Enzymatic and Mechanistic Studies into Tryptophan 2, 3-Dioxygenase

Sarah J. Thackray

Thesis presented for the degree of Doctor of Philosophy

University of Edinburgh

February 2009

Acknowledgements

I would like to thank my supervisors, Prof. Steve Chapman and Dr Simon Daff for the opportunity to work in their laboratories and their guidance and support over the past three years. In addition, particular thanks must also go to Dr. Chris Mowat and Dr Ross Anderson for all their help throughout this PhD, and to Dr Chiara Bruckmann and Laura Campbell for all the beautiful crystals and the associated crystallography. I would also like to thank all the members of the Chapman, Daff and Reid groups, both past and present, for making the lab such an enjoyable place to work over the last few years.

I am also grateful to Professor Emma Raven (University of Leicester) for allowing me to work within her laboratory, and to her research group for making me so welcome. Particular thanks must go to Nishma Chaudran and Sara Rafice for their assistance and useful discussions.

Most of all I would like to thank my Mum, Dad, Granny, Grandad, brother Steven and partner Allan for all their support and encouragement.

Abstract

Tryptophan 2,3-dioxygenase (TDO) from *Xanthomonas campestris* (xcTDO) is a highly specific heme-containing enzyme from a small family of homologous enzymes, that includes indoleamine 2,3-dioxygenase (IDO). Both enzymes catalyse the dioxygenation of L-tryptophan (L-Trp) to N-formylkynurenine, in the first step of the kynurenine pathway and play a central role in the physiological regulation of tryptophan flux in the human body

The structure of catalytically active, ferrous xcTDO in complex with L-Trp has been determined to 1.6 Å. In addition, the structure of the catalytically inactive, substrate-free xcTDO has been determined to 2.7 Å. These structures show the substrate binding interactions at the active-site and reveal that TDO is an induced-fit enzyme, with significant reorganisation of the active-site upon substrate binding. A thousand fold increase in the L-Trp binding affinity is observed upon heme reduction (K_d Fe(III) = 3800 μM, K_d Fe(II) = 4μM), disfavouring the mechanistically unproductive binding of L-Trp to the oxidized enzyme (1).

The catalytic mechanisms employed by TDO and IDO have not yet been fully elucidated and a number of mechanisms for tryptophan dioxygenation have been proposed. One proposed mechanism of dioxygen activation suggests that the base-catalysed deprotonation of the indole nitrogen of the substrate is necessary for catalysis, and the crystal structure of xcTDO has revealed a histidine residue (histidine 55) in the active site. Histidine 55 hydrogen bonds to the indole nitrogen atom of L-Trp, and could function as an active site base. However, on comparison of the active sites of TDO and IDO it can be seen that IDO contains a serine residue (serine 167) in the analogous position to histidine 55 in TDO. This serine residue is unlikely to act as an active site base, suggesting the possibility that a base may not be needed. In this study we attempt to resolve the question of whether an active site base is necessary for catalytic activity.

Active-site mutants where histidine 55 was replaced by alanine or serine (H55A and H55S) were created and crystal structures of the H55A and H55S mutant forms in complex with L-Trp were determined to 2.15 Å and 1.90 Å resolution respectively (2). Only a small change in the L-Trp binding affinity is observed upon enzyme

reduction for H55A (K_d, Fe(III) = 12μM, K_d Fe(II) = 4μM) and H55S (K_d, Fe(III) = 18μM, K_d Fe(II) = 5μM)), allowing unproductive binding of L-Trp to the oxidized enzyme. These data, in conjunction with structural, potentiometric and kinetic studies, revealed that histidine 55 was not essential for turnover, but greatly disfavoured the mechanistically unproductive binding of L-Trp to the oxidized enzyme, allowing control of catalysis.

1-Methyl-tryptophan was also studied as a possible substrate or inhibitor of xcTDO activity. This study reveals that whilst 1-methyl-tryptophan is not a substrate for TDO, and is not an inhibitor of its action, the active site mutants H55A and H55S can dioxygenate 1-methyl-tryptophan. These catalytic differences are explained by comparison of the active sites of the enzymes, and support the proposal that a catalytic base is not necessary for enzymatic activity. In addition, these data provide new insight into the future of 1-methyl-tryptophan as an inhibitor of IDO activity in cancer treatments.

Contents

Abbreviations

General

Abs	Absorbance
CN^-	Cyanide
DMSO	Dimethyl sulfoxide
E°	Standard reduction potential
EPR	Electron paramagnetic resonance
EDTA	Ethylene diamine tetra-acetic acid
ΔG°	Standard Gibb's free energy change
IDO	Indoleamine 2,3-dioxygenase
IPTG	Isopropyl-β-D-thiogalactopyranoside
hIDO	*Homo sapiens* indoleamine 2,3-dioxygenase
hTDO	*Homo sapiens* tryptophan 2,3-dioxygenase
H55A	Histidine 55 to alanine mutant
H55S	Histidine 55 to serine mutant
IDO	Indoleamine 2,3-dioxygenase
k_{cat}	Rate constant at substrate saturation
K_d	Dissociation constant
K_i	Inhibition constant
K_m	Michaelis constant
k_{obs}	Rate constant observed at a specified substrate concentration
L-Trp	L-tryptophan
LC-MS	Liquid chromatography- mass spectrometry
LB	Luria Bertani
MCD	Magnetic circular dicroism
MS-MS	Mass spectrometry – mass spectrometry
NMR	Nuclear magnetic resonance
OTTLE	Optically transparent thin layer electrochemistry
PAGE	Polyacrylamide gel electrophoresis
PEG	Polyethylene glycol

PI	4-Phenylimidazole
PrnB	Pyrrolnitrin biosynthetic enzyme
SDS	Sodium dodecyl sulfate
SHE	Standard hydrogen electrode
sIDO	*Shewanella oneidensis* indoleamine 2,3-dioxygenase
TDO	Tryptophan 2,3-dioxygenase
UV	Ultraviolet
Vis	Visible
wtTDO	Wild-type tryptophan 2,3-dioxygenase
xcTDO	*Xanthomonas campestris* tryptophan 2,3-dioxygenase
1-Me-L-Trp	1-methyl-L-tryptophan
1-Me-D-Trp	1-methyl-D-tryptophan
5-F-Trp	5-fluoro-tryptophan
5-Me-Trp	5-methyl-tryptophan
6-F-Trp	6-fluoro-tryptophan
6-Me-Trp	6-methyl-tryptophan
7-Cl-Trp	7-chloro-tryptophan

Standard Symbols

m	metre	M	molar
g	gram	°C	degree Celcius
l	litre	V	volt
s	second	Å	Angstrom

Amino Acids

A	Ala	Alanine	**M**	Met	Methionine
C	Cys	Cysteine	**N**	Asn	Asparagine
D	Asp	Aspartic acid	**P**	Pro	Proline
E	Glu	Glutamic acid	**Q**	Gln	Glutamine
F	Phe	Phenylalanine	**R**	Arg	Arginine
G	Gly	Glycine	**S**	Ser	Serine
H	His	Histidine	**T**	Thr	Threonine
I	Ile	Isoleucine	**V**	Val	Valine
K	Lys	Lysine	**W**	Trp	Tryptophan
L	Leu	Leucine	**Y**	Tyr	Tyrosine

Chapter 1

Introduction

1.1 Introduction

Heme is a versatile cofactor in biology and heme-containing proteins have a wide variety of functions, ranging from oxygen transport to single-electron transfers (3, 4). Many biological oxidation reactions are catalysed by oxygen-binding heme proteins and they are specific and powerful oxidation catalysts. Classic examples include: the cytochromes P450 (4), which catalyse the monoxygenation of a range of inert substrates, and heme oxygenases which catalyse the first step in heme catabolism, the oxidative degradation of heme to biliverdin and carbon monoxide (5). A wide variety of mechanisms are employed by heme enzymes to accomplish such oxygenation reactions, and our understanding of how protein structure relates to the catalytic mechanism is of intense interest.

Dioxygen serves two essential functions in aerobic life. It is both a terminal electron acceptor and a biosynthetic reagent. It is this latter role for dioxygen that will be the focus of this thesis: the incorporation of both of the oxygen atoms of dioxygen into the amino acid L-tryptophan (L-Trp).

Tryptophan 2,3-dioxygenase, E.C. 1.13.11.11 (TDO) and indoleamine 2,3-dioxygenase, E.C. 1.13.11.52 (IDO) are members of a small family of heme enzymes that includes PrnB, the second enzyme in the pyrrolnitrin biosynthesis pathway from *Pseudomonas fluorescens* (6) and SO4144, a bacterial IDO-like protein from *Shewanella oneidensis* (sIDO) (1). TDO and IDO catalyse the dioxygenation of L-Trp to N-formyl-L-kynurenine in the first and rate-limiting step of the kynurenine pathway. This is achieved by the activation of molecular oxygen, and the insertion of both atoms into the pyrrole ring of L-Trp (Figure 1.1). TDO activity is highly specific, and is limited to L-Trp, and a few derivatives substituted in the 5- and 6-

positions of the indole ring (4). In comparison, IDO exhibits broader substrate specificity, also catalysing the dioxygenation of D-tryptophan, 5-hydroxy-tryptophan, serotonin and tryptamine. As yet, the precise catalytic mechanism employed has not been fully elucidated.

L-Trp is the least abundant of the essential amino acids, accounting for ~1% of the total amino acids in cellular proteins. L-Trp is up taken by the body, as it cannot be efficiently synthesized by cells. The L-kynurenine pathway is the major catabolic route for L-Trp metabolism in the body and ultimately leads to the formation of nicotinamide adenine dinucleotide (NAD^+), an essential energy source (7). IDO and TDO therefore play a central role in the physiological regulation of tryptophan flux in the human body, controlling the kynurenine and serotogenic pathways (8, 9). TDO and IDO are currently of intense scientific interest due to their roles in many diverse physiological and immunological diseases, in particular the role of IDO in tumour induced tolerance (10, 11). Recently IDO-initiated immune tolerance has attracted interest because of its great potential for understanding, treating, and preventing human diseases. Investigation of the protein structure and catalytic mechanism employed by TDO and IDO would greatly aid our understanding of these important enzymes, and enlighten study into possible future disease treatments.

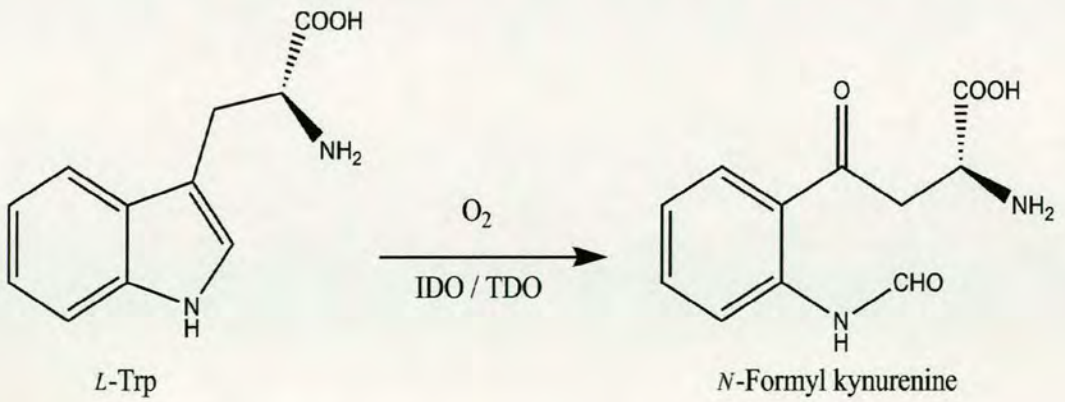

L-Trp *N*-Formyl kynurenine

Figure 1.1 Reaction catalysed by TDO and IDO.

1.2 Discovery and Occurrence

TDO was first called "tryptophan pyrrolase" when initially isolated by Kotake and Masayama in 1936 (12) and is a soluble homotetrameric protein. It is found in both eukaryotes and prokaryotes, and in mammals its expression is normally restricted to the liver. However, TDO expression has been discovered in the brain and epididymis of some species (13) and in some tissues TDO production can be induced in response to stimuli such as glucocorticoids and heme (14). It is currently unknown as to why this clear compartmentalisation of TDO expression exists, or its role in biological tryptophan regulation. TDO is homotetrameric, and eukaryotic TDOs contain around 400 amino acids whilst prokaryotic TDOs contain approximately 300 amino acids. Sequence identities between prokaryotic and eukaryotic TDOs are around 20-40%. A sequence alignment between different TDO species is displayed in Figure 1.2.

IDO was first identified in 1967 (15) and first purified in 1978 (16), and is found in many eukaryotes where it is expressed ubiquitously throughout the body, except for in the liver. IDO expression is induced in several tissues by a number of pro-inflammatory mediators, such as endotoxin and interferon-γ (17). In addition, IDO is up-regulated by the immune system in response to specific stimuli, and performs a number of roles in the body's immune response (17). Mammalian IDO is monomeric and contains approximately 400 amino acids, displaying high sequence identity between eukaryotic species, at around 20-30%. Bacteria are also believed to use members of this family for the aerobic metabolism of L-Trp via the kynurenine pathway, and some prokaryotic IDO-like proteins, such as sIDO have been identified (1). Bacterial IDOs display high sequence similarity between species, although they bear little sequence similarity to eukaryotic IDO proteins, and homology is based on their predicted 3-D structures. The recent 3-D structure of sIDO has confirmed its high structural homology to IDO, but as yet little is known about the function or expression of these proteins.

Recently a new enzyme with the ability to catalyse L-Trp dioxygenation known as INDOL1 or IDO2, has been identified (18, 19). It is encoded by a gene adjacent to

that for IDO in many eukaryotes and is predicted to be closely related to IDO in terms of its structure and function. However, it is thought that biological expression of IDO2 in the human body is different to that of IDO, and it is unknown what role this differential expression may play physiologically. IDO plays an active role in the body's immune response, and it is currently of interest as to what role IDO2 may also play in this process. Further study is needed to discover the differences between these two proteins and their physiological roles.

PrnB was first isolated and studied in *Pseudomonas* species and catalyses the second step in the pyrrolnitrin biosynthetic pathway, the conversion of 7-chlorotryptophan (7-Cl-trp) to monodechloro-aminopyrrolnitrin. This biosynthetic pathway is common to many organisms such as *Myxococcus fulmus* (21) and *Aspergillus nidulans* (22) and a number of PrnB enzymes have been identified. Pyrrolnitrin itself is a potent anti-fungal agent used to treat skin infections, and is proposed to operate via the inhibition of the fungal respiratory electron transport system (21, 23).

Sequence identity between members of this family of proteins is low and homology is generally only apparent from their 3-D structures and the conservation of certain amino acids in their active sites.

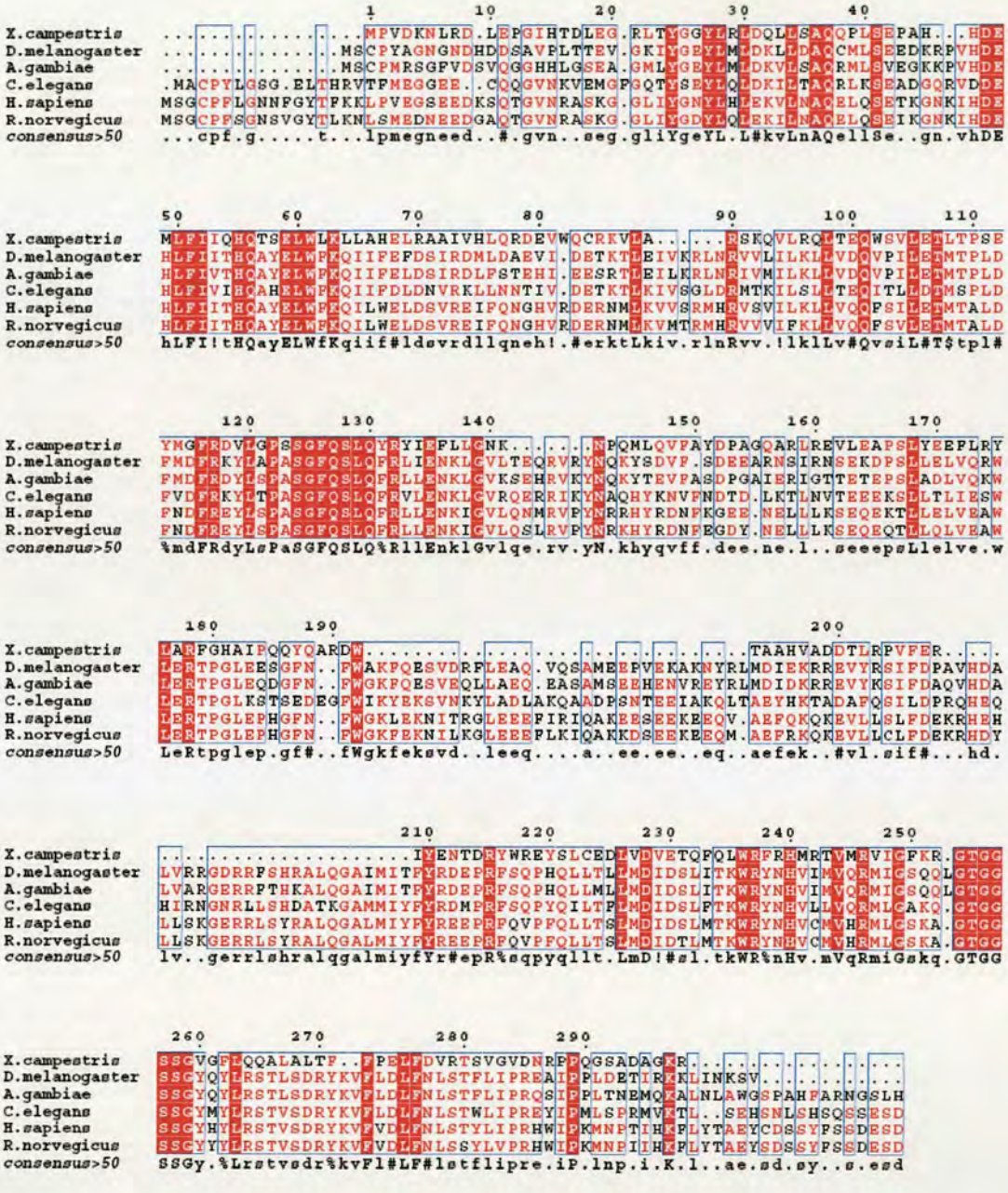

Figure 1.2 Amino acids sequence alignment of X. campestris TDO (xcTDO) (top line) and a range of eukaryotic TDOs. X. campestris TDO shares 34% sequence identity with H. sapiens TDO. Conserved residues are highlighted in red (20).

1.3 Biological Function

IDO and TDO both play a central role in the physiological regulation of tryptophan flux in the human body, controlling the kynurenine pathway and influencing serotogenic regulation. Studies have implicated these proteins in many wide-ranging and seemingly unconnected physiological and patho-physiological conditions, as discussed below. Although both enzymes catalyse the same reaction, the compartmentalisation of IDO and TDO expression is thought to reflect their differing biological roles. IDO and TDO production can be induced in certain tissues in response to specific stimuli, this specificity of cellular induction suggests little crossover of function. IDO plays an active role in the human body's immune response, but there is little evidence to suggest that TDO plays a part in this process.

1.3.1 The Kynurenine Pathway

The kynurenine pathway accounts for the processing of over 90 % of L-Trp utilised by humans, leading ultimately to the formation of NAD, an essential coenzyme, as shown in Figure 1.3 (8).

The kynurenine pathway is important as a source of metabolites, and the build up of pathway metabolites can lead to numerous physiological conditions. Some of these metabolites are neuroactive and one such example is quinolinic acid. Quinolinic acid causes neural death when injected into the brain, or when applied to neurons *in vitro* (24). Up-regulation of TDO or IDO activity in the brain may result in the accumulation of quinolinic acid and the accumulation of quinolinic acid in cerebrospinal fluid may be involved in various neurological disorders, including cerebral malaria (25), Alzheimer's disease (24), multiple sclerosis (26) and AIDS related dementia (27). Kynurenine pathway metabolites have also been implicated in cataract formation (28). The kynurenine pathway metabolites 3-hydroxyanthranilic acid and 3-hydroxykynurenine are UV filters found in the lens of the eye which protect the retina from UV light (29). These filters are synthesised from tryptophan

in the lens, and with increasing age, less turnover of metabolites occur. 3-hydroxyanthranillic acid and 3-hydroxykynurenine accumulate in the lens and "kynurenilation" occurs, causing the lens to turn opaque (30). In addition, some kynurenine pathway metabolites are immunomodulatory and can consequently contribute to immunosuppressive pathways and suppress proliferation (or cause apoptosis) of T-cells (31, 32) however the mechanisms of such metabolites are currently unknown.

The kynurenine pathway is important not only as a source of metabolites, but also due to the effect of IDO or TDO on the local tryptophan concentration. The antimicrobial response to intracellular bacteria is part of the innate host defence against certain pathogens, as some microorganisms cannot synthesise their own tryptophan, and depend upon its uptake (33). The local depletion of tryptophan in a specific tissue by enzymatic action is mainly associated with an antimicrobial response by IDO or TDO, or immune regulation by IDO, which is discussed below.

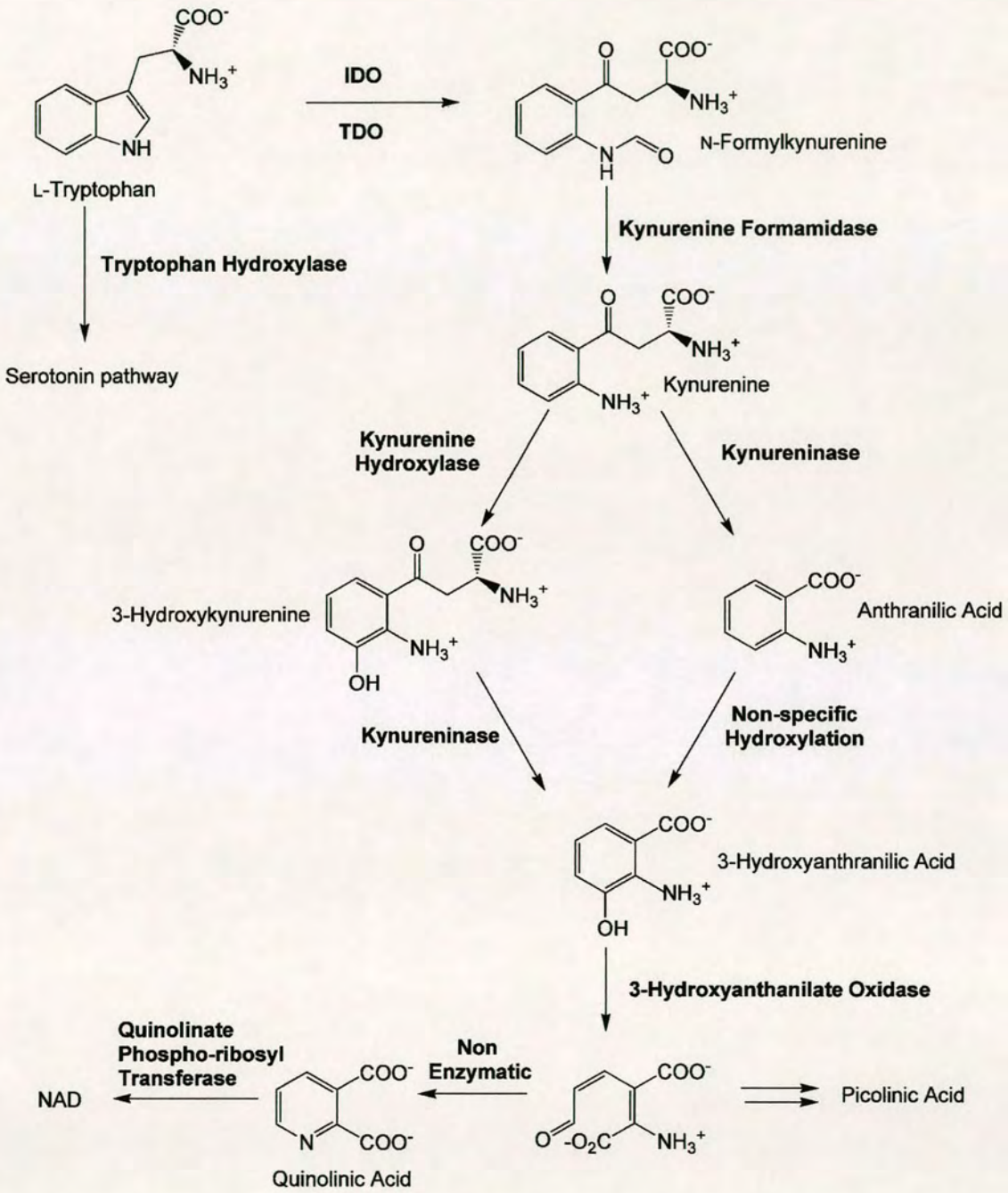

Figure 1.3 Schematic representation of the kynurenine pathway. Greater than 90% of L-Trp is metabolised via the kynurenine pathway in mammals (7).

1.3.2 Immune Regulation

Simply put, the immune system exists to discriminate between self and non-self. The mechanisms which exist to regulate the many differing and sometimes complementary processes that make up the immune system are currently very poorly understood and extremely complicated. IDO plays an active role in the human body's immune response, but there is little evidence to suggest that TDO plays a part in this process. Although TDO is induced in response to some stimuli in confined locations (34-36), it is not induced or regulated by the immune system. In contrast, IDO is subject to complex regulation by a number of immunoregulatory stimuli, and IDO-expressing cells are found in many tissues throughout the body, including dendric cells (17) and human fibroblasts (37). The evolutionarily ancient structural gene that encodes IDO pre-dates adaptive immunity, even though the promoter is easily regulated by the immune system (38). This suggests that IDOs initial, tryptophan degrading function has been re-used in regulatory mechanisms as the immune system evolved. The regulation of IDO can be influenced by many factors including tryptophan depletion, the accumulation of immunosuppressive metabolites, and interactions with signalling or immunoregulatory pathways (10, 17, 24).

IDO is a normal effector of peripheral tolerance in the immunoregulatory pathway of tryptophan metabolism and helps create a balanced immune response between inflammation and tolerance, suppressing excessive immune activation (17). Initially, IDO was associated with peripheral tolerance and immunosupression by the immune system, such as that displayed by the immune activated anti-microbial response. During the immune activated anti-microbial response, specific and local activation of dendric cells induces inferon-γ production, which in turn induces IDO production, which depletes L-Trp levels (17, 24). As some pathogens such as viruses (Herpes viruses), intracellular bacteria (*Chlamydia* and *Rickettsia*) and extracellular bacteria (*Staphylococci)* are sensitive to L-Trp depletion this may be an effective mechanism for controlling their ability to proliferate. As an example of this behaviour, L-Trp depletion is an effective mechanism against *Toxoplasma gondii* in human fibroblasts

(33, 37). However, the delicate balance between suppression and activation of the immune response by the body is not well understood, and over-induction of IDO by inferon-γ outside of a specific location can cause detrimental effects to the host (39). Side effects include depression, anxiety and diarrhoea, limiting the possible therapeutic applications of inferon-γ in humans.

IDO is now also thought to play an essential role in acquired immune tolerance. During pregnancy, the immune system does not reject the genetically different (allogenic) foetus as non-self (40). Maternal tolerance towards the allogenic foetus is not fully understood, but it is thought that cells expressing IDO in the placenta can suppress T-cell responses that mediate rejection, and this induces tolerance towards the foetus (40). Inhibition of IDO activity in mice has been shown to lead to allogenic fetal rejection, displaying the delicate balance between tolerance and rejection, which may be controlled by only one enzyme (41). If this adaptive immunity is caused solely by IDO regulation of T-cells, IDO can be targeted as a potent regulator of adaptive immune responses in immune therapy. Other examples of this adaptive immune regulation include renal allograft failure, where increased IDO activity induces acceptance of the allograft (40, 42).

It has also been discovered that IDO is involved in the proliferation of numerous cancers in the human body (10, 43, 44). IDO expression allows tumours to induce tolerance from the host's immune system by interacting with T-cells and depleting L-Trp levels. This is crucial for tumour progression, and certain cancers can be highlighted due to their IDO expression. In recent studies it has been suggested that monitoring IDO concentrations in these cancers may be an effective system for developing prognosis reports, as the most aggressive forms of these cancers show a high level of IDO expression (Figure 1.4) (10, 44). It is unknown exactly how tumours evade local immune destruction from tumour-reactive T-cells, but in consequence IDO has emerged as an attractive drug target in cancer treatments (45-47).

(33, 37). However, the delicate balance between suppression and activation of the immune response by the body is not well understood, and over-induction of IDO by inferon-γ outside of a specific location can cause detrimental effects to the host (39). Side effects include depression, anxiety and diarrhoea, limiting the possible therapeutic applications of inferon-γ in humans.

IDO is now also thought to play an essential role in acquired immune tolerance. During pregnancy, the immune system does not reject the genetically different (allogenic) foetus as non-self (40). Maternal tolerance towards the allogenic foetus is not fully understood, but it is thought that cells expressing IDO in the placenta can suppress T-cell responses that mediate rejection, and this induces tolerance towards the foetus (40). Inhibition of IDO activity in mice has been shown to lead to allogenic fetal rejection, displaying the delicate balance between tolerance and rejection, which may be controlled by only one enzyme (41). If this adaptive immunity is caused solely by IDO regulation of T-cells, IDO can be targeted as a potent regulator of adaptive immune responses in immune therapy. Other examples of this adaptive immune regulation include renal allograft failure, where increased IDO activity induces acceptance of the allograft (40, 42).

It has also been discovered that IDO is involved in the proliferation of numerous cancers in the human body (10, 43, 44). IDO expression allows tumours to induce tolerance from the host's immune system by interacting with T-cells and depleting L-Trp levels. This is crucial for tumour progression, and certain cancers can be highlighted due to their IDO expression. In recent studies it has been suggested that monitoring IDO concentrations in these cancers may be an effective system for developing prognosis reports, as the most aggressive forms of these cancers show a high level of IDO expression (Figure 1.4) (10, 44). It is unknown exactly how tumours evade local immune destruction from tumour-reactive T-cells, but in consequence IDO has emerged as an attractive drug target in cancer treatments (45-47).

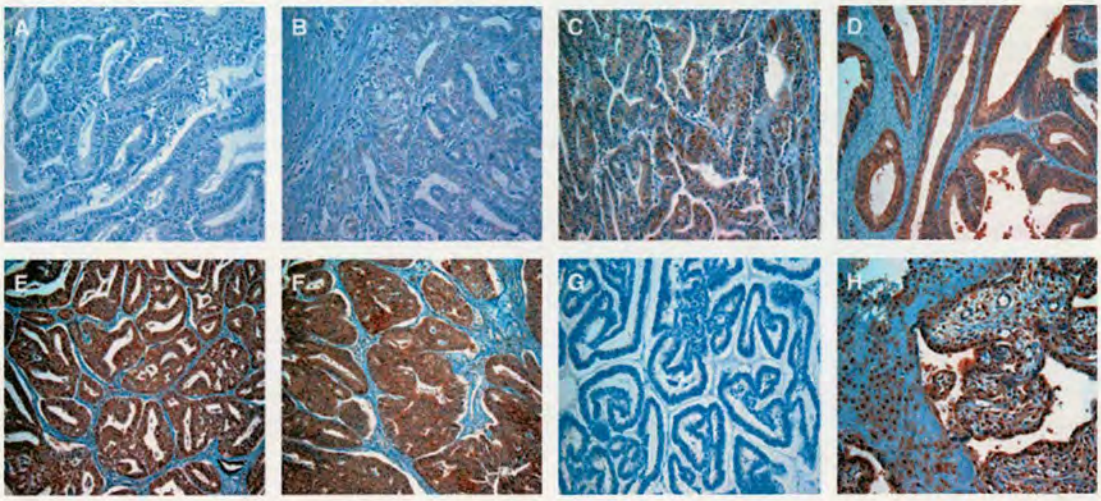

Figure 1.4 Representative immunological staining for IDO expression in endometrical cancer tissues, where IDO expression is often up-regulated. (A) IDO- (negative), (B) IDO1+ (sporadic/weak), (C) IDO2+ (focal/moderate), (D-F) (diffuse/ strong), (G) negative control, (H) positive control (normal placenta) (48).

1.3.3 TDO and IDO inhibition

IDO is a therapeutic target for the development of new anticancer drugs and importance has been given to the design of new inhibitors of its action (43, 49). Most strategies targeting the inhibition of IDO activity have utilised the indole ring structure of tryptophan as a base, and most known inhibitors are based around this structure (50, 51). Some known inhibitors of IDO activity are shown in Figure 1.5 (49, 52, 53). The most-studied inhibitor of IDO is 1-methyl-tryptophan (1-Me-Trp), a competitive inhibitor. Recently it was shown that the combination of 1-Me-Trp with a number of clinically relevant chemotherapeutic agents was able to cause regression of established tumours in murine breast cancers (45). However, 1-Me-Trp exists as two stereoisomers with potentially different biological properties, and it is unclear which isomer affects the greatest inhibitory response *in vitro* (45, 51). Most studies have employed a racemic mixture of 1-Me-Trp, leaving unanswered the question of which stereoisomer to employ in human trials. Recent studies have showed that whilst 1-Me-L-Trp is a more potent inhibitor of purified IDO than in cell–based

assays (45), 1-Me-D-Trp is more effective than 1-Me-L-Trp as an anticancer agent when tested in mouse cancer cells. These findings supported the suitability of 1-Me-D-Trp for human cancer trials, which have since commenced (54). However, since these reports it has been suggested that 1-Me-D-Trp may be inhibiting INDOL1 activity, rather than the activity of IDO (51, 55). Considering the importance of developing new cancer treatments, clearly more information is needed on both IDO and INDOL1, and the effects of L-and D-Me-Trp upon their enzymatic activity.

In comparison 1-Me-Trp is ineffective against TDO activity (56). However, a few potent inhibitors of TDO have been discovered, including norharman (57), a β-carboline derivative. In addition, a number of 2-(2-pyridylethenyl) indole derivatives have been investigated, although research in this area is less extensive (58-60).

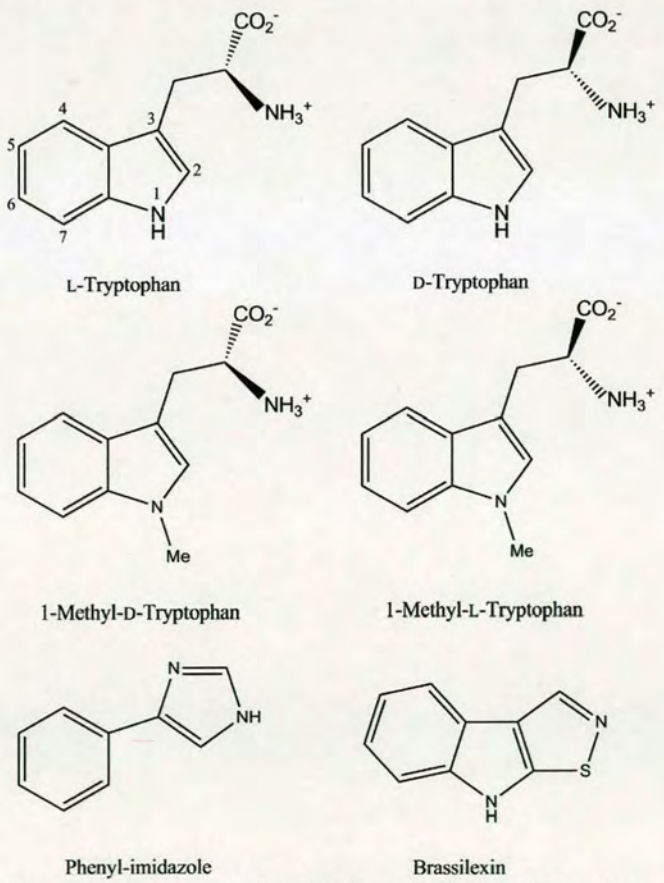

Figure 1.5 L-Trp is a substrate for TDO and IDO. D-Trp is a weak inhibitor of TDO and a substrate for some IDOs. 1-methyl-L-tryptophan, 1-methyl-D-tryptophan, phenyl imidazole and brassilexin are all IDO inhibitors.

1.4 The Role of Dioxygen

1.4.1 Chemical Properties of Dioxygen

Dioxygen is essential to aerobic life, and it is now known to play a role in a wide variety of biological processes. Oxygen is a powerful oxidising agent, due to its high electronegativity and thermodynamically favourable reactivity. Molecular dioxygen is primarily used in biological reactions for its oxidising capabilities, whereby it is reduced to water.

Oxygenase reactions involve the cleavage of the oxygen-oxygen bond, which is a thermodynamically favourable reaction (61). However, the chemical reactivity of dioxygen with organic molecules under standard conditions is very low. Indeed if this were not the case, dioxygen would be harmful rather than useful for living organisms. This low reactivity is due to the ground state of molecular oxygen. It is a triplet, diradical in the ground state with two unpaired electrons residing in antibonding π* orbitals, Figure 1.6. The molecular orbital energy level configuration of triplet dioxygen is $(1s\sigma)^2\ (1s\sigma^*)^2\ (2s\sigma)^2\ (2s\sigma^*)^2\ (2p\sigma)^2\ (2p\pi)^4\ (2p\pi x^*)^1\ (2p\pi y^*)^1$. This unusual paramagnetic ground state arises from two electrons residing in the antibonding $2p\pi x^*$ and $2p\pi y^*$ orbitals, resulting in dioxygen having a formal bond order of two.

Singlet oxygen is more readily reactive than triplet dioxygen, and two singlet states exist (Figure 1.6). Nearly all stable organic compounds are singlets with paired electrons, and direct reactions between singlet and triplet species are spin forbidden because chemical reaction rates are much faster than spin inversion rates. Therefore the reaction of triplet dioxygen with these compounds under standard conditions can only proceed via the spin-allowed, high energy formation of an unstable triplet intermediate by the organic molecule. This undergoes reaction with triplet dioxygen, followed by slow spin inversion to form a singlet product. In addition triplet dioxygen will react readily with organic radicals. Non-enzymatic conversion of triplet to singlet dioxygen requires photolysis or an external energy source to

overcome the high kinetic barrier inherent to reactivity. Both singlet states of dioxygen are higher in energy than the triplet state, and 22.5 k_{cal} mol^{-1} is required to convert triplet dioxygen to the lower energy singlet state.

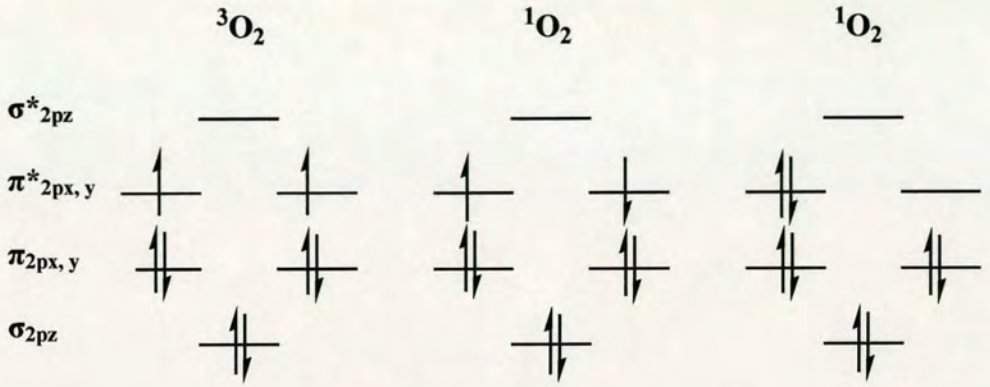

Figure 1.6 Molecular orbital diagrams for the triplet and singlet states of dioxygen, (a) $^3O_2$, (b) $^1O_2$ ($^1\Sigma$) and (c) $^1O_2$ ($^1\Delta$).

1.4.2 Enzymatic Oxygen Activation

Nature has devised a large number of redox active groups, utilising transition metal ions, heme porphyrins and organic cofactors to mediate dioxygen activation. Oxygenases catalyse the enzymatic addition of oxygen to substrates, and utilise all of these different redox strategies to promote their reactions. The most commonly used metals in oxygenases are iron and copper, and they are employed because in their lower oxidation states these metals can form complexes with dioxygen, organic substrates, or both, and affect the electronic structure of the bound compound to alter its reactivity. They achieve this by promoting the reaction between dioxygen and an organic substrate in two main ways. Firstly, they can activate triplet dioxygen to attack organic substrates. Secondly, they can activate organic substrates to attack triplet dioxygen. Easily oxidisable singlet organic molecules can react by first forming resonance-stabilised, (one-electron oxidised) radicals, which then react with

triplet dioxygen. This is obviously a simplification and in reality an enzyme may utilize a combination of these approaches, either in synergy or sequentially.

Cofactor-less oxygenases also activate dioxygen, but the reactions catalyzed by these enzymes are poorly understood in mechanistic terms (62). Catalysis is thought to proceed via a radical mechanism, and the enzymes are thought to stabilise anionic intermediates in the catalytic cycle.

1.4.3 Oxygen Activation by Heme

The heme system consists of an iron atom coordinated in a square-planar arrangement by four nitrogen atoms, provided by pyrrole groups. The axial ligands to the heme iron are provided by either one or two amino acid side-chains or exogenous ligands. The most common heme prosthetic group is iron protoporphyrin IX, heme *b* (Figure 1.7 (b)). There are a number of naturally occurring variations to the protoporphyrin IX system giving rise to the classes of heme *a, b, c,* and *d* (Figure 1.7).

Heme is generally a one-electron cofactor, with the iron atom accessing the two most stable oxidation states available; the ferrous (Fe^{2+}) and ferric (Fe^{3+}) forms. However, some systems, e.g. the P450 enzymes and the heme-copper oxidases, are known to utilise the ferryl (Fe^{IV}) oxidation state of the iron (63, 64). The conjugated heme governs the activation of dioxygen, allowing the formation of low-spin states, stabilising highly oxidised iron intermediates that can undergo reactions.

The mechanism of dioxygen activation by heme iron enzymes involves an initial reversible, complex formation between the ferrous high-spin (d^6, S = 2) heme iron and triplet dioxygen. This yields a low-spin complex that is generally described as either Fe^{2+}-O_2 or Fe^{3+}-$O_2^{\bullet-}$ or a resonance hybrid of these two forms because the actual electronic structure may involve partial electron transfer between iron and bound dioxygen. For the Fe^{2+}-O_2 structure, σ bond formation occurs *via* back donation from a ferrous ion orbital (e.g., d_{xz}) to the empty σO_2* orbital. Transfer of one electron from iron to the bound dioxygen yields the ferric superoxide structure,

Fe^{3+}-$O_2^{\bullet-}$. An unpaired electron on the superoxide resides in its antibonding σ orbital (σO_2^*), while a second unpaired electron resides in a nonbonding iron orbital (d_{xy}). In either the ferrous dioxygen or ferric superoxide configuration, the complex is *diamagnetic*.

Substrate activation by heme enzymes involves initial complex formation between the (singlet) substrate and the ferric or ferrous heme iron, such as that catalysed by the extradiol dioxygenases (65).

For TDO and IDO, the ferrous dioxygen structure is the best model of the electron configuration, as further reduction of the heme-bound dioxygen is not required in its mechanistic cycle (see "Catalytic Mechanism"). However, the complex formed between ferrous heme iron and triplet O_2 must be a singlet for the reaction to proceed. The bound dioxygen is not singlet O_2, but can react by either an ionic or a radical mechanism to give products that are similar to those that would be produced by the reaction of singlet O_2.

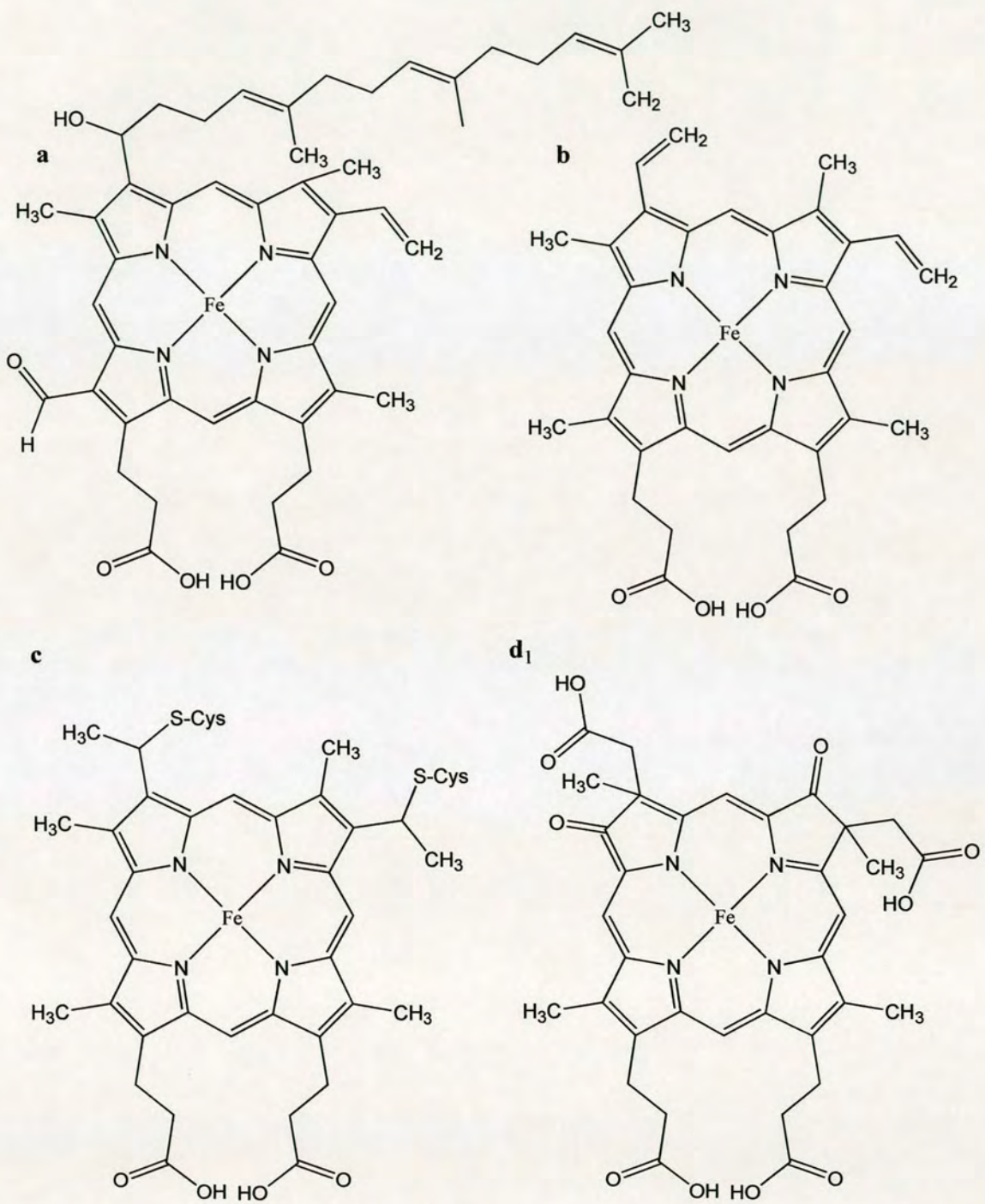

Figure 1.7 : Structures of some of the naturally occurring heme groups. The heme groups a, b, c, and d_1 are represented. The protoporphyrin IX system is the heme b.

1.5 Oxygenases

Early biochemical studies assumed that the oxygen found in organic substrates came from water and that dioxygen was only utilised by the body in some oxidase and dehydrogenase reactions. Then in 1955 Hayaishi and Mason unambiguously demonstrated that isotopically labelled dioxygen could be incorporated into organic compounds directly, and designated the enzymes which catalyse such reactions oxygenases (66, 67). Hayaishi and Mason demonstrated that these oxygenases can catalyse the incorporation of one or both atoms of molecular oxygen into organic substrates – by processes of monooxygenation or dioxygenation. We now know that monooxygenases insert an atom of molecular oxygen into the substrate of interest and reduce the other atom of dioxygen to water, whilst dioxygenases are either intermolecular or intramolecular, incorporating oxygen into separate substrates or into a single substrate. Oxygenases may be enantio-, chemo-, or regioselective and can produce optically pure products when traditional chemical reactions are unspecific, consequently they are becoming widely exploited in industrial processes (68). Monooxygenases and dioxygenases may employ transition metal ions, heme porphyrins and inorganic cofactors in their catalytic reactions. Described below are some examples of monooxygenase and dioxygenase enzymes.

1.5.1 Monooxygenases

Monooxygenases require two electrons to reduce the unincorporated oxygen atom of O_2 to water. The two electrons may be obtained from a reducing agent or agents, or from the substrate itself. Monooxygenases can utilise inorganic compounds, transition metal ions or heme porphyrins to activate the reaction, and often also contain non-metal cofactors such as flavins or tetrahydrobiopterin as an electron source to reduce the second atom of O_2 to water (69).

Heme-containing monooxygenases include cytochrome P450's (4), secondary amine monooxygenase (4) and heme oxygenase (70). The cytochromes P450 are perhaps

the most well known monooxygenases, catalysing the oxidation of a huge variety of organic compounds. The most common function of the P450 enzymes is the catalysis of regio- and stereo-specific hydroxylation reactions on non-activated hydrocarbons under physiological conditions. These properties have recently lead to the investigation of P450s as potential biocatalysts since uncatalysed reactions require high temperatures and are non-specific (71). All P450s contain a *b*-type heme coordinated to the enzyme *via* a cysteine ligand in the fifth ligation site (72). It has been proposed that the strong electron donating character of the cysteine thiolate provides an 'electron push' onto the heme allowing it to achieve reduction potentials necessary to stabilise the oxygen species required in the catalytic mechanism.

Non-heme iron monooxygenases include tryptophan hydroxylase which catalyses the hydroxylation of L-Trp to 5-hydroxy-tryptophan (73), and methane monooxygenase (70, 74), which is found in methanotropic bacteria. Methanotropic bacteria respire on methane and catalyse the oxidation of methane to methanol, in the first step of the conversion of methane to carbon dioxide. There are many different forms of methane monooxygenase, including both membrane bound and soluble forms, and these are thought to contain copper and iron centres, although this remains a widely debated issue. One soluble form (soluble methane monooxygenase) is known to contain only iron centres, and in this enzyme dioxygen is activated at a di-iron cluster by a reductive process that results in the formation of a high valency iron-oxo species prior to substrate binding (74).

Quinone-forming monooxygenases are cofactor-less oxygenases involved in polyketide tailoring (62). They catalyse the synthesis of a number of aromatic polyketides by the oxidation of naphthacenone- and anthrone-type precursors of polyketides to form the corresponding quinine derivatives. Polyketides are of enormous therapeutic and commercial importance, since they exhibit antibiotic, antitumour and immunosuppressive activities. The quinone-forming monooxygenase requires only dioxygen for activity and uses its substrate as a reducing equivalent for the reduction of dioxygen to water, making it an internal monooxygenase.

1.5.2 Dioxygenases

Non-heme iron oxygenases include the Rieske cis-dihydrodiol-forming dioxygenases (75) and the extradiol aromatic ring cleaving dioxygenases (65, 75). The extradiol aromatic ring cleaving dioxygenases convert complex aromatic compounds to single or double-ring compounds in bacteria. The rings of these molecules are opened by dioxygenases that usually contain Fe^{2+} or Fe^{3+} at their active-sites. The active metal centre in most of these extradiol dioxygenases contains a ferrous iron ion bound by two histidine residues, and a glutamate or aspartate side chain, whilst the other three positions can contain up to three solvent molecules. Whilst the reactions catalysed can vary greatly, the initial oxygen activation mechanism is often similar between enzymes. Substrate coordinates to the metal first concurrently displacing two solvent molecules from the metal centre. Dioxygen then coordinates to the iron centre in site adjacent to the substrate, and the reaction between the two is facilitated by the iron atom allowing electron transfer between them. This is thought to induce radical character, allowing the otherwise spin-forbidden reaction to proceed

Heme-containing dioxygenases include TDO and IDO, where the heme porphyrin coordinates and activates dioxygen whilst in the ferrous state (4). This is similar to the phenol ring cleavage catalysed by non-heme iron dioxygenases such as catechol 3,4-dioxygenases (73) and protocatechuate 4,5-dioxygenase (76). But in contrast to heme iron and non-heme iron-containing monooxygenases such as P450 which are able to oxygenate completely unactivated alkanes, TDO and IDO require a substrate containing a functionalised double bond for catalytic activity.

Cofactor-less dioxygenases involved in the degradation of N-heteroaromatic compounds have been identified (62). Biochemical and spectroscopic studies of the purified 2,4-dioxygenases termed Qdo (1H-3-hydroxy-4-oxoquinoline 2,4-dioxygenase) and Hod (1H-3-hydroxy-4-oxoquinaldine 2,4-dioxygenase) have shown that neither enzyme contains any metal or organic cofactors, however, little more is known of these proteins to date, and their mode of operation is unknown.

1.6 Catalytic Mechanism

The catalytic mechanism employed by TDO and IDO are poorly understood, and little characterisation of reactive intermediates has been reported. Proposals for the catalytic mechanism for tryptophan oxidation by TDO and IDO are illustrated in Figures 1.8 and 1.9.

1.6.1 Reduction of TDO and IDO

Turnover of L-Trp by TDO or IDO occurs with the enzyme in the ferrous state. Some reports of weak catalytic activity by ferric IDO and TDO exist (77, 78), but this is likely due to small amounts of the ferrous form being present. Reduction of the heme iron is therefore required to facilitate the observation of catalytic activity (4). Under physiological conditions it has been proposed that cytochrome b_5 acts as an electron transfer protein, donating an electron to ferric IDO (79). It is unknown whether cytochrome b_5 also reduces TDO, but a similar mechanism would appear likely.

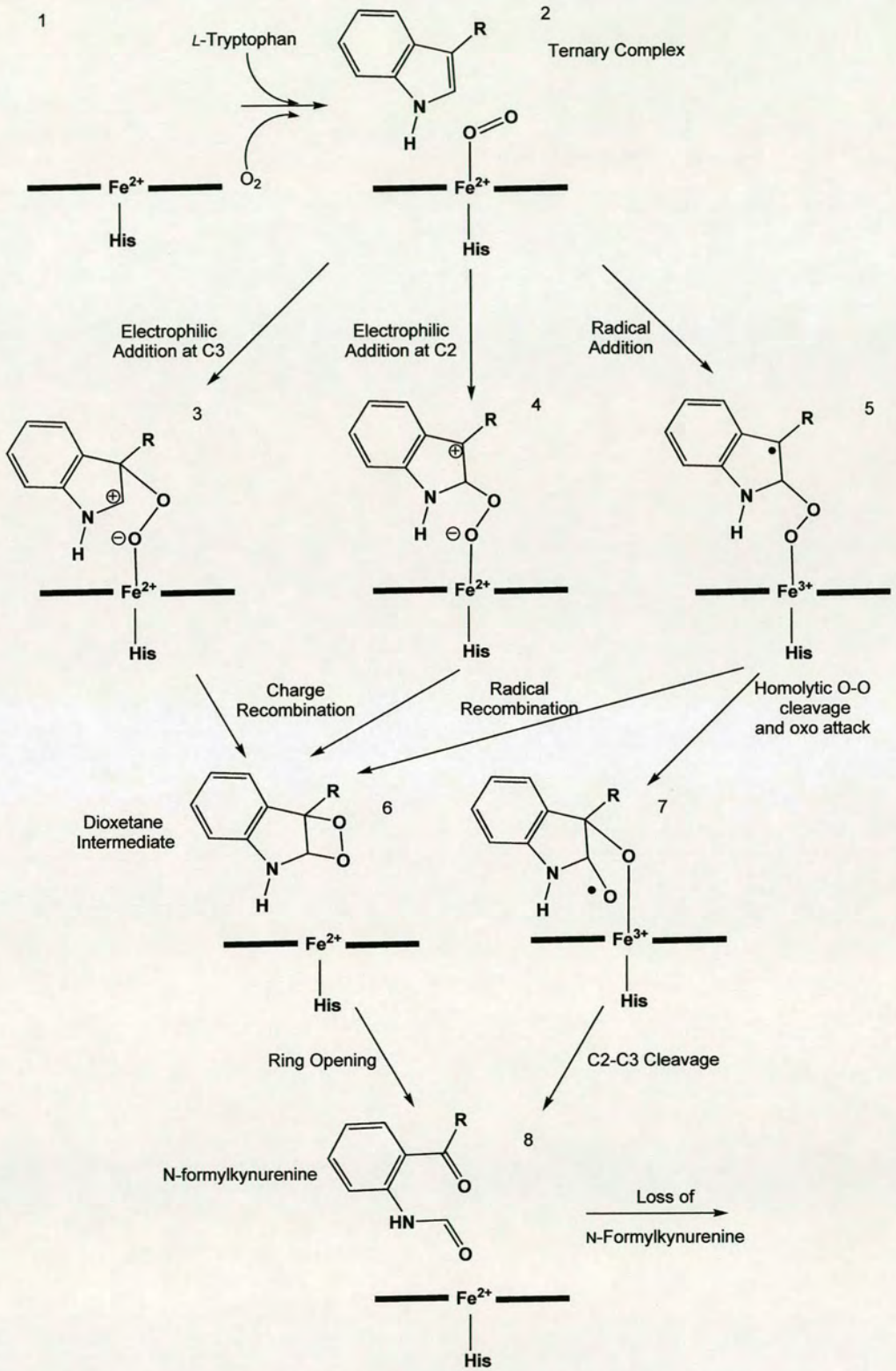

Figure 1.8 Proposed catalytic mechanisms for TDO and IDO dioxygenation.

1.6.2 Ternary Complex Formation

In the enzyme active site, O_2 and L-Trp must both bind to the active site, forming a ternary complex [2], before any reaction can take place (Figures 1.8 and 1.9). Trapping of this ternary adduct (substrate-Fe^{2+}-O_2) for both TDO and IDO has confirmed its formation [reviewed in 4].

TDO

In TDO, the binding of substrate and dioxygen to the reduced enzyme to form the ternary complex (Trp-Fe^{2+}-O_2) is thought to be an ordered process with L-Trp binding first, then O_2 (1, 4). Reduced TDO does not readily bind O_2 in the absence of substrate and addition of dioxygen leads directly to the oxidised enzyme, with no detectable intermediates (77). The oxidised enzyme does not bind dioxygen while substrate binding is disfavoured compared to the reduced enzyme, making it impossible for the oxidised enzyme to form the ternary complex. The ternary complex activates O_2, and allows the otherwise spin-forbidden reaction between L-Trp and O_2 to proceed. TDO is not thought to utilise superoxide, although some generation of reactive oxygen species by TDO *in vivo* has been reported (80).

IDO

In the case of IDO it appears that both the ferric and ferrous forms of the enzyme can react with specific oxygen species to form products. It is thought that *in vivo* IDO is reduced by an external factor such as cytochrome b_5, before reacting with substrate and dioxygen to form the ternary species (79). However, ferric IDO is also capable of reacting with superoxide and substrate to form the ternary species (81).

Ferrous IDO is able to bind either the substrate or dioxygen to form stable binary complexes. The formation of the ternary complex can occur as it does in TDO, by substrate binding followed by dioxygen binding. In addition, reaction of the binary

oxy-Fe^{2+} adduct (which is stable with a lifetime of seconds) with a substrate yields the appropriate product (78) and it seems reasonable that ternary complex formation probably occurs via both routes.

Ferric IDO binds superoxide to form the binary Fe^{2+}-O_2 adduct, which can then bind substrate as described above (81, 82). However, it is not clear if the binary Fe^{3+}-L-Trp adduct can react with superoxide. It has been shown by equilibrium binding studies of L-Trp to both the ferric and ferrous forms of IDO that L-Trp binds more readily to the ferrous enzyme (83). Therefore it seems unlikely that the Fe^{3+}-L-Trp adduct would form *in vivo* and react with superoxide. Some studies have suggested that even if this reaction is favourable, any product formation via this route would be minimal (81, 84). Unlike TDO, IDO undergoes auto-oxidation during catalytic turnover, producing ferric enzyme and superoxide (4, 82). IDO needs to be continually reduced *in vitro* and *in vivo* to retain catalytic activity.

1.6.3 Dioxygen Activation in the Ternary Complex

Various mechanisms have been proposed for the initial step in the dioxygenation of L-Trp by IDO and TDO. Catalysis can proceed either *via* an ionic or a radical mechanism, and these routes involve the same intermediates in product formation. Early work by Wiseman et al. suggested that it would be energetically unfavourable to proceed via a radical mechanism (85) (Figure 1.8). However, the proposed radical mechanism involved base-catalyzed deprotonation of the indole NH group to generate the Trp anion, which is then reversibly oxidized by (Fe^{3+}-O_2) to form a tryptophan radical and (Fe^{2+}-O_2) (86). Formation of such a tryptophan radical is a highly thermodynamically unfavourable reaction and such a radical mechanism became discounted as a valid route for product formation (4). Subsequent work has generally proposed ionic catalytic mechanisms with electrophilic addition of the bound dioxygen to the indole ring, concerted with proton transfer (an oxygen-ene type reaction) (87, 88). Until very recently this was the most accepted mechanism for

dioxygen activation. However, a recent density functional theory study into the catalytic intermediates involved in TDO and IDO catalysis does not support this concerted oxygen-ene type pathway (Figure 1.9) (89). On the basis of DFT calculations Chung *et al* propose that dioxygen activation occurs either *via* direct electrophilic addition of the bound dioxygen or direct radical addition to the Fe^{3+}-$O_2^{\bullet-}$ species. Each of these possible mechanisms will now be discussed in detail.

Formation of a Hydroperoxide Intermediate

This is an ionic mechanism, proposed on the basis of biochemical studies, whereby catalysis proceeds via the formation of a hydroperoxide intermediate. Addition of O_2 to the C3 position of the substrate occurs prior to O-O bond cleavage (4, 88). It has been proposed that formation of this hydroperoxide intermediate could be catalysed by three possible mechanisms – base-catalysed deprotonation of the indole nitrogen atom, proton abstraction by bound dioxygen or base catalysed deprotonation by solvent, these are discussed below.

It has been proposed that base catalysed deprotonation of the indole nitrogen could facilitate nucleophilic attack from the C3 position of the indole ring to the bound dioxygen (4, 88). This mechanism is displayed in Figure 1.9 (a). However, although this mechanism may be possible for TDO, which has a histidine residue in its active site, IDO does not contain a residue capable of acting as a catalytic base. In fact IDO contains a serine residue (ser 127) in the analogous position to histidine in TDO.

Catalysis by the iron-bound dioxygen in an "oxygen-ene" type reaction is generally proposed in the absence of a base (Figure 1.9 (b)) where proton abstraction by the iron-bound dioxygen is concerted with electrophilic attack. The indole NH group interacts with the proximal oxygen atom, weakening the O-O bond, facilitating electrophilic addition at the C3 position (87-89). Until recently this "oxygen-ene" type reaction was favoured as a possible catalytic mechanism. However, the recent DFT calculations have suggested that the energy barrier for formation of the transition state is high, and therefore unfavourable.

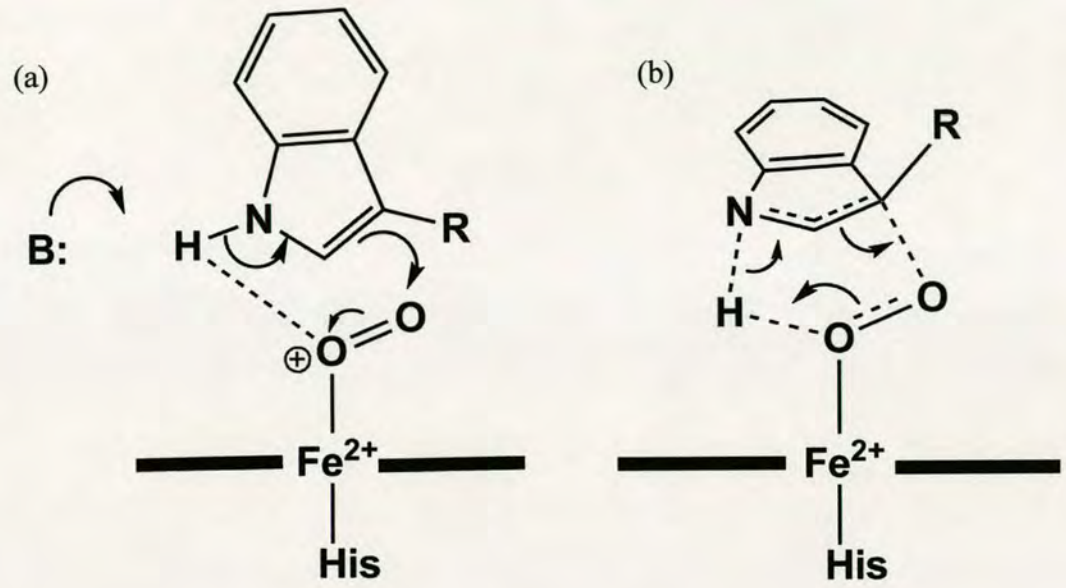

Figure 1.9 The ternary complex (Fe^{2+}-L-Trp-O_2) is displayed in both (a) and (b). (a) Shows base-catalysed attack on the ternary complex, whilst (b) displays a non-based catalysed mechanism whereby the reaction proceeds by an "oxygen-ene"-type rearrangement.

Another possibility that has been considered is that proton abstraction is catalysed by a solvent molecule in the active site. If this was to occur the pKa values of the groups involved must be similar. However, whilst the p*K*a of enzyme bound L-Trp is unknown, that of free L-Trp is quite high (16.9), and any solvent must be more basic than this (Figure 1.10) (90). Additionally, as the most probable solvent is water, and the crystal structure of xcTDO shows that no water is bound in the appropriate position in the substrate-bound active-site this mechanism is consequently considered unlikely (1, 2).

Direct Electrophilic Addition of the Iron-Bound Oxygen

Dioxygen activation in the ternary complex, by direct electrophilic addition of the iron-bound dioxygen to the electron-rich indole ring of tryptophan is predicted to be

favourable by DFT calculations (89), and is shown in Figure 1.8. Addition of oxygen to either the C2 or C3 position of the indole ring, uncoupled to proton transfer, is predicted to be favourable (Figure 1.8 [3] and [4]). The addition is calculated to have the lowest energy barrier when the electronic configuration of dioxygen is a closed-shell singlet for reaction to either the C2 or C3 positions.

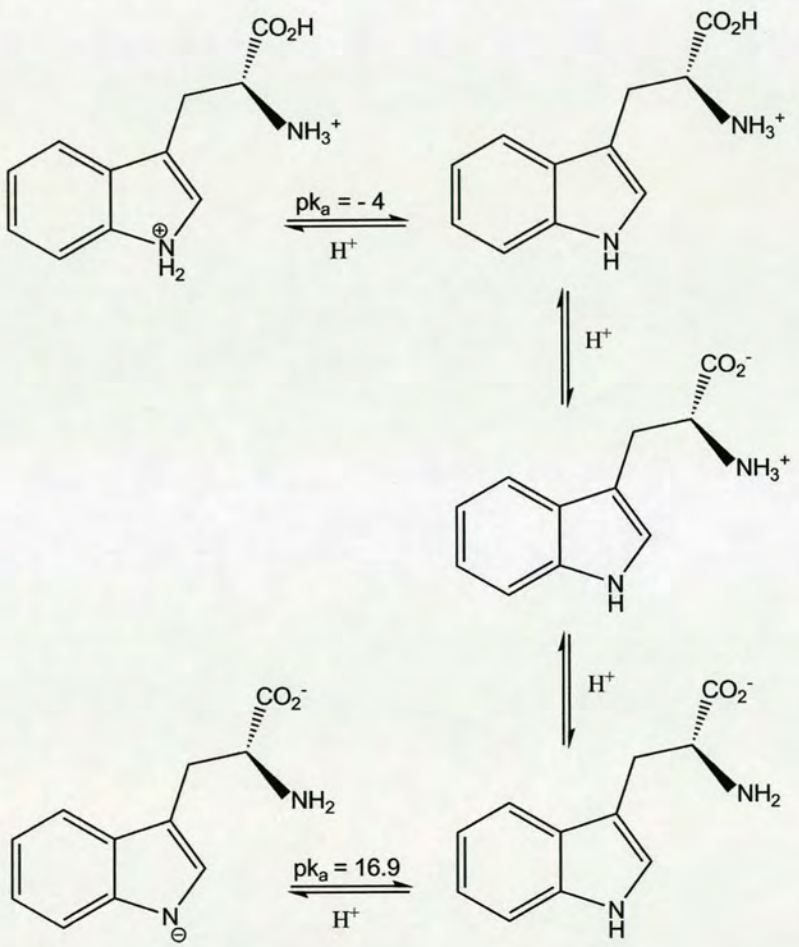

Figure 1.10 pH-dependant properties of tryptophan. Deprotonation of the indole nitrogen atom occurs at a pKa of 16.9, whist formation of the doubly protonated species occurs at a theoretical pKa of - 4.

Direct Radical Addition

Direct radical addition of Fe^{3+}-superoxide species to the C2 position without the involvement of proton transfer is predicted by DFT to be favourable in energy, displaying a low energy barrier to reaction. The superoxide species must be in a triplet or open-shell singlet state for the reaction to be favourable. The diradical intermediate is shown in Figure 1.8 [5].

1.6.4 Rearrangement of Addition Intermediate

The rearrangement of the addition intermediate to form the product has been proposed until recently to be catalysed by either a Criegee or a dioxetane pathway. However, the recent suggestion of different addition pathways has lead to the proposal of new rearrangement mechanisms. All of the proposed rearrangements will now be discussed.

Criegee Rearrangement

The hydroperoxide intermediate [3], can rearrange via the Criegee or dioxetane rearrangements to form the product N-formylkynurenine. The Criegee rearrangement is shown in Figure 1.11, and requires an antiperiplanar arrangement of the O-O bond and the indole C2-C3 bond to form an intermediate [4] that further rearranges [5] to form the product N-formylkynurenine [6]. DFT calculations have suggested that the Criegee rearrangement is unfavourable since formation of the antiperiplanar conformation required for catalysis demands a very high barrier from the neutral indoleine intermediate (89). These calculations cast doubt on the feasibility of a Criegee rearrangement in the mechanism of L-Trp dioxygenation.

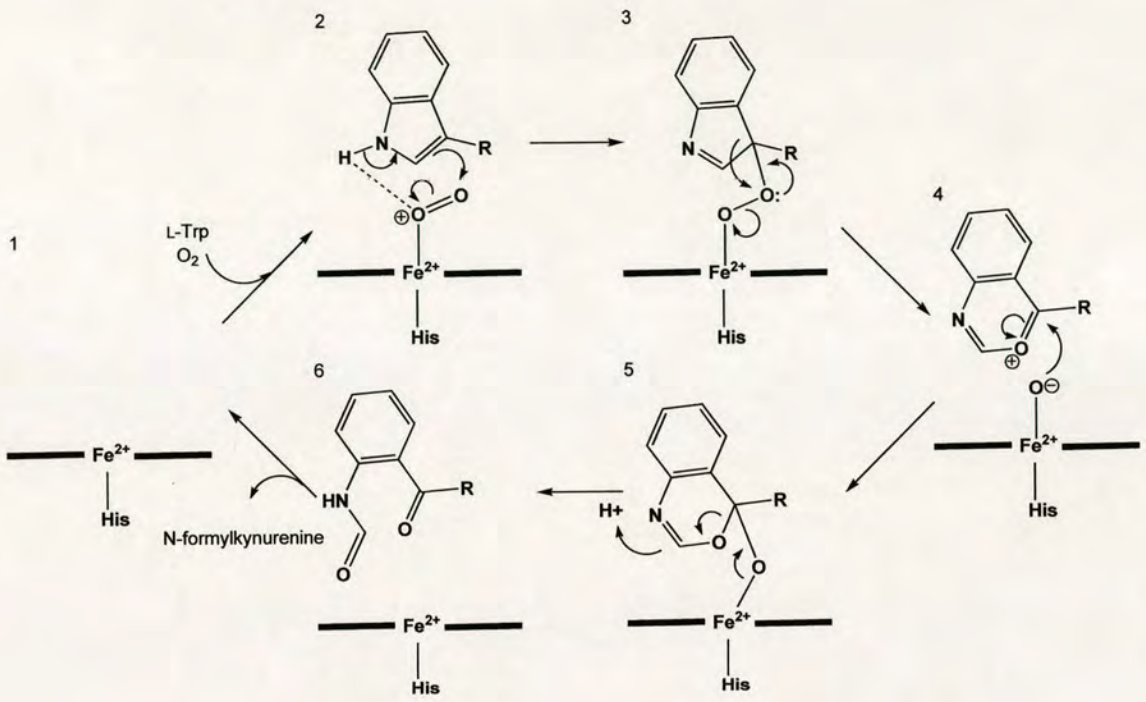

Figure 1.11 The proposed Criegee rearrangement of the hydroperoxide intermediate in the dioxygenation of L-Trp by TDO and IDO.

Dioxetane Mechanism

All of the catalytic intermediates proposed to form from initial dioxygen activation (Figure 1.8 [3], [4] and [5] and Figure 1.11 [3]) can undergo rearrangement to products via a dioxetane rearrangement. The dioxetane mechanism requires a sin-coplanar configuration of intermediate [6] (Figure 1.8) which then undergoes a retro [2+2] cycloaddition to form the product. DFT calculations modelling the Michaelis complex indicate that formation of the highly strained dioxetane intermediate and its decomposition are energetically favourable. However, no chemiluminescence has been detected on decomposition of the dioxetane, which could be expected upon decomposition of the four-membered ring.

Radical Rearrangement

After initial radical intermediate formation (Figure 1.8 [2] to [5]), catalysis can proceed via a nearly barrier-less charge-recombination step to form the dioxetane intermediate and rearrange to products, or alternatively undergo a radical mechanism.

The proposed radical mechanism involves homolytic O-O bond cleavage from the diradical intermediate followed by oxo attack and facile C2-C3 bond cleavage to products. However, the formation of strong oxidant ferryl-oxo species may lead to undesired by-products (64).

1.6.5 Conclusions

Currently there is little biochemical data to support any particular mechanistic route of L-Trp dioxygenation. In this study we attempt to determine detailed information on the mechanism of L-Trp dioxygenation, via biochemical and structural characterisation of xcTDO. Throughout this thesis the impact of key results on the mechanism of ternary complex formation, dioxygen activation in the ternary complex and the rearrangement of the addition intermediate will be discussed and mechanistic conclusions drawn. These results will provide the basis for the proposal of a catalytic mechanism in Chapter 6.

1.7 Crystal Structures

Crystal structures of five members of this family of heme proteins have now been published, and crystallographic information is shown in Table 1.1.

(The structure of xcTDO was solved by our research group in collaboration with Liang Tong (Columbia University, NY, USA) in 2007 and is discussed both below, and in Chapter 1).

Table 1.1 Crystallographic data regarding the heme dioxygenase family of proteins.

	Ligand	Resolution (Å)	PDB codes
xcTDO (1)	None, L-Trp, 6-F-Trp	2.7, 1.6 and 1.8	2NW7, 2NW8, 2NW9
rmTDO (88)	None	2.4	2N0X
hIDO (87)	PI, CN^-	2.3 and 3.4	2D0T, 2D0U
sIDO (1)	None	2.4	1ZEE
PrnB (6)	None, L and D-Trp, L and D-7-Cl-Trp	1.75, 2.0, 1.75, 2.4, 2.0	2V7I-2V7M

1.7.1 TDO Structure

Two structures of TDOs have been published, those of *X. campestris* TDO (xcTDO) (1) and *R. metallidurans* TDO (rmTDO) (88). The crystal structures show that the proteins are essentially identical (they share 47 % sequence identity), with the regions of the highest sequence similarity located near to the active-site. As the structure of *X. campestris* TDO is at a higher resolution, and it is the only structure available in the ferrous, active form with substrate bound (L- or 6-F-Trp) it is the best available model of substrate binding interactions.

The structure of TDO is an intimately associated homotetramer with approximately 4500 $Å^2$ of the surface area of each monomer being buried within the tetramer interface (Figure 1.12(a)). The structure of the monomer contains 12 α-helices and no β-strands and belongs to the family of bacterial TDO-like protein folds, represented in Figure 1.13(a). The tetramer may best be described as a dimer of dimers as the N-terminal residues of each monomer form part of the substrate-binding site in the adjacent monomer (residues 21-40 of xcTDO). A "dimer" of xcTDO is shown in Figure 1.12(b) and (c). The N-terminal loop from the adjacent monomer points down directly to the heme binding site with two tyrosine residues (Tyr 24 and Tyr 27) each hydrogen bonding with glutamate residues on the αA-helix forming the back wall of the active site pocket (Figure 1.13(b)). It is unknown what function this dimerisation may play in the function of TDO *in vivo,* but similar arrangements are seen in a number of allosteric proteins (3).

In the substrate bound structure of xcTDO a flexible loop (encoding residues 250-260) just outside the heme pocket has been fully resolved crystallographically. This loop appears to be involved in binding both the ammonium and carboxylate moieties of L-Trp, and may be acting as a "lid" closing the active site upon substrate binding.

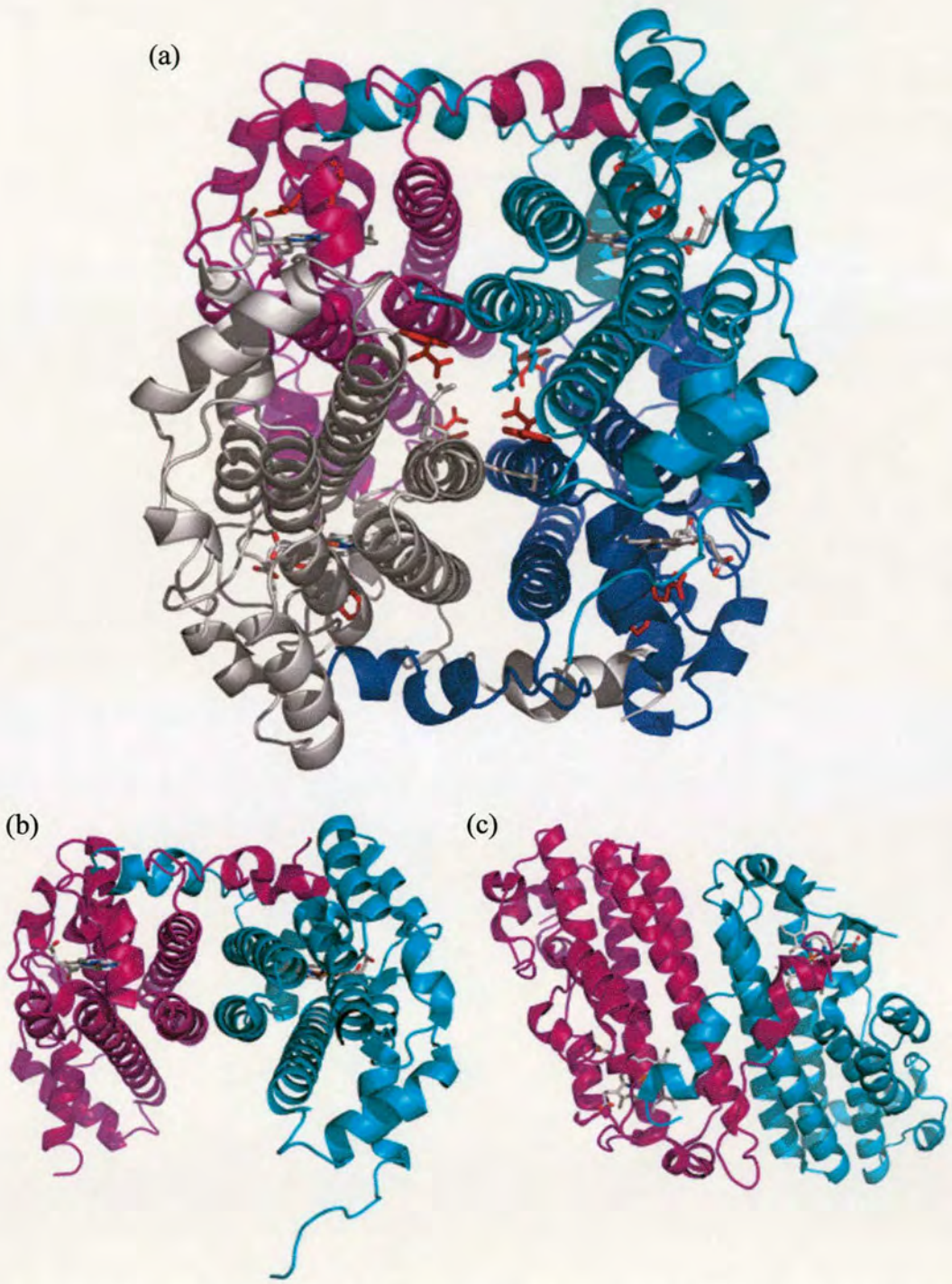

Figure 1.12 (a) Tetrameric TDO, with the different monomers shown in magenta, cyan, grey and blue. Heme is displayed in grey and 8 bound L-Trp molecules are shown in red. Displayed in (b) and (c) are two views of the "dimeric" arrangement of TDO

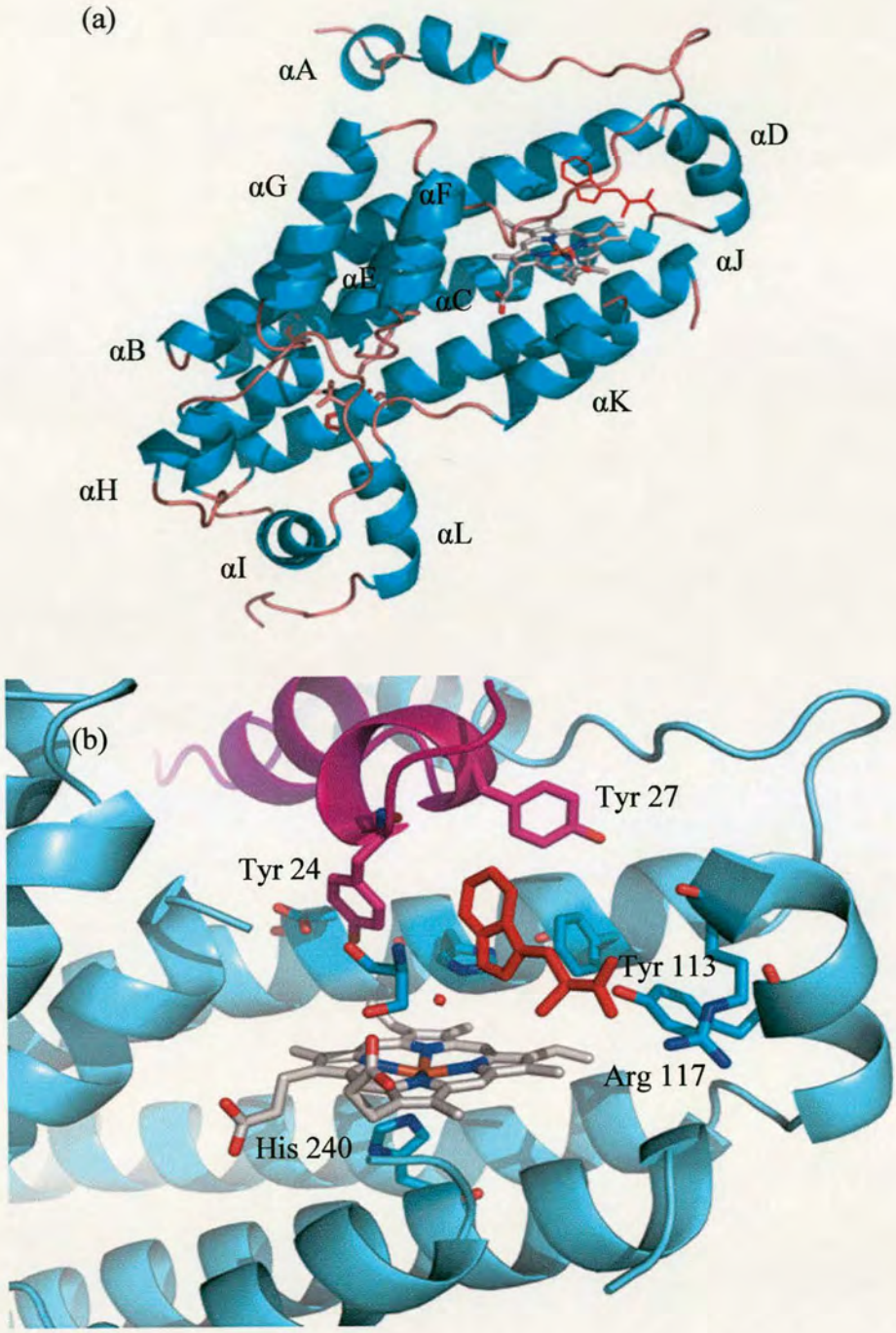

Figure 1.13 (a) A monomer of xcTDO with all the helixes labelled. Helices are displayed in cyan and loop and joints in pink, (b) active-site and heme environment of xcTDO, one monomer is shown in cyan and the N-terminal arm of the adjacent monomer is shown in magenta. Key residues involved in the active site have been shown as stick models.

Active-site Structure

Figure 1.13(b) shows the active site of TDO in the reduced, L-Trp-bound form, displaying the heme environment. The proximal site of the heme porphyrin is occupied by a histidine residue (His 240), whilst the distal heme pocket comprises residues from both monomeric TDO and the N-terminal arm of its partner subunit. The distal site is the substrate binding pocket where the sixth coordination site of the iron is empty.

The active-site has a preponderance of hydrophobic residues, such as Phe 51, Tyr24 and Tyr 27, creating a "greasy pocket", similar to that found in globins that encourage hydrophobic substrate binding (3). Interactions of the substrate with the active site can be split into two categories – interactions with the carboxylate and ammonium groups of L-Trp, and those with the indole ring system.

The interactions of the substrate carboxylate and ammonium groups include an electrostatic interaction between the side chain of Arg117 and the substrate carboxylate group, which is also hydrogen-bonded to the phenolic group of Tyr113 and the main chain amide group of Thr254. This carboxylate-binding motif appears to be essential for substrate binding; arginine reorientates in the presence of substrate, coordinating the carboxylate group of L-Trp, with "open" and "closed" conformations observed (Figures 1.14 (a) and (b)). The closed conformation is only observed in TDO crystals grown in the presence of tryptophan (Figure 1.14(b)), although no L-Trp is bound to rmTDO (This absence is probably due to a low affinity of L-Trp binding to oxidised rmTDO, similar to that observed for xcTDO (K_d, Fe^{3+} = 3.8 mM), whilst only 1mM L-Trp was present in the crystallization solution (88)).

The substrate ammonium group is hydrogen-bonded to the side chain hydroxyl group of Thr254, the 7-propionate group of the heme, and a water molecule. Thr254 is involved in binding both the ammonium and carboxylate moieties of L-Trp and is part of a flexible loop (comprising residues 250-260 of xcTDO) located just outside the active-site. This loop is only ordered in the structures grown in the presence of L-

Trp (xcTDO and rmTDO), because substrate binding appears to induce ordering. In the absence of L-Trp this loop region is also disordered in the TDO structure.
In xcTDO the substrate indole ring binds into a hydrophobic pocket, interacting with the side chain of Phe51 and several other hydrophobic residues, including Tyr24 and 27 from the adjacent monomer, anchoring the indole ring of tryptophan in the active-site. This extensive network of enzyme-substrate interactions serves to stabilise the active site and control substrate binding and catalysis.

Secondary Allosteric Binding Site

In the crystal structure of L-Trp-bound xcTDO in the ferrous state there is a second L-Trp binding site in the tetramer interface, and this is shown in Figures 1.15(a) and (b). It would appear that this is a specific interaction with L-Trp, and in light of reports of allosteric activation of TDO by L-Trp it is possible that this site represents an allosteric effector site. This site is not occupied in the 6-F-Trp complex, possibly because of the lower concentration of the substrate in the crystallization solution.

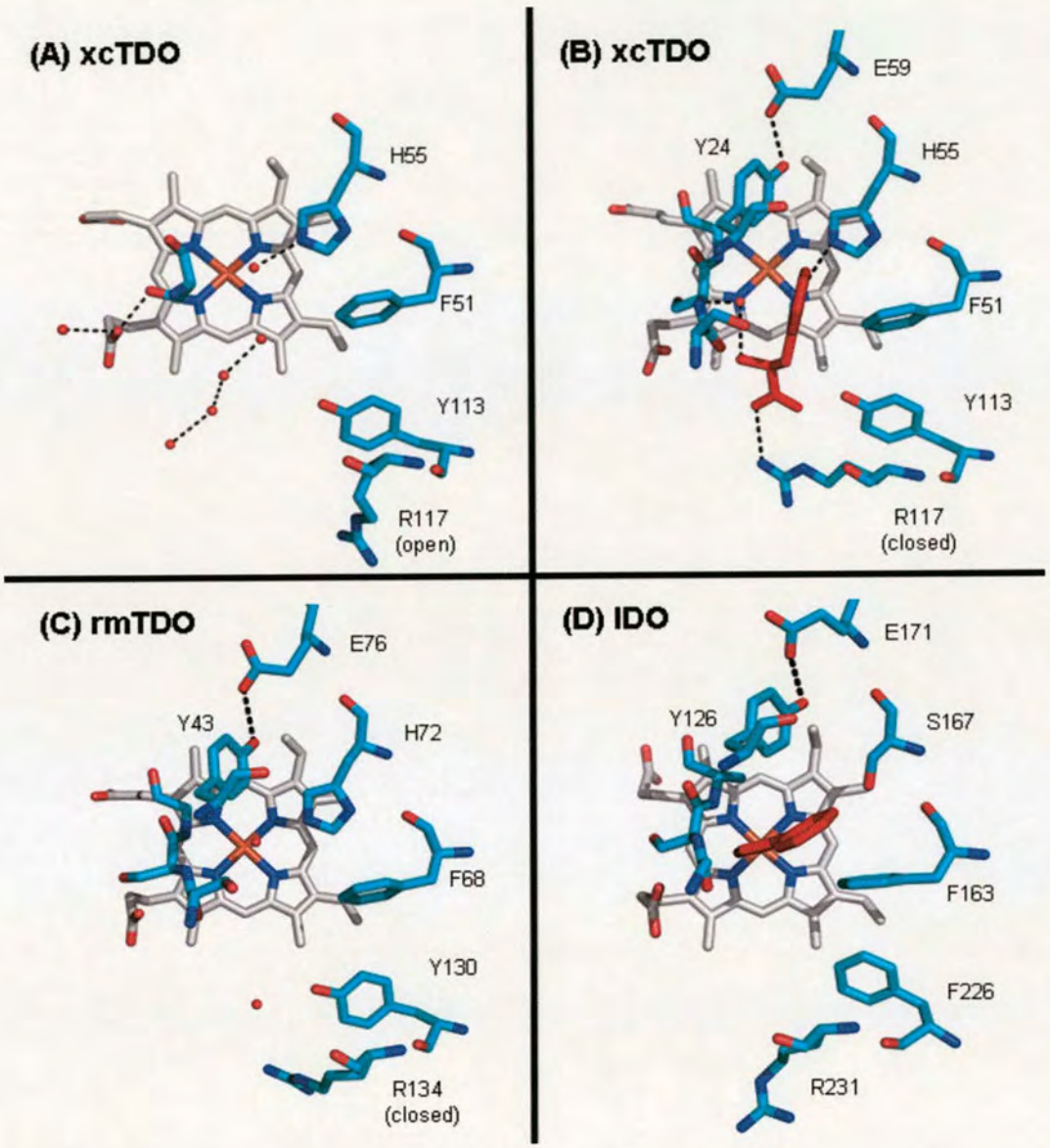

Figure 1.14 Active site stick structures of (a) ferric, substrate free xcTDO, (b) ferrous, substrate bound xcTDO, (c) ferric, substrate free rmTDO, (d) ferric, PI-bound hIDO. The heme porphyrin is shown in grey, and tryptophan and PI are shown in red.

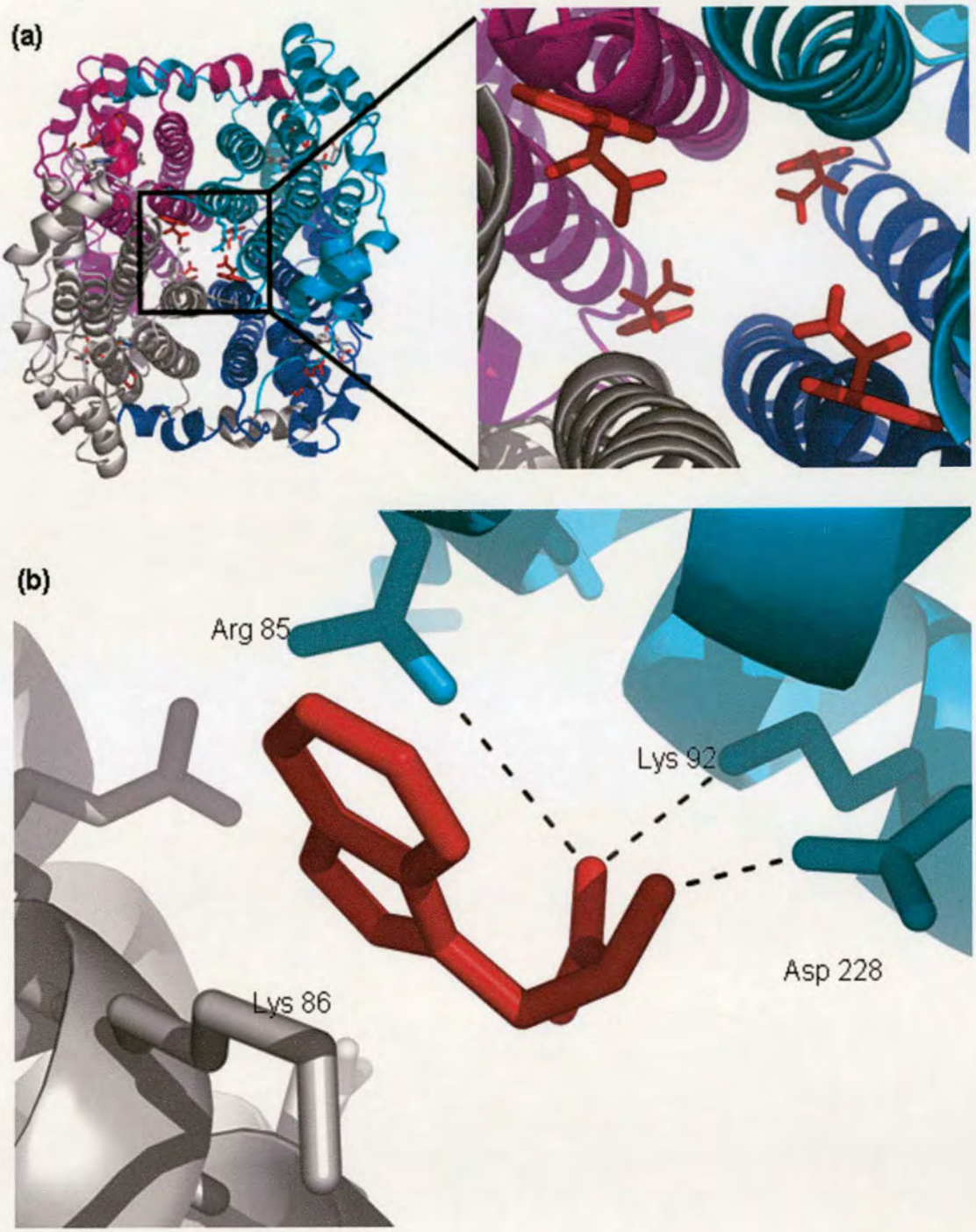

Figure 1.15 (a) Interfacial binding of four additional L-Trp molecules to xcTDO, (b) specific interactions at the interfacial binding site, L-Trp is bound diagonally across the tetramer, interacting with two monomers in separate "dimers".

1.7.2 IDO

The first crystal structure of a member of the heme dioxygenase family to be published was that of eukaryotic IDO by Sugimoto *et al* (87), in complex with 4-phenylimidazole (PI), a known inhibitor and heme ligand, and with cyanide (CN^-) (Table 1.1). The PI bound enzyme structure of IDO is shown in Figure 1.16 and shows that hIDO is a monomeric protein, with the structure divided into two distinct domains, a large (C-Terminal) domain and a small (N-Terminal) capping domain. Inter-domain contact is extensive, with a buried surface area of 3100 $Å^2$, and the two domains are linked by a long loop, comprising residues 250-267. The larger domain is completely helical, with thirteen α-helices and two 3_{10} helices, and belongs to the family of IDO-like protein folds, while the smaller N-terminal domain consists of six α-helices, two short β-strands, and three 3_{10} helices, and displays some similarity to the C-terminal domain of glutathione S-transferase. The larger domain is essentially topologically identical to a protomer of tetrameric TDO, and the structures readily super imposable (Figure 1.16). The heme-binding pocket of hIDO is located mainly within the larger domain, close to the domain interface buried within the protein architecture. The loop region connecting the two domains lies above the distal face of the heme, providing part of the binding cavity. In the IDO structures, residues comprising a flexible loop (of a similar length to that resolved in the TDO structure) just outside the heme pocket have not been fully resolved crystallographically. It is thought that this flexible loop may play a role in substrate binding like that in TDO, and substrate binding may aid its resolution crystallographically.

Active-site

In contrast to TDO, the structure of IDO is not available with any substrate bound, but has been solved with the inhibitor PI at the active site. This model shows PI binds to the heme iron as expected, but does not yield any information regarding the mode of substrate binding in IDO. Figure 1.14 (d) shows the active site of IDO in the PI-

bound form, displaying the heme environment with the proximal site of the heme porphyrin occupied by a histidine residue (His 346). The heme pocket is formed by residues from the small domain (Tyr126, Cys129) and from the large domain (Phe163, Phe164, Phe226, Arg231, Ser263, Gly261 and Gly262) and has a preponderance of hydrophobic residues.

1.7.3 Comparison of IDO and TDO

With the exception of the smaller N-terminal domain of IDO, the structures of IDO and TDO are very similar. Indeed, in comparing 201 structurally equivalent Cα atoms between xcTDO and the large domain of hIDO the root mean square difference is only 3.1 Å (Figure 1.16). The above-mentioned 'dimeric' arrangement in TDO, which involves the N-terminal region of one monomer comprising part of the substrate-binding site in the adjacent monomer, is clearly not possible in monomeric IDO. However, the two tyrosine residues in TDO that are proposed to be important in this arrangement, Tyr24 and Tyr27, are in equivalent positions to Tyr126 and Cys129 in IDO. These tyrosine residues all hydrogen-bond to glutamate residues, and this tyrosine / glutamate motif is conserved in most TDO and IDO species, linking either the N-terminal loop of the adjacent monomer to the active site in TDO, or between the capping and larger domains in IDO (Figure 1.16 and 1.17).
However, in addition to these similarities, it should be noted that the equivalent region in IDO of the loop comprising residues 250–260 of TDO is disordered in the IDO structure. This region is particularly important in TDO because it includes Thr254 that, as mentioned above, is involved in binding the ammonium and carboxylate moieties of L-Trp. In the absence of L-Trp this loop region is disordered in the TDO structure, and substrate binding is required to induce its ordering. This may also be the case for IDO, but the possibility exists that there is no equivalent interaction between IDO and L-Trp.

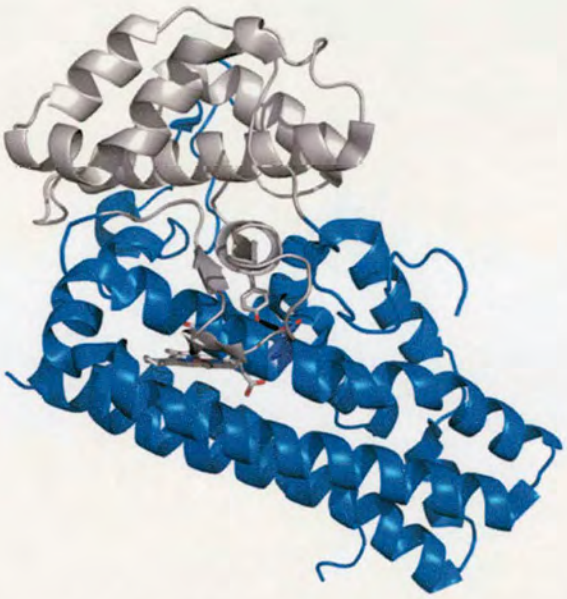

Figure 1.16 Homo sapiens IDO in the ferric, PI bound state. The smaller C-terminal capping domain is shown in grey, and the larger N-terminal domain in blue. The heme porphyrin is shown in grey and Try 126 is shown as sticks, linking the capping domain to the active site.

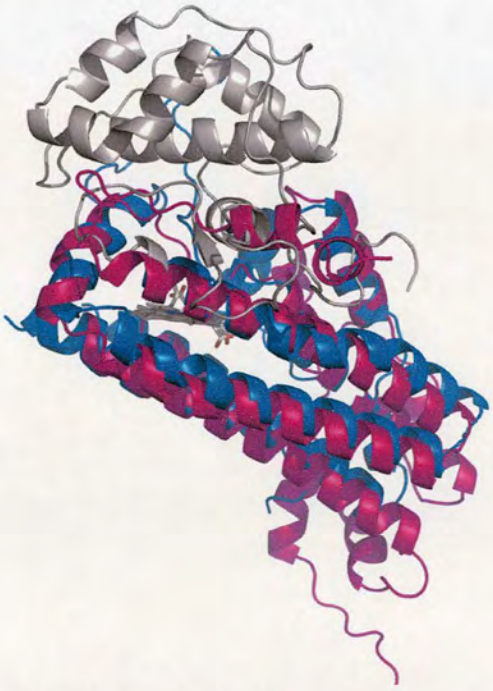

Figure 1.17 TDO and IDO overlaid. IDO is shown in grey and blue as in whilst monomeric TDO is shown in magenta.

In contrast to TDO, the structure of IDO is not available with any substrate bound, but has been solved with the inhibitor PI at the active site. Currently, the only structures available with substrate bound at the active site are of xcTDO or PrnB (6). Since PrnB has no proven dioxygenase ability in its purified form little information therefore exists on the mode of substrate binding in the heme dioxygenase family. Given the similarity between the active sites of TDO and IDO, it is perhaps reasonable to assume a similar substrate-binding mode in the active-site.

In a comparison of the active-sites of TDO and IDO it can be seen that many residues are equivalent to each other - Arg117 in TDO to Arg231 in IDO, Phe51 in TDO to Phe163 in IDO, and Tyr24 in TDO to Tyr126 in IDO. Similarly, the position occupied by Tyr113 in TDO is taken by the similar amino-acid Phe226 in IDO.

Perhaps the most obvious difference between the active sites of the two enzymes is the presence of His55 in xcTDO and its equivalent Ser167 in hIDO. In TDO, the histidine side chain is hydrogen bonded with the indole nitrogen atom of L-Trp, and the role of His55 would appear to be for regulating substrate binding. The role of Ser167 in IDO is less clear in the absence of a substrate-bound crystal structure, but it is unlikely that this residue plays any crucial role in IDO.

Residues equivalent to xcTDO Arg117 and Tyr113 are found in all TDO and IDO enzymes, although tyrosine 113 is replaced by phenylalanine in approximately 50% of IDO species. As discussed above, this carboxylate-binding motif appears to be essential for substrate binding; arginine reorientates in the presence of substrate, interacting with the carboxylate group of L-Trp, with "open" and "closed" conformations observed (Figures 1.14 (a), (b), and(c)).

Table 1.2 Active-site bond distances

Enzyme	Atoms	Distance (Å)
xcTDO	H240 – Fe	2.3 ± 0.2
	Fe – Water 1	3.5 ± 0.2
	Water 1 – G125 amide N	2.8 ± 0.2
	Water 1 – L-Trp α-amino N	3.0 ± 0.2
	Water 1 – L-Trp indole N	3.3 ± 0.2
	H55 – L-Trp indole N	2.6 ± 0.2
rmTDO[α]	H257-Fe	2.2 ± 0.3
hIDO	H346 – Fe	2.1 ± 0.3
	Fe – 4-PI	2.1 ± 0.3

1.8 Allostery

Allosteric regulation is the ability of an effector molecule to influence binding at an allosteric site, and relates to enzymes containing one or more binding sites. Effectors which enhance the proteins activity or binding capabilities are known as allosteric activators, and those which decrease these properties are known as allosteric inhibitors. Allosteric regulation is often used in biological systems to regulate substrate concentrations in metabolic pathways, or to transport molecules around the body (91, 92).

Cooperativity can be displayed only by enzymes with multiple binding sites. Cooperativity refers to the binding of substrate or an effector at one active site influencing the binding at another or all other binding sites. Confusingly this can also be referred to as allostery, and literature on this subject appears to use the two terms almost interchangeably. For example, the most commonly known allosteric protein is hemoglobin, and hemoglobin is commonly used in textbooks to describe basic concepts of allostery and cooperativity (93, 94).

Cooperativity in binding of substrate or molecules to a protein is diagnostic of the protein's interaction between binding sites- the binding of one molecule at a binding site affects the binding of others. A sigmoidal binding curve (dissociation or association) for a substrate is seen, which is analysed by the Hill equation (95). The Hill equation gives n, the Hill constant, which increases with the degree of cooperativity of a reaction. This provides a simplistic characterisation of ligand binding: if n=1, the reaction is non-cooperative and equal to Michaelis-Menton kinetics, when n >1, positive cooperativity is observed, where effector ligand binding increases the affinity of the protein for further reaction or ligand binding. The maximal value of n is equal to the number of ligand binding sites accessible. Negative cooperativity is displayed when n < 1, where effector ligand binding decreases the affinity of the enzyme to further reaction or binding.

Previous studies of TDO have indicated some degree of cooperativity in its binding of substrates (96, 97) and the recent crystal structure of xcTDO showed the specific binding of four L-Trp residues in the interface of the tetramer (1). These additional binding sites raise the possibility that these may be allosteric effector sites, where binding of substrate changes the conformation of the protein, affecting the binding of further molecules at the active site (which is the "allosteric site" described above).

For TDO there is an apparent activation towards binding of diatomic ligands, such as oxygen, cyanide, nitric oxide and carbon monoxide at the active site, in the presence of L-Trp, tryptamine and 5-hydroxy-L-tryptophan (4, 96, 98, 99), as evidenced by dramatically decreased K_d values. In addition there is an increased affinity for oxygen in the presence of α-methyl-tryptophan, a substrate analogue that is neither a substrate nor an inhibitor of enzyme activity (96). This is strong evidence that substrate binding alters the conformation of the protein, although it is unknown if this allosteric activation is occurring within one monomer, with binding at the active site or the effector site influencing binding in each monomer separately, or if it is a more global, cooperative activation between active sites and effector sites in different monomers of the protein.

The reaction velocity of allosteric enzymes can be regulated by small changes in substrate concentration and often regulate metabolic pathways where the substrate concentration fluctuates over a narrow range. It is possible that TDO may play such a "housekeeping" role, regulating the tryptophan concentration and keeping it within certain parameters (38).

1.9 Spectroscopy of TDO and IDO

Electron paramagnetic resonance (EPR), resonance Raman, magnetic circular dicroism (MCD), and nuclear magnetic resonance (NMR) spectroscopies have been used to characterize this family of proteins, and the results of these studies are discussed below. EPR data of the substrate-free and L-Trp-bound forms of IDO and TDO, in the ferric state, are shown in Table 1.3.

1.9.1 Spectroscopic Investigations of TDO

The heme environment of TDO is well characterised due to the availability of crystal structures with and without the presence of L-Trp in the active-site (bond distances are shown in Table 1.2). EPR experiments on human, rat liver and *Pseudomonas* TDOs in the ferric state have shown the presence of two distinct species in solution, a high-spin form and a low-spin form (77, 96, 100). At acidic pH only the high-spin state has been reported and on increasing the pH a transition to a mixed-spin state occurs, containing a mixture of the two forms. The spin state of the alkaline form of ferric TDO is temperature-dependent, and the proportion of high spin species increases with elevating temperature. Histidine occupies the axial coordination position to the heme iron, whilst sixth ligand in the high-spin species is postulated to be a water molecule whilst that of the low-spin species is postulated to be hydroxide (77). This is possible for substrate-free TDO since a histidine residue is present in the active site to deprotonate a bound water molecule that is present in the *X.campestris* substrate free active site (1). This is in contrast to IDO where no equivalent residue is available, but data so far are inconclusive.

EPR data on rat liver and *Pseudomonas* enzymes show that addition of L-Trp to the ferric enzyme causes an increase in the low-spin component at neutral pH, with a decrease in the high-spin component (96, 100). MCD studies have suggested that this high spin component may be distinct from that observed in the substrate-free enzyme, but little data are available for analysis at present (101). The spectral

changes indicate that L-Trp binding to the ferric protein causes increased deprotonation of the heme bound water. L-Trp binding to the ferric enzyme also significantly modifies the pH of the spin state transition, decreasing the pH at which this transition occurs by about 1.6 units. This substrate-induced shift could be caused by the bound L-Trp deprotonating the bound water molecule, as in IDO, rather than the active site histidine. Deprotonation of the water by the indole nitrogen is possible, since the bond distance is 3.3 Å (Table 1.2).

Contrary to the data on the prokaryotic TDO, recent EPR analysis has shown that addition of L-Trp to human TDO causes the creation of an additional low-spin species (Table 1.3) (77). The high-spin and two low-spin species observed have similar g-values to those of human IDO under analogous conditions, and they are proposed to have similar ligands in their distal position (78, 102). This result is clearly different to that of the prokaryotic TDO species studied, and poses many questions as to the differences in the heme environment and substrate binding interactions between TDO enzymes from different species and between IDO and TDO.

1.9.2 Spectroscopic Characterization of IDO

UV/Visible, EPR and MCD spectra of ferric human IDO show the presence of two distinct species in solution, high- and low-spin heme, in approximately equal population at pH 6 (77, 101-103). The two species are shown to be in equilibrium, and on increasing the pH there is an increase in the low spin component, with a concomitant decrease in the high spin component. Histidine is the proximal ligand to the heme iron in both species, with a nitrogen-iron bond distance of 2.1 Å (87). The high-spin species is confirmed by MCD and resonance Raman spectroscopy as arising from water ligation in the distal position. The identity of the sixth ligand in the low-spin species is thought to be an as yet unidentified nitrogenous ligand, as there is not an available nitrogen ligand in the active-site (102). The spectra are

shown to be pH independent – indicating that no ionisable residue affects binding, and there is no formation of hydroxide bound heme whilst substrate is absent.

In the presence of L-Trp at pH 8 MCD and EPR confirm that there are three distinct species in solution, one of which is high-spin and the other two are low-spin (102). The sixth heme ligand for the additional low-spin species is hydroxide, and this is the predominant species in solution. The bound L-Trp provides a hydrogen-bond acceptor to stabilize deprotonation of the bound water molecule. Ferric substrate-free human IDO does not form a hydroxide-bound species because IDO lacks a hydrogen-bond acceptor to facilitate deprotonation of the bound water molecule. In contrast, for the ferric substrate-bound enzyme, the spectra are pH dependent due to an ionisable interaction affecting the formation of the hydroxide species in the active site. L-Trp is thought to act as a proton acceptor, deprotonating the bound water molecule and forming the hydroxide bound species and this is supported by resonance Raman studies (104, 105). The relation of these studies and those above to the active site structure is currently limited by the lack of a substrate bound crystal structure.

Resonance Raman spectra of CO and NO binding to ferric, L-Trp bound human TDO (104) and human IDO (105, 106) enzymes suggests that in TDO the C2-C3 double bond of the tryptophan ring faces the distal diatomic ligand of the heme. This is in contrast to IDO, where the indole nitrogen appears to hydrogen-bond with the diatomic heme ligand.

Table 1.3 EPR identification of all species observed in the absence or presence of L-Trp for TDO and IDO

Enzyme	Species	g-value
H. sapiens TDO (77)	High spin	5.71 and 2.01
	Low spin	2.89, 2.30 and 1.62
	Low spin [α]	2.63, 2.20 and 1.84
P. acidovorans TDO (96) [γ]	High spin	5.8
	Low spin [α]	3.67, 2.20 and 1.80
H. sapiens IDO (102)	High spin (H_2O)	5.96 and 1.99
	Low spin (N)	2.94, 2.25 and 1.50
	Low spin (OH)[α]	2.52 2.19 and 1.86

([α] Only observed in the presence of L-Trp, [γ] Similar data are observed in the study by Brady et al (107)).

1.10 Objectives

At the beginning of this PhD, a very limited understanding of the molecular details of tryptophan oxidation existed, since there was no published structure for TDO. The nature of substrate and dioxygen binding to the enzymes were unclear and little biochemical data on substrate binding, redox states or reaction intermediates existed. Detailed information on the mechanism of L-Trp oxidation by TDO and IDO, and its control at the molecular level needs to be determined and the ultimate aim is the complete description of the mechanism of TDO. The catalytic mechanisms employed by TDO and IDO have not yet been fully elucidated although a number of mechanisms for tryptophan dioxygenation have been proposed. In this study we attempt to resolve the question of whether an active site base is necessary for catalytic activity, utilising a TDO from *Xanthomonas campestris* (xcTDO). *Xanthomonas campestris* is a pathogenic gram-negative aerobic bacterium that infects plants, such as the crucifers Brassica and Arabidopsis (108, 109). *Xanthomonas campestris* TDO shares 34% sequence identity with human TDO, making it a good model for investigating TDOs biochemical properties (Figure 1.2).

To this end, the bacterial xcTDO was isolated and was characterised using a range of biochemical, potentiometric and structural techniques. To achieve this, firstly, an efficient bacterial expression system was designed and implemented to provide useful quantities of pure protein.

Secondly, structural studies provided information on the enzyme structure, revealing the substrate binding interactions of the active site and allowing the construction of active-site mutants based on these critical residues. Biochemical and potentiometric characterisation of the wild-type enzymes and its variants has provided insight into binding characteristics and oxidation state of the enzyme in the catalytically active form. From this mechanistic conclusions have been formed and provide insight into the mechanism of TDO.

Chapter 2

Materials and Methods

2.1 Molecular biology and Mutagenesis

A full-length *Xanthomonas campestris* TDO (*xc*TDO) construct was created at the centre for Advanced Biotechnology and Medicine (Northeast Structural Genomics Consortium), Rutgers University, Piscataway, NJ 08854. The expression plasmid was produced by cloning full-length *xc*TDO (Q8PDA8_XANCP, NESG ID XcR13) into a pET21d (Novagen) derivative, generating the plasmid pXcR13-21.3, with a C-terminal hexa-histidine tag. The full length amino-acid sequence for *xc*TDO is shown in Appendix C. The resulting XcR13 contains eight non-cleavable, non-native residues at its C terminus to allow efficient purification. BL21(DE3) pMGK cells were used for initial colony identification, as they allow efficient plasmid transformation, and the plasmid was then extracted using a Qiagen QIAprep® Spin Miniprep Kit. The extracted plasmid was then transformed and expressed using the One Shot® BL21(DE3) (Invitrogen), *E. coli* expression system, which produces high levels of xcTDO protein expression.

The point mutation of histidine 55 to alanine (H55A) was created by Rong Xiao and Li Zhao at the Centre for Advance Biotechnology and Medicine, Rutgers University, Piscataway, NJ 08854, whilst the point mutation histidine 55 to serine (H55S) was created in our laboratory. In both cases point mutations were created by employing the QuikChange II sitedirected mutagenesis kit (Stratagene, La Jolla, CA). DNA polymerases require a short sequence of single stranded DNA called a primer, which can bind to the wild type-sequence at the location where the mutation is to be introduced. The oligonucleotide primers directing the mutation were designed in an automated fashion by using the Primer Prim'er program, www.nmr.cabm.rutgers.edu/bioinformatics/Primer_Primer/ and the primers designed are displayed in Appendix C. All mutations and their associated open reading frames

were verified by DNA sequence analysis the Edinburgh University SSBS sequencing lab. Mutated plasmids were extracted and expressed in the same manner as wild-type TDO, using the One Shot® BL21(DE3) Invitrogen, *E. coli* expression system. Bacterial strains expressing TDO and its mutant forms were stored long term as dimethyl sulfoxide (DMSO) stocks (923 µl starter culture, 77 µl DMSO) at –80 °C.

2.2 Growth and Expression

Wild-type TDO and its mutants H55A and H55S were all expressed and purified in the same way. Bacterial cultures were grown in Luria Bertani broth (LB), previously sterilised at 121 °C for 20 minutes in a Kestral autoclave (Table D.1, Appendix D). All solutions were prepared with Millipore Q Ultrapure water. Agar plates were prepared with sterilised LB/agar solution and allowed to cool prior to solidification in sterile Petri dishes with ampicillin (Table D.1, Appendix D).

Starter cultures for large scale growth were prepared by inoculating 20 ml of sterile media with DMSO stock via a sterile pipette tip and incubated for 24 hours at 37 °C, 225 rpm in a Gallenkamp shaker. Growth flasks (1 l flasks containing 400 ml LB broth) were inoculated with 1ml of starter culture and 500 µl of 25 mM ampicillin and grown for 12 hours at 37 °C and 150 rpm. Protein production was then induced with isopropyl-β-D-thiogalactopyranoside (IPTG) at a final concentration of 250 mg l^{-1} and 1 ml of 7 mM hemin solution added to encourage heme incorporation into the protein. The temperature was also decreased to 30 °C and left for a further 12 hours at 150 rpm until the cells were harvested by centrifugation (10 minutes at 8000 rpm) using a Sorvall RC-5B refrigerated centrifuge at 4 °C. The resulting cell pellets were either lysed and purified immediately (as described below) or stored at –20 °C until required.

2.3 Enzyme Extraction and Purification

2.3.1 Cell Lysis

All buffers used in purification of the enzymes are described in Table D.2, Appendix D. The harvested cells were re-suspended in buffer A (5 ml of buffer per gram of cell culture) and cell lysis was initiated by incubating the cell suspension with egg white lysosyme (1mg per ml of suspension) for 30 minutes with phenylmethylsulfonyl fluoride present (1 mg per ml of suspension) in order to inhibit proteolytic enzymes present. Lysis was completed by ultrasonication of the suspension, (20 second bursts at 10 microns amplitude, Sanyo soniprep 150). This was performed on ice, resting for 1 minute and stirring between bursts in order to minimise overheating and protease activity, and was complete when the viscosity of the lysed material decreased. Cell debris was then removed via ultracentrifugation, 1 hour at 20,000 rpm, 4 °C, and the supernatant collected.

2.3.2 Chromatographic Purification

Purification of the protein was achieved using column chromatography – the His-tagged protein can be separated from the cell supernatant by specific, reversible, binding of the His tag to a nickel agarose (Ni-NTA) gel column (Qiagen). Selective binding of the protein to the resin allows impurities to be washed off and the subsequent elution of the protein provides purified material. All purification steps were performed in a cold room at 4 °C and purification buffers are described in Appendix D.

A Ni-Agarose column containing 20 ml Ni-Agarose resin solution (Qiagen) was suspended in a minimal amount of buffer A and packed to form a column 6×2 cm in dimensions. The column was washed with buffer A and the supernatant was loaded onto the column where it bound strongly to form a tight red band. The column was then washed with a further two column volumes of buffer A to remove supernatant and any unbound proteins. It was further washed with four column volumes of buffer

B, then four column volumes of buffer C to remove further protein impurities. Elution was achieved using a minimal amount of buffer D, with the dark red protein fraction collected and subsequently concentrated by centrifugation using a FALCON 6-300 centrifuge and Amicron Centriprep concentrators with a membrane cut-off of 30 kDa at 2500 rpm for 1 hour until there was ~5 ml of protein solution.

G-25 sephadex resin was suspended in a minimum amount of buffer E and packed to form a column 2×15 cm in dimensions. The column was equilibrated with 5 column volumes of buffer E, and the 5 ml of protein loaded onto the column. When all the protein was loaded, buffer E was passed down the column and the dark red imidazole free protein was collected and concentrated by centrifugation at 2500 rpm as before, until the required concentration was achieved (typical protein concentrations were 0.5-1.5 mM but the protein can be concentrated to ~5 mM before precipitation occurs). Aliquots of 200 µl purified and concentrated protein were flash frozen in cryovials using liquid nitrogen and stored at –80 °C until required.

2.4 Purity Determination

2.4.1 SDS-PAGE analysis

SDS-PAGE (Sodium Dodecyl Sulfate Polyacrylamide Gel Electrophoresis) was used to verify the purity of the protein, and monitor the degree of purification. SDS-PAGE shows the different proteins present in a sample over a fixed range and can therefore be used to verify the purity of a protein sample.

2.4.2 Gel Loading and Electrophoresis

Samples for gel electrophoresis were loaded onto a gel and a potential difference applied causing a migration of proteins through the gel. The distance travelled is determined by their effective mass, which is then estimated according to how far they migrate compared to a known set of standards.

Samples were prepared by placing 75 µl distilled water, 25 µl SDS sample buffer (Invitrogen) and 1 µl protein in an eppendorf tube and boiling the sample for 3 minutes to denature the polypeptide chain.

Pre-poured 4–12 % Bis-Tris gels (Invitrogen) were used and prepared by washing with distilled water before use. Prepared protein samples were loaded into the wells at the top of the gel, including one lane of pre-prepared marker samples (typically 5 µL molecular marker (Seeblue Plus 2, Invitrogen). The gel was placed in a gel tank filled with running buffer. A voltage of 150 V, (120 mA, 60 W for ~ 1 hour) was applied, until the dye front reached the foot of the gel. The gel was removed from the tank and stained for both heme and total protein content. The gel buffers are outlined in Table D.3, and a representative gel is shown in Figure 2.1.

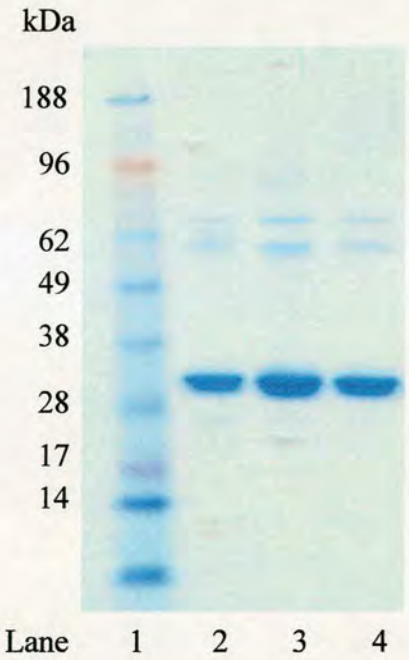

Figure 2.1: Coomassie stained SDS-PAGE analysis of TDO. Lane 1 is a molecular weight marker lane, with weights indicated to the left hand side. Invitrogen SeeBlue® Plus 2 marker system was used. Lane 2 shows purified wild-type TDO (wtTDO), Lane 3 shows purified H55A and lane 4 shows purified H55S.

2.4.3 Coomassie Staining

Coomassie stain can be used to detect the presence of any polypeptide in the samples run by staining them blue. Coomassie stain was applied to each gel for 15 minutes, before removal. The gel was then immersed in a destaining solution for several hours. An example is shown in Figure 2.1. Coomassie blue can be used on gels previously stained for heme presence, in order to assess polypeptide content.

2.4.4 Heme Staining

As *c*-type cytochromes are covalently bound to the protein backbone, they are not lost during denaturation of the protein by boiling. As a result, any *c*-type cytochromes present in the protein sample can be stained by a hydrogen peroxide / , 3', 5, 5'-Tetramethylbenzidine stain. In addition, some proteins containing *b*-type heme porphyrins can be analysed via this method. An enzyme containing *b*-type heme or hemes may sometimes still retain contact with the porphyrin after denaturation by boiling.

The gel was equilibrated in the heme stain equilibration buffer as shown in Table D.3. After 30 minutes, a small quantity of 3, 3', 5, 5'-Tetramethylbenzidine (10 mg) was added and incubated for 15 minutes in the dark. Hydrogen peroxide was then added, and the colour due to heme presence developed within minutes.

2.4.5 Purity Determination via Spectrophotometric Observation

UV/ Visible spectra were recorded over the range 250-800 nm using a Shimadzu UV-2101PC spectrophotometer and quartz cuvette with a 1 cm path length, and the relative absorbance ratio of the Soret band to the peak at 270 nm was recorded. The absorption at 270 nm is due to the aromatic residues in the protein, and so is indicative of the protein concentration, whilst the peak at 405 nm (the Soret Band) is due to absorbance by the heme groups. For wtTDO and its mutants a ratio of $A_{405}/A_{270} > 2$ is an indication of pure protein.

2.5 Enzyme Concentration Determination

2.5.1 Bradford Assay

Initial protein concentration was determined by employing a Bradford assay (110), using the Bio-Rad (Bradford) Protein Assay Kit with bovine plasma albumin standard. This kit utilises the shift in the absorbance maximum of Coomassie Brilliant Blue G-250 from 465 nm to 595 nm upon protein binding. This method is particularly useful as the extinction coefficient of the dye-albumin complex is constant over a 10-fold concentration range, allowing a large range of proteins to be analysed. Firstly a standard graph is plotted utilising bovine plasma albumin, shown in Figure 2.2, and then samples of the protein of interest are reacted with Coomassie Brilliant Blue G-250, and compared to the standard to calculate the protein concentration. Results are obtained in triplicate and repeated at two different protein concentrations to ensure accuracy.

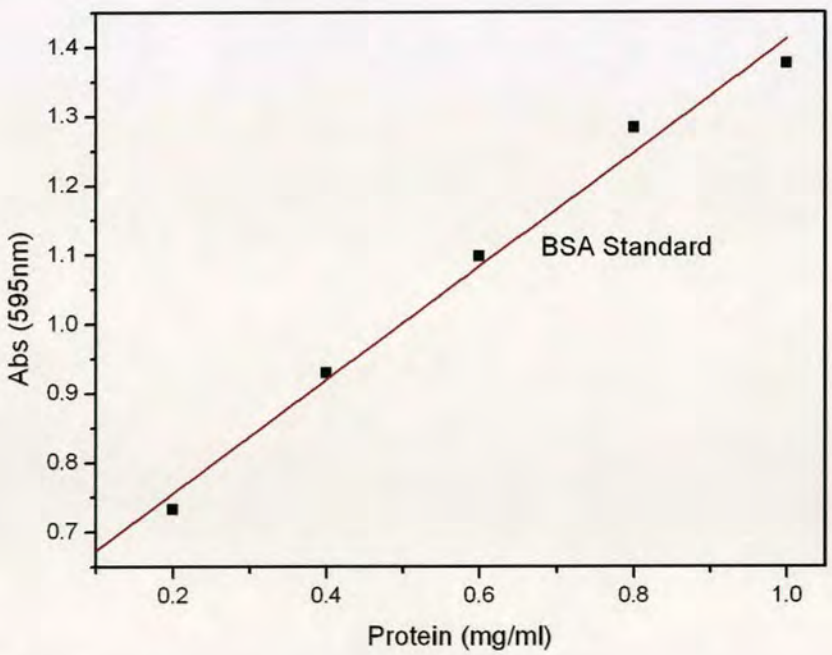

Figure 2.2: Standard graph of bovine plasma albumin concentration against absorbance displaying straight line characteristics

2.5.2 Liquid Chromatography - Mass Spectrometry (LC-MS)

The molecular mass of wt TDO was determined using LC-MS. LC-MS was carried out using a mass spectrometer utilising a Alliance™HT, Waters™ 2795 separations module, Micromass platform and Waters™ 486 Tunable Absorbance Detector. Samples consisted of 10 mM protein in a 0.1 % formic acid solution. Analysis and recording of data was achieved by using MassLynx V4.0 Global Mass-Informatics.

2.5.3 Heme Content Determination

Knowledge of the degree of heme incorporation is crucial to this work. Failure to incorporate heme would result in altered activities and heme content is assessed via the pyridine hemochrome assay (111). In addition, the initial determination of enzyme concentration and the heme extinction coefficient was based on the total heme content, and total protein content, determined by the pyridine hemochromagen assay and Bradford assays (110) respectively.

A solution of TDO (5 μM) was thoroughly mixed with an equal volume of reagent A (Table D.4, Appendix D), followed by the immediate addition of 10 μl of 5 mg per ml $Na_2S_2O_4$ solution. Spectra of the reduced pyridine hemochromagen was recorded over the range 250-800 nm using a Shimadzu UV-2101PC spectrophotometer and quartz cuvette with a 1 cm path length. Heme concentrations were calculated using the difference extinction coefficient $\Delta\varepsilon_{556\text{-}540} = 22.1\ mM^{-1}cm^{-1}$. The appearance of the reduced pyridine hemochromagen was time dependent and so sufficient equilibration was allowed following the addition of dithionite. Each determination was performed in triplicate to ensure accuracy. Comparison of the calculated Bradford assay protein concentration with the heme concentration calculated from the pyridine hemochrome assay gives an indication of heme incorporation. In all cases, heme incorporation was determined to be greater than 90%.

Extinction coefficients at 404nm and 431nm were calculated per protomer for the ferric and ferrous enzymes respectively by comparing the Soret maxima of the ferric

and ferrous enzymes with the corresponding protein concentration determined via the Bradford assay. Calculated extinction coefficients are shown in Table 2.1.

During experimental procedures protein concentration was determined from the absorbance of the ferric (oxidised) Soret band, by applying the Beer-Lambert Law, taking into account the dilution of the protein sample, and using the extinction coefficients outlined in Table 2.1.

Table 2.1 Calculated Extinction Coefficients

Enzyme	E_{405} ($M^{-1}cm^{-1}$)	E_{431} ($M^{-1}cm^{-1}$)
wtTDO	180,500	113,000
H55A	130,400	120,000
H55S	132,000	116,000

2.6 Binding of Exogenous Ligands

Substrate binding titrations give a measure of the affinity that the enzyme has for substrate. The addition of substrate to ferric or ferrous wtTDO and its mutants causes a shift in the Soret peak and this change can be monitored spectrophotometrically as a shift in the absorption spectrum. Dissociation constants (K_d) were determined spectrophotometrically by monitoring the change in absorbance at the appropriate wavelength stimulated by addition of small aliquots of substrate, using Equation 2.1;

$$\Delta Abs = (K_D\, Abs_{initial} + [L]_{tot}\, Abs_{final}) / (K_D + [L]_{tot}) \qquad \text{Equation 2.1}$$

Where $Abs_{initial}$ and Abs_{final} are the initial and final absorbance values, respectively, and $[L]_{tot}$ is the total concentration of the ligand. Absorbance changes upon substrate binding are small (~ 5-10 % of initial peak absorbance) but usually easily quantifiable due to tight substrate binding.

The K_d is a measure of the affinity that the substrate has for the enzyme and is equivalent to the substrate concentration at half the maximum absorbance change. K_d values for binding to ferric and ferrous wtTDO and mutant enzymes were determined in a Belle Technology anaerobic glove box with $[O_2]$ maintained below 5 ppm.

An enzyme concentration of 5 μM was used and aliquots of substrate (0.5-15 μl maximal volume) were added sequentially to the cuvette using a Hamilton® syringe. Where reduced enzyme was required, the stock enzyme solution was reduced by titration with sodium dithionite and excess reductant was removed via gel filtration (BioRad G-25, 10 cm^3 column). Aliquots of concentrated ligand prepared in the same buffer as the enzyme solution were added to the cuvette and the spectra recorded from 250 to 800 nm using a Shimadzu UV-PC 1501 spectrophotometer. Spectra were recorded after each addition of ligand at 25°C, as shown in Figure 2.3. Spectral changes were monitored and difference spectra calculated from ((TDO_{405})-(TDO_{405}+substrate)). Dissociation constants were determined by plotting the maximal absorbance changes calculated from each difference spectrum against the concentration of ligand using Microcal Origin 7.5.

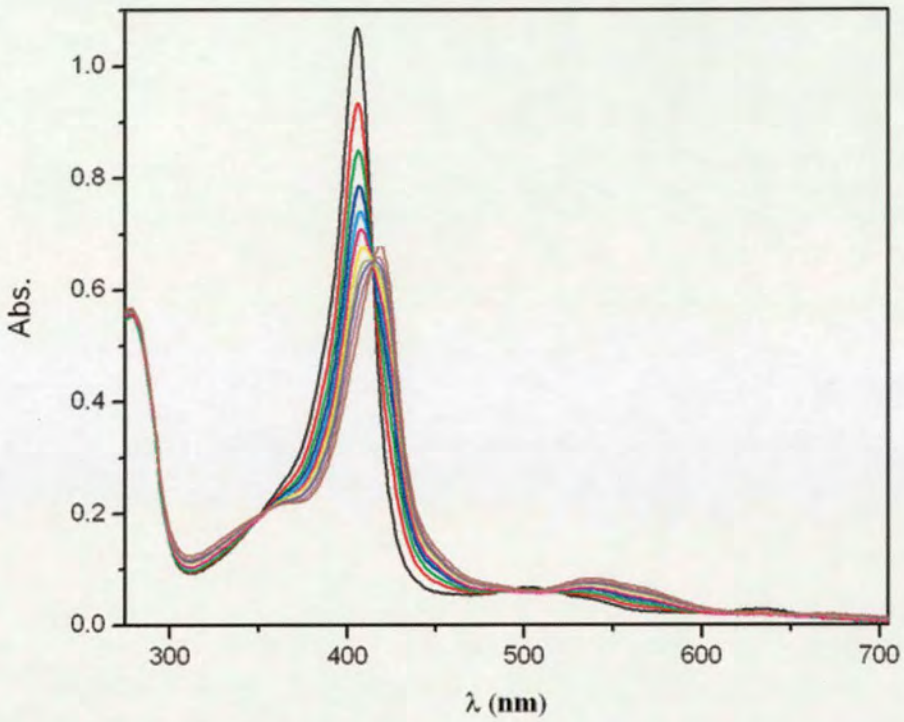

Figure 2.3: Example of the spectral changes observed upon L-Trp binding to ferric wtTDO, on addition of 0.5-30 mM L-Trp to the enzyme. The deviations from ligand free (black) are shown in red through brown, plotted against the wavelength.

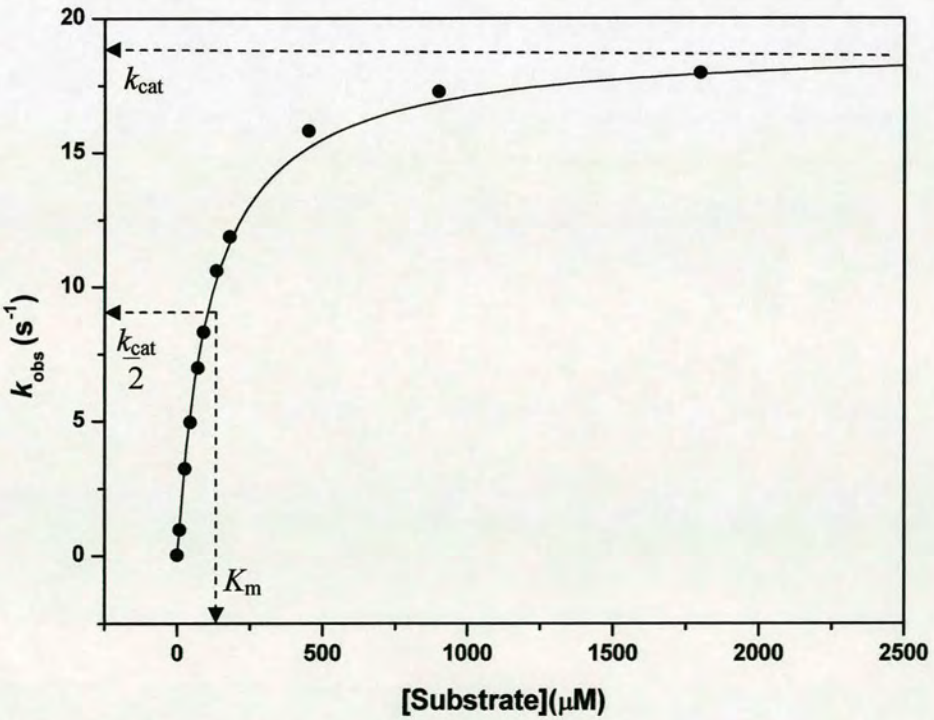

Figure 2.4 Michaelis-Menten plot of substrate concentration against calculated rate of turnover (k_{obs}).

2.7 Steady-State Kinetics

Substrate-dependent steady-state turnover is a quantitative study of enzyme catalysis used to calculate maximal rates of enzymatic turnover. The derivation of the Michaelis-Menten equation and other equations used in this thesis are described in Appendix B. The formation or depletion of one of the components necessary for turnover must be observed over a set time period – observing at a variety of substrate concentrations allows for plotting observed rates against substrate concentration, and from this the rate constant k_{cat} and the Michaelis constant, K_m, calculated.

The rate of formation of N-formylkynurenine was monitored by measuring the change in absorbance at 321 nm (ε_{321} of N-formylkynurenine = 3750 $M^{-1}cm^{-1}$) in a Shimadzu UV-2101PC spectrophotometer and quartz cuvette with a 1 cm path length. Kinetic data were fitted to both the Michaelis-Menten and the Hill equation using Origin software (MicroCal, Northampton, MA). All assays were performed at 25 °C by means of a thermostatically controlled water bath. Assay buffer F was used throughout, with 20 mM ascorbate, 10 μg catalase and 10 μM methylene blue present. Substrate concentration was varied dependent on the substrate of interest, (Table (e), Appendix D) and a known concentration of enzyme, (~50 nM) was added to the cuvette to initiate the reaction. Each measurement was carried out in triplicate. The rate of L-kynurenine production over a range of substrate concentrations was fitted to the Michaelis-Menten equation using Microcal Origin, Figure 2.4.

Weak catalytic activity by ferric IDO and TDO has been reported, but turnover is generally catalyzed by the ferrous protein. Reduction of heme iron is therefore required to facilitate the observation of catalytic activity. Upon reduction, some turnover can be observed in the absence of any electron transfer mediators, but full catalytic activity is not observed without their presence due to uncoupling of the reaction leading to oxidised enzyme production (and subsequent reduction in the catalytic activity). Ascorbate, catalase, and methylene blue are employed in the assay buffer to achieve this. Ascorbate and methylene blue are reducing agents, but also react with dioxygen to form superoxide and peroxide by-products, which can bleach the heme and destroy catalytic activity. Catalase is therefore present to remove any

superoxide or peroxide in solution and hence allows an efficient turnover of substrate.

2.7.2 pH Dependence of Activity

The variation of turnover rate with pH for both wild-type and mutant forms of TDO was determined by measurement of activity at saturating L-Trp concentrations, and over the range pH 6.0 - 8.3, utilising assay buffer F. The profiles obtained were fitted by least squares regression to a single pK_a value using Microcal Origin 7.5.

2.7.3 Determination of Inhibition Constants

There are two main causes of the failure of the Michaelis-Menten equation – substrate inhibition or substrate activation and equations describing different types of inhibition are described in Appendix C.

The effect on L-Trp turnover by wtTDO upon addition of an inhibitory molecule was studied *via* the steady-state method. The steady-state turnover of L-Trp was observed as described in Section 2.7.1, with no inhibitor present in the assay mixture. The assay was then repeated 5 times, with differing amounts of the inhibitor present in solution each time. For the determination of the inhibitory constant for D-Trp, the assay was repeated 6 times with 0, 3300, 6600, 10000, 15000 and 20000 mM D-Trp present in the assay mixture. The data was analysed by plotting 1 / v (the observed rate), against 1 / [L-Trp] using Microcal Origin 7.5.

2.7.4 Preparation of Deuterated Samples for Kinetic Experiments

The effect on turnover rates upon deuteration of the solvent was studied *via* the steady-state assay method. Buffer and substrate solutions were prepared in D_2O as described before but using either DCl or NaOD where appropriate. The pD of the deuterated buffer was corrected according to Equation 2.2 (112, 113);

$$pD = pH + 0.4 \qquad \text{Equation 2.2}$$

The protein solution was prepared in H_2O then concentrated such that the addition of the protonated enzyme solution was less than 0.05 % of the total volume of the assay.

2.8 Stopped-Flow Spectrophotometry

Stopped flow spectrophotometry involves the rapid mixing of two solutions and the immediate monitoring of any spectral changes over the initial reaction period. Mixing occurs within a spectrophotometric cell of fixed path length, and on mixing the instrument records the absorbance of the reacting solution, either at a fixed wavelength or over a specified range. The resolution of the instrument is restricted by its dead-time, a value which is the difference between the point at which the reaction can be traced back to ($t = 0$) and the point at which recording actually begins ($t = dt$). Data is also impaired by the mixing time for the sample of interest. Once the two solutions are entered into the reaction chamber observation will begin, however until mixing is complete the reaction will not proceed at maximum velocity and a lag will be observed. Mixing time is hard to quantify and will depend on the sample of interest and its temperature. These factors make reactions occuring at a rate faster than 1000 s^{-1} hard to quantify using single wavelength analysis. All stopped-flow experiments were conducted using an Applied Photophysics SF.17MV stopped flow spectrophotometer using either a single wavelength or diode array (multiple wavelengths) detector, with a dead time between 0.9-1.1 ms. The stopped-flow equipment was contained in an anaerobic glove box (Belle Technology), maintained under a nitrogen atmosphere ($O_2 < 5$ ppm). Unless otherwise stated, buffer F was used throughout at pH 7.5.

2.8.1 Detection of an Oxyferrous Ternary Species

For detection of the oxyferrous ternary complex, all procedures were conducted within an anaerobic glove box (Belle Technology, $O_2 < 5$ppm) at either 10 °C or 25 °C. Firstly 200 µl of 50 µM enzyme was reduced by addition of sodium dithionite,

and the dithionite was then removed via gel filtration down a G25 pre-packed column (Bio-Rad) equilibrated with buffer F. Reduction was confirmed by UV / Visible spectrometry on a Varian Cary 50 Bio spectrophotometer, also contained within the glove box. Substrates (L-Trp, 6-F-Trp or 5-F-Trp) were prepared in buffer F and concentrations varied according to substrate.

Sample A - 0.8 ml aliquot of reduced enzyme was mixed with 0.2 ml substrate, to yield a sample containing an excess of substrate (at least a 10-fold excess), and this sample was mixed with Sample B - a 1 ml sample of approximately 10 mM O_2 in the spectrophotometer (O_2 concentration was determined prior to mixing). The subsequent reaction was recorded utilising either a diode array detector between 200 and 700 nm (Figure 2.5(a)), or at a specific wavelength (Figure 2.5(b)).

2.8.2 Oxygen Dependence of Turnover

Steady-state kinetic experiments under varying [O_2] rather than [substrate] were performed using the stopped-flow apparatus. The concentration of O_2 present in the assay could be controlled due the sealed environment of the mixing chamber. This experiment allowed the calculation of the oxygen binding affinity (K_m), and the maximum rate of turnover of the enzyme of interest under saturating levels of O_2. All experiments were performed at 25° C in buffer F. The enzyme was reduced with dithionite, and the dithionite removed as described above in Section 2.8.1. Sample A containing 50 nM reduced enzyme and 25 mM L-Trp (a large excess), was then mixed with Sample B, solutions containing various concentrations of O_2 (10 – 2000 μM), in the stopped–flow apparatus. The rate of product formation (L-kynurenine) was measured, and the rate of turnover was calculated as described in Section 2.7. Results were obtained in triplicate, averaged and an error calculated. Parameters relating to the oxygen dependence (K_m of dioxygen, k_{max} and K_i) could be calculated by plotting the O_2 concentration against the apparent rate of turnover, and fitting the data to the Michaelis-Menten equation or the Michaelis-Menten equation corrected for substrate inhibition using Microcal Origin 7.5.

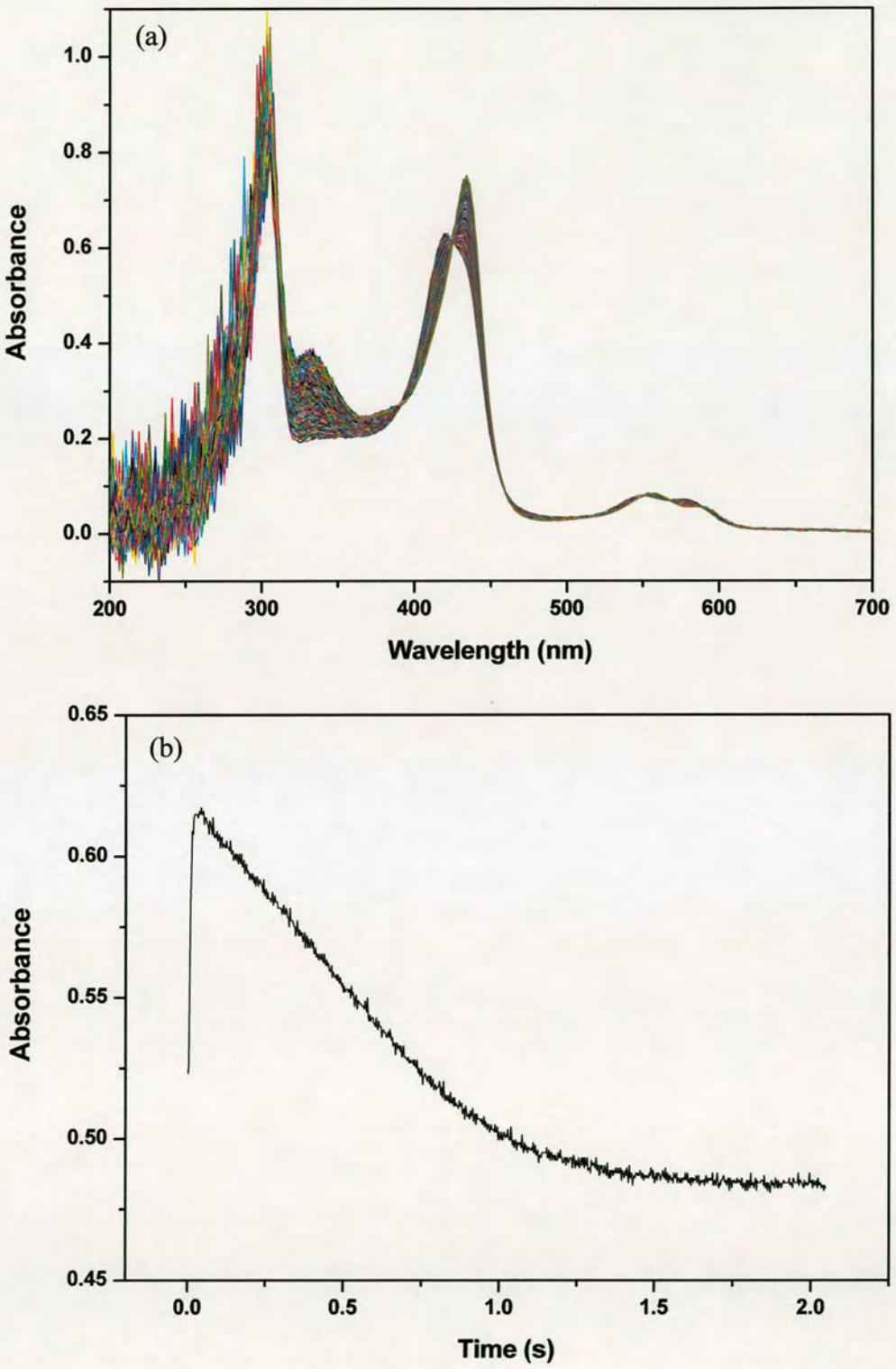

Figure 2.5 (a) Diode array spectra overlaid for formation of an oxyferrous species for wtTDO with L-Trp. (b) Single wavelength detection at 419nm for formation (fast increasing) and decay (slow decreasing) of the oxyferrous ternary species for the same reaction as in (a).

2.8.3 CO Binding Kinetics

CO binding kinetics were performed by varying [CO] and measuring the rate of formation of the Fe^{2+}-CO complex at 420 nm, allowing the calculation of the CO dissociation constant (K_d). CO binding was recorded using the stopped-flow apparatus. The concentration of CO present in the assay could be controlled due the sealed environment of the mixing chamber.

All experiments were performed at 10° C in buffer F. The enzyme was reduced with dithionite, and the dithionite removed as described above in Section 2.7. Sample A containing 50 nM reduced enzyme was then mixed with Sample B, solutions containing various concentrations of CO (100 – 500 mM), in the stopped–flow apparatus. Results were obtained in triplicate, averaged and an error calculated. Parameters relating to the oxygen dependence (K_d of CO, and k_{off}) can be calculated by plotting the CO concentration against the rate of formation and fitting the data to a straight line using Microcal Origin 7.5, where the K_d of CO is equal to minus the x-intercept and k_{off} is equal to the y-intercept.

2.9 Small Molecule Concentration

2.9.1 CO Concentration

CO-saturated buffer solutions were prepared by removing sealed aliquots of buffer F from the anaerobic environment, bubbling with appropriate gas for 5 minutes and returning to the glove box. Aliquots of saturated buffer were removed via a rubber septum using a syringe to ensure the gas concentration remained constant.

CO-saturated buffer CO concentrations were determined spectrophotometrically using the characteristic P450 CO binding technique. UV / visible spectra were recorded over the range 250-800 nm using a Shimadzu UV-2101PC spectrophotometer and quartz cuvette with a 1 cm path length. A protein sample (10 µl protein in 990 µl buffer) was reduced using sodium dithionite and a spectrum recorded. An aliquot of CO saturated buffer (1-5 µL dependent on saturation) was

then added to the cuvette and a second spectrum taken. CO concentrations were determined from the difference spectra (Enzyme-CO)-(Enzyme) at ~ 450 nm, using the Beer-Lambert law with an extinction coefficient of $\varepsilon = 92{,}000\ M^{-1}cm^{-1}$.

2.9.2 NO Solutions

NO-saturated buffer solutions were prepared in the same manner; however determination of NO concentration is difficult and was not necessary during the course of the experiments. Since the typical NO concentration of a NO saturated solution is above 100 μM, an excess of NO (at least 10 times the enzyme concentration) was used in all reactions involving NO in this thesis.

2.9.3 O_2 Concentration Determination

Oxygen concentrations were determined spectrophotometrically by UV/visible spectrophotometry, within an anaerobic glove box. Oxygen-saturated buffer solutions were prepared as for CO, and a separate buffer sample was used for each experiment to ensure O_2 concentrations were uniform. The concentration of oxygen in a prepared solution was checked on an hourly basis to record any small changes.
A solution of reduced methyl viologen (~20 μM) was prepared by electrochemical bulk reduction and the spectrum was recorded. (Methyl viologen concentrations were determined by UV/ visible spectrophotometry over the range 250-800 nm using a shimadzu UV-2101PC spectrophotometer and quartz cuvette with a 1 cm path length, contained within an anaerobic glove box. Absolute concentrations were calculated using the extinction coefficient $\varepsilon_{600} = 13{,}000\ M^{-1}cm^{-1}$. An aliquot (typically 10 μl) of oxygenated buffer was then added to the cuvette and a second spectrum taken. Oxygen concentrations were assessed from the difference of the two spectra at 600 nm assuming that four methyl viologen molecules are required to provide the 4 electrons necessary to reduce oxygen to water.

2.10 Redox Potentiometry

The mid-point reduction potential of the heme group (Fe^{3+}/Fe^{2+}) couple present in the enzyme was investigated by potentiometric titrations. The standard redox potential (E°) is a thermodynamic property dependent on the Gibbs free energy change (ΔG) between the oxidised and reduced (Fe^{3+}/Fe^{2+}) forms of the complex is described in Equation 2.3:

$$\Delta G = -nFE^{\circ} \qquad \text{Equation 2.3}$$

Where n is the number of electrons and F is the Faraday constant. In terms of electron transfer, electrons travel favourably from more negative E° to positive E° due to a negative ΔG. E° is measured sequentially by reducing and oxidising the enzyme using an applied voltage and monitoring the spectroscopic changes to the absorbance, at 25°C. Plotting the change in absorbance (ΔAbs) against the applied potential (V), and fitting to the Nernst equation, Equations 2.4 and 2.5, allows E° to be obtained.

$$E_{cell} = E^{\circ} - \frac{RT}{nF} \ln Q \qquad \text{Equation 2.4}$$

Which when expressed in terms of base 10 logarithms,

$$E_{cell} = E^{\circ} - \frac{59.1}{n} \text{ mV } \log_{10} \frac{^{a}Red}{^{a}Ox} \qquad \text{Equation 2.5}$$

At equilibrium, E = 0 and Q = *K*, therefore, substituting these values into Equation 2.3, gives Equation 2.6:

$$\text{Log}_{10}K = \frac{nE^{\circ}}{59.1\text{mV}} \qquad \text{Equation 2.6}$$

Equation 2.6 relates the standard electrode potential to the equilibrium constant of a redox reaction.

2.10.1 OTTLE Electrochemistry

Optically Transparent Thin Layer Electrode (OTTLE) potentiometry is used to calculate mid-point reduction potentials. Firstly a modified EPR tube with an optically transparent flat cell, path length 0.3 mm, is filled with the enzyme solution of interest. A platinum/ruthenium gauze working electrode, a platinum counter electrode and an Ag /AgCl reference electrode are fitted to the cell, and it can be sealed with rubber septa to exclude oxygen if an anaerobic environment is required. A potential is applied to the cell, and at each potential a spectra (250 – 700 nm) is recorded to observe the sample as shown in Figure 2.6 (a). The proportion of enzyme reduced (measured at 431 nm) against the applied potential is plotted. The potential of the working electrode was decreased in 50 mV steps and increased in 50 mV steps offset by 25 mV relative to the reductive trace. Heme reduction potentials were determined by fitting the data to a Nernst equation for a single-electron process using Microcal Origin software, as shown in Figure 2.6 (b). The Ag/AgCl reference electrode was calibrated against either indigotrisulfonic acid (-99 mV vs. SHE) or phenazine methosulfate (+82 mV vs. SHE). Applied potentials were corrected relative to SHE where [(potential Ag/AgCl) + 205 mV] = [potential SHE].

In all experiments the sample was prepared in an anaerobic environment and sealed from the atmosphere before removal from the glove box as described in (1, 114). Samples were prepared to a final enzyme concentration of approximately 50μM. Titrations were performed in the presence and absence of substrate for WT TDO (15 mM L-Trp), the H55A mutant (5 mM L-Trp) and the H55S mutant (10 mM L-Trp). On preparation of the enzyme sample a range of mediators were added (2-hydroxy-1,4-naphthoquinone (-145 mV vs. SHE), 5-hydroxy1,4-naphthoquinone (-3 mV vs. SHE), phenazine ethosulfate (+55 mV vs. SHE), phenazine methosulfate (+82 mV vs. SHE), and 1,2-naphthoquinone (+135 mV vs. SHE)) to ensure efficient reduction and re-oxidation of the protein.

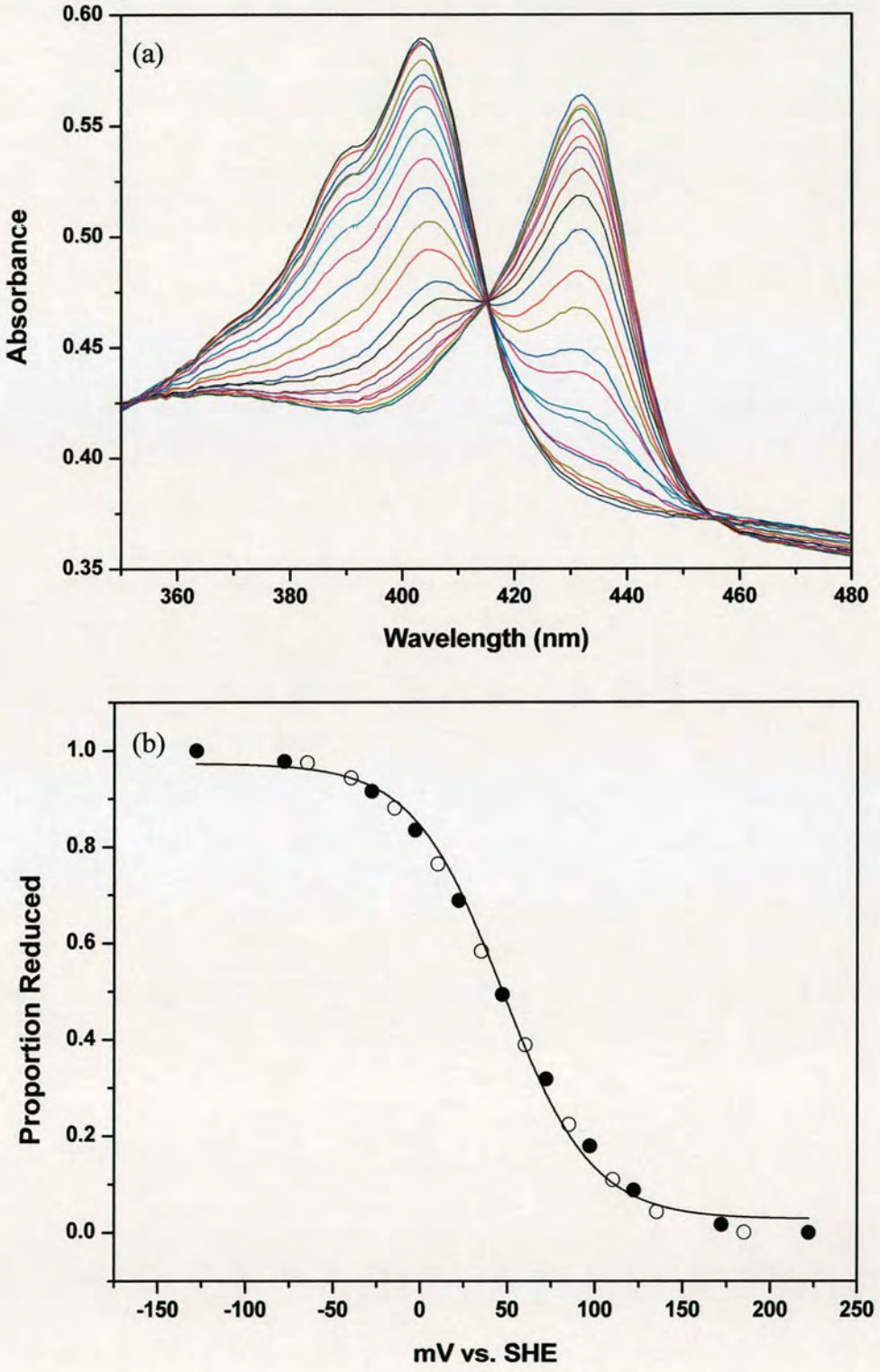

Figure 2.6 (a) Absorbance change in wtTDO spectrum (b) Relative proportion of reduced wtTDO upon oxidation (○) and reduction (●) by electrochemical potential, fitted to the Nernst equation.

2.11 Liquid Chromatography- Mass Spectrometry (LC-MS)

Liquid chromatography-mass spectrometry (LC-MS) combines the physical separation capabilities of liquid chromatography with the mass analysis capabilities of mass spectrometry. LC-MS is a powerful technique used for many applications which has very high sensitivity and specificity. Generally its application is oriented towards the specific detection and potential identification of chemicals in a complex mixture.

LC-MS was carried out to determine the mass of wild type TDO using the mass spectrometer in the University of Edinburgh, School of Chemistry, as described in Section 2.4.2.

LC-MS upon the reaction products produced by TDO and its mutants was carried out at the University of Leicester, Chemistry Department with Dr. Graham Eaton. A Micromass Quatro LC spectrometer, was used, and the sample was run with MeCN / H_2O (0.1% formic acid) as the solvent. A C18 (2.0mm × 250mm × 5μM) column was used to separate the reactants and products.

Samples for LC-MS to analyse turnover products were prepared by allowing enzyme turnover to proceed, then running the sample through the LC- MS. Aliquots of 10 μl were used as described in Section 2.7. Assay buffer F was used throughout, with 20mM ascorbate, 10 μg catalase and 10 μM methylene blue present. Substrate concentration was 4 mM for L-Trp turnover experiments and 1.5 mM for 1-Me-Trp turnover experiments. Approximately 300 nM of enzyme was added to the cuvette for each enzyme studied. The reaction was allowed to proceed for 30 minutes, and was then quenched by the addition of 200 μL of a 30% solution of trichloroacetic acid. The sample was then centrifuged to collect the degraded protein and the supernatant was then filtered using a Millipore 0.45 μM filter unit to ensure no protein remained in solution. The samples were then flash frozen and stored at -80° until required.

2.12 Mass Spectrometry-Mass Spectrometry (MS-MS)

MS-MS upon the reaction products produced by TDO and its mutants was carried out at the University of Leicester, Chemistry Department with Dr. Graham Eaton. A Micromass Quatro LC spectrometer, was used, and the sample was run with MeCN / H_2O (0.1% formic acid) as the solvent. A C18 (2.0mm * 250mm *5μM) column was used to separate the reactants and products. Samples were produced as described above for LC-MS.

2.13 Protein Crystallisation and Data Collection

2.13.1 Wild Type TDO - Oxidised substrate free structure

Crystallisation of TDO was attempted for the oxidised form of the protein by the hanging drop vapour diffusion method. Crystals were grown at 18 °C in a well solution comprising 0.1 M MES (2-(N-morpholino)ethanesulfonic acid) buffer pH 6.1, 8 % polyethylene glycol 1000 (PEG 1000), 60 mM $MnCl_2$ and 30 mM L-tryptophan. Drops were prepared by addition of 2 μl protein (10 mg/ml in buffer E) to 2 μl of well solution. After approximately one week large (0.5 × 0.4 × 0.1 mm) plate-like crystals were formed. These crystals were immersed in mother liquor supplemented with 23 % glycerol as cryoprotectant prior to mounting in nylon loops. A data set was collected at SRS Daresbury (Station 14.2, λ = 0.979 Å) to 2.6 Å resolution. The crystal was found to belong to space group $P\ 2_1\ 2_1\ 2_1$ with cell dimensions a = 89.885 Å, b = 109.767 Å, and c = 146.616 Å.

2.13.2 Wild Type TDO - Reduced substrate bound structures

To obtain the structure of TDO in the ferrous state, the protein was reduced by the addition of sodium dithionite, and all steps were performed in a Belle Technology anaerobic glove box with the O_2 concentration maintained below 5 parts per million. Excess sodium dithionite was removed by gel filtration (Sephadex G25 column) before crystallization. Crystals of TDO were grown by the sitting-drop vapour-

diffusion method with a well solution comprising 100 mM MES (pH 6.3), 10-12% (wt / volume) polyethylene glycol 4000, 60 mM $MnCl_2$, 10 mM sodium dithionite, and 2 mM L-Trp or 8 mM 6-fluoro-D/L-tryptophan. Before mounting in nylon loops and flash-freezing in liquid nitrogen, crystals were immersed in a cryoprotectant solution composed of mother liquor (with L-Trp concentration increased to 50 mM) supplemented with 23% (volume/volume) glycerol. In the case of the L-Trp complex, the solution was bubbled with nitric oxide for 15 min before use. Data sets for both crystals were collected at the BM14 beam line at the European Synchrotron Radiation Facility (Grenoble, France) to 1.60 Å resolution for the L-Trp bound enzyme, and to 1.80 Å resolution for the 6-fluoro-tryptophan bound enzyme. Crystals of the binary complex of TDO (with L-Trp or 6-F-Trp) belong to space group $P3_121$, with cell dimensions $a = b = 114.1$ Å, and $c = 96.2$ Å. In this case, the asymmetric unit contains two TDO monomers.

2.13.3 H55A and H55S mutant forms

Crystallisation of H55A and H55S TDO mutant forms was carried out by hanging drop vapour diffusion at 18 °C in Linbro plates. Crystals were obtained with well solutions comprising 9-10% (w/v) polyethylene glycol 1000, 80 mM MES buffer pH 6.3, 20 mM bicine buffer pH 9.0, 40 mM $MnCl_2$, 400 mM $MgCl_2$, 8-15 mM NaCN and 20 mM L-Trp. Hanging drops (4 µl volume) were prepared by adding 2 µl of 8 mg ml^{-1} protein (in 50 mM TrisHCl buffer pH 8.0, 5 mM in ethylenediaminetetraacetic acid (EDTA)) to 2 µl of well solution. Red tetragonal shaped crystals appeared after approximately one week, reaching full size after two weeks. Crystals were immersed in mineral oil prior to being mounted in nylon loops and flash cooled in liquid nitrogen. For crystals of the H55A and H55S enzymes, data sets were collected to a resolution of 2.15 Å and 1.90 Å respectively at station 10.1 at SRS Daresbury ($\lambda = 1.381$ Å for H55A TDO, $\lambda = 1.045$ Å for H55S). In both cases crystals belonged to space group $P2_1$ with unit cell parameters $a = 78.2$ Å, $b = 117.6$ Å, $c = 139.3$ Å, $\beta = 95.7$ ° (H55A), and $a = 77.9$ Å, $b = 117.8$ Å, $c = 139.1$ Å, $\beta = 95.7$ ° (H55S).

2.13.4 Data Processing

For wtTDO data processing was carried out using the HKL package (115). The tetrameric TDO structure (PDB ID 1YW0), stripped of water was used as the initial model for molecular replacement. Electron density fitting was carried out using the program TURBO-FRODO (116). Structure refinement was carried using Refmac5 (117).

For H55A and H55S mutants data processing was carried out using the CCP4 package (118) and PHENIX(119). The wild-type TDO Apo enzyme structure (PDB ID 1YW0), stripped of water was used as the initial model. Electron density fitting was carried out using PHENIX and TURBO-FRODO. Refinement was carried out using PHENIX and Refmac.

2.14 Molecular Graphics

Figures of crystal structures were generated using PyMOL, DeLano Scientific LLC, (www.pymol.org) (120), unless otherwise stated. Molscript and Raster3D (121) programmes have also on occasion been employed.

Chapter 3

Characterisation of *Xanthomonas campestris* TDO

3.1 Introduction

In this chapter the purification, biochemical characterisation and structure determination of wild-type xcTDO will be described. The aims of these studies were to reveal key aspects of the structure of wtTDO, and determine kinetic and thermodynamic information relating to its catalytic function.

3.2 Expression and Purification

TDO was expressed and purified as described in Section 2.2, and produced a yield of approximately 80 mg of purified enzyme per litre of culture. Denaturing SDS-PAGE analysis of the purified enzyme sample is shown in Figure 3.1(a). A wide main band is observed at ~ 35 kDa, corresponding to monomeric TDO and two bands at ~65 kDa and ~70 kDa, both corresponding to dimeric TDO (as explained by ESI-MS below). The purified enzyme sample gave a characteristic Soret absorption maximum at 405 nm, corresponding to oxidised TDO (Figure 3.2 and Table 3.1).

3.2.1 Electrospray Ionization Mass Spectrometry (ESI-MS)

The purified TDO was shown by electrospray ionisation mass spectrometry to have two forms, with either 6 or 17 amino-acid residues removed from the N-terminus of the protein by proteases. ESI-MS analysis calculated the molecular masses as 34970 ± 90 Da and 33750 ± 90 Da respectively, with equal amounts observed (Figure 3.1(b)). As the protein is non-homogeneous, all protein batches were tested for catalytic activity after purification. Catalytic activity was observed to remain constant (~20 s^{-1}), indicating that the clipping does not affect catalytic activity, allowing the purified TDO to be used for biochemical and structural analyses.

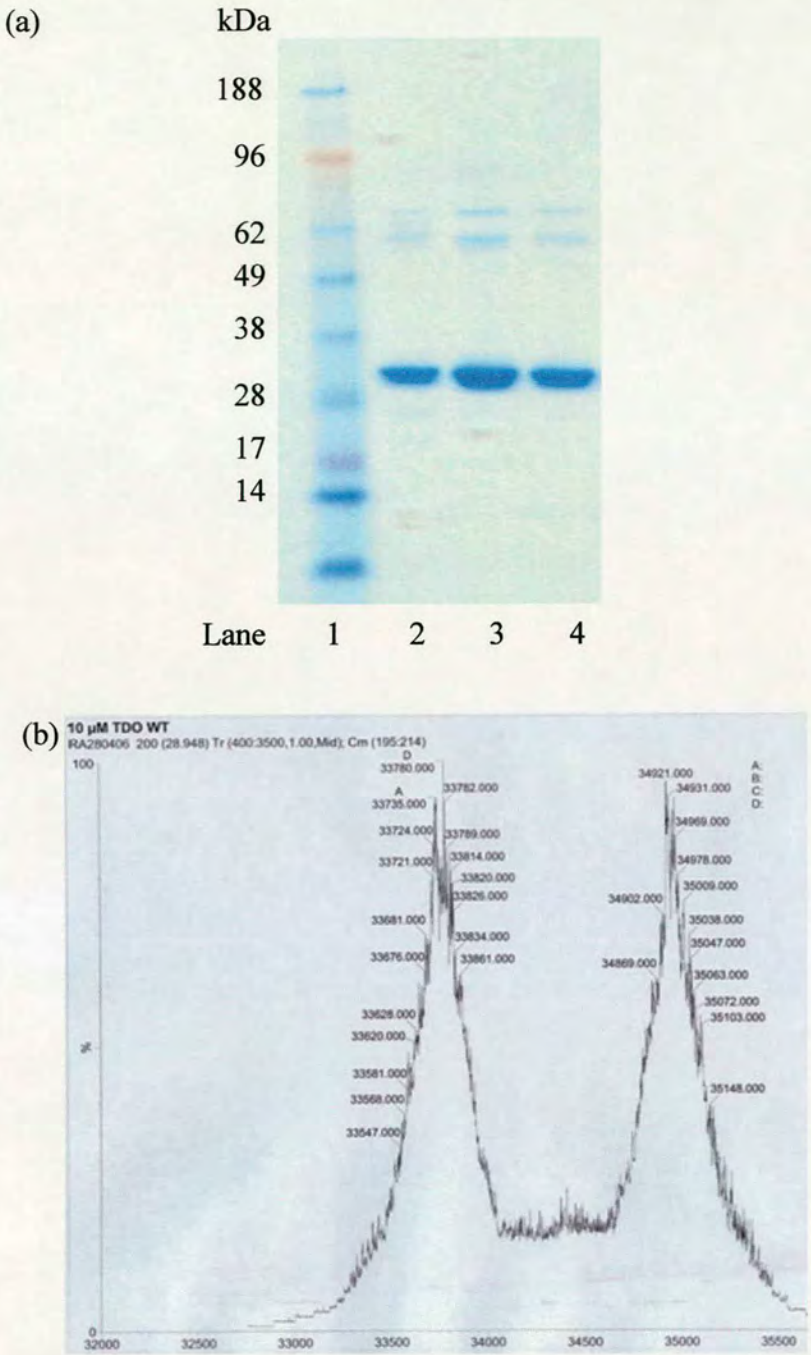

Figure 3.1 (a) Coomassie stained SDS-PAGE analysis of TDO. Lane 1 is a molecular weight marker lane, with weights indicated to the left hand side. Invitrogen SeeBlue® Plus 2 marker system was used. Lane 2 shows purified WT TDO, Lane 3 shows purified H55A and lane 4 shows purified H55S. For all three lanes one wide main band is observed at ~ 35 kDa and two bands at ~65 kDa and ~70 kDa, (b) ESI-MS analysis of purified TDO gives two proteins of molecular mass 34970 kDa and 33750 kDa due to clipping of N-terminal amino acids

.

3.3 Concentration and Heme Content Determination

The concentration of all protein samples were determined using the Bradford assay, as described in Section 2.4, with enzyme concentrations ranging from 0.2-2 mg ml^{-1}. Determination of the heme content was carried out using the pyridine hemochrome method described in Section 2.5. Heme incorporation was greater than 90 % for all samples tested when the results were compared to those calculated by the Bradford assay. This gave a value of at least 3.6 heme groups per tetramer of TDO, which can reasonably be assumed to indicate one heme group per monomeric unit of TDO. This result differs to some previous studies which observed two hemes per tetramer for mammalian TDOs (96, 122-124). However, purification methods vary greatly between studies, and in this study increased heme incorporation may be due to addition of hemin during induction of *E.coli* protein production to ensure that heme incorporation is not limited by the quantity of heme available in the cell environment, and the relatively simple method of purification.

These data allowed the calculation of the extinction coefficients for the main Soret peak of ferric and ferrous wtTDO, and extinction coefficients are displayed in Chapter 2, Table 2.1. Both the ferric and ferrous extinction coefficients calculated for wtTDO are typical of *b*-type heme proteins.

3.4 Spectroscopic Characterisation

The UV–vis absorbance spectra for this family of proteins are characteristic of *b*-type heme-containing proteins with an axial histidine ligand. Spectrochemical data are shown in Table 3.1 for wtTDO and some related proteins.

The spectrum of the ferric form of wtTDO has maxima at 405, 503 and 633 nm, consistent with a high-spin heme species (Figure 3.2). Reduction of ferric wtTDO results in a red-shift in the Soret band (from 405 to 431 nm) and the formation of two peaks in the visible region (555 and 588 nm) (Figure 3.2). The binding of L-Trp to ferrous wtTDO leads to a decrease in the Soret band, and no other visible changes to the spectrum, indicating little change of spin state upon substrate binding.

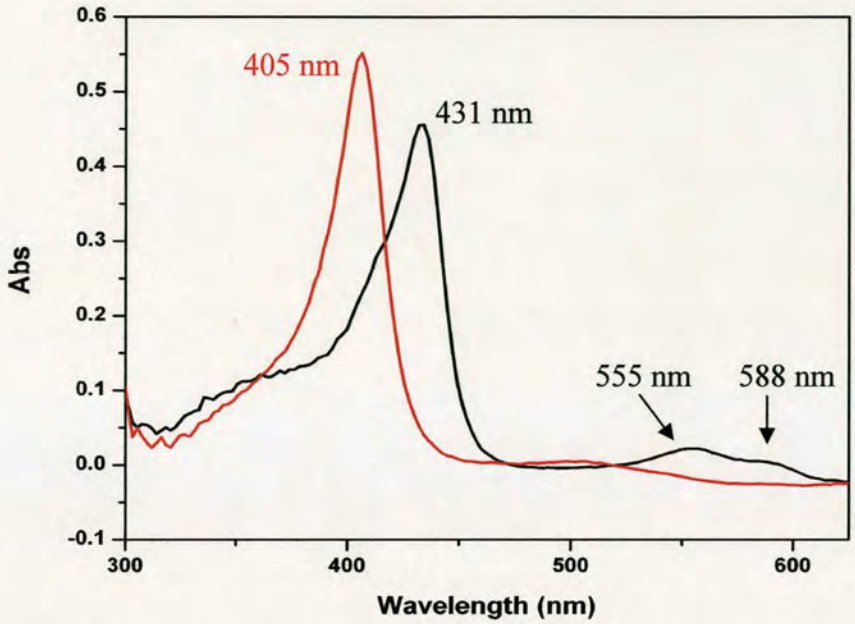

Figure 3.2 *Spectra of ferric (red) and ferrous (black) wtTDO.*

Table 3.1 *Spectroscopic data relating to some TDO and IDO proteins. Peak wavelengths are given in nm.*

Derivative	*X. campestris*[a] TDO (1)	*H. sapiens* TDO (77)	Rat liver TDO (123)	*H. sapiens* IDO (78, 102)
Fe^{3+}	405, 503, 633	408, 533, 621	406, 500, 630	404, 500, 535, 633
Fe^{3+} - L-Trp	405, 585	410, 536, 565	407, 498, 632	411, 540, 576
Fe^{2+}	431, 555, 588	428, 560	430, 557	425, 527[sh], 558
Fe^{2+} - L-Trp	433, 555, 588	426, 533, 560	421, 557	425, 556
Fe^{2+} - O_2	*dnf*	413	*dnf*	412, 539, 576
Fe^{2+} - CO	419, 541, 568	421, 540, 564	420, 538, 569	419, 539, 565
Fe^{3+} - CN^-	418, 538, 570[sh]	419, 538, 566[sh]	-	419, 540, 570[sh]

[sh] = *Shoulder*, *dnf* = *does not form.*

3.5 Structural Studies

The structure of TDO has been described in Section 1.7, and PDB codes and crystallographic information for the following structures are described in Table 1.1. All crystallisation procedures, data collection and data analysis on wild-type xcTDO were performed by Dr Chiara Bruckmann and Dr Chris Mowat.

3.5.1 Solved Crystal Structures

Crystals of TDO in the oxidised state, in the absence of substrate, were grown in aerobic conditions as described in Section 2.13.1, producing a data set to a resolution of 2.7 Å (PDB ID 2NW7). Subsequent data analysis and inspection of the electron density revealed no binding of L-Trp in the active site of any monomer, and gave a tetrameric structure for TDO, described in Section 1.7.1. The first 22 amino acids were unresolved, presumably due to a flexible N-terminal region outside the active site pocket, although some clipping of these amino-acid residues may occur during purification, as evidenced by mass spectrometry.

Crystals of TDO in the reduced state, with L-Trp or 6-F-trp bound (PDB ID 2NW8 and 2NW9), were grown in anaerobic conditions as described in Section 2.13.2, using data sets to 1.6 and 1.8 Å resolutions respectively. The structure of the 6-F-Trp binary complex is essentially identical to that of the L-Trp binary complex (Figure 3.3). In addition the structure of xcTDO in the reduced state with partial occupancy of the substrate L-Trp has been solved to a resolution of 1.95 Å. In this structure there are two monomers in the asymmetric unit (half of the physiological tetramer), and L-Trp is bound at the active site of one monomer whilst there is no L-Trp in the other. This has allowed us to compare the reduced substrate bound, reduced substrate-free and the oxidised substrate free forms of TDO.

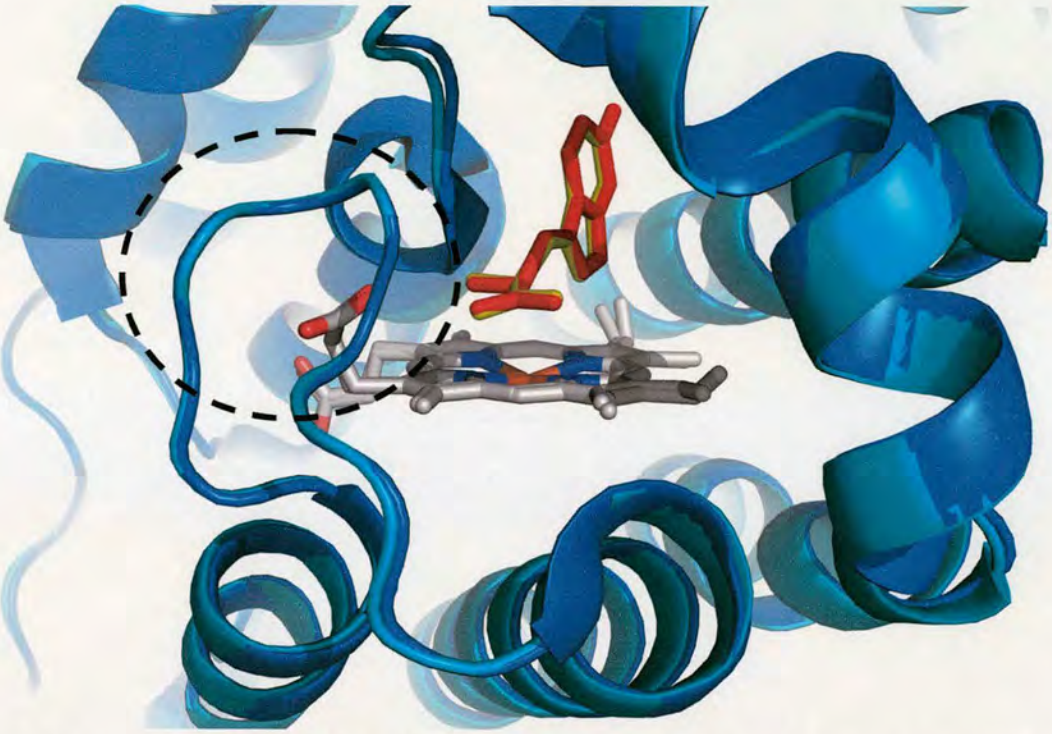

Figue 3.3 Binary complexes of wtTDO with L-Trp and 6-F-Trp bound, overlaid. The protein backbone is shown in marine blue and cyan, L-Trp is shown in yellow and 6-F-Trp is shown in red. The substrates align identically in the active-site. The αJ–αK loop is circled.

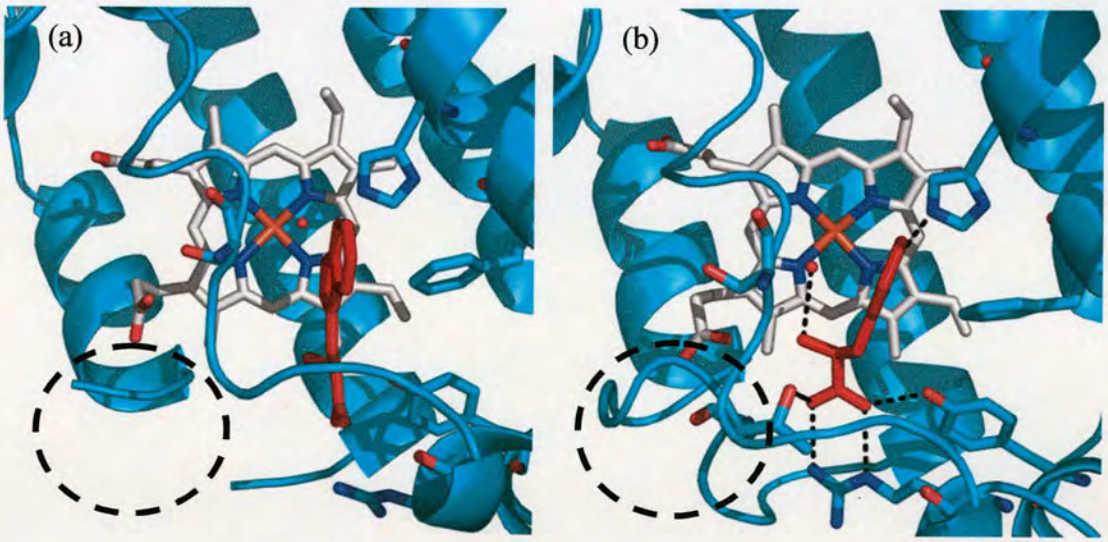

Figure 3.4 (a) Monomer B of wtTDO L-Trp bound structure (PDB ID 2NW8), displaying the active site and surrounding structure. The flexible αJ–αK loop is unresolved (b) Structure of monomer A, showing fully bound L-Trp. The flexible αJ–αK loop is resolved and is shown interacting with L-Trp.

3.5.2 TDO is an Induced-Fit Enzyme

Structural comparisons suggest that TDO is an induced-fit enzyme. Upon recognition of the L-Trp a complex and extensive network of interactions is established, thus stabilizing the active-site region. The evidence for this behaviour is described below. The active-site region is exposed to solvent in the substrate-free enzyme- but it is almost completely shielded from solvent upon L-Trp binding, with only the carboxylate group of the 6-propionate of heme visible on the surface. Substrate binding "closes" the active site-pocket, and in the L-Trp and 6-F-Trp bound structures, the αJ–αK loop, which helps to form the walls of the active-site pocket is well-defined crystallographically, whilst it is disordered in the substrate-free enzyme (Figure 3.4).

As described in Section 1.7, comparison between the substrate-bound and substrate-free structures shows reorientation of Arg 117 upon binding of tryptophan, with the side-chain undergoing a movement of ~6 Å to interact with the L-Trp carboxylate group. An Arg/Tyr pair is a common binding motif for carboxylates in proteins, also displayed in P450 BM3 (126, 127) and mandelate dehydrogenase (128, 129). This carboxylate-binding motif appears to be essential for substrate binding; arginine reorientates in the presence of substrate, interacting with the carboxylate group of L-Trp, with "open" and "closed" conformations observed (Figures 3.5 A, B and C). The movement of Arg 117 is accompanied by the movement of a loop spanning the active site, leading to a flip of serine 124 into its hydrogen-bonding position in the active site of the reduced enzyme.

Additional evidence for the induced-fit behaviour is observed in the active site of the second TDO monomer in the asymmetric unit. The binding mode of the L-Trp substrate is very different in this monomer, as shown in Figure 3.5. The L-Trp side chain is not positioned as deeply into the pocket, and the hydrogen bond between the indole nitrogen atom and His 55 is lost. Both nitrogen atoms are instead hydrogen-bonded to a water molecule, located 3.5 Å from the heme iron in a position distinct from that of the water in the active site of the other monomer. This conformation may also be stabilized by crystal packing interactions, as the 7-propionate of heme is ion-

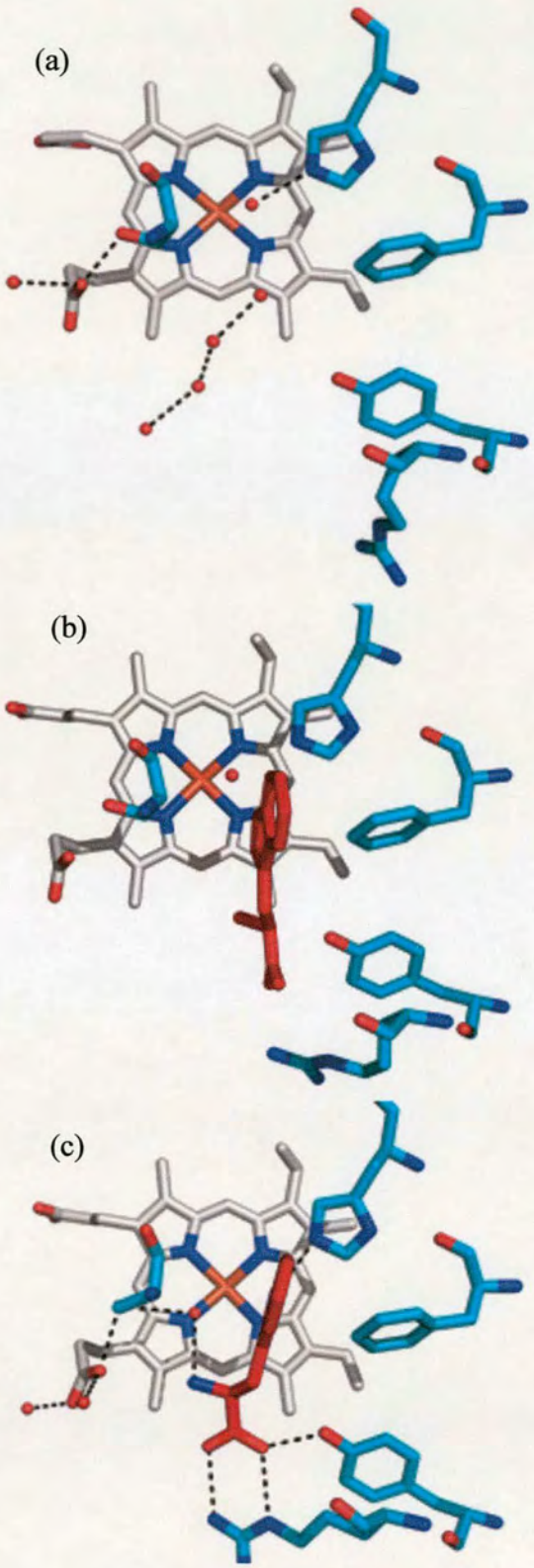

Figure 3.5 Active-site conformations of wt TDO with (a) no substrate bound (2NW7), (b) L-Trp bound, monomer B (2NW8), L-Trp bound monomer A (2NW8).

paired with an Arg residue from another TDO tetramer in the crystal. The main chain atoms of L-Trp appear to be disordered because no clear electron density was observed for them. Consistent with this finding, the αJ–αK loop is disordered in this molecule, similar to that in the substrate free enzyme (Figures 3.4 and 3.5). This complex may represent an initial stage in the formation of the Michaelis complex of TDO. Proper positioning of the L-Trp substrate for catalysis would lead to the recognition of its main chain atoms and the ordering of the αJ–αK loop.

3.5.3 A Model for the Michaelis Complex.

To help provide further insight into the catalysis by these enzymes, a model of the Michaelis complex was built using the L-Trp bound structure by placing one oxygen atom of the dioxygen substrate directly over the heme iron, at a distance of 2.1 Å (Figure 3.6). The distal oxygen atom was placed such that the O–O bond is parallel to the C2–C3 bond of indole ring, giving a Fe–O–O angle of 135°, in a trans position to the indole ring, described in Section 1.7.1 (2). The distal oxygen atom in this conformation is within 0.5 Å of the water molecule observed in our substrate-bound structure, suggesting that this water should be ejected from the active site upon dioxygen binding, leaving the active-site completely devoid of solvent molecules. In the model of the Michaelis complex, the oxygen atoms are in a trans configuration relative to the C2–C3 atoms of L-Trp

The modelled dioxygen binding mode reveals information on the activation mechanism of this ternary complex. TDO has an ordered catalytic cycle in which the protein binds L-Trp to the ferrous form, then O_2, forming the ternary complex which then undergoes reaction (4). The positioning in our modelled Michaelis complex indicates that electrophilic addition or radical addition mechanisms will be favoured over an "oxygen-ene" type addition. In the model, the distal oxygen atom interacts with the L-Trp ammonium moiety and the backbone amide nitrogen of Gly 125. The Lewis acidity of these hydrogen-bonding donors, coupled with the electron-withdrawing nature of the heme, increases the electrophilicity of the bound dioxygen, making it more reactive, and therefore more likely to facilitate electrophilic attack on the substrate C3 or C2 atoms. Studies with heme oxygenase suggest that the

hydrogen-bonding interactions with the dioxygen substrate may also help to prevent its heterolysis, and the exclusion of water probably removes a hydrogen-bond competitor with the dioxygen (72, 130)

.

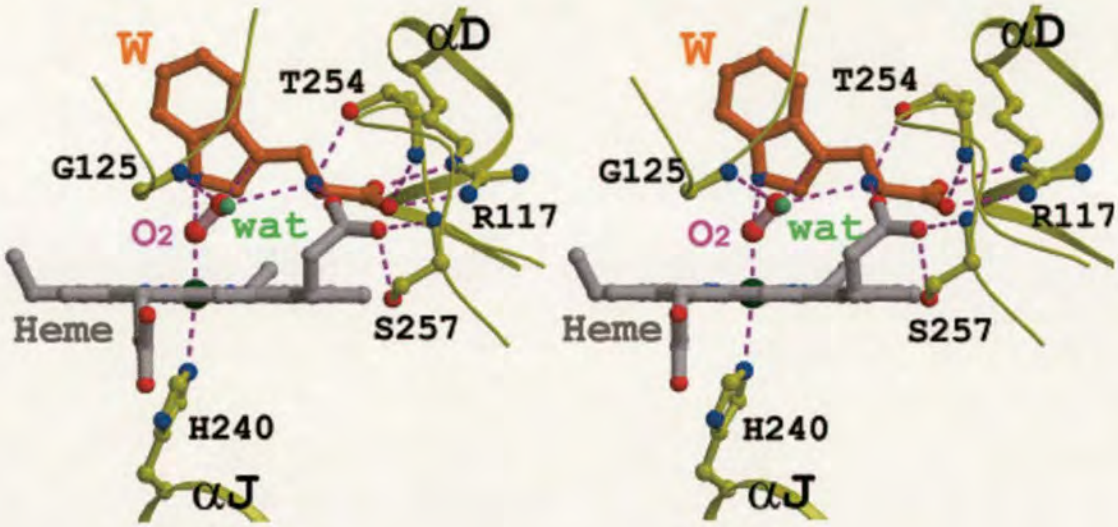

Figure 3.6 Stereo view model of the Michaelis complex. The water molecule is shown as a small sphere in green, tryptophan is shown in orange, O_2 is shown as two red spheres. Produced with Molscript and rendered with Raster3D (121).

3.5.4 A Potential Allosteric Binding Site

The crystal structure of wtTDO has revealed four secondary interfacial L-Trp binding sites, as described in Section 1.6.1. The residues Asp 228, Tyr 220, Arg 85 and Lys 92, which are located on the αJ and αC helices, interact with L-Trp, binding it to the enzyme (Figures 1.13 and 1.14). In addition the αJ helix encodes histidine 240, which coordinates directly the heme group. The αJ helix links the interfacial binding site and the active-site, and suggests a mechanism for allosteric regulation in the enzyme.

3.6 Substrate Binding Titrations

Substrate binding titrations give a measure of the affinity that the enzyme has for substrate allowing dissociation constants to be calculated as described in Section 2.6. L-Trp binds to TDO in the oxidised, non-reactive, state, causing a decrease in the Soret band at 405 nm and an increase in absorption at 565 nm. Spectrophotometric data for the binding of a number of ligands to the ferric or the ferrous protein are displayed in Table 3.2. Binding of substrate and substrate analogues to the reduced enzyme produces a decrease in the Soret peak at 431 nm. Changing pH between pH 6 and 8.3 does not affect the change in the spectrum upon binding of substrate in both the ferric and ferrous states.

These binding studies provide direct evidence for the induced-fit behaviour of TDO. Indeed, there is a large increase in the affinity of the enzyme for L-Trp when the heme iron is reduced (K_d, Fe^{3+} = 3840 μM, whereas K_d, Fe^{2+} = 4.1 μM). Binding of L-Trp to the ferric protein is described in Section 2.6 and displayed in Figures 2.3 and 3.7. L-Trp preferentially binds to ferrous protein rather than ferric, by a factor of almost a thousand. The substrates 6-F- D/L- and 5-F- D/L-Trp bind to wtTDO in a similar manner to L-Trp, with a large difference in the K_d values for binding to ferric and ferrous enzyme (Table 3.2). Slightly smaller K_d values for binding to both the ferric and ferrous enzyme indicates that these substrates may bind tighter than L-Trp, but this effect is not substantial.

The substrate analogue indolepropionic acid (IPA) binds to ferrous wtTDO with low affinity - K_d = 185 μM, displaying a binding curve analogous to that of the TDO substrates. 5-Br-Trp and tryptamine are only weakly soluble to non-saturating concentrations, causing binding values to go undetermined.

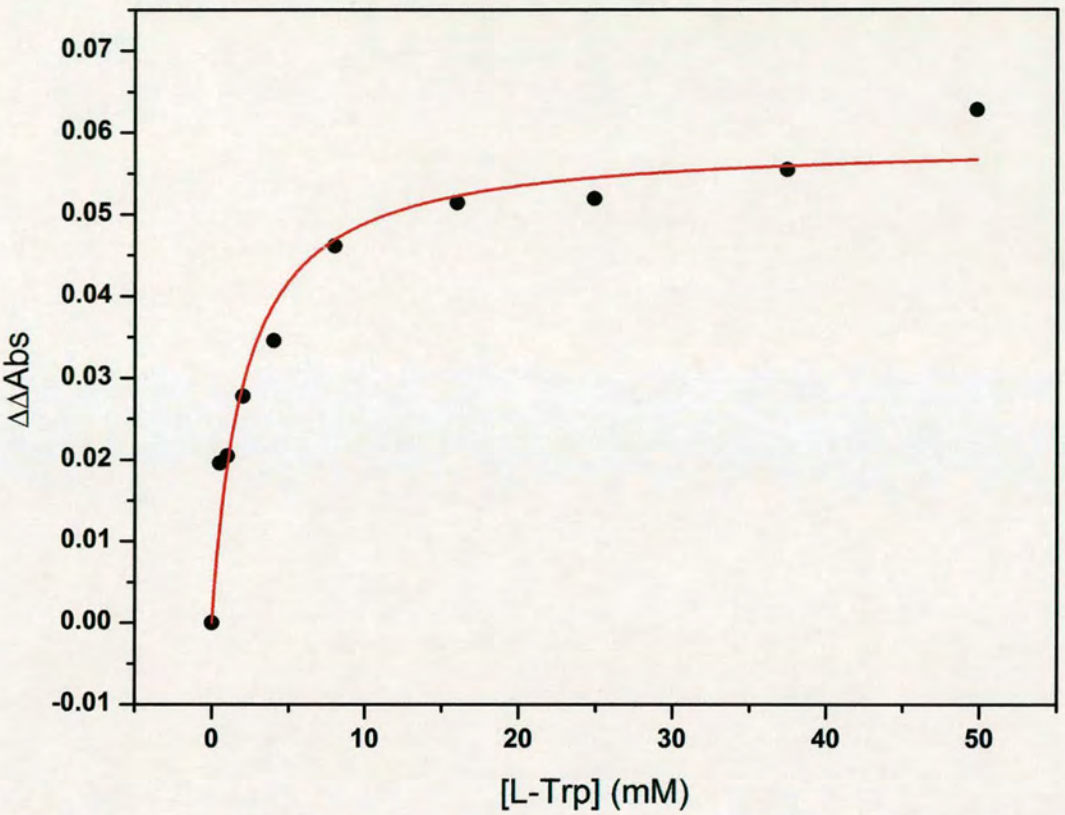

Figure 3.7 Plot of binding of L-Trp to ferric wtTDO. The change in absorbance (ΔΔabsorbance) is plotted against substrate concentration.

Table 3.2 Substrate binding to wtTDO

Substrate	Fe^{3+}, K_d, (μM)	Fe^{2+}, K_d, (μM)
L-Trp	3840 ± 140	4.1 ± 0.2
6-F-D/L-Trp	1510 ± 80	<1.00‡
6-Me- D/L-Trp	>2000*	>200
5-F- D/L-Trp	2450 ± 420	<1.00‡
5-Me- D/L-Trp	>2500*	51 ± 7
D-Trp	>50,000*	*nc*
Indole Propionic Acid	>10,000*	185
Tryptamine	>4,000*	>500

‡ *Binding was too tight to be measured. Values quoted represent the minimum K_d that can be measured under standard assay conditions.*

* *Maximum solubility of the substrate investigated.*

nc No change observed upon binding.

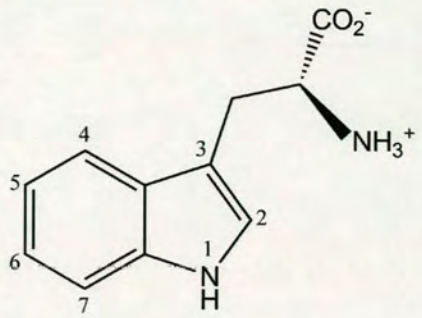

L-tryptophan

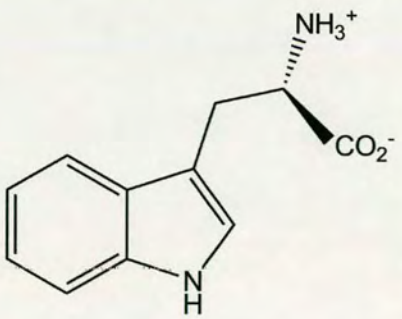

D-tryptophan

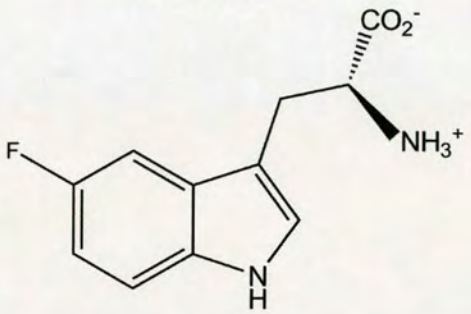

5-Fluoro-tryptophan

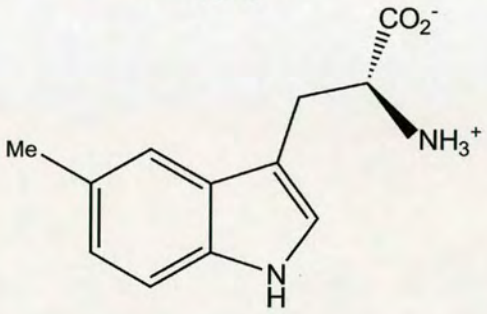

5-Methyl-tryptophan

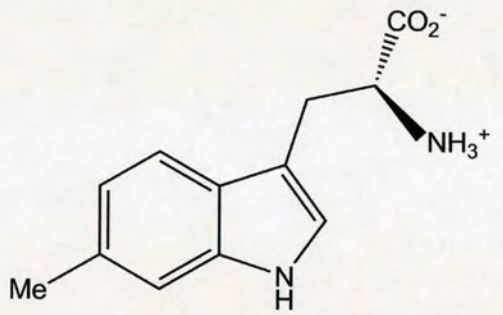

6-Methyl-tryptophan

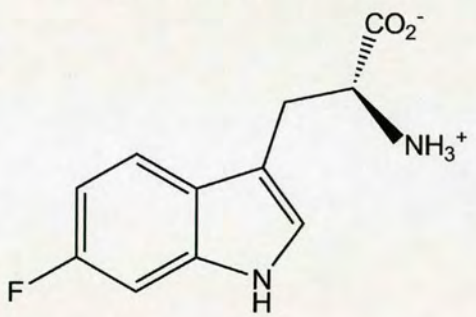

6-Fluoro-tryptophan

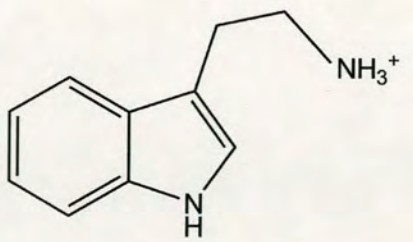

Tryptamine

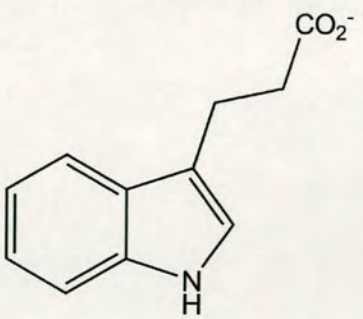

Indole propionic acid

Figure 3.8 TDO substrates, L-Trp, 5-F-Trp, 5-Me-Trp, 6-F-Trp and 6-Me-Trp, the inhibitor D-Trp, and the substrate analogues tryptamine and indole propionic acid.

3.7 .1 Steady-State Turnover Kinetics

Steady-state kinetic rates of turnover were determined as described in Section 2.7. A variety of substances have been tested for enzymatic activity, with wtTDO displaying high substrate specificity, only catalysing the dioxygenation of L-Trp, 6-F-Trp, 6-Me-Trp, 5-F-Trp and 5-Me-Trp. WtTDO is inactive toward D-Trp, tryptamine and indole propionic acid (IPA) which are substrates for IDO, confirming its designation as a TDO. Reactivity's are shown in Table 3.3 and the structures of some of these compounds are shown in Figure 3.8. WtTDO catalyses the dioxygenation of L-Trp with a k_{cat} of 19.5 s^{-1} (Figure 3.9(a)), whilst the k_{cat} for 6-F-D/L-Trp is 37 s^{-1}, twice the rate of that for L-Trp. It is probable that catalysis only occurs with the L-isomer of 6-F-Trp, indicating a 4-fold increase in k_{cat} compared to L-Trp. As fluorine is highly electron withdrawing, it can be postulated that this electron-withdrawing effect inductively activates tryptophan oxidation, decreasing the energy of activation for electrophilic addition to the indole ring by the bound dioxygen. Molecular modelling simulations (not shown), comparing the activation energy for the conversion of L-Trp, 5-F-L-Trp and 6-F-L-Trp suggest that the reaction is most favourable for 6-F-L-Trp, in agreement with the experimental observations (85).

The narrower substrate specificity of TDO compared to IDO could be due to the tight substrate binding pocket in TDO. Previous studies have shown that IDO catalyses the dioxygenation of D-Trp, although at a slower rate than for L-Trp (4, 102). As Table 3.3 shows, D-Trp is not a substrate for TDO and is in fact a weak competitive inhibitor of wtTDO at high concentrations, with a K_i of 16.5 mM as shown in Figure 3.9 (b) (The K_i was determined as described in Section 2.7.3). This different specificity can be explained by considering the binding of D-Trp to wtTDO, and comparing the structures of xcTDO and hIDO. Binding data show that D-Trp has much lower affinity for the ferrous, catalytically active state of wtTDO than L-Trp. This is consistent with our structural information - ionic interactions are important for recognizing the L-Trp ammonium ion and carboxylate group, and these make the enzyme stereospecific to L-Trp. Some of these electrostatic interactions are conserved in IDO (Arg231 and the heme 7-propionate), however, some hydrogen-

bonding interactions to the substrate are absent. For example Tyr113 of xcTDO is replaced by Phe226 in hIDO (Figure 1.2), removing at least one hydrogen bonding interaction. Additionally the xcTDO Thr 254 residue, which interacts with the substrate carboxylate, may not have an equivalent in hIDO because the flexible loop which orders on substrate binding in xcTDO is disordered and therefore absent from the hIDO crystal structure. This loop region has a highly divergent sequence in IDO species compared with TDO species and a residue able to play this role may not be present. Therefore IDO may have weaker interactions with tryptophan, and this may be the reason why it cannot completely distinguish among the indoleamine substrates, catalysing the dioxygenation of D-Trp, whilst wtTDO does not.

The catalytic activity of allosteric enzymes can often be regulated by small changes in substrate concentration, allowing regulation of metabolic pathways where the substrate concentration fluctuates over a narrow range. It has been proposed that TDO may play such a "housekeeping" role, regulating the tryptophan concentration and keeping it within certain parameters (38). However, no evidence of allostery was observed during L-Trp turnover, indicating that L-Trp is not an allosteric effector of wtTDO, and its binding does not appear to influence the activity of the enzyme.

Table 3.3 Steady-state kinetic data for xcTDO and some similar proteins.

	X.campestris TDO (1)		*H.sapiens* TDO[α] (77)		*H.sapiens* IDO[α] (78)	
Substrate	k_{cat} (s^{-1})	K_m (μM)	k_{cat} (s^{-1})	K_m (μM)	k_{cat} (s^{-1})	K_m (μM)
L-Trp	19.5 ± 1.2	114 ± 1	1.40 ± 0.02	222 ± 15	1.4 ± 0.1	7.0 ± 0.8
6-F-D/L-Trp	37.3 ± 0.6	186 ± 12	~	~	~	~
6-Me-D/L-Trp	41.0 ± 1.2	975 ± 48	~	~	~	~
5-F- D/L-Trp	2.4 ± 0.1	100 ± 6	0.18 ± 0.01	360 ± 28	0.76 ± 0.01	6.0 ± 0.8
5-Me-D/L-Trp	3.6 ± 0.1	357 ± 12	*a*	*a*	3.8 ± 0.2	98 ± 14
D-Trp	n/a	K_i = 16.5mM	*b*	*b*	3.9 ± 0.1	1570 ±100

[α] *Steady-state kinetics performed at pH 8.0 in 50mM Tris buffer.*

a *Catalytic turnover at [D-Trp] = 50 mM was measured due to low activity, and $k_{cat} \sim 0.073\ s^{-1}$.*

b *Very little reaction, maximum observed $k_{cat}/K_m = 0.0001\ \mu M^{-1}s^{-1}$*

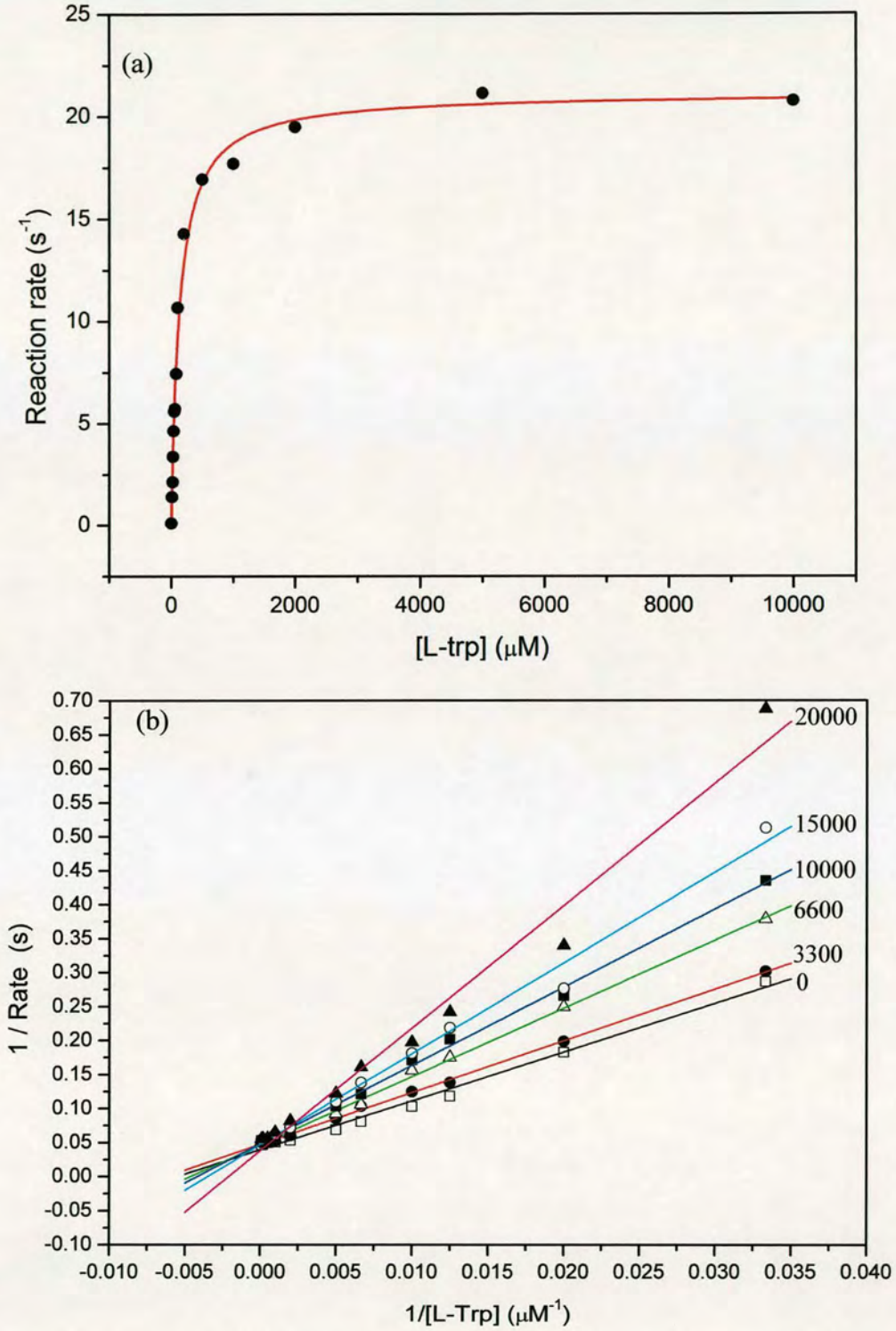

Figure 3.9 (a) L-Trp turnover by wild-type wtTDO at pH 7.5. Data is fitted to the Michaelis Menten equation, and plotted in Microcal Origin 7.5, (b) Plot of 1/[L-Trp] against 1/ Rate of turnover for xcTDO activity with differing concentrations of D-Trp (shown in μM) present in the assay.

3.7.2 pH Dependence of Turnover

Experiments were performed as described in Section 2.7.2. Figure 3.10 shows the change in k_{cat} and K_m for L-Trp dioxygenation by wtTDO with varying pH. Little variation of k_{cat} occurs between pH 5.5 and 8.3, indicating that a base may not be required for catalysis. If a base was involved in the catalytic mechanism of L-Trp dioxygenation it could be supposed that varying the pH would have an effect on the rate of turnover. However, as k_{cat} remains constant with varying pH, this would indicate that a non-base catalysed mechanism may operate.

The Michaelis constant, K_m, is shown to decrease with increasing pH between pH 6.0 and 7.0, with a pKa value of around 6.5. However, little variation in K_m is observed above pH 7.0. This indicates that turnover is optimised above pH 7, and pH 7.5 is therefore used as the standard pH throughout this thesis.

3.7.3 Steady-State Deuterium Kinetic Isotope Effect

The rate of L-Trp turnover could involve deprotonation of the indole nitrogen, or be influenced by hydrogen bonding *via* water molecules in the active site. To probe these effects deuterated water was used during turnover, using the method stated in Section 2.7.3. Catalytic turnover of L-Trp by wtTDO in deuterated conditions gave a k_{cat} almost identical to that obtained in non-deuterated solvent (21 ± 0.2 s^{-1}), indicating that proton delivery is not rate limiting to turnover. The K_m was determined to be 138 ± 5 μM, again close to that observed in non-deuterated solvent, supporting the idea that base-catalysed deprotonation of L-Trp does not play a rate limiting step in the catalytic mechanism of wtTDO.

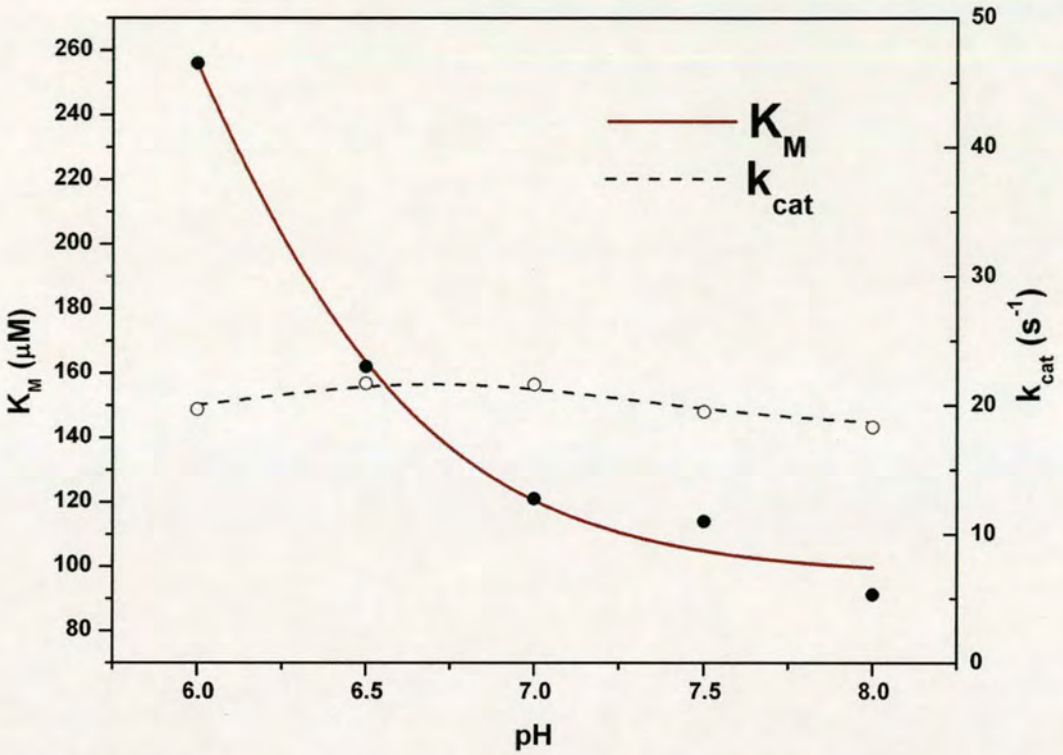

Figure 3.10 Plot of K_m and k_{cat} vs. pH for turnover of L-*Trp by TDO.*

3.7.4 LC-MS Analysis of Products

LC-MS analysis was used to detect products produced upon catalytic turnover of L-Trp by wtTDO, as described in Section 2.11. The equipment was calibrated to detect L-kynurenine (209 Da), N-formylkynurenine (237 Da) and L-Trp (205 Da). LC-MS analysis is shown in Figure 3.11, and it can be seen that both the product N-formylkynurenine, hydrolysed N-formylkynurenine, (L-kynurenine), and the reactant L-Trp are present in the sample.

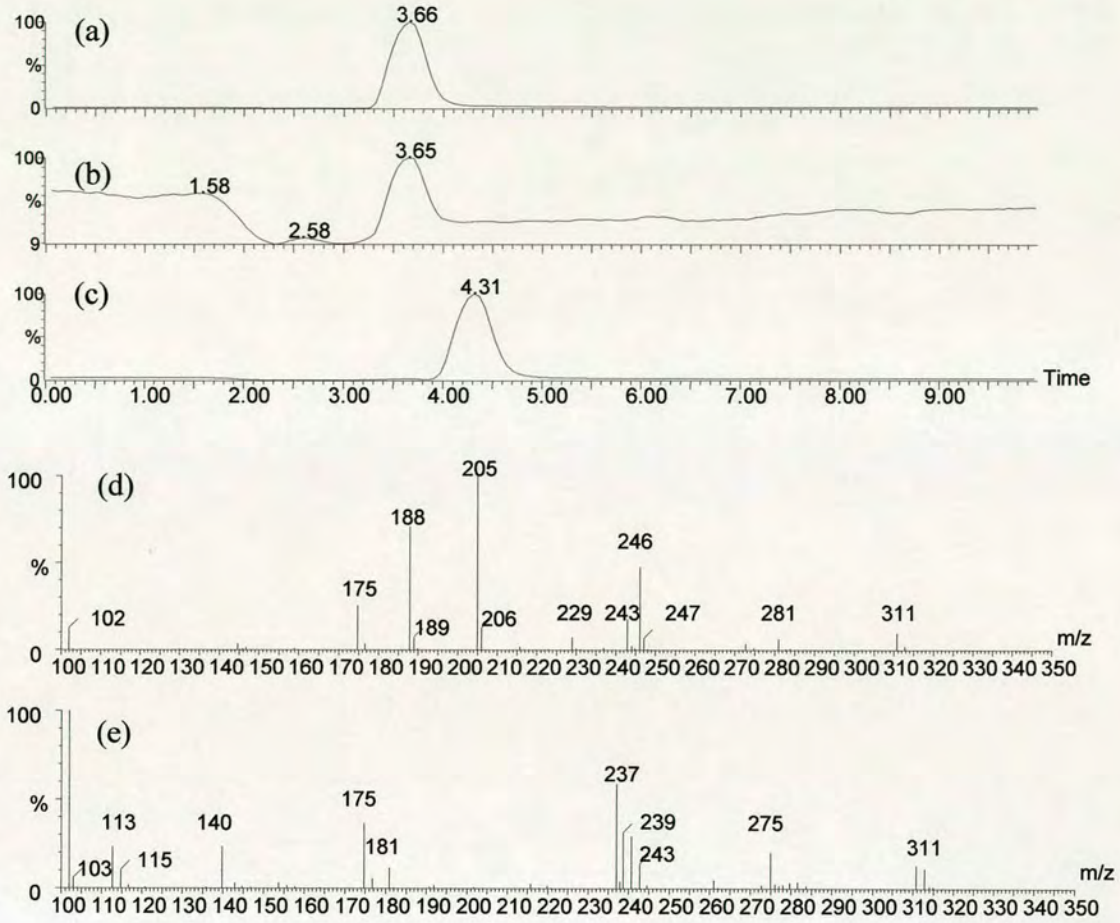

Figure 3.11 LC-MS analysis of wtTDO L-Trp turnover products, (a) LC trace calibrated to detect the ($M+H^+$) ion of L-Kynurenine (209 Da) vs. time, (b) LC trace calibrated to detect the ($M+H^+$) ion of N-formylkynurenine (237 Da) vs. time, (c) LC trace calibrated to detect the ($M+H^+$) ion of L-Trp (205 Da) vs. time, (d) MS of the ($M+H^+$) ion of L-Trp peak detected in (c), (e) MS of the ($M+H^+$) ion of N-formylkynurenine peak detected in (b).

3.7. 5 MS-MS Analysis of Products

MS-MS analysis was conducted on the same sample as that used for LC-MS, as described in Section 2.12. The data produced confirms that L-Trp, N-formylkynurenine and L-kynurenine are found in the sample. L-kynurenine is only found to be present in a small quantity. MS-MS analysis is shown in Figure F.1 in Appendix F. These data confirm that the product of the reaction of wtTDO with L-Trp is N-formylkynurenine, and that no other products are observed to be formed.

3.8 Steady-state Turnover in Varying Oxygen Concentrations

Steady-state kinetic experiments investigating the effect of oxygen on L-Trp turnover were performed as described in Section 2.8.2. Under experimental conditions TDO substrate turnover is limited only by the amount of oxygen available. The rate of turnover observed is therefore indicative of the maximal rate at the oxygen concentration used. Plotting the rates observed against oxygen concentration gives an indication of the binding affinity of oxygen and its effect on the turnover of substrate. Shown in Figure 3.12, the observed rate constant for turnover is dependent on dioxygen concentration, $[O_2]$, under saturating L-Trp concentrations (25 mM). The data is fitted to the Hill equation, indicating that the effect of varying oxygen concentration on turnover is slightly cooperative, with an n value of 1.16. As this is only a small variation from Michaelis-Menten kinetics, any cooperative behaviour displayed is highly suspect. Turnover may be occurring according to Michaelis Menten kinetics, with the variation an artefact of the method of analysis. Further, more sensitive analysis of this reaction is needed before any conclusions can be drawn as to if there is any cooperativity occurring, and if it is catalytically relevant.
At room temperature (25°C) the concentration of O_2 in assay buffer F is approximately 140-160 μM (determined spectrophotometrically via the methyl viologen assay described in Section 2.9.3). Therefore the concentration of O_2 used in the steady-state turnover experiments (described in Sections 2.7 and 3.7) was 140-160 μM, and at which concentration the observed rate is 19.5 mol s^{-1}. This correlates

with the rate displayed in Figure 3.12 at approximately 150 μM. Turnover is limited by the dioxygen concentration at 150 μM, and maximal turnover is not achieved till oxygen saturation of greater than 600 μM. The maximal rate observed $k_{cat,}$ is 35.4 s^{-1} and indicates that turnover is only ~ 60 % of maximal under standard conditions.

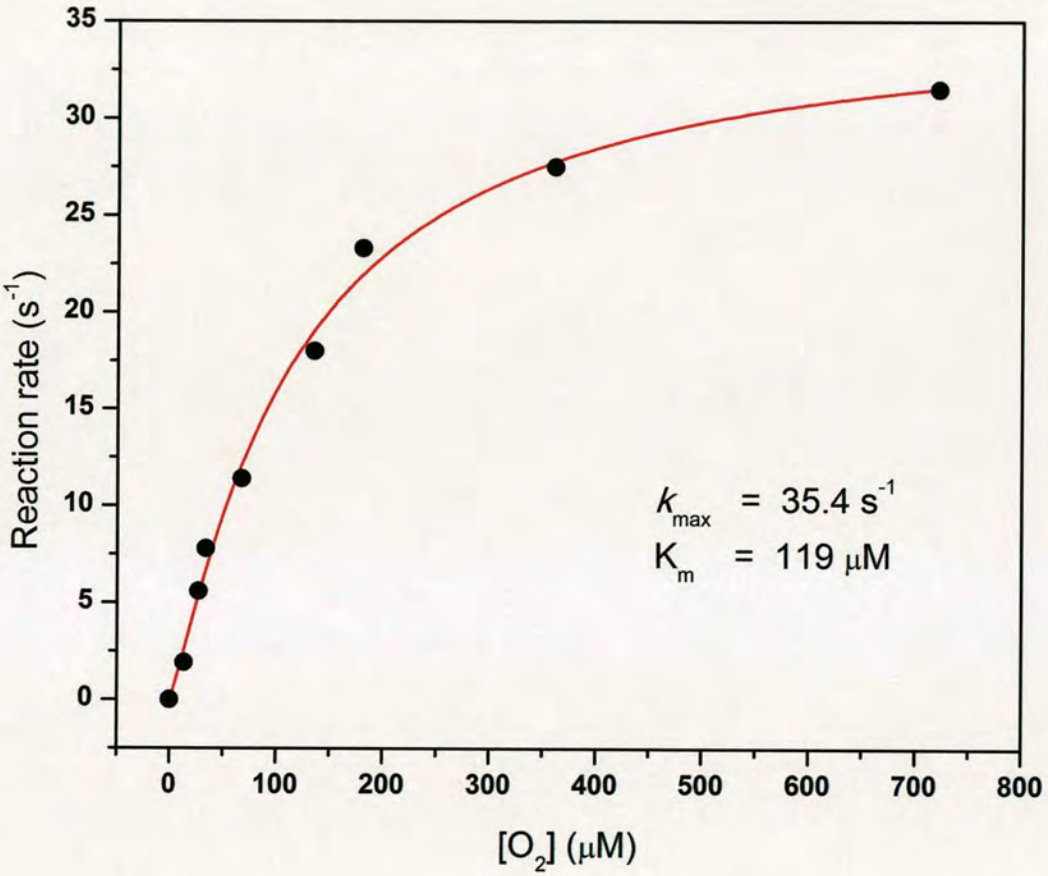

Figure 3.12 Rate of production of kynurenine (s^{-1}) against oxygen concentration for TDO, data fitted to the Hill equation using Microcal Origin 7.5.

3.9 Oxygen binding

Experiments were performed as described in Section 2.8.1. On addition of oxygen to reduced wtTDO at 25 °C, no binding is observed to occur to the active site, with the heme porphyrin becoming oxidised to the Fe^{3+} state, and a characteristic shift in the

Soret peak to 405 nm occurring. This is shown in Figure 3.13(a). When substrate is not present it can be hypothesised that the correct groups necessary to bind oxygen in the active site are not present and oxidation of the ferrous iron occurs.

On addition of oxygen to an L-Trp saturated solution of wtTDO at 25 °C a peak is observed to form at 417 nm, which quickly decays back to the reduced TDO spectrum. It is hypothesised that this is the formation of an oxy-ferrous species, which then undergoes a catalytic reaction to form the product. The product is then released by the active site, and the enzyme remains in the reduced, ferrous state, which is observed as a rapid decay back to the initial reduced species (Figure 3.13 (a)). The data fits to a second order exponential, indicating more than one mechanistic step is required to facilitate production of the stable species, consistent with mechanisms of dioxygen activation proposed in Section 1.3. It has been observed that IDO forms a similar oxy-ferrous species on dioxygen binding in the presence of L-Trp, and is predicted to catalyse substrate dioxygenation in a similar (or identical) manner to TDO.

After this initial evidence suggesting the formation of an oxy-ferrous species, experiments were carried out using other substrates and substrate analogues in the same manner, in the hope of observing a more stable oxy-ferrous intermediate. Unfortunately, as yet no stable oxy-ferrous intermediate has been discovered which displays a longer lifetime than that observed with L-Trp as the substrate.

Addition of dioxygen to a reduced, 6-F-Trp saturated solution of wtTDO produced an oxyferrous species displaying the same spectral characteristics as that formed when L-Trp was present and rates for the second order decay back to the reduced spectrum were similar to those of L-Trp. This indicated that turnover of 6-F-Trp proceeds in an analogous fashion to L-Trp turnover and is consistent with the identical binding of 6-F-Trp and L-Trp to the enzyme, (Table 3.2), which would suggest similar stabilities for any catalytic intermediates.

Addition of dioxygen to a reduced, 5-F-Trp saturated solution of wtTDO gave partial generation of an oxyferrous species, with the spectrum indicating that part of the sample remains in the dioxygen–free reduced state (Figure 3.13(b)). The oxyferrous species then decays back to the reduced species.

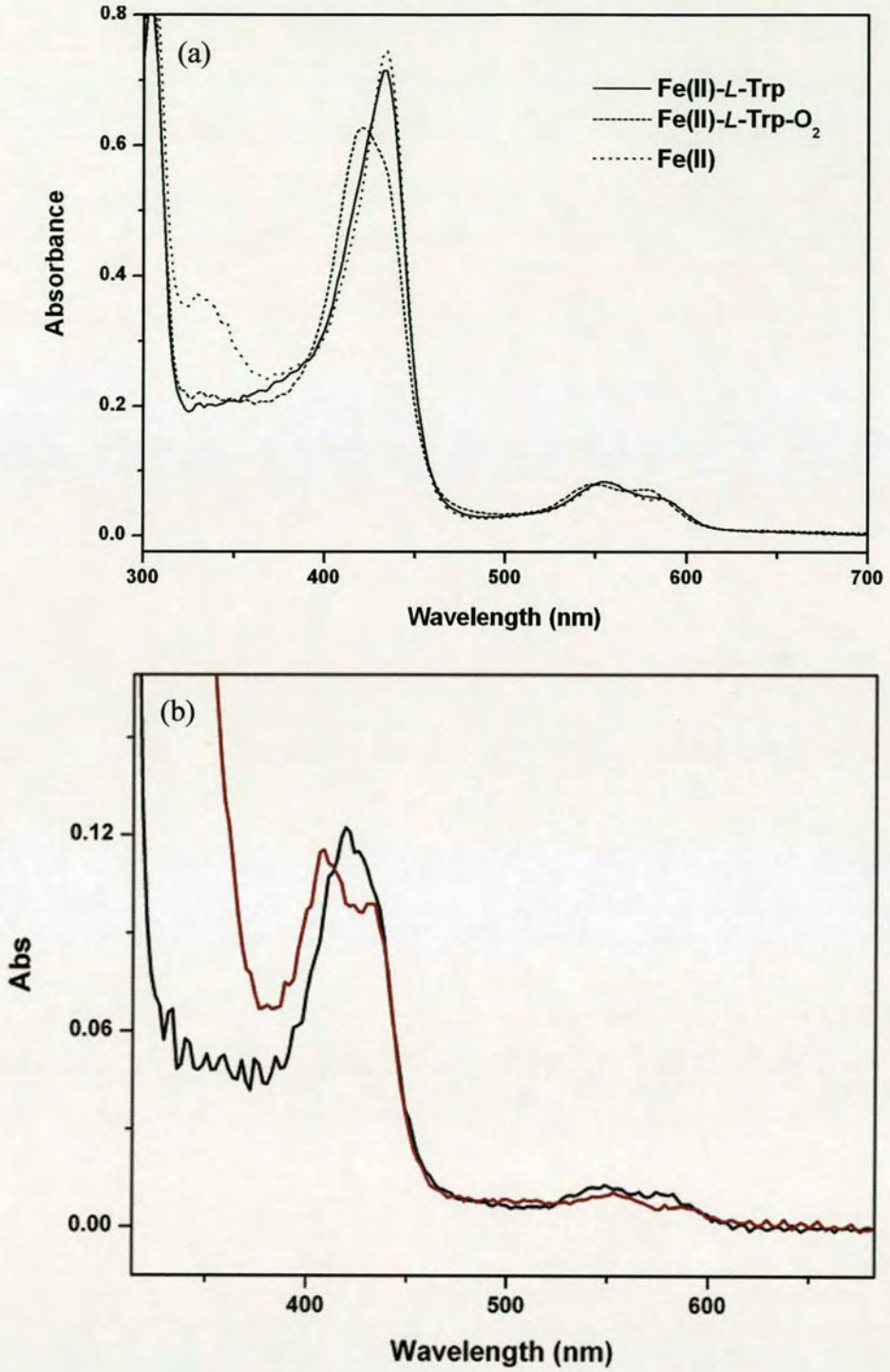

Figure 3.13 (a) Production of the wtTDO oxyferrous complex. The peak positions of the oxyferrous complex are at 420 nm, 548 nm, and 578 nm. This decays back to ferrous enzyme and product (N-formylkynurenine – peak position 321 nm), (b) Addition of oxygen to reduced, 5-F-Trp saturated wtTDO shows an oxyferrous intermediate partially formed during substrate turnover.

This indicates that the reaction is partially uncoupled i.e. inefficient turnover of 5-F-Trp is occurring, with a percentage of the ternary complex dissociating rather than forming products. Efficient, fully-coupled production of product does not occur. This uncoupling is reflected in the lower rate of 5-F-Trp turnover (only ~10 % of L-Trp), and may be caused by greater steric hindrance to the formation of reactive intermediates due to the addition of a fluorine atom to the aromatic ring.

3.10 Binding of Diatomic Molecules

Binding of diatomic molecules to TDO can mimic the effect of binding oxygen at the active site. Binding diatomic molecules in the presence of substrates and substrate analogues can aid our understanding of the formation of the ternary complex, and give insight into the residues involved in complex formation.

3.10.1 CO Binding

CO binding experiments were conducted as described in Section 2.8.3. CO coordinates to the ferrous and ferric protein, displaying tighter binding to the ferrous form. Since all catalytic activity occurs in the ferrous state, only binding to the ferrous enzyme will be considered. CO binding to the ferrous enzyme to produce (Fe^{2+}-CO), induces a shift in Soret band from 431nm to 420 nm. In addition, the Soret peak diminishes upon binding, and a change in the spectral bands at 560 and 590 nm occurs (Figure 3.14 (a)).

In the presence of L-Trp, CO binding to produce (Fe^{2+}-L-Trp-CO) leads to a shift in the Soret peak from 431 to 417 nm, with the height of the peak increasing by around 25% (Figure 3.14 (b)). The characteristic peaks at 560 and 590 nm change in height till they are no longer observed, with peaks, at around 540 and 570 nm forming.

As there is a large spectral difference between the binding of CO to wtTDO in the presence or absence of L-Trp, this change can be used to probe the possible side chain interactions between the L-Trp molecule and the bound CO. Tryptamine and indole propionic acid are L-Trp analogues which can be used to probe the effect of

the amine and carboxylate groups of tryptophan upon CO binding to the active-site, and their use is discussed below.

3.10.2 Probing the Side-Chain Interactions of L-Trp

The structures of tryptamine and IPA are shown in Figure 3.8. IPA lacks the amine group of L-Trp, whilst tryptamine lacks the carboxylate group. These two derivatives of tryptophan can be used to probe the effect of the amine and carboxylate groups of tryptophan upon binding of small molecules to the active-site. Comparison of the binding of CO to substrate-free, L-Trp-bound, IPA-bound and tryptamine-bound wtTDO will allow evaluation of the roles of the amine and carboxylate groups of L-Trp in small molecules binding.

The binding of CO to wtTDO with IPA or tryptamine bound to the active-site to produce (Fe^{2+}-IPA-CO) and (Fe^{2+}-Tryptamine-CO) are shown in Figures 3.14 (c) and (d) respectively. The binding of CO to ferrous wtTDO with IPA bound at the active-site produces a spectrum analogous to that of (Fe^{2+}-CO) in the substrate-free state. A peak is observed at 420 nm, with no decrease in the peaks at 560 and 590 nm. The binding of CO to wtTDO with tryptamine bound, gives a spectrum analogous to that of (Fe^{2+}-L-Trp-CO). The Soret band is shifted to 417 nm, and peak height is increased although not to the extent of that seen for L-Trp. Also the bands at 560 and 590 nm are replaced by ones at 540 and 570 nm.

These results suggest that the amine group of tryptophan must be important in the binding of small molecule, such as CO. Both L-Trp and tryptamine can coordinate to CO through the amine in the ternary complex, whilst in the substrate free-enzyme and IPA-bound wtTDO this is not possible due to the absence of the amine group. The amine nitrogen therefore appears to play a role in the binding of CO, and it can be hypothesised that it will also play a role in the binding of O_2 in the ternary complex. This correlates with the observed active-site structure displayed in the L-Trp bound crystal structure. The amine group coordinates to a water molecule, which is predicted to lie in the position where the distal atom of dioxygen will reside in the Michaelis complex (Figure 3.6).

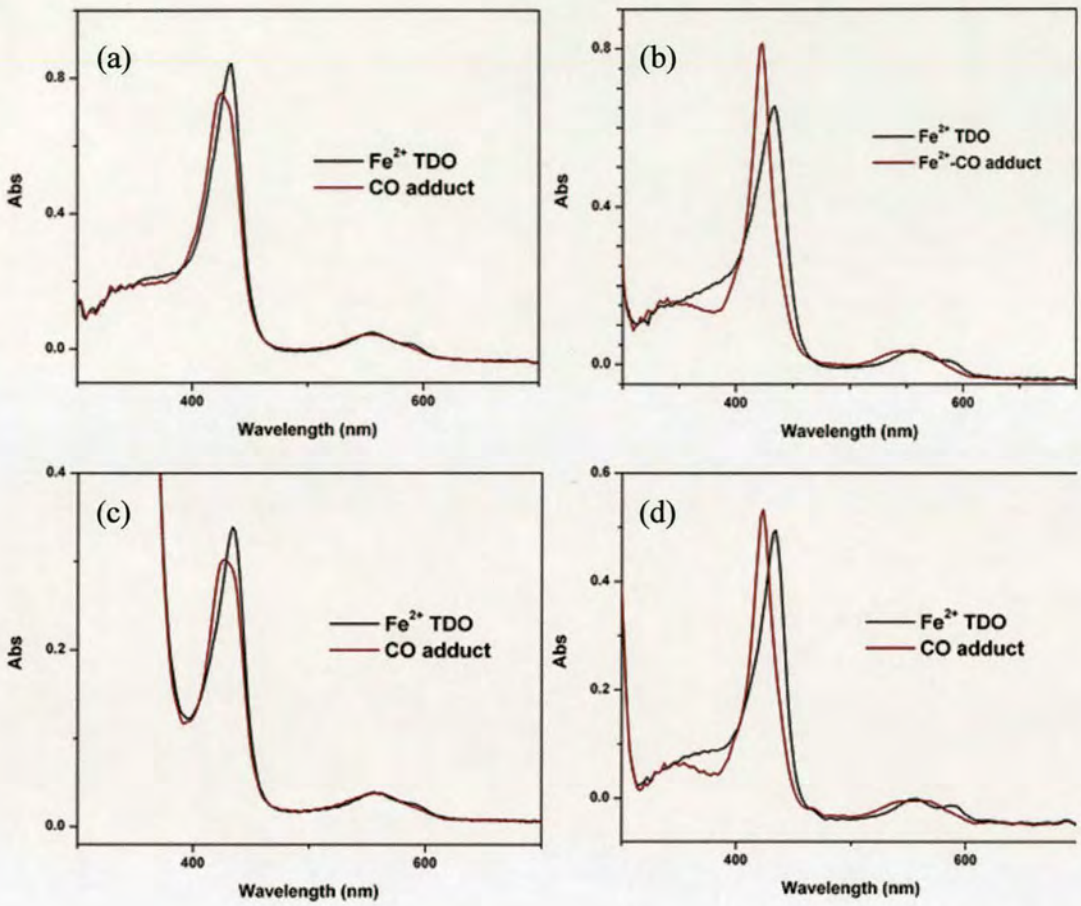

Figure 3.14 CO binding to wtTDO with (a) no substrate present, (b) L-Trp present, (c) indolepropionic acid present and (d) tryptamine present.

3.10.3 Calculating the Dissociation Constant for CO

To calculate the K_d for CO binding to both substrate-free and L-Trp bound wtTDO, experiments were performed as described in Section 2.8.3. The rate of formation of the CO adduct was measured by observing the absorbance spectrum at 420 nm (Figure 3.15(a)) (Note; a nanomolar concentration of wtTDO was used to ensure that only the availability of CO was rate limiting).

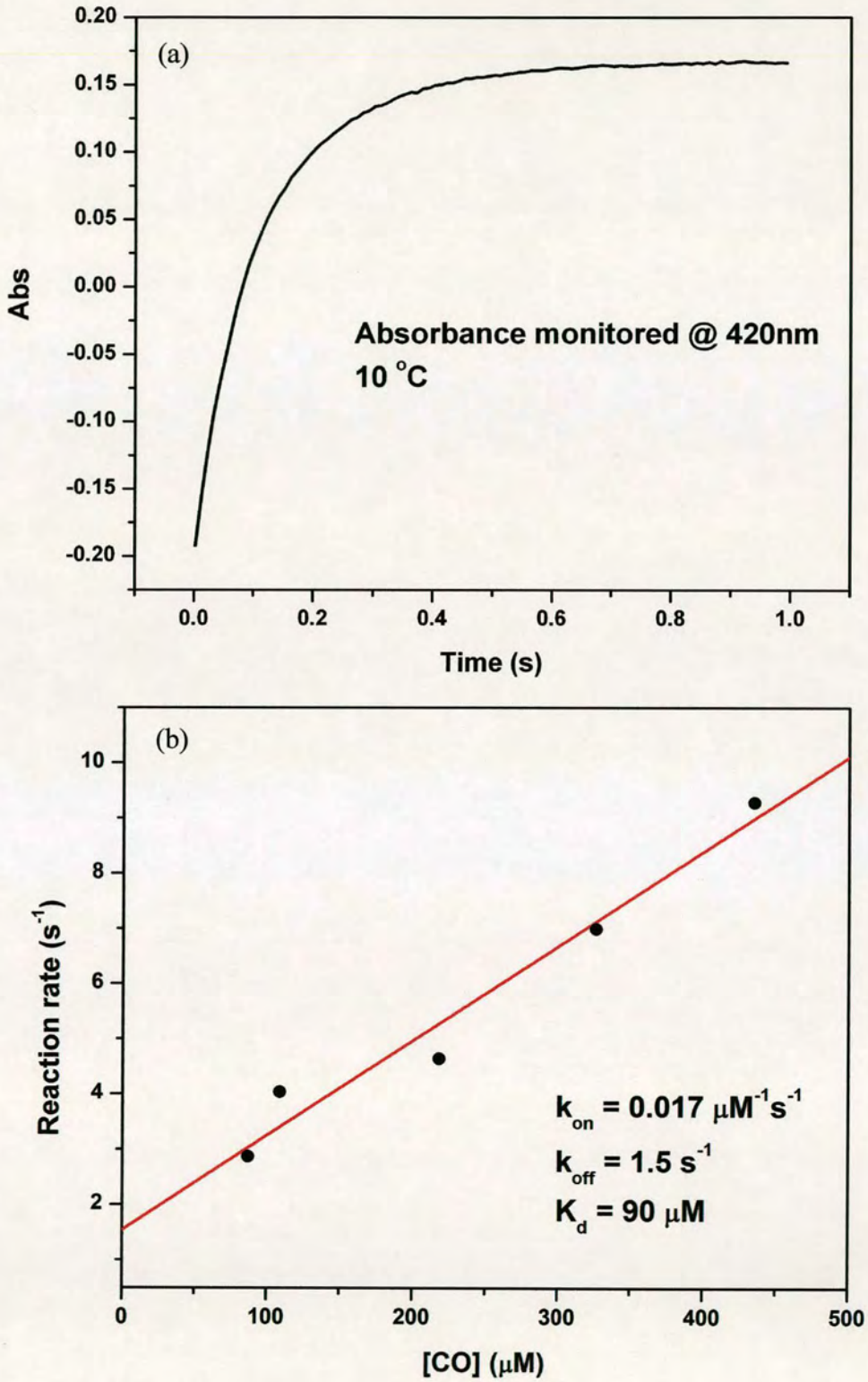

Figure 3.15 (a) Trace showing the production of the CO binding complex at 420nm over time, (b) plot of CO concentration against observed rate of formation of CO adducts fitted linearly.

These results show that CO binds to wtTDO, proportionally with increasing CO concentration (Figue 3.15 (b)). Binding is directly proportional to the CO concentration present in solution, and does not display any sigmoidal or parabolic effects which could be associated with cooperative or allosteric binding. The K_d, for CO binding is 90 μM, indicating that CO binds tightly to wtTDO. The rate of loss of CO from the complex, k_{off}, is 1.5 s^{-1}, showing that binding is reversible and decay of the CO adduct occurs over a measurable timescale. As a consequence of these properties, at standard room temperature and pressure, and *in vitro* where the concentration of CO is low, CO binding to wtTDO does not affect catalytic turnover.

3.10.4 NO Binding

Binding of NO to wtTDO was too fast to be measured by stopped-flow. The spectral characteristics of the species formed are displayed in Table 3.1. No dissociation or association constants of NO to the enzyme have been measured due to the difficulty in obtaining accurate data on the concentration of NO in solution.

3.10.5 Cyanide Binding to TDO

Cyanide was used to probe the active-site of wtTDO. Cyanide binds strongly to the oxidised heme iron producing a characteristic change in the Soret peak from position 405 nm to 424 nm, with a K_d of approximately 15 μM and no indication of cooperativity in the binding. The binding of cyanide to substrate-free TDO is stronger than the binding of L-Trp to the enzyme, which is most probably due to the direct coordination of cyanide to the heme iron.

The binding of cyanide is observed to be pH dependent, with K_d varying between around 500 μM to around 10 μM on increasing the pH from 6.0 and 8.3 (Figure 3.16 (a)). This trend can be fitted to a pH curve which gives a pKa for the binding of ~ 6.5, consistent with a histidine residue being present at the active site.

3.10.6 Cyanide binding to TDO with Substrate Present

The binding of cyanide to ferric wtTDO with L-Trp present gives a decrease in the Soret peak at 405nm, and an increase at 419 nm, with a K_d of 1.5 μM at pH 7.5. Hence the enzyme displays greater affinity for cyanide in the presence of L-Trp. This trend is displayed across the pH range from pH 6.0 to 8.3, with K_d varying from 3 to 1.5 μM, with a pKa of ~ 6.5.

Contrary to substrate free enzyme, binding of cyanide in the presence of L-Trp displays cooperative binding. This is shown in Figure 3.16 (b), where the Hill coefficient is shown to vary with pH within the range n = 1.5-2.2. The Hill coefficient is seen to peak at pH 7.5, with a maximum value of 2.2. Binding of CN^- when other substrates are present can give an indication of which parts of the active site binding pocket are involved in the reported cooperativity of the tetramer.

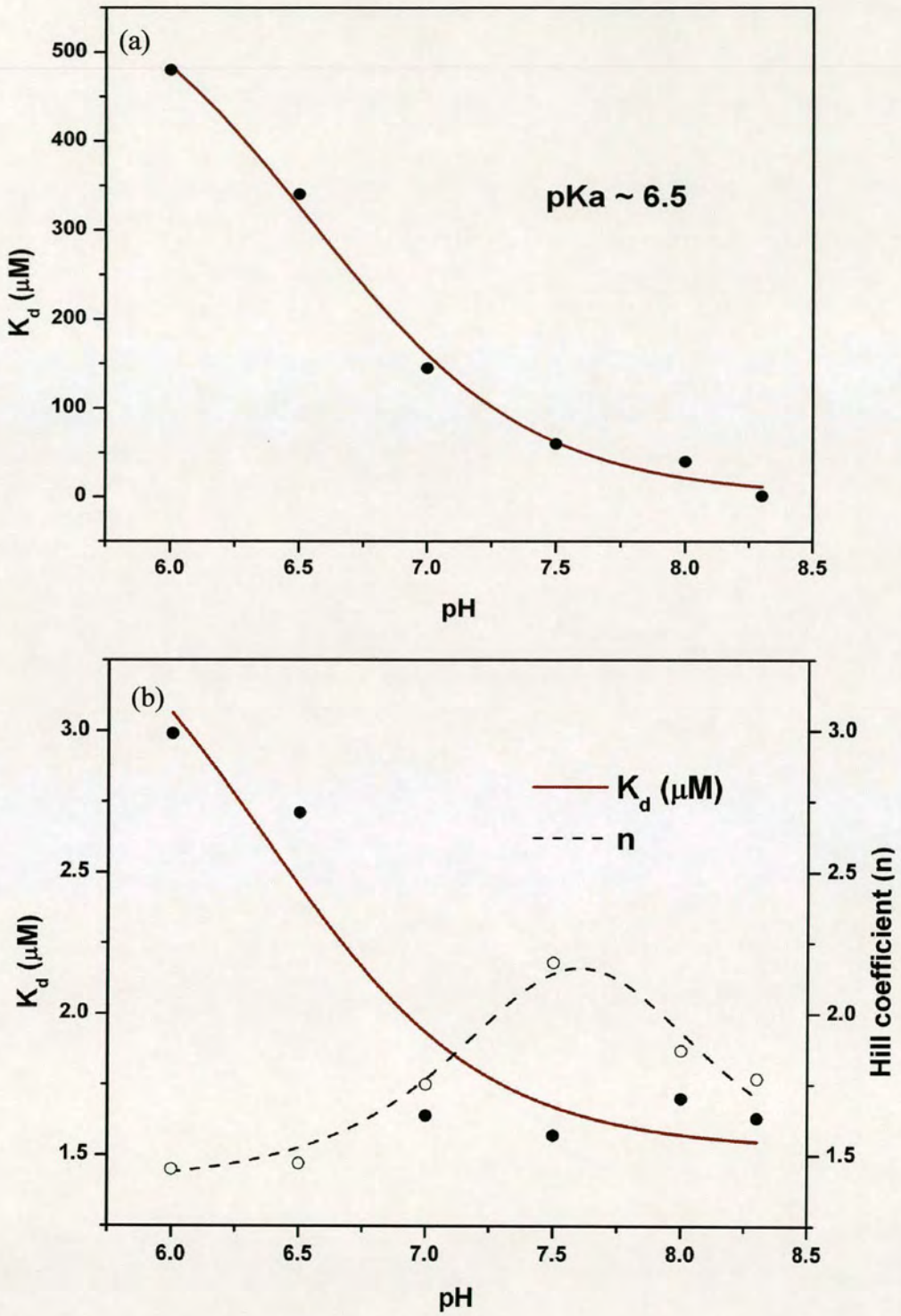

Figure 3.16 (a) K_d against pH for binding of CN^- to wtTDO with no substrate present, (b) Binding of CN^- to TDO with L-Trp present, displaying K_d against pH, and the variation of the hill coefficient (n) with pH.

3.11 OTTLE Potentiometry

Substrate-free and substrate-saturated heme reduction potentials were determined as described in Section 2.10. The heme reduction potential is a measure of the tendency of TDO to receive or accept electrons. Typically the addition of substrate leads to a positive increase in the heme reduction potential generating a more positive driving force for the electron transfer and hence acting as a thermodynamic switch.

The substrate-free and substrate-bound heme reduction potentials for wtTDO and some related proteins are shown in Table 3.4. The mid-point reduction potential of substrate free wtTDO is 8 mV and substrate-bound wtTDO is 144 mV, a shift of 136 mV on substrate binding (Figure 3.17). In fact, the shift in reduction potential almost perfectly correlates with the increase in affinity for L-Trp on reduction, both giving an estimated $\Delta\Delta G$ of 15 kJ / mol. A thousand fold increase in the L-Trp binding affinity is observed upon enzyme reduction (K_d Fe(III) = 3800 μM, K_d Fe(II) = 4μM), disfavouring the mechanistically unproductive binding of L-Trp to the oxidized enzyme.

Few reduction potentials for either IDO or TDO have so far been reported, but those available show clear trends (Table 3.4). Upon binding of the substrate, there is an increase in reduction potential for both IDO and TDO, reflecting additional stabilization of the ferrous derivative. The increase is larger for TDO proteins (with the exception of human TDO), compared to IDO proteins. For both IDO and TDO, it is not clear whether heme reduction precedes substrate binding or *vice versa*, but a thermodynamic stabilization of the reduced form would clearly favour reduction prior to substrate binding. The large positive change in the reduction potential for both enzymes suggests that there is a significant stabilization of the ferrous form when substrate is bound. This stabilization could also play a physiological role in keeping the proteins reduced, and therefore active, when L-Trp is present.

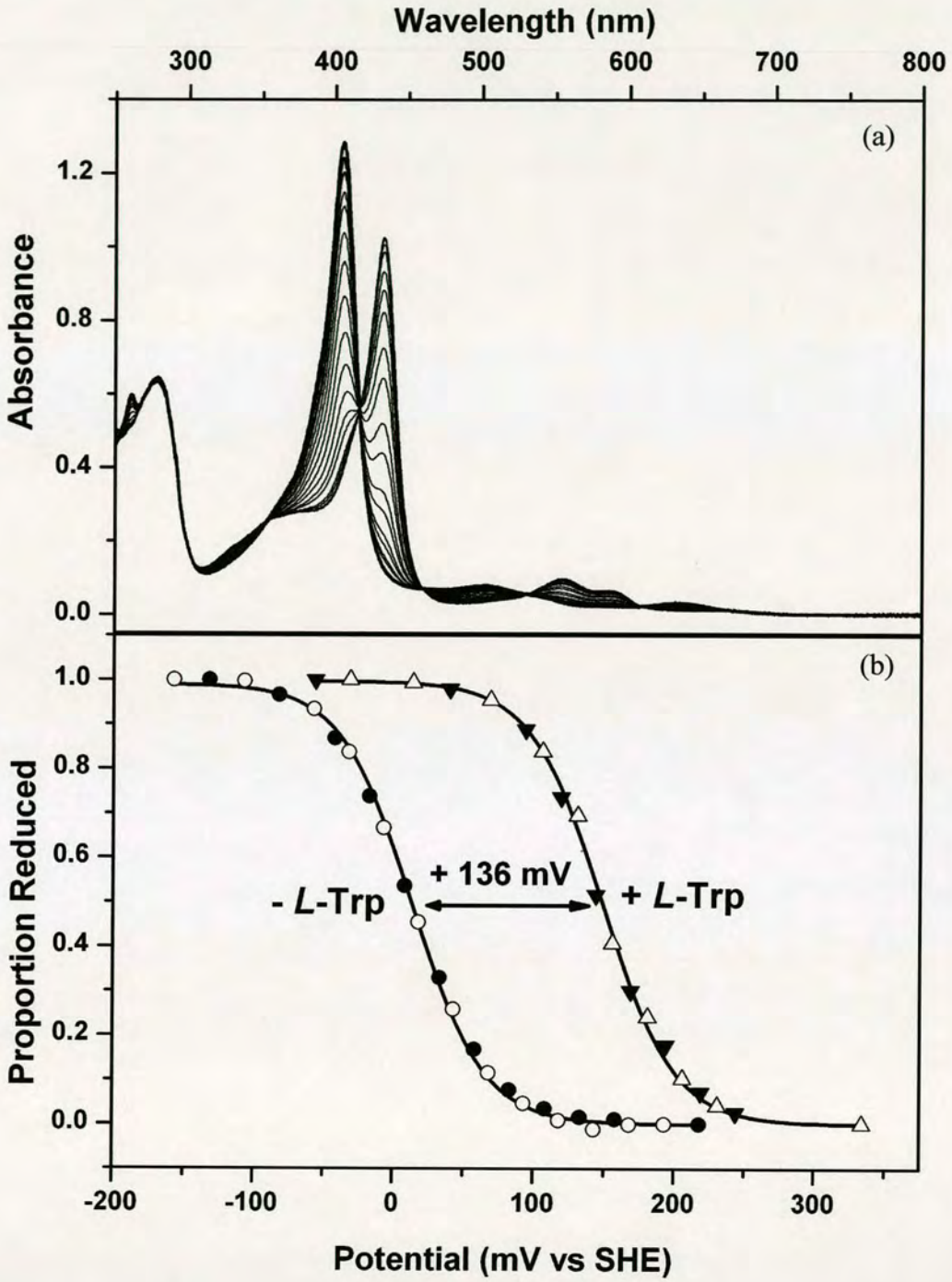

Figure 3.17 (a) Change in WTTDO spectrum on oxidation and reduction by electrochemical potential. The 405 nm peak is the oxidised protein, which gradually shifts to 430 nm on reduction and vice versa, (b) oxidative (▲and ●) and reductive (Δ and ○) potential sweeps on WTTDO, with and without L-Trp present. Curves are fitted to the Nernst equation, giving one electron equilibrium reduction potentials for the heme group with and without L-Trp.

Table 3.4 Electrochemical midpoint reduction potentials (mV vs. SHE)

Enzyme	Substrate	Substrate-free E_{mid}	Substrate Bound E_{mid}	ΔE_{mid}
X.campestris TDO (1)	L-Trp	8 ± 5	144 ± 6	+136
Rat liver TDO (100)	L-Trp	+100	+160	+60
H. sapiens TDO (77)	L-Trp	-92 ± 3	-76 ± 6	+16
H. sapiens IDO[α] (78, 102)	L-Trp	-30 ± 4 (-63)	16 ± 3	+46 (+79)
S. oneidensis IDO[β]	L-Trp	-105	-74 ± 2	+ 31
PrnB (6)	L-Trp	-109	-243	-134
PrnB (6)	7-Cl-L-trp	-109	-195	-86

[α] *Two potentials are quoted for H.sapiens IDO in separate studies*
[β] *Unpublished data*
(Note potentials for H .sapiens IDO, H. sapiens TDO and rat liver TDO obtained at pH 7.0, and those for X. campestris TDO, S. oneidensis IDO and PrnB were obtained at pH 7.5).

3.12 Conclusions

The structure of catalytically active, ferrous xcTDO in complex with L-Trp has been determined to 1.6 Å. In addition, the structure of the catalytically inactive, substrate-free oxidised xcTDO has been determined to 2.7 Å. These structures show the substrate binding interactions at the active-site and reveal that TDO is an induced-fit enzyme, with significant reorganisation of the active-site upon substrate binding.

The crystal structure of wtTDO has revealed a histidine residue is present at position 55, near to the active site, hydrogen bonding to the nitrogen of the indole ring, in an analogous position to a serine residue in human IDO (serine 167) (87). As a base is not present for proton abstraction in IDO, suggesting that substitution of histidine 55 in xcTDO to alanine or serine could reveal whether a base is necessary for catalysis.

TDO displays robust L-Trp activity with little variation of k_{cat} values occurring with pH, indicating that a catalytic base may not be required for catalysis. In addition catalytic turnover of L-Trp by wtTDO in deuterated conditions gave a k_{cat} value identical to that obtained in non-deuterated solvent, supporting this theory.

The binding characteristics of small molecules to TDO suggest that the amine group of tryptophan is important in the binding of small molecules, such as CO or O_2. The amine group of L-Trp plays a role in the binding of CO, and it can be hypothesised that it will also play a role in the binding of O_2 in the ternary complex. This correlates with the active-site arrangement in the L-Trp bound crystal structure. The amine group coordinates to a water molecule, which is predicted to lie in the position where the distal atom of dioxygen will reside in the Michaelis complex

A thousand fold increase in the L-Trp binding affinity is observed upon enzyme reduction (K_d Fe(III) = 3800 μM, K_d Fe(II) = 4μM), disfavouring the unproductive binding of L-Trp to the oxidized enzyme. This is confirmed by electrochemical data which shows a large, positive shift in reduction potential (ΔE_{mid} = 136 mV) in the presence of L-Trp, which correlates with the increase in affinity for L-Trp on reduction. These data show that there is a significant stabilization of the ferrous form when substrate is bound. This stabilization could also play a physiological role to keep the protein reduced, and therefore active, when L-Trp is present.

Chapter 4

The Role of Histidine 55

4.1 Introduction

It has been proposed that the catalytic mechanism for TDO and IDO involves the base-catalyzed deprotonation of the indole nitrogen of the substrate (131). The results discussed in the previous chapter show that in xcTDO histidine 55 hydrogen bonds to L-Trp and could possibly act as an active site base (1). This chapter reports the crystallographic and biochemical study of two TDO mutants, where the active-site residue histidine 55 has been substituted by alanine (H55A) and serine (H55S). These structural data, in conjunction with potentiometric and kinetic studies on the mutants, is used to resolve the question of whether an active site base is necessary for catalytic activity in TDO and to provide information on the molecular mechanism used by TDO to control substrate binding.

4.2 Results

4.2.1 SDS-PAGE

The H55A and H55S mutants of TDO were expressed and purified as described in Chapter 2, and produced a yield of approximately 70-100 mg of purified enzyme per litre of culture. Denaturing SDS-PAGE analysis of the purified enzyme sample is shown in Figure 3.1 (Chapter 3). Wide main bands are observed at ~ 35 kDa, corresponding to monomeric H55A and H55S and two bands at ~65 kDa and ~70 kDa, both corresponding to dimeric H55A and S mutants (as explained for wild-type TDO by mass spectrometry in Section 3.2.1). The purified enzyme samples produced absorption spectra with characteristic Soret absorption maxima at 405 nm, corresponding to oxidised H55A and H55S. No peak was observed at 430 nm, indicating that the enzymes purified in the oxidised form only.

4.3 Concentration and Heme Content Determination

The concentration of all protein samples was determined using the Bradford assay (110), as described in Section 2.5.1. Heme incorporation was greater than 95% for all H55A samples tested when the results were compared to those calculated by the Bradford assay and greater than 90% for all H55S samples. These results correlate with those obtained for wtTDO, and both mutants can be assumed to contain one heme per monomer. These data allowed the calculation of the extinction coefficients for the main Soret peaks of ferric and ferrous H55A and H55S, and these are displayed in Table 2.1.

4.4 Spectroscopic Characterisation

The UV–vis absorbance spectra for this family of proteins are characteristic of *b*-type heme-containing proteins with an axial histidine ligand. Spectrochemical data are shown in Table 4.1 for wtTDO, H55A and H55S proteins. Both H55A and H55S enzymes display similar spectra to wtTDO in both the ferric and the ferrous state, with and without substrate bound.

The spectra of the ferric forms of H55A and H55S are consistent with high-spin heme species, exactly the same as for wtTDO (Figure 3.2). Reduction of ferric H55A and H55S results in a red-shift in the Soret band (from ~405 to ~431 nm) and the formation of two peaks in the visible region (555 and ~588 nm) analogous to wtTDO (Figure 3.2).

Table 4.1 Spectroscopic data relating to wtTDO, H55A and H55S proteins. Peak positions are given in nm

Derivative	*X. campestris* wtTDO(1)	*X. campestris* H55A	*X. campestris* H55S
Fe^{3+}	405, 503, 633	405, 503, 633	404, 500, 633
Fe^{3+} - L-Trp	405, 585	405, 595sh	404, 498, 600
Fe^{2+}	431, 555, 588	431, 555, 588	431, 555, 586
Fe^{2+} - L-Trp	433, 555, 588	432, 555, 588	432, 555, 586
Fe^{2+} - CO	419, 541, 568	419, 539, 568	418, 521, 549
Fe^{2+} - NO	418, 545, 574	418, 545, 573	418, 544, 573
Fe^{3+} - CN^-	418, 538, 570^{sh}	419, 538, 570sh	419, 539, 567sh

^{sh} = shoulder

4.5 Crystallography

All crystallisation procedures, data collection and data analysis on the H55A and H55S mutants of xcTDO were performed by Dr Chiara Bruckmann, Laura Campbell and Dr Chris Mowat (2).

Crystals of the H55A and H55S mutants in the oxidised state, in the presence of substrate, were grown in aerobic conditions as described in Section 2.13.3. It was possible to obtain crystals of oxidised H55A and H55S mutant enzymes in complex with L-Trp due to the much greater affinity of L-Trp for the oxidised mutant enzymes compared to wtTDO (see Section 4.6). For the H55A mutant a data set was solved to a resolution of 2.15 Å, whilst for H55S the resolution was to 1.90 Å. The atomic coordinates have been deposited in the Protein Data Bank, accession codes 3BK9 (H55A) and 3EO8 (H55S) (2).

4.5.1 Comparison of the overall structures to wtTDO

The structure of wtTDO has been previously described (Sections 1.7 and 3.5). The average root mean square fit of all backbone atoms between all monomers of the H55A and H55S models, and wtTDO (PDB code 2NW8) is 0.6-0.8 Å, indicating no major differences between the three protein structures.

For both the H55A and H55S enzymes the N-terminal region is better defined than in the wtTDO structure. In the wtTDO structures, the N-terminus is only resolved from the 17^{th} amino acid upwards as the enzyme is lacking these residues due to protelytic cleavage, as shown in the mass spectrometry. In both of the histidine substituted enzymes the N-terminus is resolved from the 7^{th} amino acid upwards. The increased definition of the N-terminal region shows that these residues (7-21) interact with the flexible loop region which is involved in substrate binding (residues 250–260).

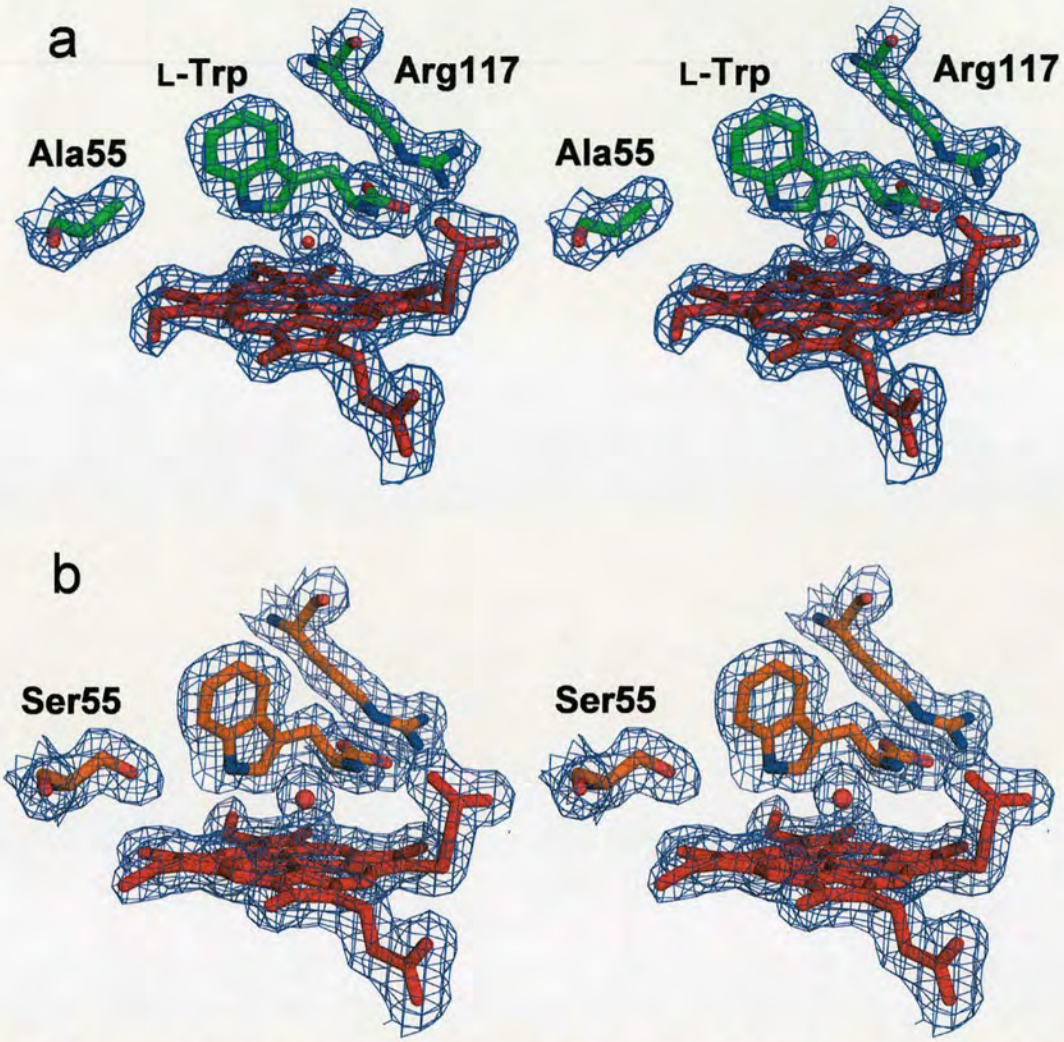

Figure 4.1 Stereoview of electron density around the heme, bound L-Trp, arginine 117, and residue 55 at the active site of (a) H55A and (b) H55S.

4.5.2 Active-Site Structure

The binding orientation of L-Trp at active site of the H55A mutant enzyme is slightly different from that observed in the wtTDO structure and stereoviews of electron density at the active-sites of H55A and H55S are shown in Figure 4.1(a) and (b).

The bound L-Trp molecules in the H55A and H55S mutant enzymes are shifted towards the side chain of residue 55 relative to the position of L-Trp in the wild-type enzyme. An overlay of the active sites of WT TDO, H55A and H55S is shown in Figure 4.2. Due to the substitution of histidine 55 by alanine or serine the hydrogen bonding interaction between residue 55 and the substrate indole nitrogen atom is lost. The positions of the side chains of other active-site residues are unperturbed by either substitution or the resultant change in substrate orientation. In particular, substrate carboxylate interactions with tyrosine 113, arginine 117 and the heme 7-propionate moiety are maintained in both mutant enzymes. Furthermore, the van der Waals interactions between the substrate indole ring and residues Phe 51, Tyr 24 and 27 and Leu 28 (the latter three belonging to the N-terminal arm of the adjacent monomer) are conserved in both mutant enzymes.

The active sites of wtTDO and both the H55A and H55S mutant enzymes contain a water molecule above the distal face of the heme, shown in Figure 4.3. In all three enzymes this water is H-bonded to the ammonium group of L-Trp and Gly 125, but is too far ($\geq$ 2.7 Å) from the heme iron to be a ligand. Further to this, an additional water molecule is found in the active site of the H55A and H55S mutant enzymes (water B in Figure 4.3) in a position which would be sterically inhibited by histidine 55 in wtTDO. In the H55A mutant enzyme water B is H-bonded to the substrate indole nitrogen, but in the H55S model water B is instead H-bonded to the side chain hydroxyl group of serine 55, which is too far away (~3.4 Å) from L-Trp to maintain a hydrogen-bonding interaction.

In wtTDO the histidine 55 imidazole moiety hydrogen bonds to a water molecule in the substrate-free ferrous state, which is displaced upon binding of substrate. The removal of the histidine side chain in either mutant enzyme would almost certainly result in the absence of a water molecule in such a position.

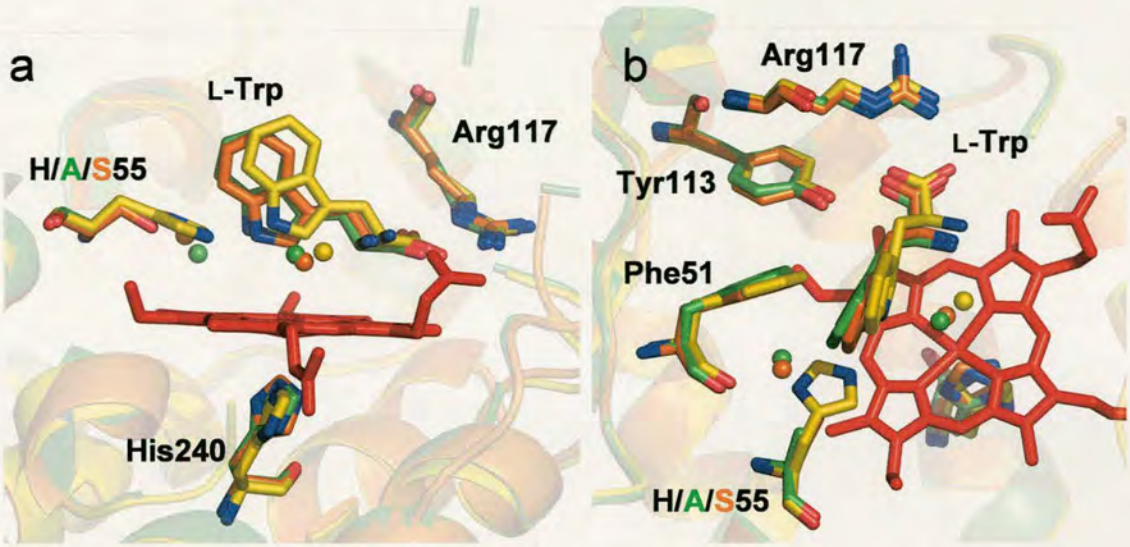

Figure 4.2 An overlay of the active site region of WT TDO (yellow), H55A (green), and H55S (orange) TDO viewed from the side (a) and from above (b). The L-Trp from the H55A enzyme (in green) is rotated toward alanine/ serine 55 and the heme, relative to the position of the substrate in WT TDO (yellow). The H-bond between histidine 55 and the substrate is lost as a result of the substitution by alanine.

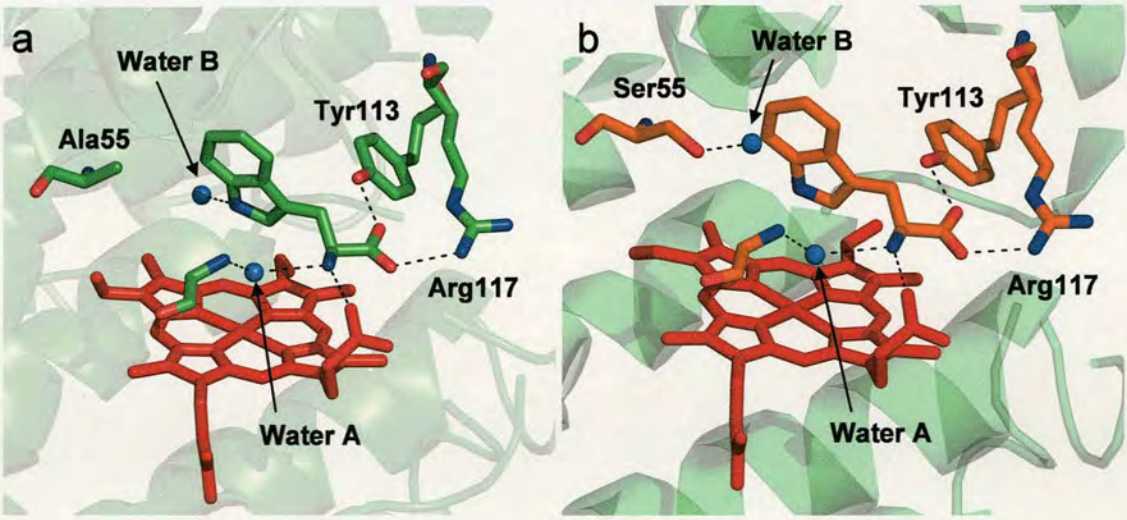

Figure 4.3 The active site of (a) H55A and (b) H55S. Hydrogen bonding interactions are indicated by dashed lines. The subtly different positions of water B in the mutant enzymes can be seen.

4.5.3 A Potential Allosteric Binding Site

An interesting finding in the structure of the substrate-bound ferrous wtTDO was the existence of a second L-Trp binding site in the tetrameric interface, and it is possible that this represents an allosteric site (Section 1.8) (1). In the structures of the H55A and H55S mutant enzyme these interfacial sites bind four L-Trp molecules per tetramer interacting with arginine 85, lysine 92 and aspartate 228 from one monomer and lysine 86 from another. (It should be noted that the H55A unit cell contains two tetramers, only one of which has four L-Trp molecules bound at the interfacial sites)

4.6 Substrate Binding

Substrate binding titrations were performed as described in Section 2.6, and the results are shown in Table 4.2. In wtTDO there is a large increase in the affinity of the enzyme for L-Trp for ferrous *vs.* ferric enzyme (K_d Fe^{3+} = 3.8 mM, K_d Fe^{2+} = 4.1 μM) (1). This is in contrast to recent findings for human TDO, where there was found to be little discrimination of binding between the ferric and the ferrous enzyme (77). For both mutant proteins this effect is essentially destroyed, with only a small increase shown in the affinity of the ferrous enzyme for L-Trp relative to ferric. This trend in K_d is repeated for other substrates. These findings suggest that one role of histidine 55 is to disfavour substrate binding to the oxidised protein, and its removal increases binding affinity by a factor >300. It can therefore be hypothesised that histidine 55 is responsible for controlling the binding affinity of the active site for L-Trp, effectively gating the binding of substrate to wtTDO. In this way histidine 55 greatly disfavours the mechanistically unproductive binding of L-Trp to the oxidized enzyme, promoting the productive binding of L-Trp to the reduced enzyme.

Table 4.2 Binding Constants

	wtTDO (K_d)		H55A (K_d)		H55S (K_d)	
Substrate	Fe^{3+} (μM)	Fe^{2+} (μM)	Fe^{3+} (μM)	Fe^{2+} (μM)	Fe^{3+} (μM)	Fe^{2+} (μM)
L-Trp	3840 ± 140	4.1 ± 0.2	11.8 ± 0.2	3.7 ± 1.3	18.4 ± 3.0	5.3 ± 1.0
6-F-D/L-Trp	1510 ± 80	<1.00‡	165 ± 44	73.0 ± 3.0	86 ± 12	6.2 ± 0.9
6-Me-D/L-Trp	>1650	>200	75 ± 11	40 ± 6	> 200	73 ± 15
5-F- D/L-Trp	2450 ± 420	<1.00‡	67 ± 20	9.0 ± 1.7	73.4 ± 5.0	<5.0‡
5-Me-D/L-Trp	>2500	51 ± 7	103 ± 10	83 ± 7	> 300	197 ± 18

‡ Binding too tight to be measured

4.7.1 Steady State Turnover Kinetics

H55A and H55S mutant enzymes show catalytic activity toward L-Trp, 6-F- D/L-Trp, 5-F-D/L-Trp, 5-methyl-D/L-tryptophan and 6-methyl-D/L-tryptophan only. Kinetic parameters are shown in Table 4.3, and there is about a 7-fold decrease in k_{cat} values, compared to wtTDO, for both mutant enzymes. Catalytic activity is observed only for the ferrous enzyme in wtTDO and its mutant forms.

The substitution of histidine 55 might have been expected to render the enzyme inactive if a base is required in the catalytic cycle, but the possibility that a water molecule could be bound in the vacant space made by the substitution of histidine 55 must be considered. This water molecule could possibly act as an active site base dependent on its pKa in the active site. A water molecule is found near this position in both the mutant enzymes, but it is not optimally aligned for the deprotonation of L-Trp. It is also located 3.3 Å away from the indole nitrogen atom, outside the range of a normal hydrogen bonding interactions, and we propose that it plays no role in the catalytic cycle. These data and the relative insensitivity of the wtTDO k_{cat} to pH support the idea that histidine 55 or a solvent molecule is not required to deprotonate the indole nitrogen atom. In IDO where the active site is devoid of solvent, the equivalent residue to histidine 55 is serine 167, which is unlikely to act as a catalytic base. Turnover still occurs, and like TDO k_{cat} is observed to be insensitive to pH.

The decrease in k_{cat} for L-Trp oxidation in both the H55A and H55S mutants may be explained by the movement of L-Trp in the active site. It can be seen from the crystal structures that for both mutants L-Trp has rotated towards the substituted amino acid (and away from the iron atom) relative to the position of L-Trp in wtTDO. The L-Trp indole ring has also shifted towards the heme. These movements are accompanied by a slight increase in the substrate K_m values, implying a small decrease in the stability of the Michaelis complex. The rotation has resulted in the displacement of tryptophan indole ring from the dioxygen binding site, thus decreasing overlap of the molecular orbitals involved in catalysis. The transition state for the reaction will be less stable, thus increasing the activation energy for catalysis. This will decrease the turnover rates for both mutants compared to wtTDO.

Table 4.3 Steady-State Kinetic Data

	wtTDO		H55A		H55S	
Substrate	k_{cat} (s^{-1})	K_m (μM)	k_{cat} (s^{-1})	K_m (μM)	k_{cat} (s^{-1})	K_m (μM)
L-Trp	19.5 ± 1.2	114 ± 1	2.86 ± 0.10	133 ± 7	2.60 ± 0.01	197 ± 2
6-F- D/L-Trp	37 ± 1	186 ± 12	3.78 ± 0.10	195 ± 1	3.80 ± 0.04	546 ± 36
6-Me-D/L-Trp	41 ± 1	980 ± 50	1.65 ± 0.03	386 ± 4	4.66 ± 0.18	1980 ± 170
5-F- D/L-Trp	2.4 ± 0.1	100 ± 6	0.68 ± 0.14	194 ± 25	0.80 ± 0.01	183 ± 12
5-Me-D/L-Trp	3.6 ± 0.1	357 ± 12	0.40 ± 0.01	395 ± 20	1.45 ± 0.01	1300 ± 20

4.7.2 LC-MS Analysis of Products

LC-MS analysis was used to detect products produced upon catalytic turnover of L-Trp by H55A and H55S, as described in Section 2.11. The equipment was calibrated to detect L-kynurenine (209 Da), N-formylkynurenine (237 Da) and L-Trp (205 Da). LC-MS analysis of the products of turnover for H55A and H55S respectively are shown in Figures 4.4 and 4.5. It can be seen that both the product N-formylkynurenine, and the reactant L-Trp are present in solution for both enzymes, showing that dioxygenation of L-Trp is occurring. Additionally a small quantity of the hydrolysed product, L-kynurenine is also detected in solution.

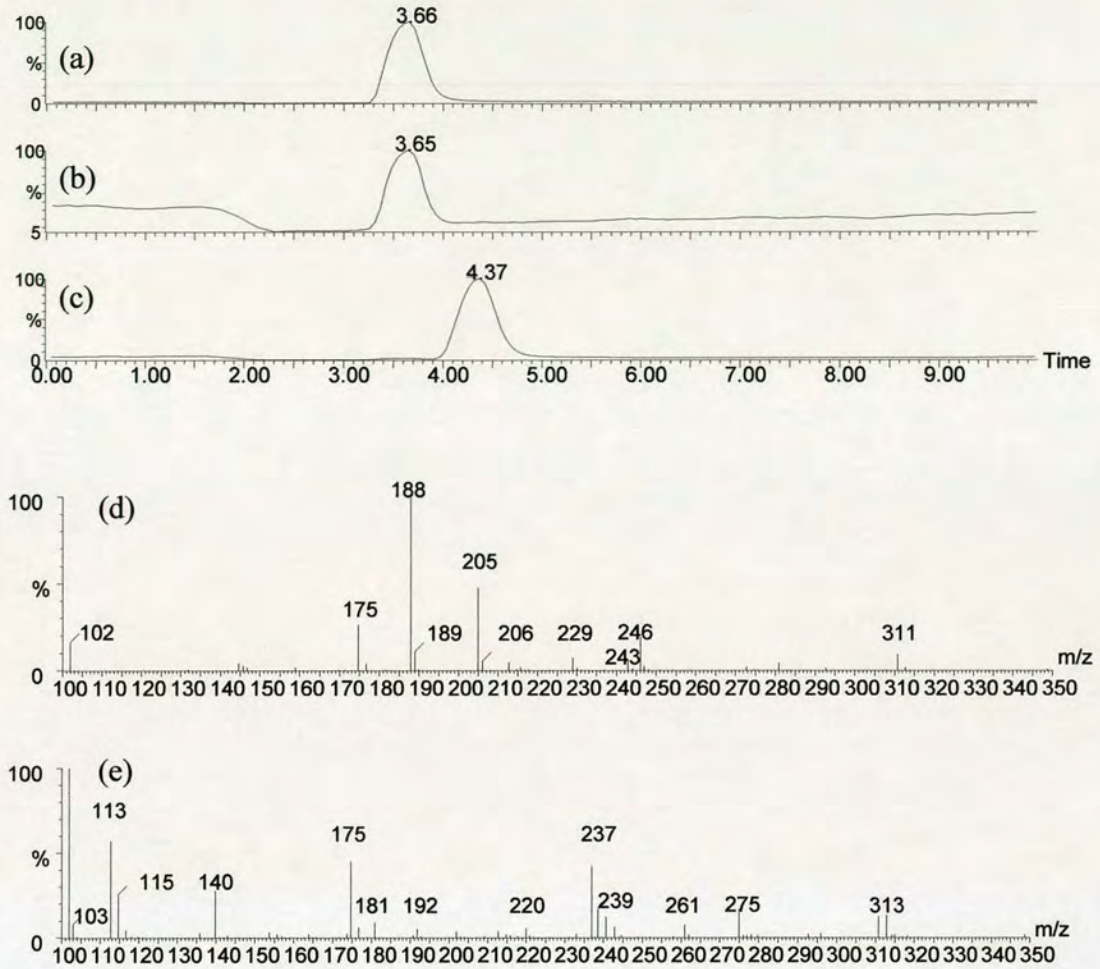

Figure 4.4 LC-MS analysis of H55A L-Trp turnover products, (a) LC trace calibrated to detect the ($M+H^+$) ion of L-Kynurenine (209 Da) vs. time, (b) LC trace calibrated to detect the ($M+H^+$) ion of N-formylkynurenine (237 Da) vs. time, (c) LC trace calibrated to detect the ($M+H^+$) ion of L-Trp (205 Da) vs. time, (d) MS of the ($M+H^+$) ion of L-Trp peak detected in (c), (e) MS of the ($M+H^+$) ion of N-formylkynurenine peak detected in (b).

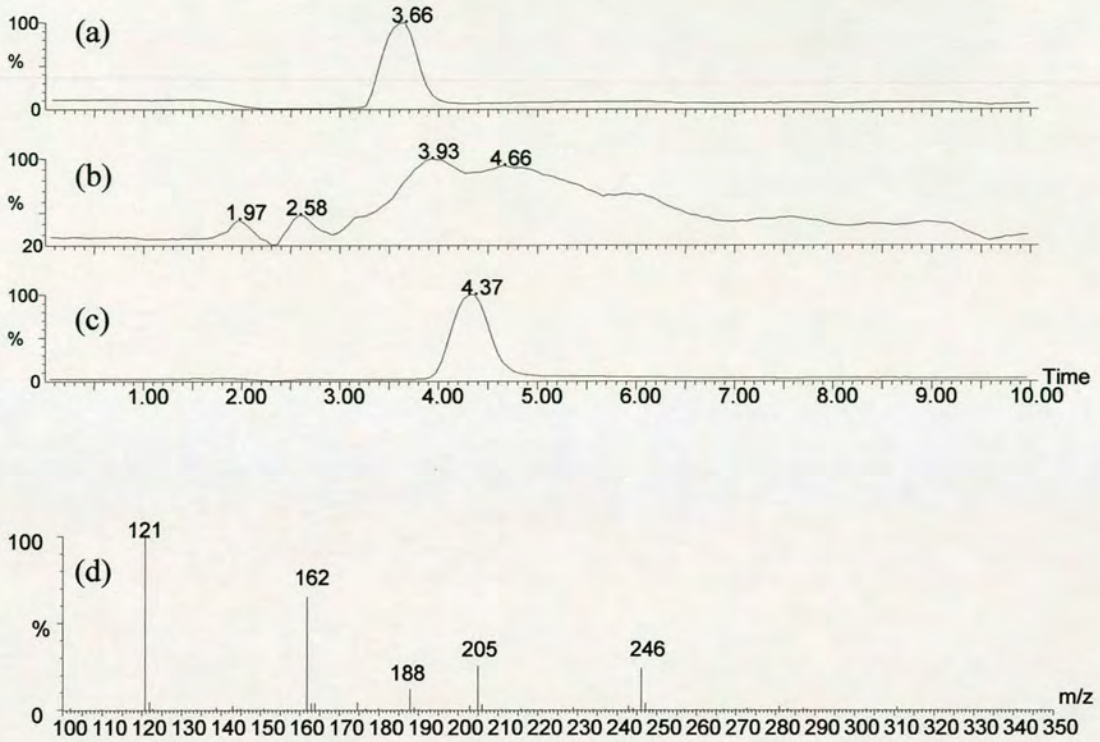

Figure 4.5 LC-MS analysis of H55S L-Trp turnover products, (a) LC trace calibrated to detect the ($M+H^+$) ion of L-Kynurenine (209 Da) vs. time, (b) LC trace calibrated to detect the ($M+H^+$) ion of N-formylkynurenine (237 Da) vs. time, (c) LC trace calibrated to detect the ($M+H^+$) ion of L-Trp (205 Da) vs. time, (d) MS of the ($M+H^+$) ion of L-Trp peak detected in (c).

4.7.3 MS-MS Analysis of Products

MS-MS analysis was conducted on the same samples as those used for LC-MS. The data produced reconfirms that L-Trp, N-formylkynurenine and L-kynurenine are found in the samples. MS-MS analysis for H55A and H55S turnover is shown in Figures F.2 and F.3 in Appendix F. These data confirm that the product of the reaction of H55A or H55S mutant enzyme with L-Trp is N-formylkynurenine, and that no other products are observed to be formed.

4.8 Oxy-Ferrous Complex Formation

WtTDO has an ordered catalytic cycle in which the reduced enzyme-substrate complex must be formed prior to O_2 binding for turnover to occur (4). No (Fe^{2+}-O_2) complex is observed in the absence of substrate (77). Addition of oxygen to ferrous wtTDO or the mutant forms in the absence of substrate leads to direct decay to the ferric state. This is also the case for human TDO, suggesting that instability of the ferrous-oxy species may be common in TDO species (77, 104). The similar L-Trp binding affinity of the reduced mutant enzymes compared to wtTDO (3.7 and 5.2 μM versus 4.1 μM) and similar K_m values for substrates shows that all enzymes can bind substrate then dioxygen in productive ternary complex formation

Formation and decay of the oxyferrous ternary species for the H55A and H55S mutants proceeds in an analogous manner to wtTDO (Section 3.9, Figure 3.10 (a) and (b)). The (Fe^{2+}- L-Trp) binary complex binds O_2, producing the oxyferrous ternary complex (Fe^{2+}- L-Trp -O_2), with a corresponding shift in the Soret peak to 419 nm. This then decays to N-formylkynurenine (shown by an increase in absorbance at 321 nm) and ferrous enzyme (displaying a Soret peak at 432 nm). These species are also observed with 6-F-D/L-Trp as the substrate, but when 5-F- D/L-Trp is employed, some uncoupling is seen. This leads to production of the inactive ferric enzyme and the superoxide anion (O_2^-), and release of the substrate in the same manner as wtTDO.

The initial rates of formation of the ternary complexes are slower for H55A and H55S compared to wtTDO, with rate constants of approximately 50 s^{-1} compared to 100 s^{-1} for wtTDO. Oxyferrous decay parallels this with rate constants of 0.4 s^{-1} and 2 s^{-1} for the mutant enzymes and wtTDO respectively. This indicates that neither substitution destabilises the ternary complex significantly, but because the rate of decay is decreased compared to wtTDO, this correlates with higher activation energy for catalysis due to the movement of the indole ring destabilising the transition state.

4.9 Steady-State turnover at Varying Oxygen Concentrations

Figure 4.6 shows how the observed rate constant for turnover is dependent on dioxygen concentration, $[O_2]$, under saturating L-Trp concentrations (25 mM). In phosphate buffer (pH 7.5) at 25 °C, K_m (O_2) is approximately 120 μM whilst the rate of L-Trp turnover by WT TDO is only 60% of maximum. However, in the case of the H55A and H55S mutant enzymes, the turnover rate is nearly maximal (Table 4.4). These data seem contrary to the Michaelis model that predicts a lower O_2 binding affinity for the mutant forms.

Substrate inhibition is observed at high oxygen concentrations for both mutant forms, whilst none is observed for wtTDO. This unexpected result may be plausibly explained by the lower rate of decay and subsequent slower expulsion of product from the active site by the mutant enzymes. As the active site cavity is larger due to the removal of histidine and its replacement by alanine or serine in the mutant forms, the product, N-formylkynurenine, may be less readily expelled at high oxygen concentrations and dioxygen may be able to bind before the product has left. This would trap the product in the active site, causing inhibition of catalytic activity.

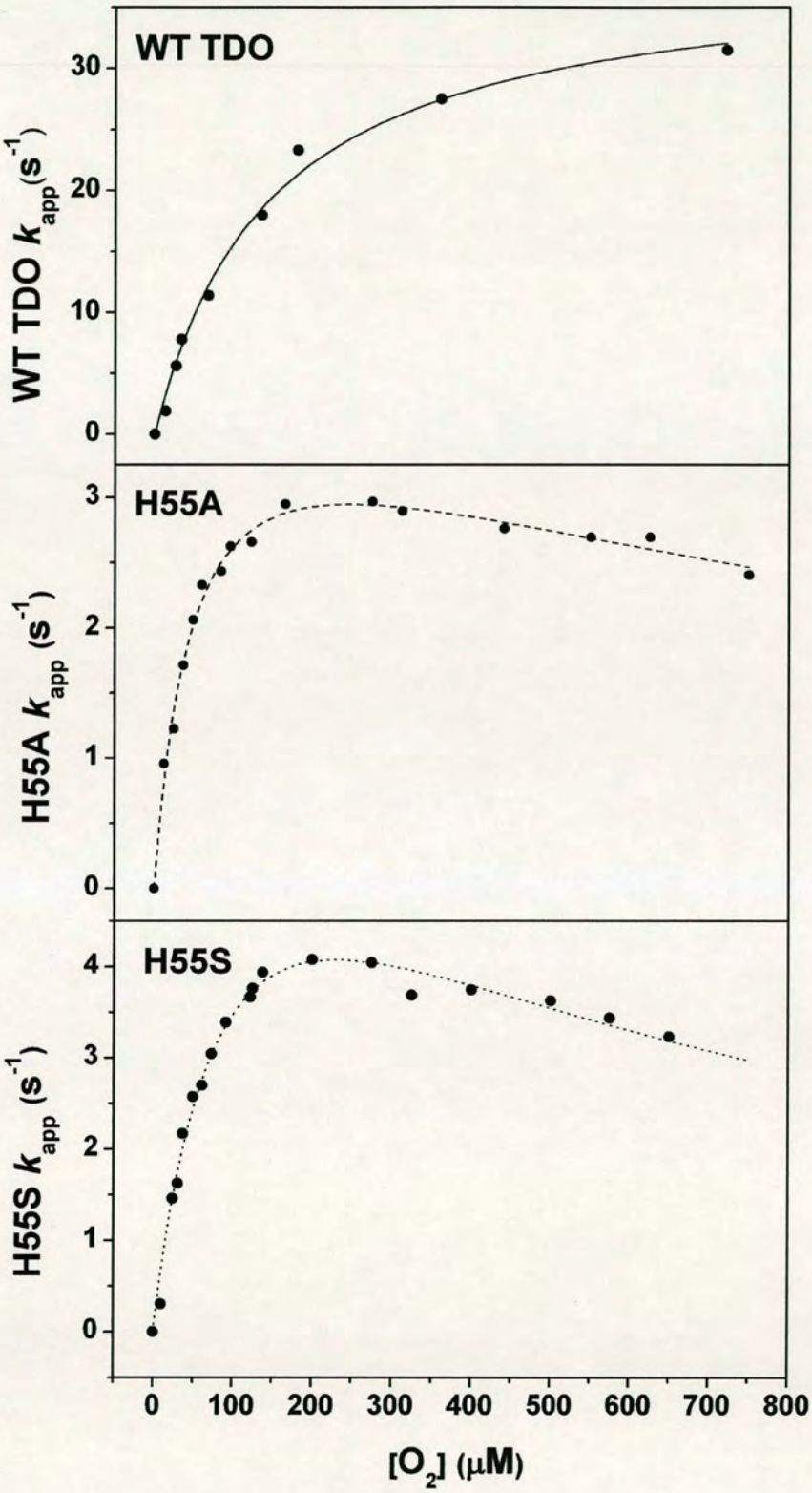

Figure 4.6 Plot of the observed steady-state turnover rate ($k_{apparent}$) versus O_2 concentration for wild type TDO (top), H55A (middle) and H55S (bottom) mutant forms.

Table 4.4 Oxygen dependence of steady-state turnover of L-tryptophan by wtTDO and its mutants.

	wtTDO	H55A	H55S
k_{max} (s^{-1})	35.4 ± 0.9	3.86 ± 0.26	7.88 ± 0.60
K_m (μM)	119 ± 2	45.7 ± 5.6	99 ± 16
K_i (μM)	----	1380 ± 140	480 ± 50

Table 4.5 Electrochemical midpoint reduction potentials (mV vs. SHE)

Enzyme	Substrate	Substrate-free E_{mid}	Substrate Bound E_{mid}	ΔE_{mid}
X.campestris TDO(1)	L-Trp	8 ± 5	144 ± 6	+136
H55A (2)	L-Trp	64 ± 3	87 ± 2	+23
H55S (2)	L-Trp	44 ± 2	101 ± 2	+57
H. sapiens IDO(78, 102)	L-Trp	-30 ± 4 (-63)	16 ± 3	+46 (+79)

4. 10 Electrochemical Studies

Electrochemical data for wtTDO and the H55A and H55S mutant enzymes are shown in Figure 4.7 and the measured midpoint potentials are displayed in Table 4.5. There is a much smaller shift in the reduction potential upon binding of substrate ($\Delta E_{mid\ H55A}$= +23 mV) ($\Delta E_{mid\ H55S}$= +57 mV) for the mutant enzymes compared to wtTDO ($\Delta E_{mid\ WT}$ = +136 mV). The shift in reduction potential of 23 mV for the H55A mutant enzyme almost perfectly correlates with the increase in affinity for L-Trp for ferrous vs. the ferric form (K_d (Fe (II)) = 3.7 μM vs. K_d (Fe (III)) = 11.8 μM), both giving an estimated ΔΔG of 3.5 kJ mol^{-1}. In fact, the difference in these ΔΔG values calculated for wtTDO and the H55A mutant enzyme is approximately 11.5 kJ mol^{-1}, within the range of energies for a single hydrogen bond. The data are less clear for H55S, with a 57 mV shift in the reduction potential on L-Trp binding. The increase in affinity for L-Trp to the ferrous H55S vs. the ferric give an estimated ΔΔG of 5.5 kJ mol^{-1}. It is possible that the lower affinity of oxidised wtTDO for substrate may be attributed to subtle changes in the structure of the active site (in terms of the hydrogen-bonding pattern) between the oxidised and reduced enzymes. Binding of L-Trp ejects solvent from the active site and results in the formation of a hydrogen-bond between His55 and the N1 atom of the indole L-Trp moiety.

In the H55A mutant the alanine side chain is unable to form the same hydrogen-bonds that His55 can in wtTDO. Consequently there may be less rearrangement of the active site hydrogen-bonding interactions to allow L-Trp binding, and the K_d for substrate binding to ferric enzyme is correspondingly low. All other amino-acid interactions binding L-Trp to the active site are analogous to wtTDO. Consequently, the absence of significant oxidation-state-dependent changes in the active site of H55A results in decreased specificity of binding to the oxidised or reduced enzyme.

The case is similar for the H55S mutant enzyme since the serine side chain is unable to form the same hydrogen-bonds that His55 can in wtTDO. It is possible that the serine could form a hydrogen-bonding interaction with a nearby solvent molecule (water 250), but the data suggest that less rearrangement of active site hydrogen-bonding interactions is necessary to allow L-Trp binding than for wtTDO.

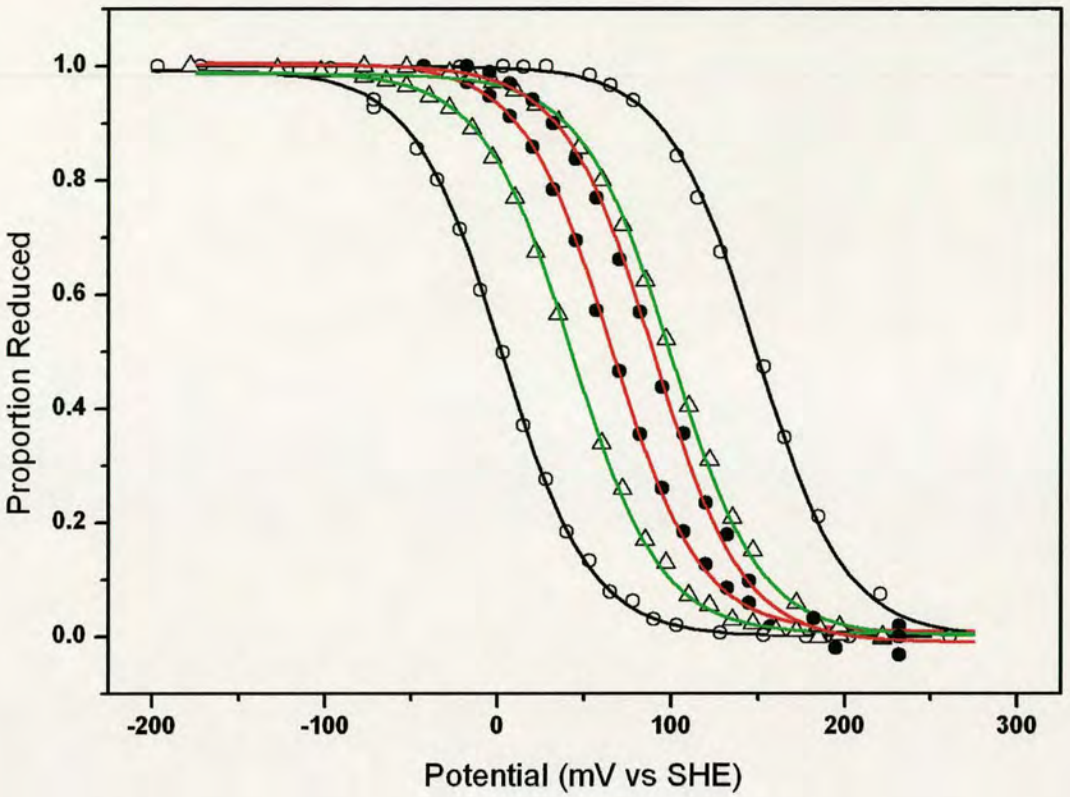

Figure 4.7 OTTLE potentiometric curves for wild type TDO (black line, open circles), H55A mutant (red line, closed circles) and H55S (green line, open triangles) with (right hand plots) and without (left hand plots) L-Trp substrate present (± L-Trp). Each curve is produced from both reduction and oxidation of the layer of interest.

4.11 Conclusions

In this chapter it has been investigated whether a putative active site base, histidine 55, is necessary for catalytic activity in TDO. The data presented show that in the mutant enzymes H55A and H55S, turnover still occurs. This indicates clearly that histidine 55 is not an essential base. Instead, a different role for histidine 55 in controlling substrate binding at the active site has been revealed. Based on structural, kinetic and electrochemical data we have proposed that the role of histidine 55 is to prevent the formation of the non-productive ferric enzyme-substrate complex. This is most likely achieved by histidine 55 controlling the water content of the substrate-free active site.

Chapter 5

1-Methyl-tryptophan

5. 1 Introduction

IDO plays an important role in the body's immune response, and has been implicated as a potential drug target for cancer treatments (43, 49). The most-studied inhibitor of IDO is 1-Me-Trp, a competitive inhibitor that exists as two stereoisomers, 1-Me-D-Trp and 1-Me-L-Trp (51). It is unclear as to which isomer effects the greatest inhibitory response *in vitro*, as discussed in Section 1.3.3, and this is currently a pertinent question since IDO is a therapeutic target for the development of new anticancer, transplant and HIV drugs (47, 132, 133). However, previous studies have shown 1-Me-D/L-Trp to be ineffective against TDO activity, raising the question as to the biochemical differences between the enzymes.

5.2 1-Methyl-tryptophan Binding

Attempts were made to bind both 1-Me-L-Trp and 1-Me-D-Trp to wtTDO and the H55A and H55S mutant forms, in both the ferric and the ferrous states. 1-Me-D-Trp does not appear to bind to any of the enzymes in either the ferric or the ferrous states, and no K_d values could be obtained. The K_d of 1-Me-L-Trp binding to wtTDO, H55A and H55S in both the ferric and the ferrous states was measured as described in Section 2.6, and results are displayed in Table 5.1.

It can be seen that 1-Me-L-Trp binds weakly to wtTDO in both the ferric and the ferrous forms, with a K_d of more than 200 μM in the ferrous form. In comparison, L-Trp binds with a K_d of only 4.1 μM. This can be explained by considering the active-site L-Trp binding interactions in wtTDO. In wtTDO the indole nitrogen of L-Trp is directly hydrogen-bonded to the His55 side chain with a distance of 2.7 Å between the nitrogen of His55 and the indole N1 atom. The addition of a methyl group to L-

Trp to produce 1-Me-L-Trp would clearly cause a steric clash with this residue, with a distance of only 1.5 Å between the methyl carbon and the nitrogen atom of His 55 (Figure 5.1). Therefore, 1-Me-L-Trp does not bind tightly to TDO, and does not inhibit its action. A comparison of the active-sites of TDO and IDO explains the differences in the inhibition of activity by 1-Me-Trp. His55 is replaced by Ser167 in hIDO (87), which creates a small pocket that can accommodate the 1-methyl group. This enables 1-Me-Trp to bind to IDO and inhibit activity. However, as IDO binds and dioxygenates both D- and L-Trp (102), we cannot rule out that both 1-Me –D-Trp and 1-Me-L-Trp could inhibit its action.

For the H55A and H55S mutants of TDO, it can be seen that the binding constants of 1-Me-L-Trp to the ferric and ferrous enzymes are approximately equal to those of L-Trp (2). Since the His55 residue has been substituted for the smaller alanine and serine residues in these mutant enzymes, a larger binding cavity has been created at the indole nitrogen. An additional methyl group on the indole nitrogen atom of L-Trp is easily accommodated in the larger binding cavity, and subsequently the K_d for 1-Me-L-Trp is similar to that of L-Trp.

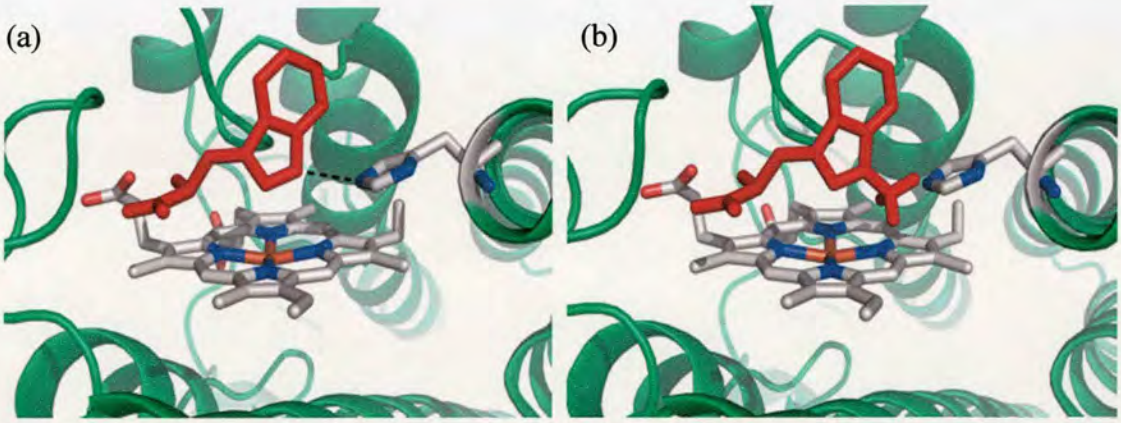

Figure 5.1 Active site of xcTDO (a) L-Trp binding (b) 1-Me-L-Trp binding model. The N1-methyl group clearly sterically clashes with the His55 residue.

5.3 Steady-State Kinetics

Steady-state turnover assays (at pH 7.5) for oxidation of 1-Me-D-Trp and 1-Me-L-Trp were performed as described in Section 2.7, but, no activity was detected in wt or mutant TDOs when utilizing 1-Me-D-Trp (purchased from sigma) as a substrate. No consistent dioxygenation of 1-Me-L-Trp could be observed for wtTDO by spectrophotometric methods, however a small amount of product (N-Me-formylkynurenine) was detected by LC-MS (Figure 5.2).). It was concluded that the rate of 1-Me-L-Trp turnover by wtTDO must be less than 0.001 s^{-1}, similar to the background level of activity from the assay components, and no accurate measurements could be obtained. In comparison, both H55A and H55S displayed robust activity toward 1-Me-L-Trp. The recorded k_{cat} was 1.7 % of that of L-Trp by H55A, and 2.0 % of that for L-Trp by H55S (Table 5.2).

On addition of 1-Me-D-Trp or 1-Me-L-Trp to wtTDO there is no inhibition of wtTDO catalytic activity upon L-Trp, as previously reported [4]. Similarly, on addition of 1-Me-D-Trp to H55A or H55S no inhibition is observed. However, addition of 1-Me-L-Trp to H55A or H55S leads to competitive inhibition of L-Trp activity.

These differences in catalytic activity between the wild-type protein and its mutant forms can be explained by the binding affinity of 1-Me-L-Trp. WtTDO is unable to bind 1-Me-L-Trp tightly in its active site, due to a steric clash between the methyl group and His 55 (Figure 5.1). Histidine 55 would need to be reoriented, or 1-Me-L-Trp adopt a different conformation to allow binding and dioxygenation. In comparison, H55A and H55S can bind 1-Me-L-Trp tightly, forming stable Michaelis complexes that undergo catalytic activity. The calculated K_m for the H55A and H55S, 1-Me-L-Trp Michaelis complexes are lower than those for L-Trp, indicating their stability.

5.4 LC-MS

LC-MS analysis was used to detect products produced upon catalytic turnover of 1-Me-L-Trp by wtTDO, H55A and H55S as described in Section 2.11. The equipment was calibrated to detect 1-Me-kynurenine (223 Da), 1-Me-formylkynurenine (251 Da) and 1-Me-Trp (219 Da). It should be noted that no stereochemical distinction of the products can be made by this method of analysis. LC-MS analysis is shown in Figures 5.2, 5.3 and 5.4 .

From the assay of 1-Me-L-Trp and wtTDO a very small amount of the product 1-Me-formylkynurenine is detected in the solution. However the quantity detected is insufficient to perform mass-spectrometry upon. The reactant 1-Me-(L)-Trp is the main component detected in the sample, and additionally a tiny quantity of hydrolysed 1-Me-formylkynurenine, (1-Me-kynurenine) is detected in solution. These data show that wtTDO does in fact catalyse the dioxygenation of 1-Me-Trp, but at a very slow rate.

For both the H55A and H55S mutant enzymes, the product 1-Me-formylkynurenine and the hydrolysed product 1-Me-kynurenine were detected in large quantities in solution.

5.5 MS-MS Analysis of Products

MS-MS analysis was conducted on the same sample as that used for LC-MS. The data produced reconfirms that 1-Me-Trp, 1-Me-formylkynurenine and 1-Me-kynurenine are found in the H55A and H55S catalysed samples. However, the quantities of 1-Me-formylkynurenine and 1-Me-kynurenine in the wtTDO sample were too small to be measured. MS-MS analysis is shown in Figure F.4, F.5 and F.6, Appendix F.

Table 5.1 1-Me-L-trp Binding to wtTDO and its mutants

	wtTDO (K_d) (1)		H55A (K_d) (2)		H55S (K_d) (2)	
Substrate	Fe^{3+} (μM)	Fe^{2+} (μM)	Fe^{3+} (μM)	Fe^{2+} (μM)	Fe^{3+} (μM)	Fe^{2+} (μM)
L-Trp	3840 ± 140	4.1 ± 0.2	11.8 ± 0.2	3.7 ± 1.3	18.4 ± 3.0	5.25 ± 1.0
1-Me-L-Trp	>2000	(>200)	15.3 ± 2.2	3.6 ± 0.7	16.2 ± 3.3	2.5 ± 0.38

Table 5.2 Steady-state kinetics for 1-Me-L-Trp turnover by xcTDO, H55A and H55S.

	wtTDO (1)		H55A (2)		H55S (2)	
Substrate	k_{cat} (s^{-1})	K_m (μM)	k_{cat} (s^{-1})	K_m (μM)	k_{cat} (s^{-1})	K_m (μM)
L-Trp	19.5 ± 1.2	114 ± 1	2.86 ± 0.10	133 ± 7	2.60 ± 0.01	197 ± 2
1-Me-L-Trp	-[α]	-	0.048 ± 0.011	59 ± 16	0.052 ± 0.009	70 ± 11

[α] *Some turnover was on occasion recorded, up to a value of 0.002 s^{-1}, but results were inconsistent and similar to the baseline rate of turnover recorded for the assay components.*

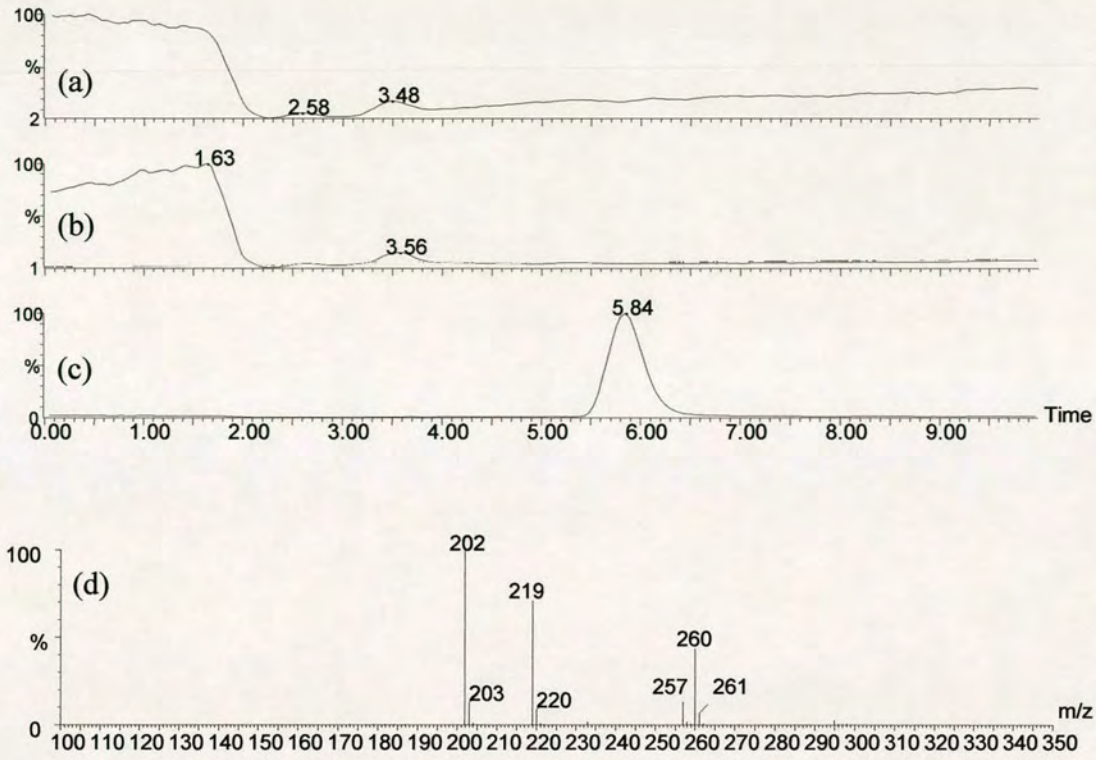

Figure 5.2 LC-MS analysis of wtTDO turnover products, (a) LC trace calibrated to detect 1-Me-Kynurenine (223 Da) against time, (b) LC trace calibrated to detect 1-Me-formylkynurenine (251 Da) against time, (c) LC trace calibrated to detect 1-Me-Trp (219 Da) against time, (d) MS of L-Trp peak detected in (c).

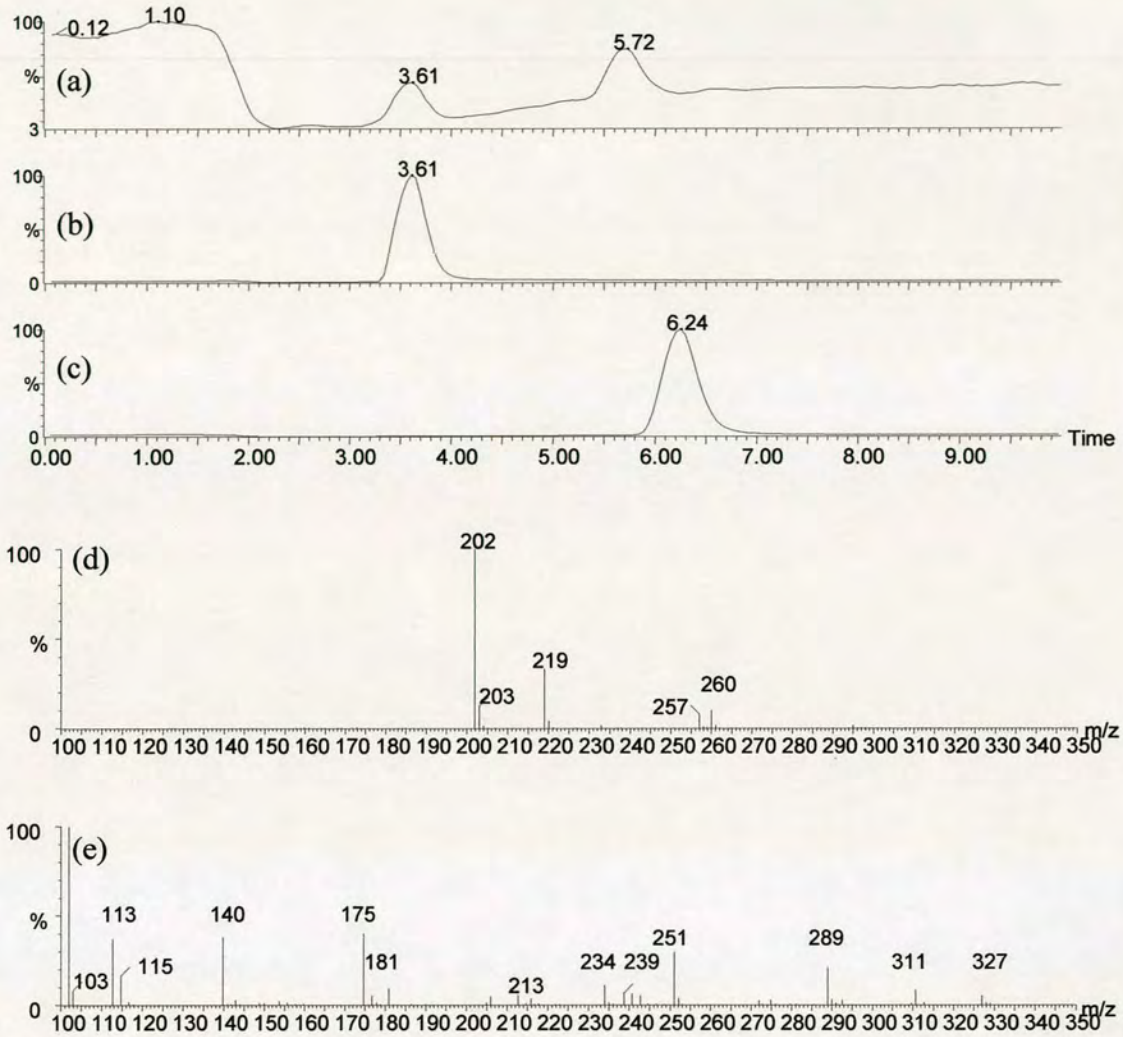

Figure 5.3 LC-MS analysis of H55A turnover products, (a) LC trace calibrated to detect 1-Me-Kynurenine (223 Da) against time, (b) LC trace calibrated to detect 1-Me-formylkynurenine (251 Da) against time, (c) LC trace calibrated to detect 1-Me-Trp (219 Da) against time, (d) MS of L-Trp peak detected in (c), (e) MS of 1-Me-formylkynurenine peak detected in (d).

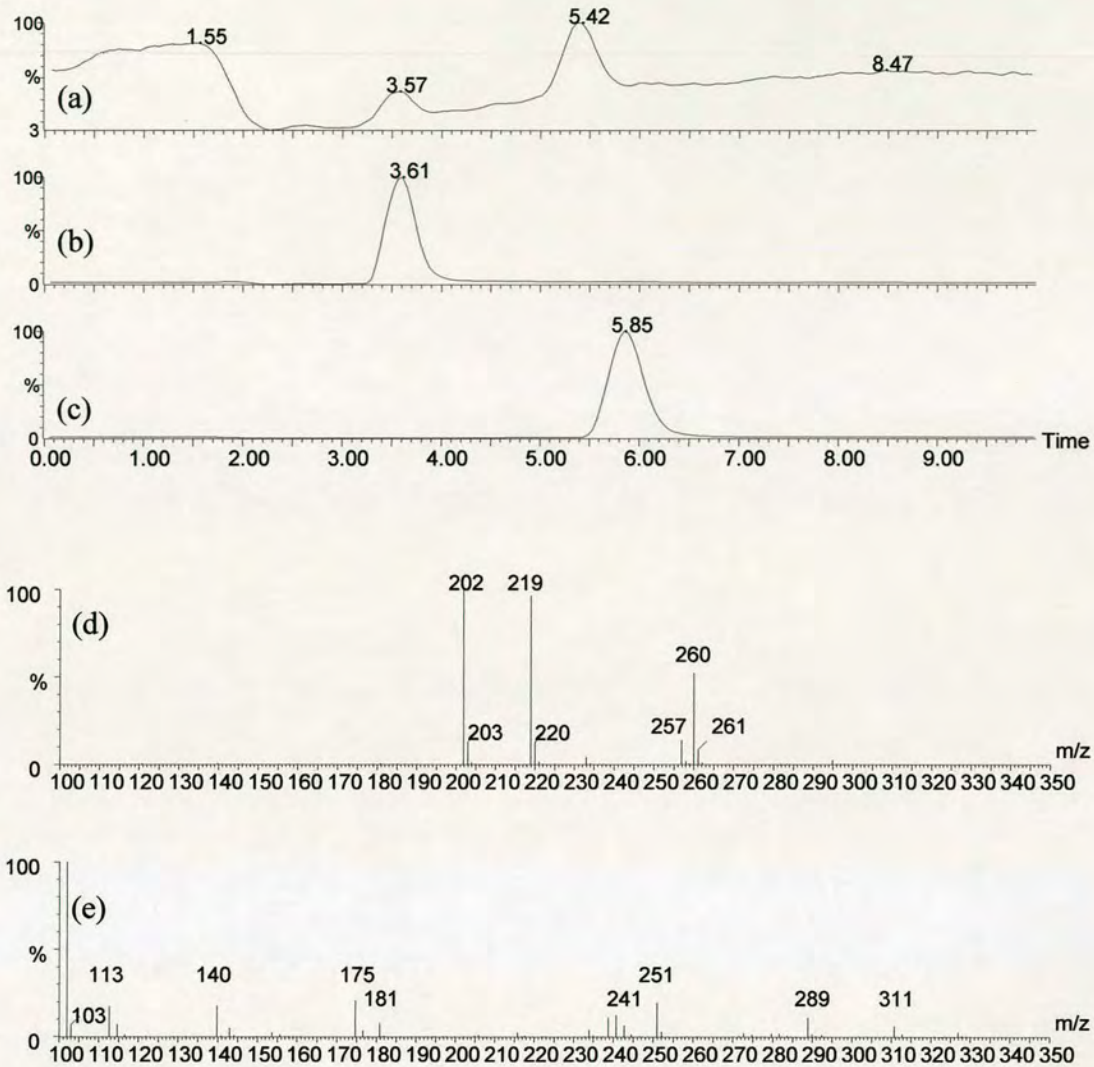

Figure 5.4 LC-MS analysis of H55S turnover products, , (a) LC trace calibrated to detect 1-Me-Kynurenine (223 Da) against time, (b) LC trace calibrated to detect 1-Me-formylkynurenine (251 Da) against time, (c) LC trace calibrated to detect 1-Me-Trp (219 Da) against time, (d) MS of 1-Me-Trp peak detected in (c), (e) MS of 1-Me-formylkynurenine peak detected in (b).

5.6 Conclusions

Analysis of wtTDO and the H55A and H55S mutant forms has shown that they all catalyse the dioxygenation of 1-Me-L-Trp, a substrate which is unable to undergo deprotonation during dioxygen activation. The catalytic differences are explained by comparison of the active sites of the enzymes, and support the proposal that a catalytic base is not necessary for enzymatic activity.

The possible catalytic mechanisms employed by TDO were discussed in Section 1.6. Dioxygen activation is proposed to occur via either base-catalysed attack, an "oxygen-ene" type rearrangement to a hydroperoxy intermediate, or by direct electrophilic or radical addition (89). In the previous chapter it has become clear that a catalytic base is not essential to catalytic activity, leaving two possible mechanisms (2). As 1-Me-L-Trp (or 1-Me-D-Trp) is unable to undergo an "oxygen-ene" type rearrangement, the dioxygenation of 1-Me-L-Trp must proceed via a direct electrophilic or radical addition pathway.

The ability of TDO and its mutants to catalyse the dioxygenation of 1-Me-L-Trp has currently been submitted for publication. Based on these results it can be theorised that IDO may display catalytic activity toward 1-Me-L-Trp. IDO contains a serine residue (serine 167 in hIDO) in an analogous place to histidine in TDO (histidine 55 in xcTDO), a much smaller residue that does not hydrogen bond to the indole nitrogen atom of L-Trp. Methylation of the indole nitrogen atom should be easily accommodated in the active-site pocket, as modelled in Figure 5.1. Therefore catalytic activity should be able to proceed unhindered, analogous to the histidine 55 substituted forms of TDO. In addition, as IDO displays wider substrate specificity than TDO, catalysing the dioxygenation of L-Trp and D-Trp it can be theorised that in addition to utilising 1-Me-L-Trp as a substrate, IDO may also be able to utilise 1-Me-D-Trp. As it is currently unknown as to which stereoisomer of 1-Me-Trp effects the greatest inhibition of activity *in vivo*, and this study raises questions as to the usefulness of 1-Me-D/L-Trp as an inhibitor in cancer treatments.

Chapter 6

Conclusions

6.1 TDO and IDO

Tryptophan 2,3-dioxygenase and indoleamine 2,3-dioxygenase constitute an important, yet relatively poorly understood, family of heme-containing enzymes and in this thesis the first crystal structure of a tryptophan 2,3-dioxygenase enzyme in complex with substrate is reported (1). The structure of catalytically active, ferrous *X. campestris* TDO in complex with L-Trp has been determined to 1.6 Å. The crystal structure of *xc*TDO displays a high level of overall structural similarity with *R. metallidurans* TDO (88), *H. sapiens* IDO (77, 102), and *S. oneidensis* sIDO (1), revealing striking evolutionary conservation between enzymes and contributing to the understanding of the structure-activity relationships in this important family of heme dioxygenases.

Our structural studies have defined the binding mode of the substrate L-Trp to TDO, identifying key interactions that are responsible for its substrate specificity. Hydrophobic interactions and hydrogen bonding interactions between the bound substrate and active-site residues are fundamental to the substrate specificity of TDO, and reveal the structural basis for the stereospecificity of this important enzyme (1).

Structural investigation of TDO has also revealed induced-fit behaviour upon substrate binding to the active site. This induced-fit behaviour is confirmed by biophysical studies and appears crucial for the exclusion of water from the active site and for stabilizing the enzyme in the presence of the substrates.

Active-site mutants where histidine 55 was replaced by alanine or serine (H55A and H55S) were created and crystal structures of the H55A and H55S mutant forms in complex with L-Trp were determined to 2.15 Å and 1.90 Å resolutions respectively (2). Kinetic, electrochemical and structural data indicate that His55 is not an active site base, but instead reveal a role for His55 in controlling substrate binding at the

active site. A thousand fold increase in the L-Trp binding affinity is observed upon enzyme reduction for xcTDO (K_d Fe(III) = 3800 μM, K_d Fe(II) = 4 μM), disfavouring the mechanistically unproductive binding of L-Trp to the oxidized enzyme. Substitution of histidine 55 greatly increases the affinity of the oxidised enzyme for substrate. Only a small change in the L-Trp binding affinity is observed upon enzyme reduction for H55A (K_d, Fe(III) = 12 μM, K_d Fe(II) = 4 μM) and H55S (K_d, Fe(III) = 18 μM, K_d Fe(II) = 5 μM)), allowing unproductive binding of L-Trp to the oxidized enzyme. Histidine 55 regulates the binding of L-Trp to the enzyme, allowing precise control of the mechanism of turnover.

Further analysis of wtTDO and the H55A and H55S mutant forms has shown that they all catalyse the dioxygenation of 1-Me-L-Trp, a substrate which is unable to undergo proton transfer during dioxygen activation. These catalytic differences are explained by comparison of the active sites of the enzymes, and support the proposal that a catalytic base is not necessary for enzymatic activity. In addition, these data provide new insight into the use of 1-Me-Trp as an inhibitor of IDO activity in cancer treatments (43). The ability of TDO and its mutants to catalyse the dioxygenation of 1-Me-L-Trp is currently unpublished. It is theorised that IDO may be expected to display a similar catalytic activity toward 1-Me-L-Trp and 1-Me-D-Trp due to its wider substrate specificity. It is currently unknown as to which stereoisomer of 1-Me-Trp effects the greatest inhibition of activity *in vivo* (51), and this study raises questions as to the usefulness of 1-Me-D/L-Trp as an inhibitor.

6.2 Catalytic Mechanism

The catalytic mechanisms employed by TDO and IDO have not yet been fully elucidated and a number of mechanisms for tryptophan dioxygenation have been proposed (89). The structural and biochemical characterisation of xcTDO presented in this thesis has shown a number of these proposals to be inaccurate. Therefore a general reaction mechanism for dioxygenation of L-Trp by TDO and IDO, based on the presented data, is summarized below and shown in Figure 6.1.

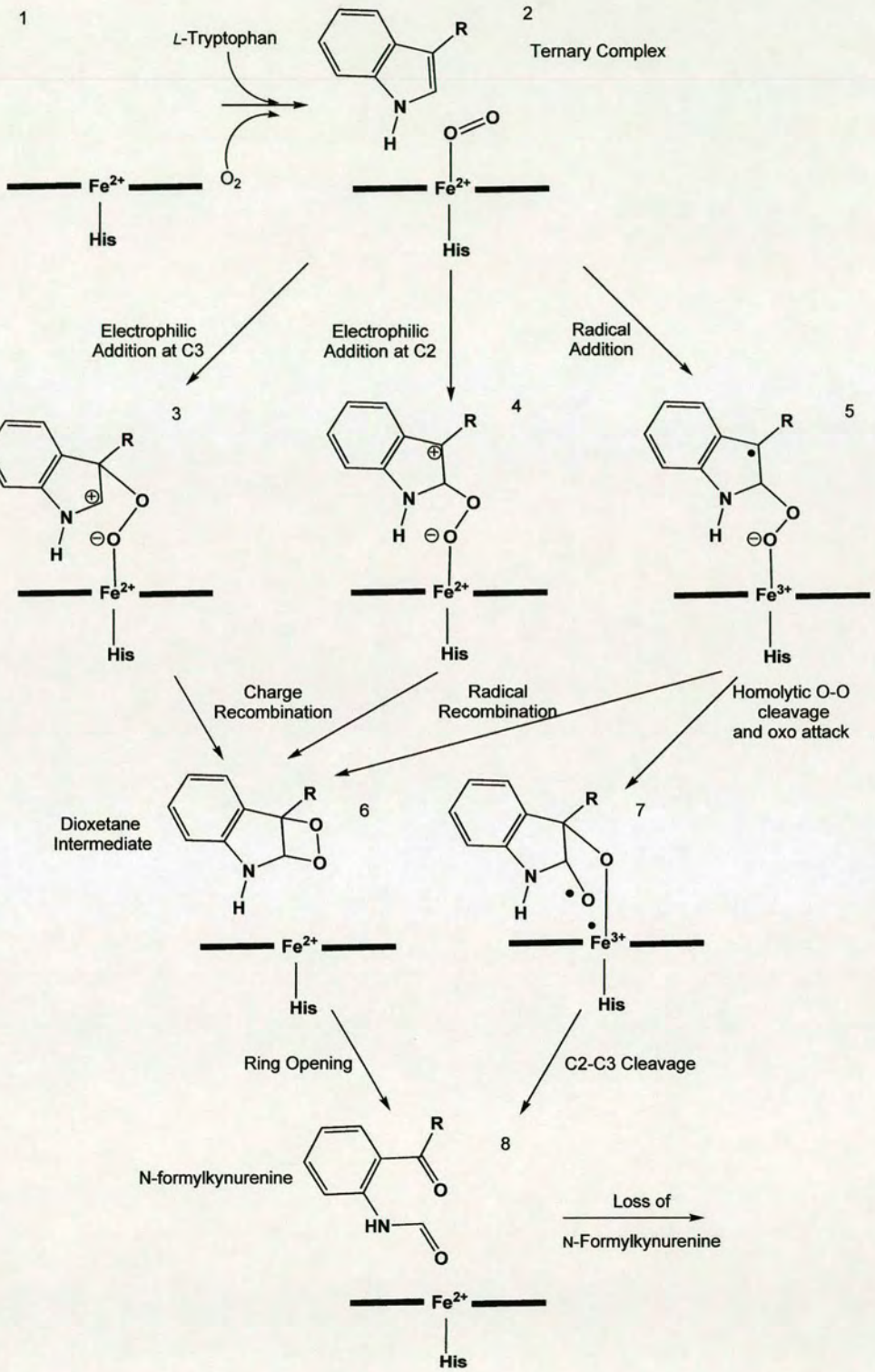

Figure 6.1 Proposed catalytic mechanism of L-Trp dioxygenation by TDO and IDO.

Formation of the Ternary Complex

In the active site of wtTDO histidine 55 greatly decreases the affinity of the oxidised enzyme for substrate and regulates the binding of dioxygen (1, 2). This prevents unproductive coupling of dioxygen to the ferrous enzyme that would lead to the production of superoxide and the dead-end ferric complex. This result confirms that substrate must bind to the enzyme first before dioxygen binding can take place, to form the ternary complex.

Dioxygen Activation

Before a crystal structure of TDO was published, previous work on rat liver TDO implicated that a histidine residue played a critical role in the dioxygenation of L-Trp at the active-site (122). These results implied that a base may be necessary for catalytic activity to occur via deprotonation of the indole proton, facilitating nucleophilic attack from the C3 position of the indole ring to the bound dioxygen (4, 88). The crystal structure of wtTDO has revealed that a histidine residue is present at position 55, near to the active site, coordinating to the nitrogen of the indole ring, in an analogous position to a serine residue in *H.sapiens* IDO (87). As a base is not present for proton abstraction in IDO, substitution of histidine 55 to alanine and serine was conducted to probe the function of histidine 55. Substitution of histidine 55 has shown that the histidine residue is not critical to TDO activity, because the mutant proteins still catalyse L-Trp dioxygenation. These data and the relative insensitivity of k_{cat} to pH indicate that a base is not necessary for catalytic function, disfavouring this route of dioxygen activation.

Modelling of the Michaelis complex for xcTDO, based on the structure of the catalytically active ferrous protein in complex with L-Trp, has shown that the highly hydrophobic active-site is devoid of solvent molecules during catalysis, suggesting that water plays no role in dioxygen activation. This proposal seems logical as the absence of solvent or a hydrogen-bonding network from the active-site may protect

transient oxygenated species, allowing them to transfer both oxygen atoms to the substrate, rather than undergo reaction with water.

Further analysis of wtTDO, H55A and H55S mutant forms has shown that they all catalyse the dioxygenation of 1-Me-Trp, a substrate which is unable to undergo proton transfer in dioxygen activation. This result shows that dioxygen activation cannot occur by electrophilic addition concerted with proton transfer, in an "oxygen-ene" type reaction. These results are supported by DFT calculations that have predicted a very high energy barrier to the "oxygen-ene" type transition state (89).

The results presented in this thesis support initial dioxygen activation occurring *via* direct electrophilic or radical addition of the bound distal oxygen to the electron-rich indole carbon. It is proposed that in TDO and IDO, a mild oxidant Fe^{2+}-O_2 species or a Fe^{3+}-$O_2^{\bullet-}$ species reacts with a very electron-rich indole. Electrophilic addition at the C2 or C3 position of the indole, or radical recombination at the C2 position are all computed to be energetically favourable by DFT (90). The proposed mechanism of dioxygen activation shown in Figure 6.2.

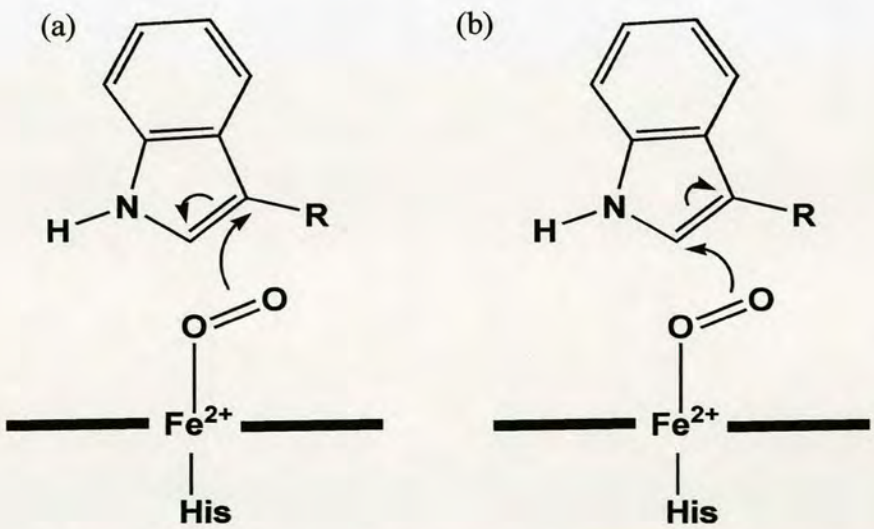

Figure 6.2 Proposed dioxygen activation intermediates, (a) direct electrophillic addition at the C3 position and at (b) the C2 position.

Rearrangement Pathway

DFT calculations have suggested that the Criegee-type rearrangement pathway requires a very high barrier from the neutral indole intermediate (90). Instead, the zwitterionic and diradical products generated from the direct addition pathways are predicted to undergo charge or radical recombination to afford the comparatively stable dioxetane intermediate. Since the results in this thesis support the direct electrophilic and diradical pathways as catalytically favourable, and do not support the formation of a hydroperoxide intermediate, a Criegee-type rearrangement must therefore be regarded as an unlikely mechanistic route. Formation of a dioxetane intermediate which can then undergo metal-catalyzed ring-opening to give the product is therefore favoured as a mechanistic pathway.

An alternative to the dioxetane formation pathway does exist - homolytic O-O bond cleavage of the radical intermediate (5) followed by oxo attack and facile C2-C3 bond cleavage could occur. However, this pathway involves the formation of a highly reactive ferryl-oxo species (64) which may lead to the formation of undesired products, and requires a number of intermediate steps in product formation, unlike the more elegant dioxetane rearrangement. Consequently this pathway appears less convincing as a possible mechanistic route, but there is no known evidence against its validity.

This study has advanced the knowledge of the biochemical and structural factors influencing the mechanism of TDO and IDO catalysis and advances our understanding of heme chemistry. However the precise catalytic mechanism employed by these important enzymes has not yet been fully elucidated and further study is necessary to fully understand their function.

6.3 Future Work

Although this study has elucidated the role of histidine 55 in substrate binding, the role of many active-site resides are currently unknown. The substitution of a number of residues, discussed below, could reveal insight into the regulation and mechanism of TDO.

Of particular interest are the amino-acid residues which coordinate to L-Trp, facilitating its precise alignment in the active-site for catalysis. The substrate binding residues arginine 113 and tyrosine 117 which interact with the amino and carboxylate moieties of L-Trp, and serine 124, which hydrogen-bonds to a water molecule in the substrate-bound crystal structure of xcTDO could be substituted to probe their function. The structure of xcTDO is composed of a "dimer of dimers" in which the N-terminus of one monomer interacts with the active-site of its partner. It is currently unknown as to what function this may play. Tyrosine 24 and tyrosine 27 of this N-terminal arm form part of the active-site pocket in the partner monomer, and their deletion or substitution should be investigated. The interfacial L-Trp binding sites discovered in the crystal structure of xcTDO suggest that this enzyme may be allosterically regulated. Site-directed mutation of key binding residues, such as lysine 92, and aspartic acid 228 in combination with identification of allosteric effectors may reveal more about this intriguing binding site.

TDO is implicated in a number of pathophysiological and physiological diseases and some studies have suggested that TDO inhibitors may be used to a treat a wide range of illnesses, including depression and ischemic brain injury (134, 135). Identification of specific inhibitors of TDO function could be beneficial in designing treatments for these conditions.

Appendix A

References

1. Forouhar, F., Anderson, J. L. R., Mowat C., G., Vorobiev S., M., Hussain, A., Abashidze, M., Bruckmann, C., Thackray S., J., Seetharaman, J., Tucker, T., Xiao, R., Ma, L.-C., Zhao, L., Acton T., B., Montelione G., T., Chapman, S., K. & Tong, L. (2007) *Proc Natl Acad Sci U S A* **104,** 473-8.
2. Thackray, S. J., Bruckmann, C., Anderson, J. L. R., Campbell, L. P., Xiao, R., Zhao, L., Mowat, C. G., Forouhar, F., Tong, L. & Chapman, S. K. (2008) *Biochem.* **47,** 10677-10684.
3. Paoli, M. & Nagai, K. (2001) *Handb. Proteins* **1,** 16-30.
4. Sono, M., Roach, M. P., Coulter, E. D. & Dawson, J. H. (1996) *Chem. Rev.* **96,** 2841-2887.
5. Unno, M., Matsui, T., Chu, G. C., Couture, M., Yoshida, T., Rousseau, D. L., Olson, J. S. & Ikeda-Saito, M. (2004) *J. Biol. Chem.* **279,** 21055-21061.
6. De Laurentis, W., Khim, L., Anderson, J. L. R., Adam, A., Phillips, R. S., Chapman, S. K., Van Pee, K.-H. & Naismith, J. H. (2007) *Biochem.* **46,** 12393-12404.
7. Schwarcz, R. (2004) *Curr. Opin. Pharmacol.* **4,** 12-17.
8. Tankiewicz, A., Pawlak, D. & Buczko, W. (2001) *Postepy Hig. Med. Dosw.* **55,** 715-731.
9. Turner, E. H., Loftis, J. M. & Blackwell, A. D. (2006) *Pharmacol. Ther.* **109,** 325-338.
10. Munn, D. H. & Mellor, A. L. (2007) *J. Clin. Invest.* **117,** 1147-1154.
11. Zamanakou, M., Germenis, A. E. & Karanikas, V. (2007) *Immunol. Lett.* **111,** 69-75.
12. Kotake, Y. & Masayama, I. (1936) *Z. physiol. Chem.* **243,** 237-44.
13. Miuller, N. & Schwarz, M. J. (2007) *J Neural Transm Suppl,* 269-80.
14. Altar, C. A., Bennett, B. L., Wallace, R. & Yuwiler, A. (1983) *Biochem. Pharmacol.* **32,** 979-84.

15. Yamamoto, S. & Hayaishi, O. (1967) *J Biol Chem* **242,** 5260-6.
16. Shimizu, T., Nomiyama, S., Hirata, F. & Hayaishi, O. (1978) *J. Biol. Chem.* **253,** 4700-6.
17. Mellor, A. L. & Munn, D. H. (2004) *Nat. Rev. Immunol.* **4,** 762-774.
18. Murray, M. F. (2007) *Curr. Drug Metab.* **8,** 197-200.
19. Ball, H. J., Sanchez-Perez, A., Weiser, S., Austin, C. J. D., Astelbauer, F., Miu, J., McQuillan, J. A., Stocker, R., Jermiin, L. S. & Hunt, N. H. (2007) *Gene* **396,** 203-213.
20. Eugene Myers, S. A., Warren Gish, David J. Lipman and Webb Miller (1990).
21. Hammer, P. E., Burd, W., Hill, D. S., Ligon, J. M. & van Pee, K. H. (1999) *FEMS Microbio. Lett.* **180,** 39-44.
22. Kafasla, P., Bouzarelou, D., Frillingos, S. & Sophianopoulou, V. (2007) *Fungal Genetics Bio.* **44,** 615-626.
23. Ligon, J. M., Hill, D. S., Lam, S. T., Hammer, P. E., van Pee, K.-H. & Kirner, S. (1998) US Patent Application.
24. Takikawa, O. (2005) *Biochem. Biophys. Res. Commun.* **338,** 12-19.
25. Sanni, L. A., Thomas, S. R., Tattam, B. N., Moore, D. E., Chaudhri, G., Stocker, R. & Hunt, N. H. (1998) *Am. J. Pathol.* **152,** 611-619.
26. Platten, M., Ho, P. P., Youssef, S., Fontoura, P., Garren, H., Hur, E. M., Gupta, R., Lee, L. Y., Kidd, B. A., Robinson, W. H., Sobel, R. A., Selley, M. L. & Steinman, L. (2005) *Science* **310,** 850-855.
27. Kerr, S. J., Armati, P. J., Pemberton, L. A., Smythe, G., Tattam, B. & Brew, B. J. (1997) *Neurology* **49,** 1671-1681.
28. Takikawa, O., Truscott, R. J. W., Fukao, M. & Miwa, S. (2003) *Adv. Exp. Med. Biol.* **527,** 277-285.
29. Serbecic, N. & Beutelspacher, S. C. (2006) *Exp. Eye Res.* **82,** 416-426.
30. Takikawa, O., Littlejohn, T. K. & Truscott, R. J. W. (2001) *Exp. Eye Res.* **72,** 271-277.
31. Schroecksnadel, K., Wirleitner, B., Winkler, C. & Fuchs, D. (2006) *Clin. Chim. Acta* **364,** 82-90.

32. Mellor, A. (2005) *Biochem. Biophys. Res. Commun.* **338,** 20-24.
33. MacKenzie, C. R., Heseler, K., Mueller, A. & Daeubener, W. (2007) *Curr. Drug Metab.* **8,** 237-244.
34. Miller, C. L., Llenos, I. C., Dulay, J. R., Barillo, M. M., Yolken, R. H. & Weis, S. (2004) *Neurobiol. Dis.* **15,** 618-629.
35. Minatogawa, Y., Suzuki, S., Ando, Y., Tone, S. & Takikawa, O. (2003) *Adv. Exp. Med. Biol.* **527,** 425-434.
36. Britan, A., Maffre, V., Tone, S. & Drevet, J. R. (2006) *Cell Tissue Res.* **324,** 301-310.
37. Dai, W. & Gupta, S. L. (1990) *Biochem. Biophys. Res. Commun.* **168,** 1-8.
38. Yuasa, H. J., Takubo, M., Takahashi, A., Hasegawa, T., Noma, H. & Suzuki, T. (2007) *J. Mol. Evol.* **65,** 705-714.
39. Szanto, S., Koreny, T., Mikecz, K., Glant Tibor, T., Szekanecz, Z. & Varga, J. (2007) *Arthritis Res Ther* **9,** R50.
40. Mellor Andrew, L., Chandler, P., Lee Geon, K., Johnson, T., Keskin Derin, B., Lee, J. & Munn David, H. (2002) *J Reprod Immunol.* **57,** 143-50.
41. Suzuki, S., Tone, S., Takikawa, O., Kubo, T., Kohno, I. & Minatogawa, Y. (2001) *Biochemical J.* **355,** 425-9.
42. Tankiewicz, A., Pawlak, D., Topczewska-Bruns, J. & Buczko, W. (2003) *Adv. Exp. Med. Biol.* **527,** 409-414.
43. Prendergast, G. C. (2008) *Oncogene* **27,** 3889-3900.
44. Feder-Mengus, C., Wyler, S., Hudolin, T., Ruszat, R., Bubendorf, L., Chiarugi, A., Pittelli, M., Weber, W. P., Bachmann, A., Gasser, T. C., Sulser, T., Heberer, M., Spagnoli, G. C. & Provenzano, M. (2008) *Eur. J. Cancer* **44,** 2266-2275.
45. Hou, D.-Y., Muller, A. J., Sharma, M. D., DuHadaway, J., Banerjee, T., Johnson, M., Mellor, A. L., Prendergast, G. C. & Munn, D. H. (2007) *Cancer Res.* **67,** 792-801.
46. Muller, A. J. & Scherle, P. A. (2006) *Nat Rev Cancer* **6,** 613-625.
47. Ou, X., Cai, S., Liu, P., Zeng, J., He, Y., Wu, X. & Du, J. (2008) *J. Cancer. Res. Clin. Onc.* **134,** 525-533.

48. Ino, K., Yoshida, N., Kajiyama, H., Shibata, K., Yamamoto, E., Kidokoro, K., Takahashi, N., Terauchi, M., Nawa, A., Nomura, S., Nagasaka, T., Takikawa, O. & Kikkawa, F. (2006) *Brit. J. Cancer.* **95,** 1555-1561.

49. Kumar, S., Malachowski, W. P., DuHadaway, J. B., LaLonde, J. M., Carroll, P. J., Jaller, D., Metz, R., Prendergast, G. C. & Muller, A. J. (2008) *J. Med. Chem.* **51,** 1706-1718.

50. Okamoto, T., Tone, S., Kanoichi, H., Ohyama, F. & Minatogawa, Y. (2007) *Int. Congr. Ser.* **1304,** 352-356.

51. Lob, S., Konigsrainer, A., Schafer, R., Rammensee, H.-G., Opelz, G. & Terness, P. (2008) *Blood* **111,** 2152-2154.

52. Banerjee, T., DuHadaway, J. B., Gaspari, P., Sutanto-Ward, E., Munn, D. H., Mellor, A. L., Malachowski, W. P., Prendergast, G. C. & Muller, A. J. (2008) *Oncogene* **27,** 2851-2857.

53. Kumar, S., Jaller, D., Patel, B., LaLonde, J. M., DuHadaway, J. B., Malachowski, W. P., Prendergast, G. C. & Muller, A. J. (2008) *J. Med. Chem.* **51,** 4968-4977.

54. Jia, L., Schweikart, K., Tomaszewski, J., Page John, G., Noker Patricia, E., Buhrow Sarah, A., Reid Joel, M., Ames Matthew, M. & Munn David, H. (2008) *Food Chem Toxicol* **46,** 203-11.

55. Metz, R., DuHadaway, J. B., Kamasani, U., Laury-Kleintop, L., Muller, A. J. & Prendergast, G. C. (2007) *Cancer Res.* **67,** 7082-7087.

56. Tanaka, S. (2002) *Kawasaki Igakkaishi* **28,** 1-9.

57. Eguchi, N., Watanabe, Y., Kawanishi, K., Hashimoto, Y. & Hayaishi, O. (1984) *Arch. Biochem. Biophys.* **232,** 602-9.

58. Madge, D. J., Hazelwood, R., Iyer, R., Jones, H. T. & Salter, M. (1996) *Bioorganic & Medicinal Chemistry Letters* **6,** 857-60.

59. Salter, M., Hazelwood, R., Pogson, C. I., Iyer, R., Madge, D. J., Jones, H. T., Cooper, B. R., Cox, R. F., Wang, C. M. & Wiard, R. P. (1996) *Adv. Exp. Med. Biol.* **398,** 61-65.

60. Salter, M., Hazelwood, R., Pogson, C. I., Iyer, R. & Madge, D. J. (1995) *Biochem. Pharmacology* **49,** 1435-42.

61. Bugg, T. D. H. (2001) *Curr. Op. Chem. Bio.* **5,** 550-555.
62. Fetzner, S. (2002) *App. Microbiol. Biotech.* **60,** 243-257.
63. Rich, P. R. & Iwaki, M. (2007) *Biochem. (Moscow)* **72,** 1047-1055.
64. Groves John, T. (2006) *J Inorg Biochem* **100,** 434-47.
65. Bugg, T. D. H. & Lin, G. (2001) *Chem. Commun.* 941-952.
66. Mason, H. S., Rowlks, W. L. & Peterson, E. (1955) *J. Am. Chem. Soc.* **77,** 2914-15.
67. Hayaishi, O., Katagiri, M. & Rothberg, S. (1955) *J. Am. Chem. Soc.* **77,** 5450-1.
68. Burton, S. G. (2003) *Trends Biotech.* **21,** 543-549.
69. Ost, T. W. B. & Daff, S. (2005) *J. Biol. Chem.* **280,** 965-973.
70. Bollinger, J. M. & Krebs, C. (2006) *J. Inorg. Biochem.* **100,** 586-605.
71. Urlacher, V. B. & Schmid, R. D. (2006) *Curr. Opin. in Chem. Biol.* **10,** 156-161.
72. Zhu, Y. & Silverman, R. B. (2008) *Biochem.* **47,** 2231-2243.
73. Foster, T. L. & Caradonna, J. P. (2004) *Compr. Coord. Chem. II.* **8,** 343-368.
74. Zhang, J., Zheng, H., Groce, S. L. & Lipscomb, J. D. (2006) *J. Molecul. Cataly. A.* **251,** 54-65.
75. Kovaleva, E. G., Neibergall, M. B., Chakrabarty, S. & Lipscomb, J. D. (2007) *Acc. Chem. Res.* **40,** 475-483.
76. Palaniandavar, M. & Mayilmurugan, R. (2007) *C. R. Chim.* **10,** 366-379.
77. Basran, J., Rafice, S. A., Chauhan, N., Efimov, I., Cheesman, M. R., Ghamsari, L. & Lloyd Raven, E. (2008) *Biochem.* **47,** 4752-4760.
78. Chauhan, N., Basran, J., Efimov, I., Svistunenko, D. A., Seward, H. E., Moody, P. C. E. & Lloyd Raven, E. (2008) *Biochem.* **47,** 4761-4769.
79. Maghzal, G. J., Thomas, S. R., Hunt, N. H. & Stocker, R. (2008) *J. Biol. Chem.* **283,** 12014-12025.
80. Li, J. S., Han, Q., Fang, J., Rizzi, M., James, A. A. & Li, J. (2007) *Arch. Insect Biochem. Physiol.* **64,** 74-87.
81. Hayaishi, O., Takikawa, O. & Yoshida, R. (1990) *Prog. Inorg. Chem.* **38,** 75-95.

82. Sono, M. (1989) *J. Biol. Chem.* **264,** 1616-22.

83. Sono, M. (1990) *Biochem.* **29,** 1451-60.

84. Kobayashi, K., Hayashi, K. & Sono, M. (1989) *J. Biol. Chem.* **264,** 15280-3.

85. Leeds, J. M., Brown, P. J., McGeehan, G. M., Brown, F. K. & Wiseman, J. S. (1993) *J. Biol. Chem.* **268,** 17781-6.

86. Hamilton, G. A. (1969) *Advan. Enzymol. Relat. Areas Mol. Biol.* **32,** 55-96.

87. Sugimoto, H., Oda, S.-i., Otsuki, T., Hino, T., Yoshida, T. & Shiro, Y. (2006) *Proc. Natl. Acad. Sci.* **103,** 2611-2616.

88. Zhang, Y., Kang, S. A., Mukherjee, T., Bale, S., Crane, B. R., Begley, T. P. & Ealick, S. E. (2007) *Biochem.* **46,** 145-155.

89. Chung, L. W., Li, X., Sugimoto, H., Shiro, Y. & Morokuma, K. (2008) *J. Am. Chem. Soc.* **130,** 12299-12309.

90. Yagil, G. (1967) *Tetrahedron* **23,** 2855-61.

91. Goodey, N. M. & Benkovic, S. J. (2008) *Nat. Chem. Biol.* **4,** 474-482.

92. Traut, T. (2007) *Handb. Proteins* **1,** 470-481.

93. Voet, D. & Voet, J. G. (1995) *Biochemistry: Second Edition.*

94. Yonetani, T. & Laberge, M. (2008) *Biochim. Biophys. Acta, Proteins Proteomics,* **1784,** 1146-1158.

95. Hill, A. V. (1910) *J. Physiol. (Lond)* **40.**

96. Makino, R., Sakaguchi, K., Iizuka, T. & Ishimura, Y. (1980) *Dev. Biochem.* **16,** 179-87.

97. Walsh, H. A., Daya, S. & Whiteley, C. G. (1994) *J. Pineal Res.* **16,** 188-92.

98. Feigelson, P. & Brady, F. O. (1974) *Bioelectrochem. Bioenerg.* **1,** 67-72.

99. Henry, Y., Ishimura, Y. & Peisach, J. (1976) *J. Biol. Chem.* **251,** 1578-81.

100. Makino, R., Sakaguchi, K., Iizuka, T. & Ishimura, Y. (1980) *J. Biol. Chem.* **255,** 11883-91.

101. Uchida, K., Shimizu, T., Makino, R., Sakaguchi, K., Iizuka, T., Ishimura, Y., Nozawa, T. & Hatano, M. (1983) *J. Biol. Chem.* **258,** 2526-33.

102. Papadopoulou, N. D., Mewies, M., McLean, K. J., Seward, H. E., Svistunenko, D. A., Munro, A. W. & Raven, E. L. (2005) *Biochem.* **44,** 14318-14328.

103. Sono, M. & Dawson, J. H. (1984) *Biochim. Biophys. Acta, Protein Struct. Mol. Enzymol.* **789,** 170-87.

104. Batabyal, D. & Yeh, S.-R. (2007) *J. Am. Chem. Soc.* **129,** 15690-15701.

105. Terentis, A. C., Thomas, S. R., Takikawa, O., Littlejohn, T. K., Truscott, R. J. W., Armstrong, R. S., Yeh, S.-R. & Stocker, R. (2002) *J. Biol. Chem.* **277,** 15788-15794.

106. Samelson-Jones, B. J. & Yeh, S.-R. (2006) *Biochem.* **45,** 8527-8538.

107. Brady, F. O., Feigelson, P. & Rajagopalan, K. V. (1973) *Arch. Biochem. Biophys.* **157,** 63-72.

108. Daniels, M. J., Barber, C. E., Dow, J. M., Han, B., Liddle, S. A., Newman, M. A., Parker, J. E., Soby, S. D. & Wilson, T. G. J. (1993) *Dev. Plant Pathol.* **2,** 53-63.

109. Alvarez, A. M. (2000) *Mech. Resist. Plant Dis.* 21-52.

110. Bradford, M. M. (1976) *Anal Biochem* **72,** 248-54.

111. Berry, E. A. & Trumpower, B. L. (1987) *Anal Biochem* **161,** 1-15.

112. Glasoe, P. K. & Long, F. A. (1960) *J. Phys. Chem.* **64,** 188-90.

113. Schowen, K. B. & Schowen, R. L. (1982) *Methods Enzymol.* **87,** 551-606.

114. Ost, T. W. B., Clark, J. P., Anderson, J. L. R., Yellowlees, L. J., Daff, S. & Chapman, S. K. (2004) *J. Biol. Chem.* **279,** 48876-48882.

115. Otwinowski, Z. & Minor, W. (1997) *Methods Enzymol.* **276,** 307-326.

116. Roussel, A., and Cambillau, C. (1991).

117. Murshudov, G. N., Vagin, A. A. & Dodson, E. J. (1997) *Acta Crystallogr.* **D53,** 240-255.

118. Anonymous (1994) *Acta Crystallogr.* **50,** 760-3.

119. Adams, P. D., Grosse-Kunstleve, R. W., Hung, L.-W., Ioerger, T. R., McCoy. A. J., Moriarty, N. W., Read, R. J., Sacchettini, J. C., Sauter, N. K., and Terwilliger, T. C. (2002) *Acta Crystallogr,* **D58,** 1948-1954.

120. DeLano, W. L. (2002).

121. Merritt, E. A. & Bacon, D. J. (1997) *Methods Enzymol.* **277,** 505-524.

122. Dick, R., Murray, B. P., Reid, M. J. & Correia, M. A. (2001) *Arch. Biochem. Biophys* **392,** 71-78.

123. Ren, S., Liu, H., Licad, E. & Correia, M. A. (1996) *Arch. Biochem. Biophys* **333,** 96-102.

124. Watanabe, Y., Fujiwara, M., Yoshida, R. & Hayaishi, O. (1980) *Biochem. J.* **189,** 393-405.

125. Manandhar, S. P., Shimada, H., Nagano, S., Egawa, T. & Ishimura, Y. (2002) *International Congress Series* **1233,** 161-169.

126. Winn Peter, J., Ludemann Susanna, K., Gauges, R., Lounnas, V. & Wade Rebecca, C. (2002) *Proc Natl Acad Sci U S A* **99,** 5361-6.

127. Cowart, L. A., Falck, J. R. & Capdevila, J. H. (2001) *Arch. Biochem. Biophys.* **387,** 117-124.

128. Gondry, M., Duboist, J., Terrier, M. & Lederer, F. (2001) *Eur. J. Biochem.* **268,** 4918-4927.

129. Sukumar, N., Dewanti, A. R., Mitra, B. & Mathews, F. S. (2004) *J. Biol. Chem.* **279,** 3749-3757.

130. Rivera, M. & Zeng, Y. (2005) *J. Inorg. Biochem.* **99,** 337-354.

131. Terentis, A. C., Thomas, S. R., Takikawa, O., Littlejohn, T. K., Truscott, R. J. W., Armstrong, R. S., Yeh, S.-R. & Stocker, R. (2002) *J Biol Chem* **277,** 15788-15794.

132. Quan, J., Tan, P. H., MacDonald, A. & Friend, P. J. (2008) *Expert Opin. Biol. Ther.* **8,** 1705-1719.

133. Boasso, A., Herbeuval, J.-P., Hardy Andrew, W., Anderson Stephanie, A., Dolan Matthew, J., Fuchs, D. & Shearer Gene, M. (2007) *Blood* **109,** 3351-9.

134. Mueller, N. & Schwarz, M. J. (2007) *Molec. Psychiatry* **12,** 988-1000.

135. Kwidzinski, E., Bunse, J., Kovac, A. D., Ullrich, O., Zipp, F., Nitsch, R. & Bechmann, I. (2003) *Adv. Exp. Med. Biol.* **527,** 113-118.

Appendix B

Derivation of Kinetic Equations

(a) The Michaelis-Menten equation

The Michaelis-Menten equation applies for an enzyme catalysed reaction in a "steady state". The concept of the steady-state is an approximation, which generally refers to the situation in which the value of a particular quantity is constant, often as its rate of formation is balanced by its destruction. In enzyme kinetics the concept is applied to enzyme-bound intermediates, when an enzyme is mixed with a large excess of substrate.

In deriving the Michaelis–Menten equation, we assume that the concentration of enzyme is negligible compared to that of substrate (as is generally true in practice due to the high catalytic efficiency of enzymes), and that substrate binding is rapid and reversible, with no chemical changes taking place. It is also assumed that what is measured is the initial rate, v, of formation of products, since under these conditions changes in substrate concentrations are generally small.

The catalytic reaction is divided into two processes, formation of the enzyme-substrate complex, ES, from the enzyme, E, and the substrate, S, and product formation, P, which is rate determining, e.g.

$$E + S \underset{K_{-1}}{\overset{K_1}{\rightarrow}} ES \overset{K_2}{\rightarrow} E + P \qquad \text{Equation 1}$$

The rate of change of concentration of the intermediate species, ES (enzyme-substrate complex), is given by:

$$\frac{d[ES]}{dt} = k_1[E][S] - k_{-1}[ES] - k_2[ES] \qquad \text{Equation 2}$$

Under steady-state conditions the concentration of the intermediate ES is assumed constant as the concentration of substrate is depleted, hence the rate of formation of

the ES complex equals the rate of decay into the product and free enzyme, therefore equation 2 is equal to zero. During the reaction the instantaneous concentration of free enzyme is not directly measurable, hence it must be expressed in terms of the initial concentration at time t = 0, and is defined as $[E_0]$.

$$[E] = [E_0] - [ES] \qquad \text{Equation 3}$$

Substitution of Equation 3 into Equation 2,

$$0 = ([E_0]-[ES])\, k_1[S] - k_{-1}[ES] - k_2[ES] \qquad \text{Equation 4}$$

Which rearranges to Equation 5:

$$[ES] = \frac{[E_0][S]}{\frac{(k_{-1} + k_2)}{k_1} + [S]} \qquad \text{Equation 5}$$

The rate of the reaction, V, is given by:

$$V = \frac{d[P]}{dt} = k_2[ES] \qquad \text{Equation 6}$$

Substitution of Equation 6 into Equation 5 gives the Michaelis-Menten equation:

$$V = \frac{[E]_0[S]k_2}{\frac{(k_{-1} + k_2)}{k_1} + [S]} \qquad \text{Equation 7}$$

From this the rate of reaction, k_{cat} is given as k_2, and the Michaelis constant, K_m is defined as:

$$K_m = \frac{(k_{-1} + k_2)}{k_1} \qquad \text{Equation 8}$$

(b) Significance of the Michaelis-Menten Parameters

(i) k_{cat}

In the case of the Michaelis-Menten kinetics, k_{cat} is the first order rate constant for the conversion of the enzyme-substrate complex, ES, to the enzyme-product complex, EP. It is often called the turnover number of the enzyme as it represents the maximum number of substrate molecules converted to products per unit time.

(ii) K_m

For simple Michaelis-Menten kinetics K_m is the apparent dissociation constant, which may be treated as the overall dissociation of all enzyme-bound species.

(iii) k_{cat} / K_m

k_{cat} / K_m is an apparent second-order rate constant that refers to the properties and the reactions of the free enzyme and free substrate.

(c) Analysis of the Michaelis-Menten Equation

Graphical analysis of the Michaelis-Menten equation is usually completed by its transformation into a linear form (Equation 8), by inverting both sides of Equation 7 and substituting v_{max} for $k_{cat}[E]_0$, where v_{max} is the limiting velocity. Graphical analysis of this equation yields the Lineweaver-Burke plot.

$$\frac{1}{V} = \frac{K_m}{k_{cat}[S]_0} + \frac{1}{k_{cat}}$$

Equation 8

The main disadvantage of the Lineweaver-Burke plot is that at low substrate concentrations, data are emphasised, whilst those at high concentrations are compressed.

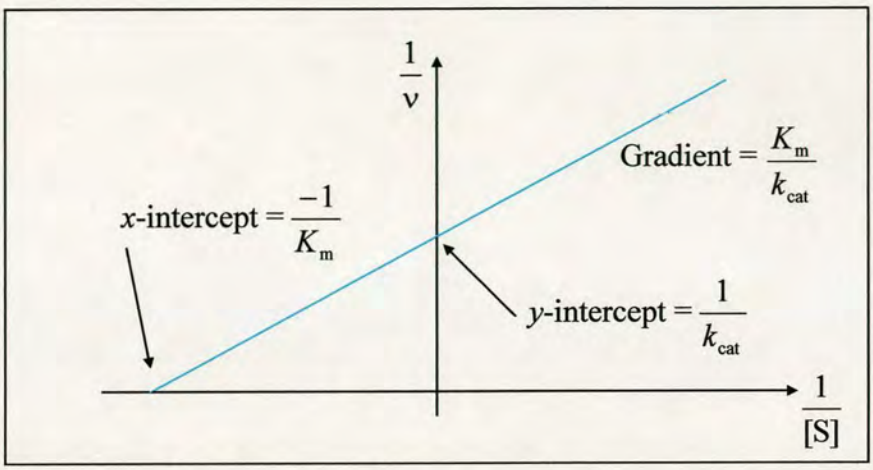

Figure B.1: Lineweaver-Burk Plot. The double reciprocal plot gives a linear relationship, with the y-intercept being inversely proportional to the maximum turnover rate k_{cat}, and the x-intercept inversely proportional to the Michaelis constant, K_m.

(d) Breakdown of the Michaelis Menten Equation

There are two main causes of the failure of the Michaelis-Menten equation – substrate inhibition, or substrate activation.

Substrate inhibition is generally caused by a second molecule of substrate binding to give an enzyme-disubstrate complex, ES_2, which is catalytically inactive. If this second binding event is modelled into the Michaelis-Menten equation, representing the second dissociation constant as K_m^* then the observed velocity is represented by Equation 15.

$$v = \frac{[E]_0[S]k_{cat}}{K_m^* + [S] + [S]^2/K_m^*} \qquad \text{Equation 15}$$

At low substrate concentrations, the rate is similar to that observed under normal Michaelis-Menten conditions, but as the substrate concentration increases a maximum value of v is observed, followed by a decrease.

Competitive Inhibition

Enzymes may be reversibly inhibited by the non-covalent binding of inhibitors. Competitive inhibitors often closely resemble the substrates whose reactions they inhibit, allowing them to compete for the same substrate binding site in an enzyme. In the case of the Michaelis-Menten equation, an additional equilibrium must be considered (Equation 9).

$$\begin{array}{ccccc} & & \overset{k_1}{\rightarrow} & & \overset{k_2}{\rightarrow} \\ \mathrm{E} + \mathrm{S} & & & \mathrm{ES} & & \mathrm{E} + \mathrm{P} \\ K_i & \uparrow\downarrow & \underset{k_2}{} & & & \\ & \mathrm{EI} & & & & \end{array} \qquad \text{Equation 9}$$

Here I is the inhibitor, EI is the enzyme-inhibitor complex and K_I is the inhibitor dissociation constant.

$$K_i = \frac{[E][I]}{[EI]} \qquad \text{Equation 10}$$

The total enzyme concentration must now take into account the quantity of the enzyme-inhibitor complex, EI, therefore

$$K_m = \frac{[E][S]}{[ES]} \qquad \text{Equation 11}$$

In this case the total concentration of enzyme must take into account EI, hence equation 12:

$$[E]_0 = [E] + [ES] + [EI] \qquad \text{Equation 12}$$

Expressing Equation 12 in terms of [EI] and substituting into Equation 4 gives:

$$[E]_0 = [E] + [ES] + \frac{[E][I]}{K_i} \qquad \text{Equation 13}$$

$$[E] = \frac{[E]_0 - [ES]}{(1 + [I]/K_i)} \qquad \text{Equation 14}$$

Expressing Equation 11 in terms of [E] and substituting into Equation 14 gives:

$$K_m\frac{(1 + [I])}{K_i} = \frac{([E]_0 - [ES])[S]}{[ES]} \qquad \text{Equation 15}$$

Finally substituting $[ES] = v/k_{cat}$ into Equation 15 gives:

$$v = \frac{[E]_0[S]k_{cat}}{[S] + K_m(1 + [I]/K_i)} \qquad \text{Equation 16}$$

Equation 16 is expressed in the same form as the Michaelis-Menten equation and shows that for competitive inhibition v is unchanged but K_m is apparently increased by $(1 + [I]/K_i)$.

Appendix C

C. 1 Protein Sequences of TDO and IDO

(a) Amino acid sequence of *Xanthamonas campestris* TDO.

```
1
MPVDK NLRDL EPGIH TDLEG RLTYG GYLRL DQLLS AQQPL SEPAH
46
HDEML FIIQH QTSEL WLKLL AHELR AAIVH LQRDE VWQCR KVLAR
91
SKQVL RQLTE QWSVL ETLTP SEYMG FRDVL GPSSG FQSLQ YRYIE
136
FLLGN KNPQM LQVFA YDPAG QARLR EVLEA PSLYE EFLRY LARFG
181
HAIPQ QYQAR DWTAA HVADD TLRPV FERIY ENTDR YWREY SLCED
226
LVDVE TQFQL WRFRH MRTVM RVIGF KRGTG GSSGV GFLQQ ALALT
271
FFPEL FDVRT SVGVD NRPPQ GSADA GKR
```

(b) Amino acid sequence of *Homo sapiens* IDO

```
1
MAHAM ENSWT ISKEY HIDEE VGFAL PNPQE NLPDF YNDWM FIAKH
46
LPDLI ESGQL RERVE KLNML SIDHL TDHKS QRLAR LVLGC ITMAY
91
VWGKG HGDVR KVLPR NIAVP YCQLS KKLEL PPILV YADCV LANWK
136
KKDPN KPLTY ENMDV LFSFR DGDCS KGFFL VSLLV EIAAA SAIKV
```

```
181
IPTVF KAMQM QERDT LLKAL LEIAS CLEKA LQVFH QIHDH VNPKA
226
FFSVL RIYLS GWKGN PQLSD GLVYE GFWED PKEFA GGSAG QSSVF
271
QCFDV LLGIQ QTAGG GHAAQ FLQDM RRYMP PAHRN FLCSL ESNPS
316
VREFV LSKGD AGLRE AYDAC VKALV SLRSY HLQIV TKYIL IPASQ
361
QPKEN KTSED PSKLE AKGTG GTDLM NFLKT VRSTT EKSLL KEG
```

C. 2 Primer Sequences and Site-Directed Mutants of TDO

H55A - Primer 1

```
  50  51  52  53  54  55  56  57  58  59
G TTC ATC ATC CAG AGC GCG ACC TCC GAG CTG
```

H55A - Primer 2

```
59  58  57  56  55  54  53  52  51  50
CAG CTC GGA GGT CAC GCT CTG GAT GAT GAA C
```

H55S - Primer 1

```
  50  51  52  53  54  55  56  57  58  59
G TTC ATC ATC CAG AGC CAG ACC TCC GAG CTG
```

H55S - Primer 2

```
59  58  57  56  55  54  53  52  51  50
CAG CTC GGA GGT CTG GCT CTG GAT GAT GAA C
```

Appendix D

(a) Growth Media and Solutions

Table D.1 Growth Media and Solutions

Luria-Bertani Broth	Per litre: 10 g Tryptone extract 10g NaCl 5g Yeast
Agar	15 g/l Agar dissolved in LB Broth 62.5 µg / l Ampicillin (Stored @ 4°C, used within 1 week of manufacture)
Ampicillin	25 mg/ml
Hemin	7 mM Hemin 1 mM NaOH

(b) Purification Buffers

Table D.2 Purification Buffers

Buffer A	50 mM NaH_2PO_4 300 mM NaCl 10 mM Imidazole	pH 8.0
Buffer B	50 mM NaH_2PO_4 300 mM NaCl 20 mM Imidazole	pH 8.0
Buffer C	50 mM NaH_2PO_4 300 mM NaCl 40 mM Imidazole	pH 8.0
Buffer D	50 mM NaH_2PO_4 300 mM NaCl 250 mM Imidazole	pH 8.0
Buffer E	50 mM Tris/HCl 1 mM EDTA	pH 8.0
Buffer F	100 mM NaH_2PO_4, pH 5.5-8.3 100 mM Na_2HPO_4	pH 5.5-8.3

(c) SDS-PAGE solutions

Table D.3 SDS-PAGE Solutions

Running Buffer	500 ml water 4.9 g MES 3.0 g Tris 5.0 g SDS 0.15 g EDTA
Heme Stain	60 ml H_2O 10 ml 2.5 M Sodium Acetate (pH 5.2) 30 ml Methanol 10 mg 3, 3', 5, 5'-Tetramethylbenzidine 150 ml Hydrogen Peroxide (100 vols)
Coomassie Stain	50 mL water 40 ml Methanol 10 ml Acetic Acid 1 ml Coomassie Brilliant Blue
Destain	50 ml water 40 ml Methanol 10 ml Acetic acid

(d) Pyridine Hemochromagen Assay

Table D.4 Reagents for pyridine hemochromagen assay

Reagent A	200 µl of 5 M NaOH 2.5 ml pyridine 2.3 ml H_2O
Reductant	10 µl of 0.05 M $Na_2S_2O_4$ in H_2O
Pyridine Hemochromagen Characteristics	$\Delta E_{556-540}$ = 22.1 $mM^{-1}cm^{-1}$ α-band = 556 nm β-band = 524 nm γ-band = 420 nm

(e) Substrate Concentrations for Steady-State Kinetics

Table D.5 Substrate concentrations employed in steady-state kinetic experiments

Substrate (Solubility in water μM)	Substrate concentrations employed in steady-state kinetic assays (μM)
L-Trp (50,000)	0, 10, 20, 40, 80, 160, 320, 500, 1000, 2000, 5000
D-Trp (50,000)	0, 10, 20, 50, 100, 200, 500, 1000, 5000, 10000, 25000
5-F-Trp (8,000)	0, 10, 20, 40, 80, 160, 320, 500, 1000, 2000, 5000
6F-Trp (20,000)	0, 10, 20, 40, 80, 160, 320, 500, 1000, 2000, 5000, 16000
5-Me-Trp (5000)	0, 10, 20, 40, 80, 160, 320, 500, 1000, 2000, 4750
6-Me-Trp (8500)	0, 10, 20, 40, 80, 160, 320, 500, 1000, 2000, 4250
Indole propionic acid (1000)	0, 10, 20, 40, 80, 160, 320, 500
Tryptamine (4000)	0, 10, 20, 40, 80, 160, 320, 500, 1000, 2000
1-Me-L-Trp (10,000)	0, 10, 20, 40, 80, 160, 320, 500, 1000, 2000, 5000

Appendix E

Mass Spectrometry – Mass Spectrometry

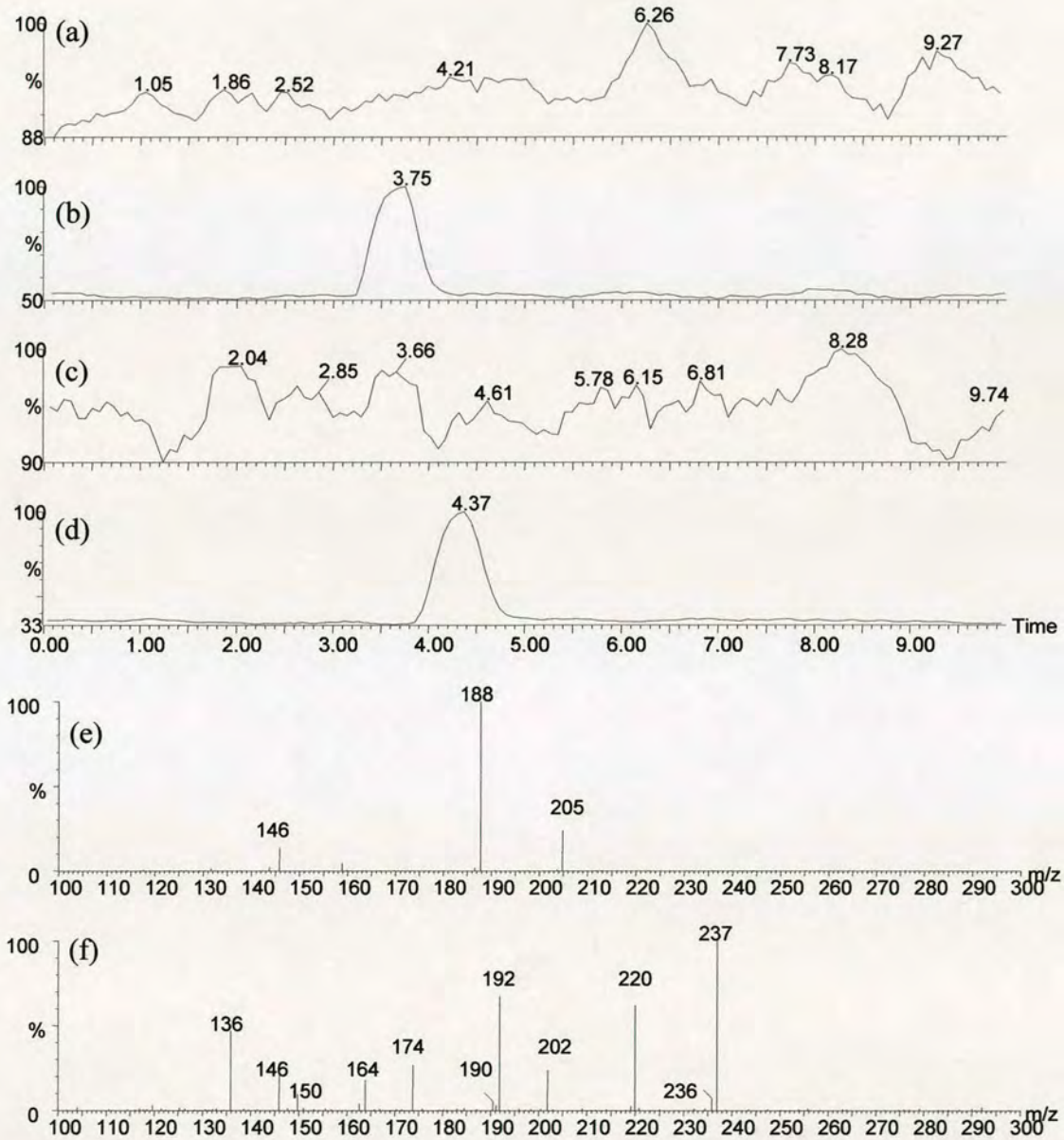

Figure F.1 MS-MS analysis of wtTDO L-Trp turnover products (a) MS trace calibrated to detect 1-Me-Trp (219 Da), (b) MS trace calibrated to detect the ($M+H^+$) ion of L-Kynurenine (209 Da) vs. time, (c) MS trace calibrated to detect the ($M+H^+$) ion of N-formylkynurenine (237 Da) vs. time, (d) MS trace calibrated to detect the ($M+H^+$) ion of L-Trp (204 Da) vs. time, (e) MS of L-Trp peak detected in (d), (f) MS of N-formylkynurenine peak detected in (c).

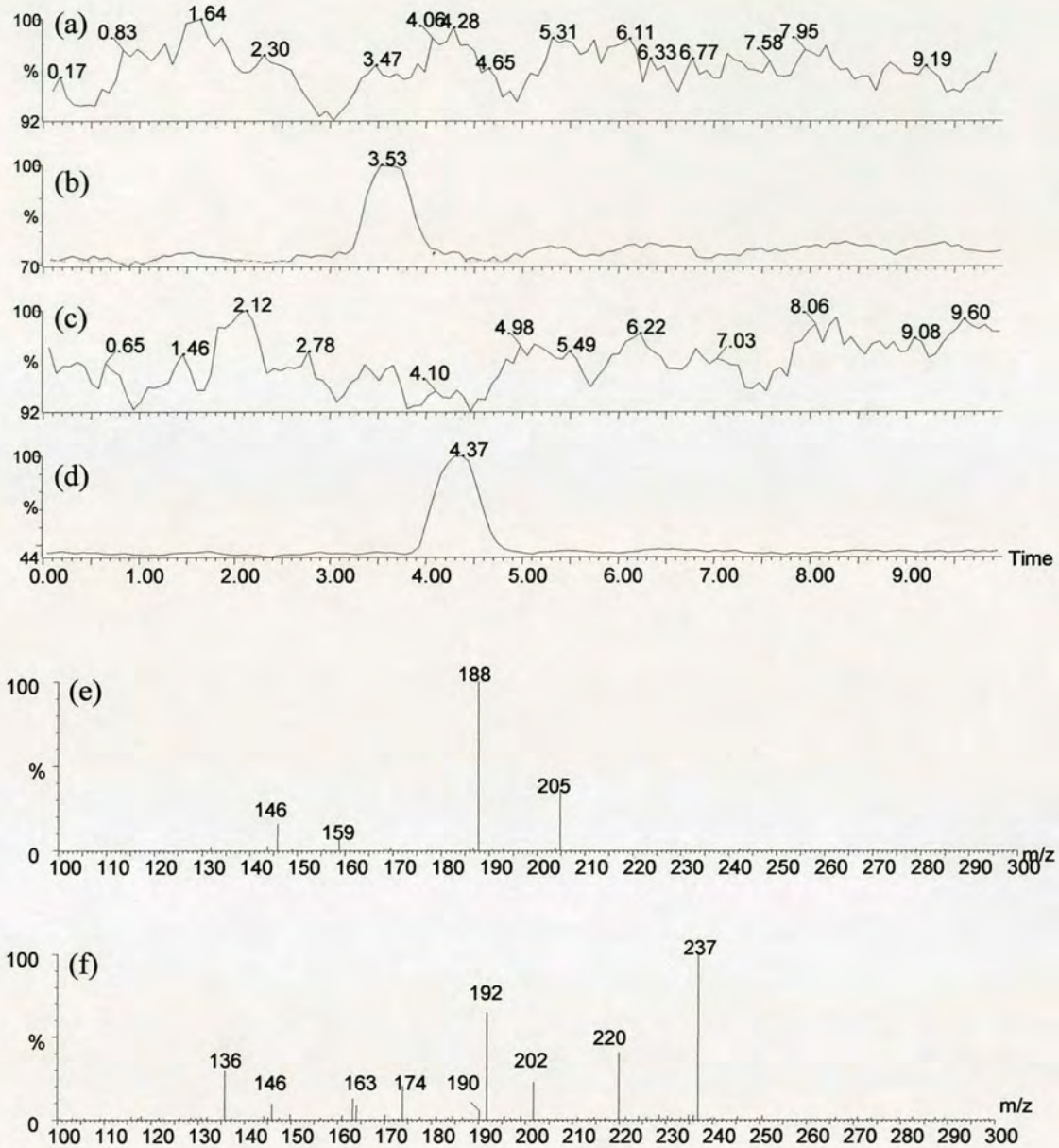

Figure F.2 MS-MS analysis of H55A L-Trp turnover products (a) MS trace calibrated to detect 1-Me-Trp (219 Da), (b) MS trace calibrated to detect the ($M+H^+$) ion of L-Kynurenine (209 Da) vs. time, (c) MS trace calibrated to detect the ($M+H^+$) ion of N-formylkynurenine (237 Da) vs. time, (d) MS trace calibrated to detect the ($M+H^+$) ion of L-Trp (204 Da) vs. time, (e) MS of L-Trp peak detected in (d), (f) MS of N-formylkynurenine peak detected in (c).

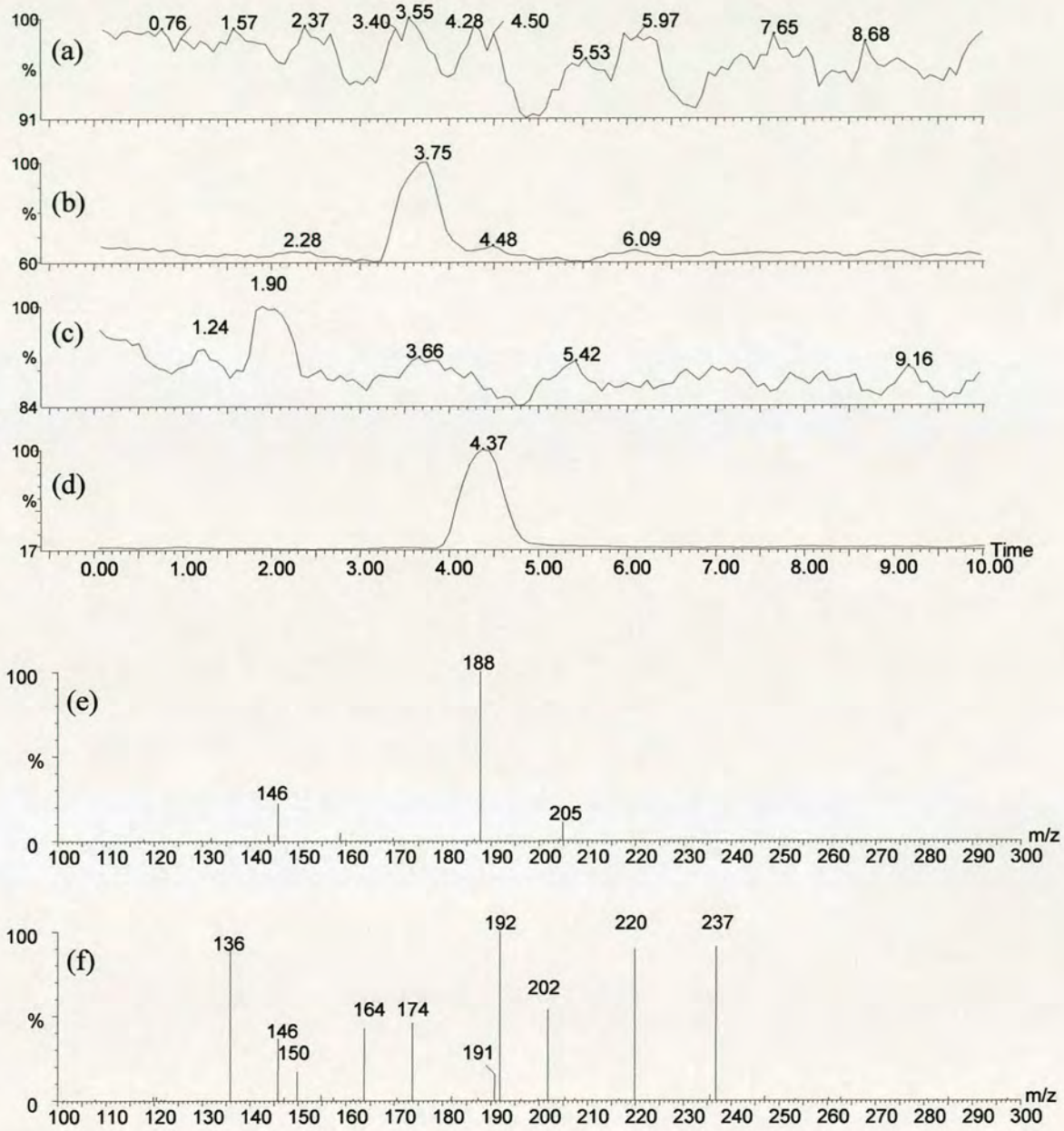

Figure F.3 MS-MS analysis of H55S L-Trp turnover products, (a) MS trace calibrated to detect 1-Me-Trp (219 Da), (b) MS trace calibrated to detect the ($M+H^+$) ion of L-Kynurenine (209 Da) vs. time, (c) MS trace calibrated to detect the ($M+H^+$) ion of N-formylkynurenine (237 Da) vs. time, (d) MS trace calibrated to detect the ($M+H^+$) ion of L-Trp (204 Da) vs. time, (e) MS of L-Trp peak detected in (d), (f) MS of N-formylkynurenine peak detected in (c).

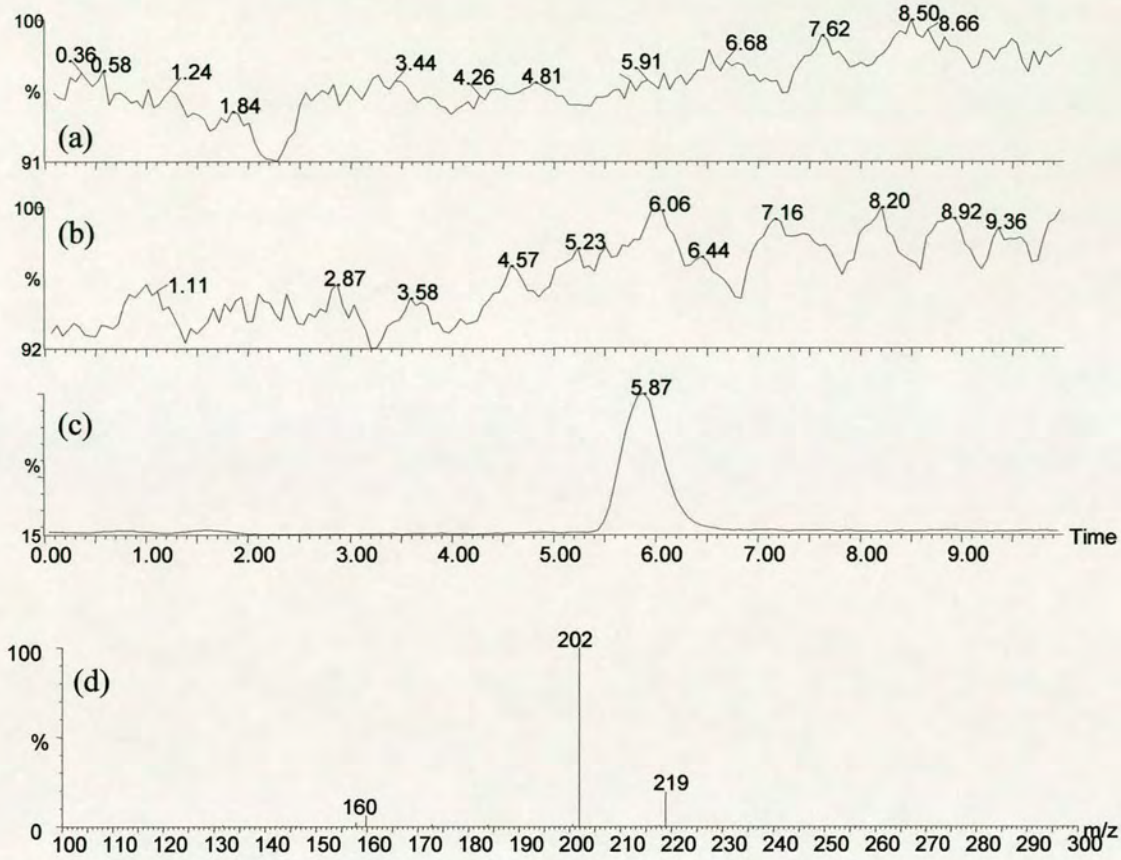

Figure F.4 MS-MS analysis of wtTDO 1-Me-Trp turnover products, (a) MS trace calibrated to detect 1-Me-Kynurenine (223 Da) vs. time, (b) MS trace calibrated to detect 1-Me-formylkynurenine (251 Da) vs. time, (c) MS trace calibrated to detect 1-Me-Trp (219 Da) vs. time, (d) MS of 1-Me-Trp peak detected in (c).

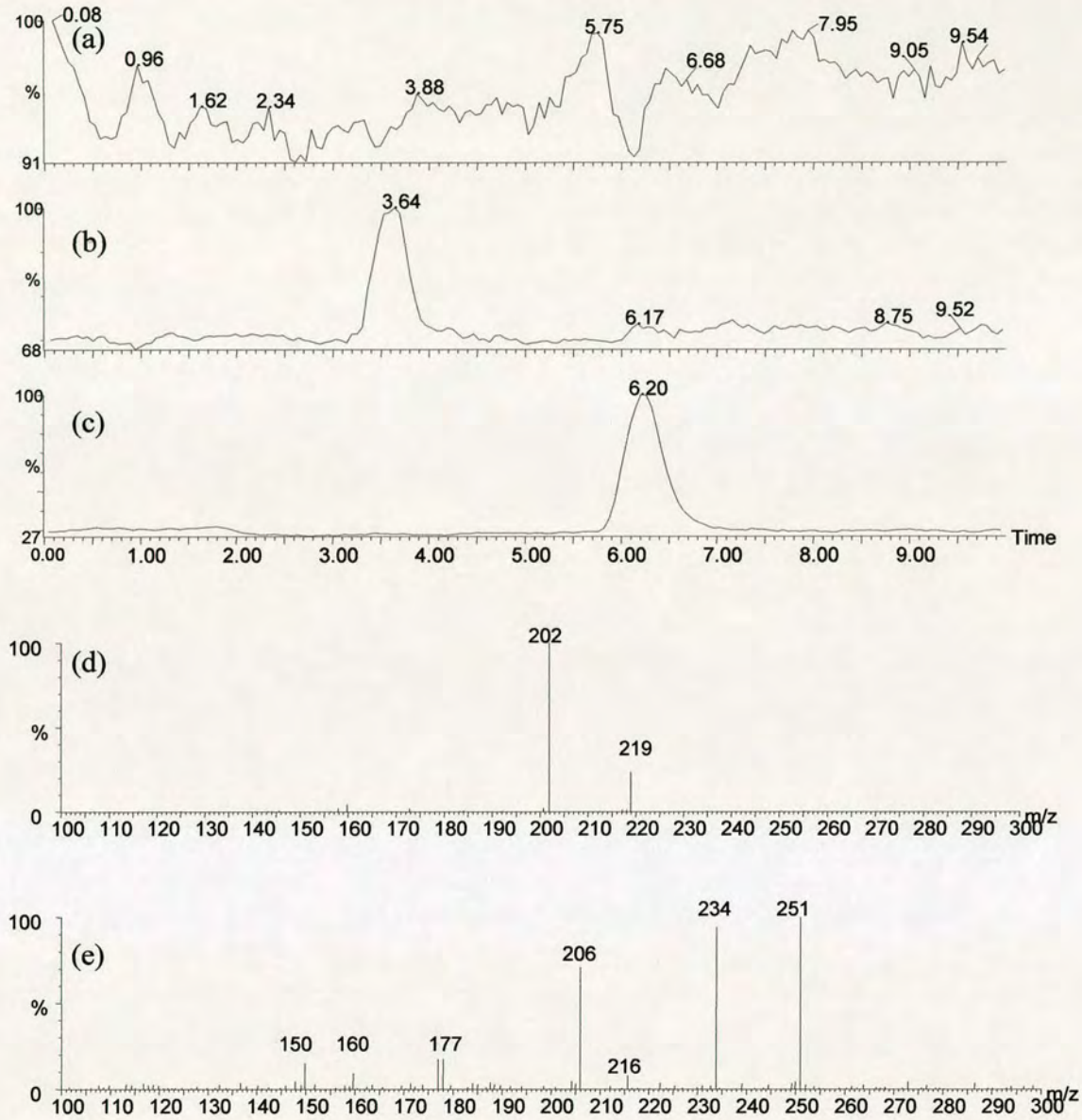

Figure F.5 MS-MS analysis of H55A 1-Me-Trp turnover products, (a) MS trace calibrated to detect 1-Me-Kynurenine (223 Da) vs. time, (b) MS trace calibrated to detect 1-Me-formylkynurenine (251 Da) vs. time, (c) MS trace calibrated to detect 1-Me-Trp (219 Da) vs. time, (d) MS of 1-Me-Trp peak detected in (c), (e) MS of 1-Me-formylkynurenine peak detected in (b).

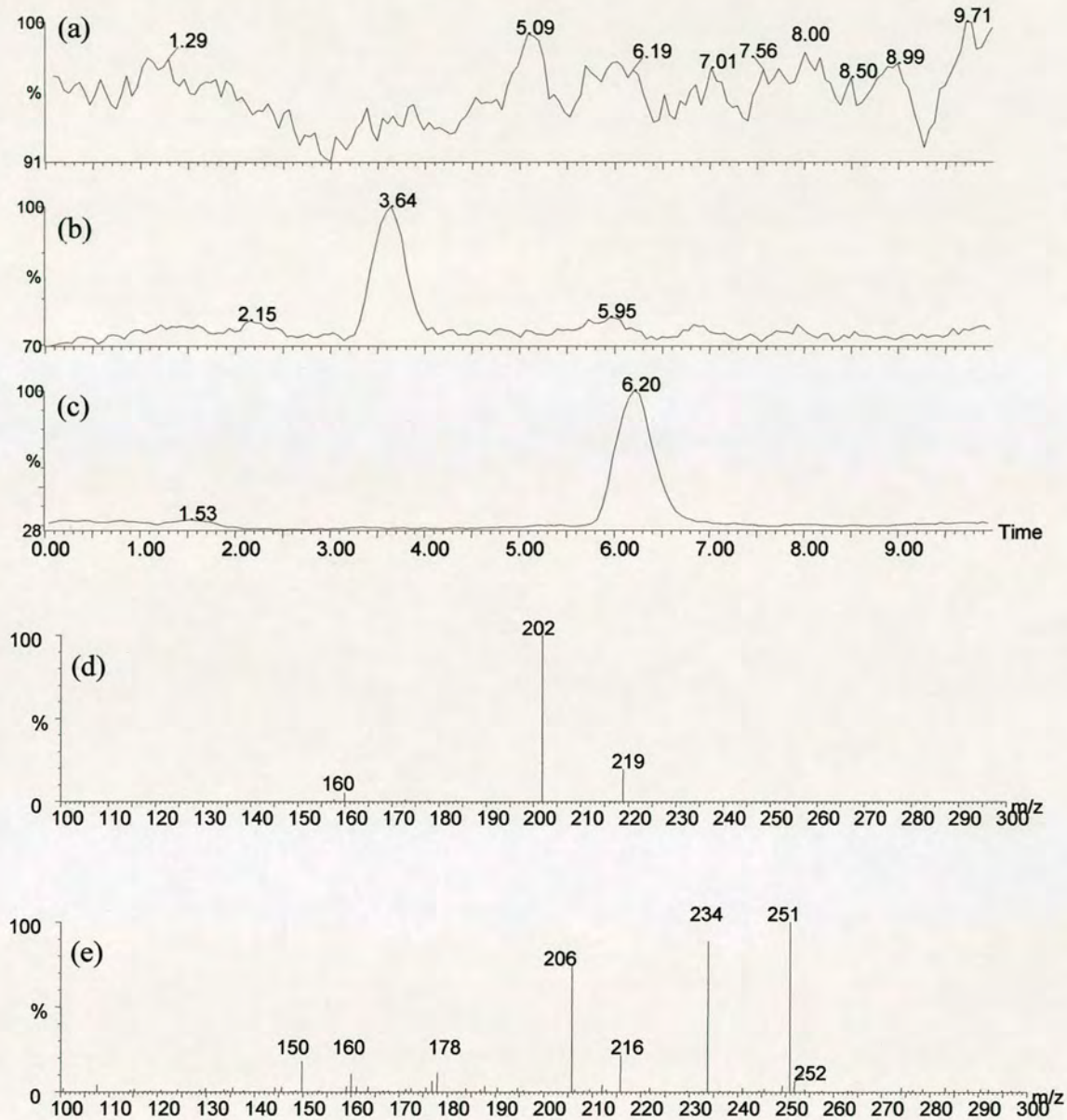

Figure F.6 MS-MS analysis of H55S 1-Me-Trp turnover products, (a) MS trace calibrated to detect 1-Me-Kynurenine (223 Da) vs. time, (b) MS trace calibrated to detect 1-Me-formylkynurenine (251 Da) vs. time, (c) MS trace calibrated to detect 1-Me-Trp (219 Da) vs. time, (d) MS of 1-Me-Trp peak detected in (c), (e) MS of 1-Me-formylkynurenine peak detected in (b).

Appendix F

Publications and Meetings Attended

(a) Publications

Copies of the publications listed below are bound at the back of the thesis.

Molecular insights into substrate recognition and catalysis by tryptophan 2,3-dioxygenase. Forouhar, F., Anderson, J. L. R., Mowat C. G., Vorobiev S. M., Hussain, A., Abashidze, M., Bruckmann, C., Thackray S. J., Seetharaman, J., Tucker, T., Xiao, R., Ma, L.-C., Zhao, L., Acton T. B., Montelione G. T., Chapman S. K. & Tong, L. (2007) *Proc Natl Acad Sci U S A*, 104(2): p. 473-8.

Indoleamine 2,3-dioxygenase and Tryptophan 2,3-dioxygenase. Thackray, S. J., Bruckmann, C., Mowat, C. G, Forouhar, F., Chapman, S. K., and Tong, L. (2008) *Handbook of Metalloproteins*, (in press).

Histidine 55 of tryptophan 2,3-dioxygenase is not an active site base but regulates catalysis by controlling substrate binding. Thackray, S. J., Bruckmann, C., Anderson, J. L. R., Campbell, L. P., Xiao, R., Zhao, L., Mowat, C. G., Forouhar, F., Tong, L., and Chapman, S. K. (2008) *Biochemistry* **47,** 10677-10684.

Exploring the Mechanism of Tryptophan 2,3-Dioxygenase. Thackray, S. J., Mowat, C. G., and Chapman, S. K. (2008) *Biochem. Trans* 36(6), 1120-1123.

Reassessment of the Reaction Mechanism in the Heme Dioxygenases. Chauhan, N., Thackray, S. J., Rafice, S. A., Mowat, C. G., Eaton, G., Lee, M., Jenkins, P. R., Chapman, S. K., and Raven, E. L. (2008) *Submitted to J. Amer. Chem. Soc.*

Molecular insights into substrate recognition and catalysis by tryptophan 2,3-dioxygenase

Farhad Forouhar*, J. L. Ross Anderson†, Christopher G. Mowat†, Sergey M. Vorobiev*, Arif Hussain*, Mariam Abashidze*, Chiara Bruckmann†, Sarah J. Thackray†, Jayaraman Seetharaman*, Todd Tucker*, Rong Xiao‡, Li-Chung Ma‡, Li Zhao‡, Thomas B. Acton‡, Gaetano T. Montelione‡, Stephen K. Chapman†, and Liang Tong*§

*Department of Biological Sciences, Northeast Structural Genomics Consortium, Columbia University, New York, NY 10027; †School of Chemistry, University of Edinburgh, West Mains Road, Edinburgh EH9 3JJ, United Kingdom; and ‡Center for Advanced Biotechnology and Medicine and Northeast Structural Genomics Consortium, Rutgers University, Piscataway, NJ 08854

Communicated by Wayne A. Hendrickson, Columbia University, New York, NY, November 13, 2006 (received for review September 25, 2006)

Tryptophan 2,3-dioxygenase (TDO) and indoleamine 2,3-dioxygenase (IDO) constitute an important, yet relatively poorly understood, family of heme-containing enzymes. Here, we report extensive structural and biochemical studies of the *Xanthomonas campestris* TDO and a related protein SO4414 from *Shewanella oneidensis*, including the structure at 1.6-Å resolution of the catalytically active, ferrous form of TDO in a binary complex with the substrate L-Trp. The carboxylate and ammonium moieties of tryptophan are recognized by electrostatic and hydrogen-bonding interactions with the enzyme and a propionate group of the heme, thus defining the L-stereospecificity. A second, possibly allosteric, L-Trp-binding site is present at the tetramer interface. The sixth coordination site of the heme-iron is vacant, providing a dioxygen-binding site that would also involve interactions with the ammonium moiety of L-Trp and the amide nitrogen of a glycine residue. The indole ring is positioned correctly for oxygenation at the C2 and C3 atoms. The active site is fully formed only in the binary complex, and biochemical experiments confirm this induced-fit behavior of the enzyme. The active site is completely devoid of water during catalysis, which is supported by our electrochemical studies showing significant stabilization of the enzyme upon substrate binding.

cancer | heme enzymes | immunomodulation | indoleamine 2,3-dioxygenase

Tryptophan 2,3-dioxygenase (TDO) and indoleamine 2,3-dioxygenase (IDO) catalyze the oxidative cleavage of the L-tryptophan (L-Trp) pyrrole ring, the first and rate-limiting step in L-Trp catabolism through the kynurenine pathway (1–3). In addition, IDO has been implicated in a diverse range of physiological and pathological conditions, including suppression of T cell proliferation, maternal tolerance to allogenic fetus, and immune escape of cancers (4–8), and is an attractive target for drug discovery against cancer and autoimmune and other diseases (2, 9–12).

Despite catalyzing identical biochemical reactions (Fig. 1*a*), the sequence similarity between TDO and IDO is extremely low. An alignment of their sequences is only possible based on their structures, which suggests a sequence identity of 10% between them (Fig. 1*b*). In comparison, *Xanthomonas campestris* TDO shares 34% sequence identity with human TDO (Fig. 1*b*), demonstrating the remarkable evolutionary conservation of this enzyme. TDO is a homotetrameric enzyme and is highly specific for L-Trp and related derivatives such as 6-fluoro-Trp as the substrate. In comparison, IDO is monomeric, and shows activity toward a larger collection of substrates, including L-Trp, D-tryptophan (D-Trp), serotonin, and tryptamine (3), although the K_m for D-Trp is ≈100-fold higher than that for L-Trp (13). The structure of human IDO in the catalytically inactive, ferric [Fe(III)]-heme state in complex with the 4-phenylimidazole inhibitor has recently been reported (14). Although this structure gave information about important active site residues, the inhibitor is coordinated to the heme iron and does not provide any information regarding Trp or oxygen binding.

To provide direct insight into substrate recognition and catalysis by these enzymes, we report here the crystal structures at up to 1.6-Å resolution of the active, reduced (Fe(II)) TDO from *X. campestris* in a binary complex with the substrate L-Trp or 6-fluoro-Trp. Our structures reveal for the first time the structural basis for the stereospecificity of this important enzyme. Our structural information is confirmed by biochemical studies and offers significant molecular insight into tryptophan dioxygenation by TDO and IDO.

Results

Structure Determination. Crystals of the reduced (Fe(II)) TDO from *X. campestris* in a binary complex with the substrate L-Trp or 6-fluoro-Trp were obtained after extensive efforts and by using anaerobic conditions, because the oxidized (Fe(III)) enzyme has much lower affinity for L-Trp (see below). The structures at up to 1.6-Å resolution of these binary complexes [Table 1; and see supporting information (SI) Table 3] as well as that of the free enzyme were determined by molecular replacement based on the structure of the apo enzyme, in the absence of heme, which we had determined by the selenomethionyl single-wavelength anomalous diffraction method (PDB entry 1YW0) (15).

The structure of the SO4414 protein from *Shewanella oneidensis* (16) was determined at 2.4-Å resolution by molecular replacement based on our structure of the apo enzyme (PDB entry 1ZEE).

Structure of TDO. The structure of *X. campestris* TDO monomer contains 12 helices (named αA through αL) and no β-strands (Figs. 1*b* and 2*a*). TDO is an intimately associated tetramer (Fig. 2*b*), and ≈4,500 Å^2 of the surface area of each monomer is buried in the tetramer. Helices αB and αC are located in the extensive, mostly hydrophobic interface between two of the monomers. The N-terminal segments (residues 21–40, including helix αA) of the two monomers are swapped in this dimer (Fig.

Author contributions: F.F., J.L.R.A., and C.G.M. contributed equally to this work; F.F., J.L.R.A., C.G.M., G.T.M., S.K.C., and L.T. designed research; F.F., J.L.R.A., C.G.M., S.M.V., A.H., M.A., C.B., S.J.T., J.S., T.T., R.X., L.-C.M., L.Z., and T.B.A. performed research; F.F., J.L.R.A., C.G.M., S.M.V., A.H., M.A., C.B., S.J.T., J.S., R.X., L.-C.M., T.B.A., G.T.M., S.K.C., and L.T. analyzed data; and F.F., J.L.R.A., C.G.M., T.B.A., G.T.M., S.K.C., and L.T. wrote the paper.

The authors declare no conflict of interest.

Abbreviations: D-Trp, D-tryptophan; IDO, indoleamine 2,3-dioxygenase; L-Trp, L-tryptophan; TDO, tryptophan 2,3-dioxygenase.

Data deposition: The atomic coordinates have been deposited in the Protein Data Bank, www.pdb.org (PDB ID codes 1YW0, 2NW7, 2NW8, 2NW9, 1ZEE, and 2NWB).

§To whom correspondence should be addressed. E-mail: ltong@columbia.edu.

This article contains supporting information online at www.pnas.org/cgi/content/full/0610007104/DC1.

BIOCHEMISTRY

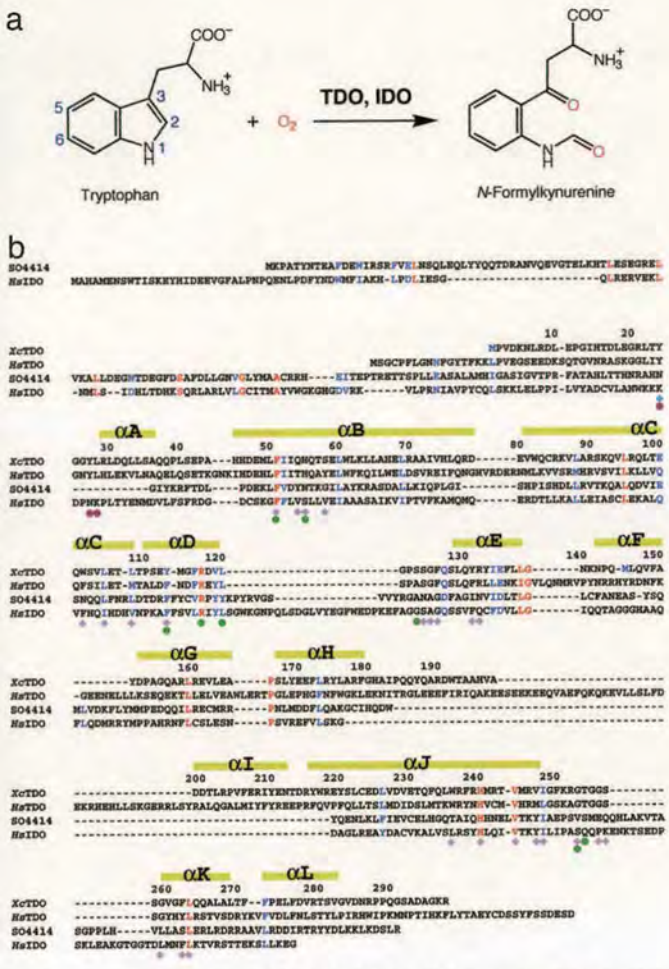

Fig. 1. Primary structures of TDO and IDO. (*a*) The biochemical reaction catalyzed by TDO and IDO. (*b*) Amino acid sequence alignment of *X. campestris* TDO (*Xc*TDO), human TDO (*Hs*TDO), *S. oneidensis* SO4414 (SO4414), and human IDO (*Hs*IDO). The filled circles indicate residues involved in binding L-Trp, and the diamonds indicate residues involved in binding heme. The symbols for residues before helix αA are given different colors, to indicate that they are from another monomer of the tetramer.

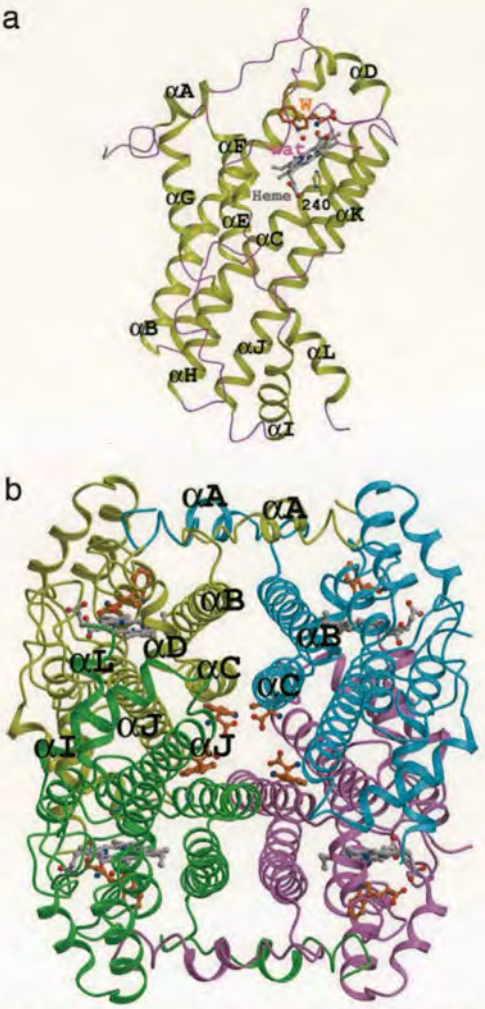

Fig. 2. The structure of TDO. (*a*) Schematic representation of the structure of the monomer of *X. campestris* TDO. The α-helices are shown in yellow and labeled. Heme is shown in gray, and L-Trp is shown in orange (labeled W). The water molecule is shown as a red sphere (labeled wat). (*b*) Schematic representation of the tetramer of *X. campestris* TDO. The four monomers are colored in yellow, cyan, violet, and green. Helices in the tetramer interface are labeled. The Trp molecules in the tetramer interface are also shown. Produced with Molscript (35) and rendered with Raster3D (36).

2*b*), which is important for the catalysis by TDO because several residues in this segment are part of the binding site for the Trp residue in the active site (see below).

Binding Mode of the L-Trp Substrate to TDO. Our structure of the binary complex defines the molecular mechanism for the recognition of the L-Trp substrate by TDO. Clear electron density was observed for heme and L-Trp in the active site based on the crystallographic analysis at 1.6-Å resolution (Fig. 3*a*). The L-Trp substrate is located in a pocket over the distal face of the heme, having interactions with residues in helices αB and αD, and the αD–αE and αJ–αK loops (Figs. 1*b* and 3*b*). The carboxylate group of Trp is recognized by bidentate ion-pair interactions with the side chain of Arg 117 (in helix αD). The carboxylate group is also hydrogen-bonded to the side chain hydroxyl of Tyr113 (helix αD) and the main chain amide of Thr 254 (αJ-αK loop). The ammonium ion of L-Trp is recognized by the 7-propionate side chain of the heme group (Fig. 3*b*), and it is also hydrogen-bonded to the side chain hydroxyl of Thr 254. The indole ring is located ≈3.5 Å above and perpendicular to the heme and is held in place by van der Waals interactions with the side chains of Phe 51 (helix αB) and several other hydrophobic residues, including Tyr 24, Tyr 27, and Leu 28 from the N-terminal segment of another monomer of the tetramer (Fig. 3*b*). In addition, the N1 nitrogen of the indole ring is hydrogen-bonded to the side chain of His 55 (helix αB) (Fig. 3*b*).

A water molecule is present in the active site of this binary complex (Fig. 3*a*), hydrogen-bonded to the ammonium ion of L-Trp and the main-chain amide of residue Gly 125 (Fig. 3*b*). The water is 3.5 Å from the ferrous atom in the heme, too far for ligating interactions. The iron atom is still 0.3 Å out of the plane of the heme, on the side of the proximal His 240 ligand (SI Fig. 5).

The crystal was exposed to a solution saturated with nitric oxide (NO) before being flash-frozen, but we did not observe the binding of this dioxygen analog in the structure. This is confirmed by our structure of the binary complex with 6-fluoro-Trp, which was not exposed to NO but contained the same density for the water molecule (SI Fig. 6). The structure of the 6-fluoro-Trp binary complex is essentially identical to that of the L-Trp binary complex (SI Fig. 6). NO probably dissociated from the heme during the cryofreezing manipulations in the anaerobic box.

Induced-Fit Behavior of TDO. Our structural information suggests that TDO is an induced-fit enzyme. Although the active site

Table 1. Summary of crystallographic information

Protein	TDO (holoenzyme)	TDO (holoenzyme)	TDO (holoenzyme)	TDO (apoenzyme)	SO4414 (holoenzyme)	SO4414 (apoenzyme)
Ligand	L-Trp	6-fluoro-Trp	None	None	None	None
Maximum resolution, Å	1.6	1.8	2.7	2.7	2.4	2.3
R_{merge}, %*	6.9 (52.7)	8.6 (60.9)	13.0 (32.3)	16.6 (74.0)	10.4 (63.0)	6.6 (30.6)
Beam line	ESRF BM14	ESRF BM14	NSLS X4A	APS 21BM	NSLS X4A	NSLS X4A
Completeness, %	87 (65)	87 (61)	72 (54)	82 (68)	83 (60)	87 (71)
R factor, %†	17.1 (18.9)	16.6 (17.9)	25.7 (25.7)	25.0 (32.1)	21.7 (23.5)	23.4 (26.7)
Free R factor, %	18.9 (22.0)	18.4 (21.1)	26.3 (26.2)	29.4 (35.1)	22.5 (24.1)	27.5 (31.5)
rms deviation in bond lengths, Å	0.005	0.005	0.008	0.011	0.007	0.006
rms deviation in bond angles, °	1.0	1.0	1.2	1.6	1.1	1.0
Most-favored region, %	92	91	89	86	92	91

*$R_{merge} = \Sigma_h \Sigma_i |I_{hi} - \langle I_h \rangle| / \Sigma_h \Sigma_i I_{hi}$. The numbers in parentheses are for the highest-resolution shell.
†$R = \Sigma_h |F_h^o - F_h^c| / \Sigma_h F_h^o$.

pocket is well defined in the binary complex (Fig. 3*b*), the αJ–αK loop, which helps to form the walls of this pocket, is disordered in the free enzyme, and the αD-αE loop has a somewhat different conformation (Fig. 3*c*; and see SI Fig. 7). Moreover, the Arg 117 side chain assumes a different conformation in the free enzyme (Fig. 3*c*). Upon recognition of the L-Trp substrate, a complex and extensive network of interactions is established (Fig. 3*b*), thus stabilizing the active site region. Although this region is exposed to the solvent in the free enzyme, it is completely shielded from the solvent in the binary complex, and only the carboxylate group of the 6-propionate of heme is visible on the surface.

Additional evidence for the induced-fit behavior is observed in the active site of the second TDO monomer in the asymmetric unit. The binding mode of the L-Trp substrate is very different in this monomer (Fig. 3*d*; and see SI Fig. 7). The Trp side chain is not positioned as deeply into the pocket, and the hydrogen bond between the ring nitrogen and the side chain of His 55 is lost (distance of 3.8 Å). Both nitrogen atoms are instead hydrogen-bonded to a water molecule, located 3.5 Å from the heme iron but at a position distinct from that of the water in the active site of the other monomer (Fig. 3*d*). This conformation may also be stabilized by crystal packing interactions, as the 7-propionate of heme is ion-paired with an Arg residue from another TDO tetramer in the crystal. The main chain atoms of the Trp substrate appear to be disordered, because no clear electron density was observed for them (Fig. 3*e*). Consistent with this finding, the αJ–αK loop is disordered in this molecule, similar to that in the free enzyme (Fig. 3*d*). This complex may represent an initial stage in the formation of the Michaelis complex of TDO. Proper positioning of the L-Trp substrate for catalysis would lead to the recognition of its main chain atoms and the ordering of the αJ–αK loop.

Implications for Substrate Binding by IDO. Our structure of the binary complex of TDO also has significant implications for substrate recognition by the IDOs. The rms distance for 201 structurally equivalent Cα atoms between TDO and the large domain of human IDO (PDB entry 2D0T) (14) is 3.1 Å (SI Fig. 8), calculated with the program Dali (17). Despite sharing only 10% overall sequence identity, key active-site residues are similar in TDO and IDO (Fig. 1*b*; and see SI Table 4), and L-Trp may have the same binding mode to the active site of IDO (SI Fig. 9). Ionic interactions that are important for recognizing the L-Trp ammonium ion and carboxylate group are conserved in IDO (Arg 231 and 7-propionate), explaining why L-Trp is a much better substrate than D-Trp for IDO. At the same time, hydrogen-bonding interactions to these atoms may be absent in IDO, because Tyr 113 of TDO is replaced by Phe 226 in IDO (SI Fig. 9), and the Thr 254 residue may not have an equivalent in IDO because the αJ–αK loop, disordered in the IDO structure (SI Fig. 9) (14), has highly divergent sequences in IDO compared with TDO (Fig. 1*b*). Therefore, IDO may have weaker interactions with tryptophan, which may be the reason why it cannot completely distinguish among the indoleamine substrates.

The structure comparison explains why 1-methyltryptophan is a micromolar inhibitor of IDO (18) but is essentially inactive against TDO (10). The N1 atom is directly hydrogen-bonded to the His 55 side chain in TDO (Fig. 3*b*), and its methylation will cause steric clash with this residue. In comparison, His 55 is replaced by Ser 167 in IDO (SI Table 4), which creates a small pocket that can accommodate the 1-methyl group (SI Fig. 9).

Structural similarity is also observed with the SO4414 protein from *S. oneidensis* (SI Fig. 8) (16), with an rms distance of 4.4 Å for 206 equivalent Cα atoms, suggesting that SO4414 may also be a dioxygenase. Moreover, the structure contains an extra domain that is formed by residues at the N terminus, similar to the small domain in human IDO (SI Fig. 8). In contrast to human IDO, SO4414 is a tetramer but with a different organization compared with that of TDO (SI Fig. 10). Our biochemical efforts so far have not been able to demonstrate IDO (or TDO) activity for this protein, suggesting that SO4414 may prefer a different substrate for oxygenation.

A Model for the Michaelis Complex. To help provide further insight into the catalysis by these enzymes, we built a model for the Michaelis complex, by placing one oxygen atom (O1) of the dioxygen substrate directly over the heme iron, at a distance of 2.1 Å (Fig. 4*a*). The distal oxygen atom (O2) was placed such that the O1–O2 bond is parallel to the C2–C3 bond of indole ring, giving a Fe–O1–O2 angle of 135°. This conformation places the O2 atom within 0.5 Å of the water molecule observed in our structure (Fig. 4*a*), suggesting that this water should be ejected from the active site upon dioxygen binding. The active site is therefore completely devoid of solvent molecules in this Michaelis complex.

The modeled dioxygen-binding mode reveals the activation mechanism of this substrate for the reaction. It has been established that TDO has an ordered catalytic cycle in which the protein first binds L-Trp to the ferrous form, and then binding of dioxygen is facilitated, and nucleophilic attack from the substrate C3 is initiated (3, 13, 19). In the model, the distal oxygen atom interacts with the L-Trp ammonium moiety and the backbone amide nitrogen of Gly 125 (Fig. 4*a*). The Lewis acidity

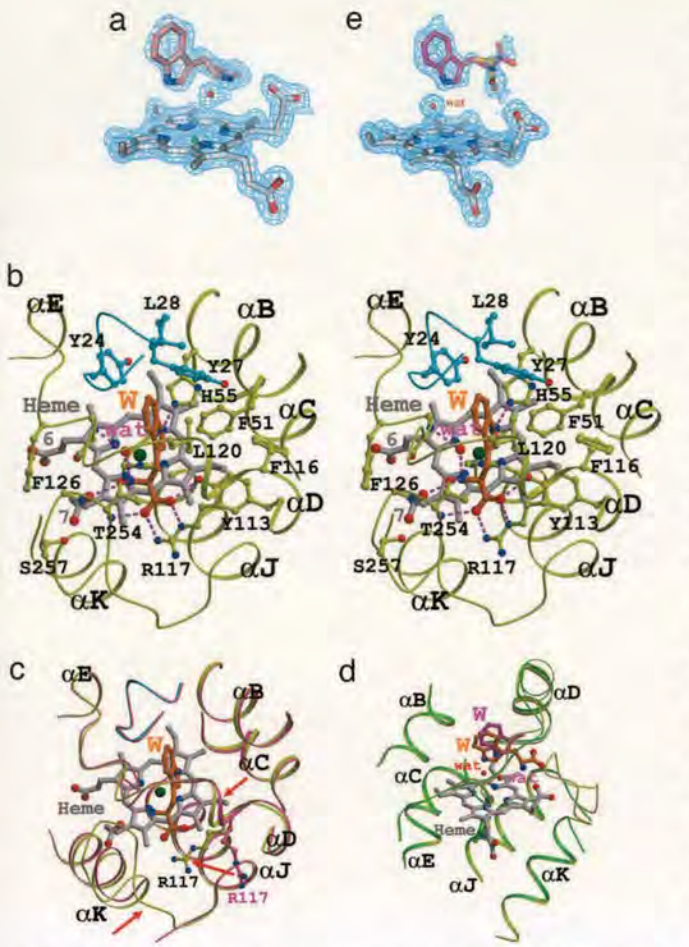

Fig. 3. Molecular basis for substrate recognition by TDO. (*a*) Final $2F_o-F_c$ electron density at 1.6-Å resolution for heme, L-Trp, and a water in the active site. Contoured at 1σ. (*b*) Stereo drawing showing the active site of *X. campestris* TDO in the binary complex with L-Trp. The segment in cyan is from another monomer of the tetramer. Hydrogen-bonding interactions are indicated with dashed lines in magenta. (*c*) Overlay of the structures of the free enzyme (in orchid) and the binary complex (yellow and cyan) in the active-site region. Regions of conformational differences are indicated with the red arrows. (*d*) Overlay of the active-site region of the second monomer (in green) and that of the first monomer (in yellow). Only the side-chain atoms of Trp are shown in the second monomer (in magenta). (*e*) Final $2F_o-F_c$ electron density at 1.6-Å resolution for heme, L-Trp, and a water in the active site of the second TDO molecule in the crystal. Contoured at 1σ. Two conformations for the main chain atoms are shown, but neither fit the density well. For the stereo version of *c* and *d*, please see SI Fig. 7. Produced with Molscript (35) and rendered with Raster3D (36).

of the hydrogen-bonding donors, coupled with the electron-withdrawing nature of the heme, would increase the electrophilicity of the bound dioxygen and render it more susceptible to nucleophilic attack by the substrate C3 atom. The increased hydrophobicity of the active site upon the exclusion of water would also aid the stabilization of an oxyferrous species. Studies with heme oxygenase suggest that the hydrogen-bonding interactions to the dioxygen substrate may also help to prevent its heterolysis (20), and the exclusion of water probably removes a hydrogen-bond competitor to the dioxygen. After the initial attack by the C3 atom, the reaction may proceed via a Criegee rearrangement or a dioxetane intermediate (SI Fig. 11). In the model, the O1–O2 atoms are in a trans configuration relative to the C2–C3 atoms of L-Trp (Fig. 4*a*), which may favor the Criegee rearrangement pathway (SI Fig. 11) (19). The Criegee pathway is also favored based on chemical, thermodynamic, and quantum mechanical considerations (3).

Our model for the Michaelis complex shows that the O1 atom is 2.6 Å from the N1 atom of L-Trp and therefore can act as the general base to extract the proton from the N1 atom (SI Fig. 11) (19). The N1 atom is hydrogen-bonded to His 55 in TDO. However, our biochemical studies show that the k_{cat} of TDO is relatively insensitive to pH over the range examined (pH 6 to pH 8) (Fig. 4*b*), and the H55A mutant had only a 10-fold decrease in the k_{cat} (Table 2), suggesting that this residue is not essential for catalysis, consistent with its replacement with a Ser residue in IDO. On the other hand, the K_m shows a marked increase at lower pH (Fig. 4*b*), probably because of the protonation of this residue.

An Allosteric Binding Site in the Tetramer Interface. We also observed the binding of four L-Trp residues to an allosteric site in the interface of the tetramer (Fig. 2*b*), with well defined electron density (SI Fig. 12). The L-Trp residue appears to be recognized specifically by the enzyme in this pocket (SI Fig. 12). There have been reports of allosteric activation by the substrate L-Trp (21, 22), and our observations offer a possibility for this effector site. Unfortunately, our kinetic studies so far have not shown any allosteric effects with *X. campestris* TDO. This site is not occupied in the 6-fluoro-Trp complex, possibly because of the lower concentration of this compound in the crystallization solution.

Biochemical Studies Confirm the Structural Observations. *X. campestris* TDO has robust catalytic activity toward L-Trp and 6-fluoro-Trp but is inactive toward D-Trp, tryptamine or indolepropionic acid (Table 2), confirming its designation as a TDO. In fact, D-Trp is a weak, competitive inhibitor of the enzyme at high concentrations (Table 2). Our binding data show that D-Trp has much lower affinity for the enzyme than L-Trp (Table 2), consistent with our structural information and explaining why D-Trp cannot be oxygenated by TDO.

The biochemical studies also provide direct evidence for the induced-fit behavior of TDO. There is a large increase in the affinity of the enzyme for L-Trp when the heme iron is reduced (K_d [ferric Fe(III) heme] = 3.8 mM, whereas K_d [ferrous Fe(II) heme] = 4.1 μM) (Table 2). The electrochemistry data show a large, positive shift in reduction potential (+136 mV) in the presence of 15 mM L-Trp (Fig. 4*c*). In fact, the shift in reduction potential almost perfectly correlates with the increase in affinity for L-Trp on reduction, both giving an estimated $\Delta\Delta G$ of 15 kJ/mol. These data show that there is a significant stabilization of the ferrous form when substrate is bound. This stabilization could also play a physiological role to keep the protein reduced, and therefore active, when L-Trp is present.

Our structural studies have defined the binding mode of the substrate L-Trp to TDO, revealing the structural basis for the stereospecificity of this important enzyme. The induced-fit behavior of TDO, confirmed by our biophysical studies, appears crucial for the exclusion of water from the active site and for stabilizing the enzyme in the presence of the substrates. Finally, structural comparisons among these enzymes reveal the striking evolutionary conservation of the heme-dependent dioxygenases.

Materials and Methods

The experimental protocols are summarized here. More detailed information can be found in *SI Materials and Methods*.

Protein Expression and Purification. Full-length *X. campestris* TDO (NESG ID XcR13) and *S. oneidensis* SO4414 (NESG ID SoR52) were cloned into a pET-21d (Novagen, San Diego, CA) derivative, with a C-terminal hexahistidine tag, and overexpressed at 17°C in *Escherichia coli* BL21(DE3) pMGK cells. Hemin (7 μM

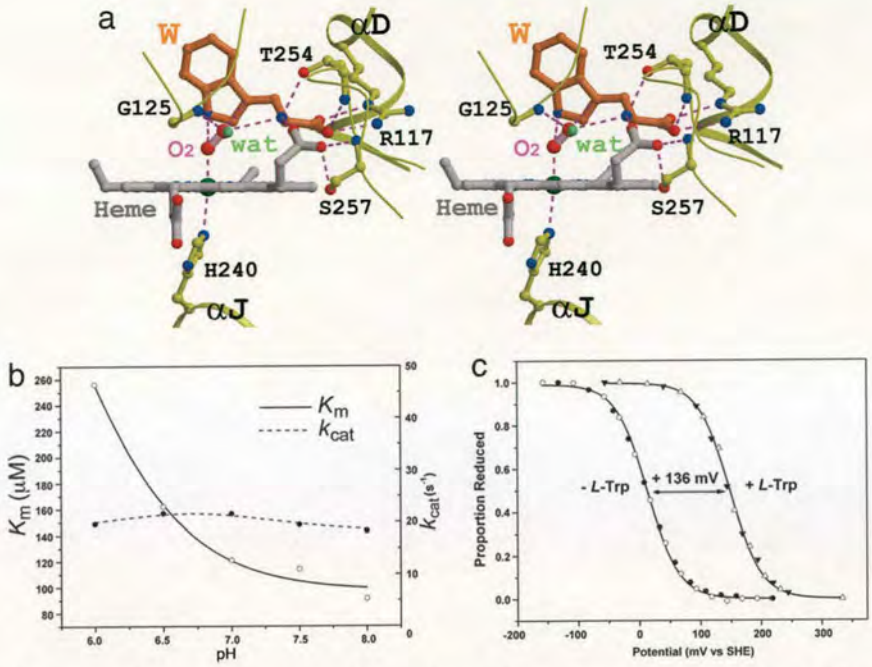

Fig. 4. Molecular insights into the catalysis by TDO. (*a*) Model of the Michaelis complex. The water molecule is shown as a small sphere in green. Produced with Molscript (35) and rendered with Raster3D (36). (*b*) The pH dependence of the k_{cat} and K_m values of *X. campestris* TDO. (*c*) The presence of L-Trp causes a large, positive shift in the reduction potential of TDO. SHE, standard hydrogen electrode.

final concentration) was included in the media for preparation of the holoenzyme samples (23). The protein was purified by using nickel-affinity and gel-filtration chromatography.

Point mutations were created with the QuikChange II site-directed mutagenesis kit (Stratagene, La Jolla, CA). The mutations and their associated ORFs were verified by DNA sequence analysis.

Protein Crystallization. To obtain the structure of TDO in the ferrous state, the protein was reduced by the addition of sodium dithionite, and all steps were performed in an anaerobic glove box (Belle Technology, Dorset, U.K.), with the O_2 concentration maintained <2 ppm. Excess sodium dithionite was removed by gel filtration (Sephadex G25 column) before crystallization. Crystals of TDO were grown by the sitting-drop vapor diffusion method with a well solution comprising 100 mM Mes (pH 6.3), 10–12% (wt/vol) PEG 4000, 60 mM $MnCl_2$, 10 mM sodium dithionite, and 2 mM L-Trp. Before mounting in nylon loops and flash-freezing in liquid nitrogen, crystals were immersed in a cryoprotectant solution composed of mother liquor (with L-Trp concentration increased to 50 mM) supplemented with 23% (vol/vol) glycerol and bubbled with nitric oxide for 15 min before use.

Data Collection and Processing. X-ray diffraction data were collected at the X4A beam line of National Synchrotron Light Source (Brookhaven National Laboratory, Upton, NY), the 21BM beam line at Advanced Photon Source (Argonne National Laboratory, Argonne, IL), and the BM14 beam line at the

Table 2. Summary of kinetic data on *X. campestris* TDO

Enzyme	Substrate	k_{cat}·(s^{-1})	K_m, μM	K_d Ferric heme, mM	K_d Ferrous heme, μM
Wild type					
	L-Trp	19.5 ± 1.2	114 ± 1	3.84 ± 0.14	4.12 ± 0.24
	D-Trp	0	16.5 mM ± 3.3*	>50†	NC
	6-F-D/L-Trp	37.3 ± 0.6	186 ± 12	2.45 ± 0.42	<1†
	5-F-D/L-Trp	2.40 ± 0.10	100 ± 6	1.51 ± 0.08	<1‡
	Indolepropionic acid	0	0	>10†	126 ± 11
	O_2§	35.4 ± 0.9	119 ± 2	0	NA
H55A mutant	L-Trp	2.86 ± 0.10	133 ± 7	ND	3.7 ± 1.3

NA, K_d for O_2 cannot be measured in the absence of substrate because of oxidation or in the presence of substrate because of turnover; NC, No spectral change detected; ND, not done.

*Inhibitory constant, K_i.

†Although a spectral change was evident, substrate solubility prevented accurate measurement of K_d. Values were estimated based on the maximum substrate concentration attainable.

‡Binding was too tight to be measured. Values quoted represent the minimum K_d that can be measured under standard assay conditions.

§The peak positions of the oxyferrous complex (O_2-TDO) are at 420 nm, 548 nm, and 578 nm.

European Synchrotron Radiation Facility (Grenoble, France). The diffraction images were processed and scaled with the HKL package (24). The data-processing statistics are summarized in Table 1, and more complete information can be found in SI Table 3.

Structure Determination and Refinement. The structures of the apo enzymes of TDO and SO4414 were determined by the selenomethionyl single-wavelength anomalous diffraction method (15). The selenium sites were located with SnB (25), and the reflection phases were calculated with Solve/Resolve (26). The structures of the holoenzymes and the ternary complex were determined by the molecular-replacement method, with the programs COMO (27) and AMoRe (28). The atomic models were built with the program XtalView (29) and TURBO-FRODO (30), and the structure refinement was carried out with CNS (31).

Electronic Spectroscopy, Steady-State Assays, and Dissociation Constant Measurements. Electronic absorption spectra were recorded by using a Cary 50-Probe UV-Visible spectrophotometer at 25°C. Assays for the steady-state turnover (at pH 7.5) of L-Trp and derivatives were performed as described (32, 33), except that substrate concentrations of 0–15 mM were used. The kinetic data were fitted to the Michaelis–Menten equation. The pH dependence of the steady-state kinetics was determined in the same manner, by using phosphate (pH 6.0–8.0) and Tris (pH 8.0–9.0) buffers. The electronic absorption spectra of the steady state were recorded by using a stopped-flow spectrophotometer (SX.17MV; Applied-Photophysics, Surrey, U.K.) in conjunction with a diode array detector, housed in an anaerobic glove box ([O_2], <5 ppm; Belle Technology).

OTTLE Electrochemistry. Anaerobic potentiometric titrations were carried out as described (34) at 25°C by using a modified quartz EPR OTTLE cell. Titrations were performed in both the absence and presence of L-Trp (15 mM), and the heme reduction potentials were determined by fitting the data to the Nernst equation for a single-electron process by using Origin software (MicroCal, Northampton, MA). Reduction potentials are quoted versus the standard hydrogen electrode.

We thank Randy Abramowitz and John Schwanof at the National Synchrotron Light Source (Brookhaven National Laboratory, Upton, NY) and Hassan Belrhali at the European Synchrotron Radiation Facility (Grenoble, France) for setting up the beam lines and G. DeTitta of Hauptman Woodward Research Institute (Buffalo, NY) for crystallization screening. This research was supported by Grants P50 GM62413 and U54 GM074958 from the Protein Structure Initiative of the National Institutes of Health.

1. Yoshida R, Hayaishi O (1987) *Methods Enzymol* 142:188–195.
2. Takikawa O (2005) *Biochem Biophys Res Commun* 338:12–19.
3. Sono M, Roach MP, Coulter ED, Dawson JH (1996) *Chem Rev* 96:2841–2887.
4. Mellor A (2005) *Biochem Biophys Res Commun* 338:20–24.
5. Munn DH, Zhou M, Attwood JT, Bondarev I, Conway SJ, Marshall B, Brown C, Mellor AL (1998) *Science* 281:1191–1193.
6. Mellor AL, Munn DH (2004) *Nat Rev Immunol* 4:762–774.
7. Grohmann U, Fallarino F, Puccetti P (2003) *Trends Immunol* 24:242–248.
8. Uyttenhove C, Pilotte L, Theate I, Stroobant V, Colau D, Parmentier N, Boon T, van den Eynde BJ (2003) *Nat Med* 9:1269–1274.
9. Schwarcz R (2004) *Curr Opin Pharmacol* 4:12–17.
10. Muller AJ, DuHadaway JB, Donover PS, Sutanto-Ward E, Prendergast GC (2005) *Nat Med* 11:312–319.
11. Miller CL, Llenos IC, Dulay JR, Weis S (2006) *Brain Res* 1073–1074, 25–37.
12. Platten M, Ho PP, Youssef S, Fontoura P, Garren H, Hur EM, Gupta R, Lee LY, Kidd BA, Robinson WH, *et al.* (2005) *Science* 310:850–855.
13. Littlejohn TK, Takikawa O, Truscott RJW, Walker MJ (2003) *J Biol Chem* 278:29525–29531.
14. Sugimoto H, Oda S-I, Otsuki T, Hino T, Yoshida T, Shiro Y (2006) *Proc Natl Acad Sci USA* 103:2611–2616.
15. Hendrickson WA (1991) *Science* 254:51–58.
16. Daraselia N, Dernovoy D, Tian Y, Borodovsky M, Tatusov R, Tatusova T (2003) *OMICS* 7:171–175.
17. Holm L, Sander C (1993) *J Mol Biol* 233:123–138.
18. Cady SG, Sono M (1991) *Arch Biochem Biophys* 291:326–333.
19. Terentis AC, Thomas SR, Takikawa O, Littlejohn TK, Truscott RJW, Armstrong RS, Yeh S-R, Stocker R (2002) *J Biol Chem* 277:15788–15794.
20. Unno M, Matsui T, Chu GC, Couture M, Yoshida T, Rousseau DL, Olson JS, Ikeda-Saito M (2004) *J Biol Chem* 279:21055–21061.
21. Ishimura Y, Makino R, Iizuka T (1980) *Adv Enzyme Regul* 18:291–302.
22. Sono M (1989) *Biochem* 28:5400–5407.
23. Littlejohn TK, Takikawa O, Skylas D, Jamie JF, Walker MJ, Truscott RJW (2000) *Protein Expr Purif* 19:22–29.
24. Otwinowski Z, Minor W (1997) *Methods Enzymol* 276:307–326.
25. Weeks CM, Miller R (1999) *J Appl Crystallogr* 32:120–124.
26. Terwilliger TC (2003) *Methods Enzymol* 374:22–37.
27. Jogl G, Tao X, Xu Y, Tong L (2001) *Acta Crystallogr D* 57:1127–1134.
28. Navaza J (1994) *Acta Crystallogr A* 50:157–163.
29. McRee DE (1999) *J Struct Biol* 125:156–165.
30. Roussel A, Cambillau C (1991) *TURBO-FRODO. Silicon Graphics Geometry Partners Directory* 86 (Silicon Graphics, Mountain View, CA).
31. Brunger AT, Adams PD, Clore GM, DeLano WL, Gros P, Grosse-Kunstleve RW, Jiang J-S, Kuszewski J, Nilges M, Pannu NS, *et al.* (1998) *Acta Crystallogr D* 54:905–921.
32. Ishimura Y (1970) *Methods Enzymol* 17A:429–434.
33. Papadopoulou ND, Mewies M, McLean KJ, Seward HE, Svistunenko DA, Munro AW, Raven EL (2005) *Biochem* 44:14318–14328.
34. Ost TW, Clark JP, Anderson JLR, Yellowlees LJ, Daff S, Chapman SK (2004) *J Biol Chem* 279:48876–48882.
35. Kraulis PJ (1991) *J Appl Crystallogr* 24:946–950.
36. Merritt EA, Bacon DJ (1997) *Methods Enzymol* 277:505–524.

Histidine 55 of Tryptophan 2,3-Dioxygenase Is Not an Active Site Base but Regulates Catalysis by Controlling Substrate Binding‡

Sarah J. Thackray,§ Chiara Bruckmann,§ J. L. Ross Anderson,§ Laura P. Campbell,§ Rong Xiao,|| Li Zhao,|| Christopher G. Mowat,§ Farhad Forouhar,⊥ Liang Tong,⊥ and Stephen K. Chapman*,§

EaStCHEM, School of Chemistry, University of Edinburgh, West Mains Road, Edinburgh EH9 3JJ, U.K., Department of Biological Sciences, Northeast Structural Genomics Consortium, Columbia University, New York, New York 10027, and Center for Advance Biotechnology and Medicine, Rutgers University, Piscataway, New Jersey 08854

Received June 27, 2008; Revised Manuscript Received August 6, 2008

ABSTRACT: Tryptophan 2,3-dioxygenase (TDO) from *Xanthomonas campestris* is a highly specific heme-containing enzyme from a small family of homologous enzymes, which includes indoleamine 2,3-dioxygenase (IDO). The structure of wild type (WT TDO) in the catalytically active, ferrous (Fe^{2+}) form and in complex with its substrate L-tryptophan (L-Trp) was recently reported [Forouhar et al. (2007) *Proc. Natl. Acad. Sci. U.S.A. 104*, 473−478] and revealed that histidine 55 hydrogen bonds to L-Trp, precisely positioning it in the active site and implicating it as a possible active site base. In this study the substitution of the active site residue histidine 55 by alanine and serine (H55A and H55S) provides insight into the molecular mechanism used by the enzyme to control substrate binding. We report the crystal structure of the H55A and H55S mutant forms at 2.15 and 1.90 Å resolution, respectively, in binary complexes with L-Trp. These structural data, in conjunction with potentiometric and kinetic studies on both mutants, reveal that histidine 55 is not essential for turnover but greatly disfavors the mechanistically unproductive binding of L-Trp to the oxidized enzyme allowing control of catalysis. This is demonstrated by the difference in the K_d values for L-Trp binding to the two oxidation states of wild-type TDO (3.8 mM oxidized, 4.1 μM reduced), H55A TDO (11.8 μM oxidized, 3.7 μM reduced), and H55S TDO (18.4 μM oxidized, 5.3 μM reduced).

Oxidative cleavage of the L-tryptophan (L-Trp)[1] pyrrole ring and the insertion of molecular oxygen to produce *N*-formylkynurenine is the first and rate-limiting step in the kynurenine pathway and is catalyzed by tryptophan 2,3-dioxygenase (TDO) and indoleamine 2,3-dioxygenase (IDO) (*2, 3*). The kynurenine pathway processes 95% of L-Trp utilized by humans, leading ultimately to the formation of nicotinamide adenine dinucleotide (NAD^+), an essential coenzyme (*4*). Kynurenine pathway metabolites have been implicated in a number of diseases ranging from neurological disorders, such as cerebral malaria and multiple sclerosis, to cataract formation (*5, 6*). Recent findings have implicated tryptophan catabolism via the kynurenine pathway in immune tolerance, including immune suppression in maternal fetal tolerance and the immune escape of cancers (*7*−*10*). These properties make elucidation of the precise catalytic mechanism of these enzymes extremely important.

TDO and IDO belong to a little-characterized family of dioxygenases that occurs in both prokaryotes and eukaryotes (*11*). These enzymes have homologous 3-D structures but dissimilar primary structures, with sequence identity often less than 10% between family members (*12*). First identified in 1936 (*13*), TDO is mainly found in the liver of mammals but has also been recently identified in mammalian mucous membranes, epididymis, and brain (*14, 15*). The enzyme discussed here is a prokaryotic TDO from *Xanthomonas campestris* (the causative agent of black rot in cabbages), which shares 34% sequence identity with human TDO. The enzyme is a homotetramer that displays high substrate specificity, catalyzing the oxidation of L-Trp, 5-F-Trp, and 6-F-Trp (*1*). In contrast, IDO is found throughout the body in mammals, except for in the liver, and no prokaryotic IDO protein has yet been identified. IDO is monomeric and catalyzes the dioxygenation of L-Trp, D-Trp, serotonin, tryptamine, and 5-OH-Trp, displaying less substrate specificity than TDO (*11, 16*). The crystal structures of WT *X. campestris* TDO (*1, 17*) and human IDO (*12*) have been published recently, revealing similarities between the two enzymes and allowing the identification of potentially important active site residues.

The catalytic mechanisms employed by TDO and IDO have, as yet, not been elucidated, but two proposed mechanisms for tryptophan dioxygenation are shown in Figure 1.

‡ The atomic coordinates for H55A and H55S mutant enzymes of TDO have been deposited in the Protein Data Bank, entries 3BK9 and 3E08, respectively.

* To whom correspondence should be addressed. E-mail: S.K.Chapman@ed.ac.uk. Tel: +44 131 650 4760. Fax: +44 131 650 6453.

§ University of Edinburgh.

|| Rutgers University.

⊥ Columbia University.

[1] Abbreviations: TDO, tryptophan 2,3-dioxygenase; IDO, indoleamine 2,3-dioxygenase; L-Trp, L-tryptophan; 5-F-Trp, 5-fluoro-DL-tryptophan; 6-F-Trp, 6-fluoro-DL-tryptophan; WT, wild type; H55A, histidine 55 → alanine; H55S, histidine 55 → serine; SHE, standard hydrogen electrode; OTTLE, optically transparent thin-layer electrochemistry.

10.1021/bi801202a CCC: $40.75
Published on Web 09/11/2008

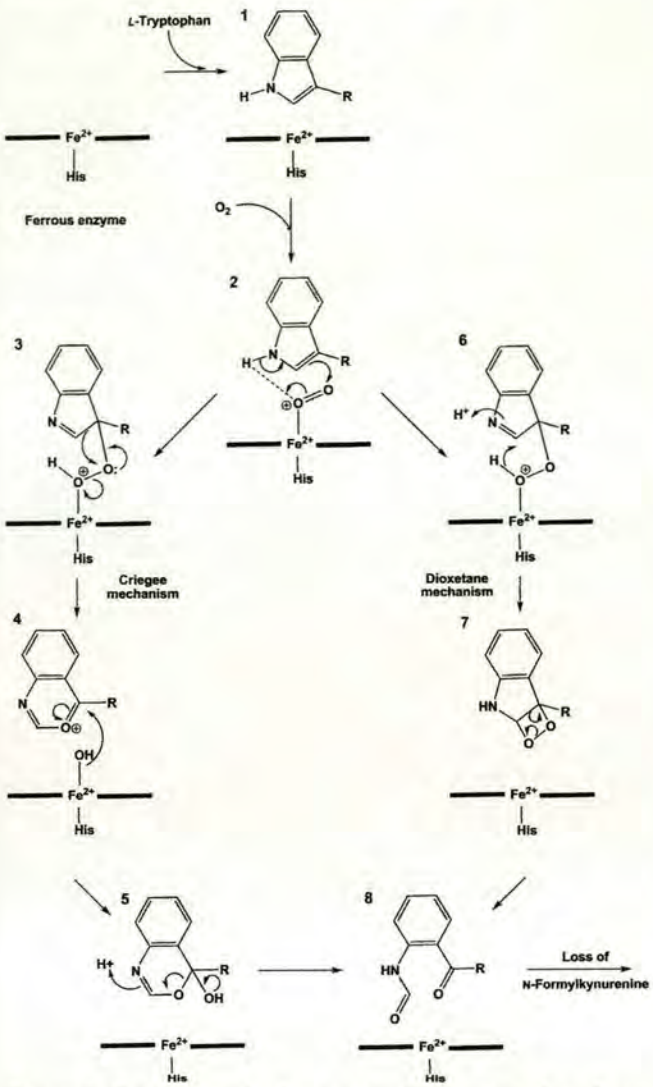

FIGURE 1: Catalytic mechanism proposed for L-tryptophan dioxygenation by TDO. The figure displays an ionic, base-catalyzed mechanism of L-Trp dioxygenation. The first substrate binds to the protein (1), followed by dioxygen binding to form the ternary complex (2). The mechanism proceeds by the formation of a hydroperoxide intermediate (3 and 6), which can undergo two different rearrangements to form the product, *N*-formylkynurenine (8), a Criegee rearrangement (4 and 5), or a dioxetane rearrangement (7). The product is then released leaving the protein in the active ferrous state.

It is proposed that the catalytic mechanism involves the base-catalyzed deprotonation of the indole nitrogen of the substrate. However, the structures of TDO and IDO show that while TDO contains a histidine residue in its active site, IDO does not contain any residues in its active site capable of performing base-catalyzed deprotonation. Instead, it has been proposed that proton abstraction is facilitated by a bound dioxygen molecule (Figure 2).

In the TDO active site histidine 55 hydrogen bonds to L-Trp and is implicated as the active site base. In this study we attempt to resolve the question of whether an active site base is necessary for catalytic activity in TDO. To accomplish this, histidine is replaced by alanine or serine (H55A and H55S mutants of TDO). These substitutions were chosen due to the inability of alanine to act as an active site base and the presence in IDO of a serine residue in the analogous position to histidine 55. We report the crystal

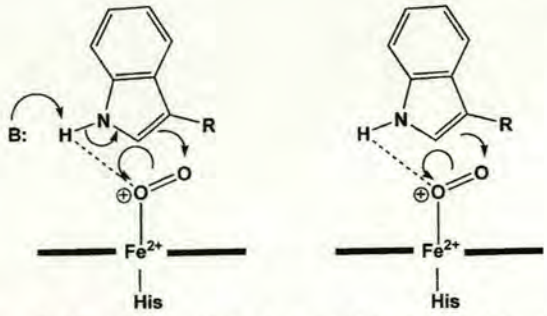

FIGURE 2: Proposed catalytic intermediates involved in proton abstraction of the indole nitrogen of L-tryptophan. The ternary enzyme−substrate−dioxygen complex can either undergo (a) a base-catalyzed proton abstraction or (b) proton abstraction by the bound dioxygen.

structure of the H55A mutant to 2.15 Å resolution and the crystal structure of the H55S mutant to 1.90 Å resolution and relate these to electrochemical and kinetic data for the mutant enzymes.

EXPERIMENTAL PROCEDURES

Genetic Manipulation, Protein Expression, and Purification. Full-length *X. campestris* TDO (NESG (Northeast Structural Genomics Consortium) ID XcR13) was cloned into a pET-21d (Novagen, San Diego, CA) derivative with a C-terminal hexahistidine tag and overexpressed at 17 °C in *Escherichia coli* BL21(DE3) pMGK cells. Point mutations H55A and H55S were created by employing the QuikChange II site-directed mutagenesis kit (Stratagene, La Jolla, CA). Oligonucleotide primers directing mutations were designed in an automated fashion by using the Primer Prim'er program, accessible at www-nmr.cabm.rutgers.edu/bioinformatics/Primer_Primer/. The mutations and their associated ORF were verified by DNA sequence analysis (*1*).

WT TDO and its mutant forms were purified using nickel-affinity and gel-filtration chromatography. Protein and heme concentrations were determined by the Bradford and pyridine hemochrome methods, respectively (*18, 19*). For WT TDO extinction coefficients ε_{404nm} and ε_{431nm} of 180.5 (±0.1) mM^{-1} cm^{-1} and 113.0 (±0.1) mM^{-1} cm^{-1} per protomer were calculated for the ferric and ferrous enzymes, respectively (*1*). For the H55A mutant enzyme extinction coefficients ε_{405nm} and ε_{431nm} were 130.4 (±0.3) mM^{-1} cm^{-1} and 120.0 (±0.1) mM^{-1} cm^{-1} per protomer. For the H55S mutant extinction coefficients ε_{405nm} and ε_{431nm} were 132.0 (±0.3) mM^{-1} cm^{-1} and 116.0 (±0.2) mM^{-1} cm^{-1} per protomer.

Protein Crystallization and Data Collection. Crystallization of H55A and H55S TDO was carried out by hanging drop vapor diffusion at 18 °C in Linbro plates. Crystals were obtained with well solutions comprising 9−10% (w/v) PEG 1000, 80 mM MES buffer, pH 6.3, 20 mM bicine buffer, pH 9.0, 40 mM $MnCl_2$, 400 mM $MgCl_2$, 8−15 mM NaCN, and 20 mM L-Trp. Hanging drops (4 μL volume) were prepared by adding 2 μL of 8 mg mL^{-1} protein (in 50 mM Tris-HCl buffer, pH 8.0, 5 mM in EDTA) to 2 μL of well solution. Red tetragonal shaped crystals appeared after approximately 1 week, reaching full size after 2 weeks. Crystals were immersed in mineral oil prior to being mounted in nylon loops and flash cooled in liquid nitrogen. For crystals of both H55A and H55S enzymes, data sets were collected to a resolution of 2.15 and 1.90 Å, respectively, at station

10.1 at SRS Daresbury (λ = 1.381 Å for H55A TDO, λ = 1.045 Å for H55S). In both cases crystals belonged to space group $P2_1$ with unit cell parameters a = 78.2 Å, b = 117.6 Å, c = 139.3 Å, and β = 95.7 ° (H55A) and a = 77.9 Å, b = 117.8 Å, c = 139.1 Å, and β = 95.7 ° (H55S).

Data processing was carried out using the CCP4 package (*20*) and PHENIX (*21*). The wild-type TDO apoenzyme structure (PDB ID 1YW0), stripped of water, was used as the initial model. Electron density fitting was carried out using PHENIX and Turbofrodo (*22*), and structure refinement was carried out using PHENIX and Refmac (*23*).

Steady-State Kinetic Analysis and Binding Constant Assays. UV−visible spectra were recorded at 25 °C using a Cary 50-Probe UV−visible spectrophotometer. Steady-state turnover assays (at pH 7.5) for oxidation of L-Trp and fluorinated derivatives were performed as described by Ishimura (*24*), except that substrate concentrations of up to 15 mM L-Trp were used. The rate of formation of *N*-formylkynurenine was monitored by measuring the change in absorbance at 321 nm (ϵ_{321}(*N*-formylkynurenine) = 3750 M^{-1} cm^{-1}). Kinetic data were fitted to the Hill equation using Origin software (MicroCal, Northampton, MA). Dissociation constants (K_d) for binding to ferric and ferrous WT TDO and mutant enzymes were determined by established procedures in a Belle Technology anaerobic glovebox with [O_2] maintained below 5 ppm. The electronic absorption spectra at the steady state were recorded by using a stopped-flow spectrophotometer (SX.17MV; Applied-Photophysics, Surrey, U.K.) in conjunction with a diode array detector, housed in an anaerobic glovebox. The oxygen binding affinity (K_m) was measured by standard methods by adding varying concentrations of O_2 ($\leq$1 mM) to the L-Trp saturated (25 mM) assay and by calculating the steady-state parameters as described above. Oxygen concentration was determined spectrophotometrically by titrating aliquots of oxygenated buffer into a solution of electrochemically reduced methyl viologen. The subsequent change in absorbance at 540 nm (ϵ_{540}(methyl viologen) = 13000 M^{-1} cm^{-1}) due to reduction of molecular oxygen was used to calculate [O_2] (*1*).

OTTLE Electrochemistry. Anaerobic potentiometric titrations on WT TDO and mutant enzymes were carried out as previously described (*1, 25*) at 25 °C using a modified quartz EPR OTTLE cell, with the exception that 100 mM Tris-HCl buffer, pH 7.5, and 300 mM KCl (with or without 10% glycerol) buffer was used. A range of mediators were added (2-hydroxy-1,4-naphthoquinone (−145 mV vs SHE), 5-hydroxy-1,4-naphthoquinone (−3 mV), phenazine ethosulfate (+55 mV), phenazine methosulfate (+82 mV), and 1,2-naphthoquinone (+135 mV)) to ensure efficient reduction and reoxidation of the protein. Titrations were performed in both the absence and presence of substrate for WT TDO (15 mM L-Trp), the H55A mutant (5 mM L-Trp), and the H55S mutant (10 mM L-Trp). Heme reduction potentials were determined by fitting the data to a Nernst equation for a single-electron process using Origin software. Reduction potentials are quoted versus the standard hydrogen electrode.

RESULTS AND DISCUSSION

Crystal Structures of H55A and H55S TDO. It was possible to obtain crystals of the ferric H55A and H55S mutant enzymes in binary complex with the substrate due to the much greater affinity of L-Trp for the oxidized mutant enzymes compared to WT TDO (see below and Table 3). For H55A TDO a data set to 2.15 Å resolution was used to refine the structure to a final *R*-factor of 20.5% (R_{free} = 28.5%), while for H55S TDO data to a resolution of 1.90 Å were used to refine the structure to a final *R*-factor of 17.8% (R_{free} = 21.6%). Data collection and refinement statistics are summarized in Table 1.

Table 1: H55A and H55S Data Collection and Refinement Statistics

	H55A	H55S
resolution (Å)	59.66−2.15	17.56−1.90
total no. of reflections	312593	362159
no. of unique reflections	131764	189203
completeness (%)	96.9	93.6
$I/[\sigma(I)]$	9.5	7.3
R_{merge} (%)[a]	10.0	7.8
R_{merge} in outer shell (2.27−2.15 Å) (%)	47.4	48.0
R_{cryst} (%)[b]	20.5	17.8
R_{free} (%)[b]	28.5	21.6
rmsd from ideal values		
bond lengths (Å)	0.022	0.007
bond angles (deg)	2.004	0.952
Ramachandran analysis		
most favored (%)	91.9	92.2
additionally allowed (%)	8.1	7.8
average *B*-factor (overall) (Å^2)	23.2	23.2
average *B*-factor (substrate) (Å^2)	25.7	24.1

[a] $R_{merge} = \sum_h\sum_i|I(h) - I_i(h)|/\sum_h\sum_i I_i(h)$, where $I_i(h)$ and $I(h)$ are the ith and mean measurement of reflection h, respectively. [b] $R_{cryst} = \sum_h|F_o - F_c|/\sum_h F_o$, where F_o and F_c are the observed and calculated structure factor amplitudes of reflection h, respectively. R_{free} is the test reflection data set, 5% selected randomly for cross-validation during crystallographic refinement.

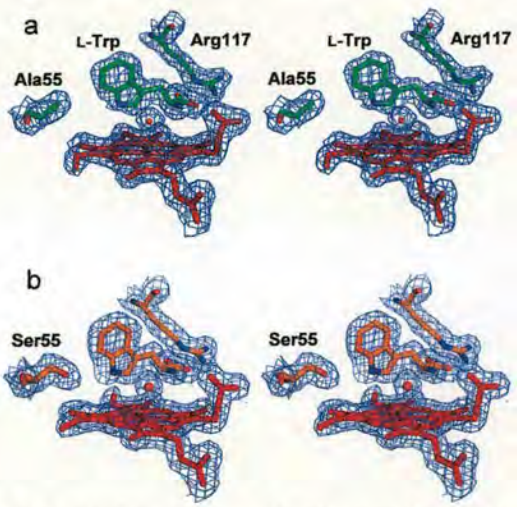

FIGURE 3: Stereoview of electron density around the heme, bound L-Trp, arginine 117, and residue 55 at the active site of (a) H55A TDO and (b) H55S TDO. The electron density map was calculated using Fourier coefficients $2F_o - F_c$, where F_o and F_c are the observed and calculated structure factors, respectively, the latter based on the final model. The contour level is 1σ, where σ is the rms electron density. This figure was generated using PYMOL (*30*).

For each of the H55A and H55S mutant enzymes the final model consists of two TDO tetramers (1 and 2), one of which (tetramer 1) is better defined than the other in the electron density map. The quality of the final electron density map around the active site of chain A of tetramer 1 of both mutant enzymes is shown in Figure 3.

In both mutant enzymes each monomer also binds one heme group and one substrate molecule. Further to this, a

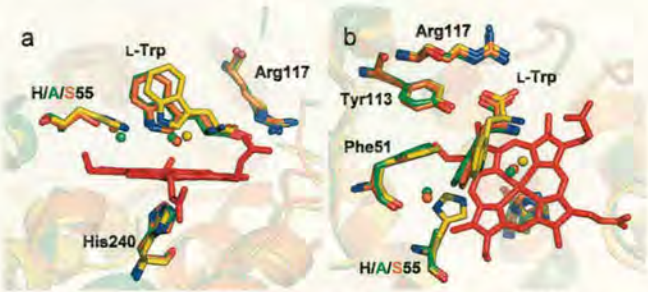

FIGURE 4: An overlay of the active site region of WT TDO (yellow), H55A TDO (green), and H55S TDO (orange) viewed from the side (a) and from above (b). The L-Trp from the H55A and H55S enzymes (in green and orange, respectively) are rotated toward alanine/serine 55 and the heme, relative to the position of the substrate in WT TDO (yellow). The H-bond between histidine 55 and the substrate is lost as a result of the substitution by alanine/serine. The position of the water molecule (water A; see Figure 5) above the heme group in H55A and H55S TDOs is slightly different than in WT enzyme due to the altered substrate binding. This figure was generated using PYMOL (*30*).

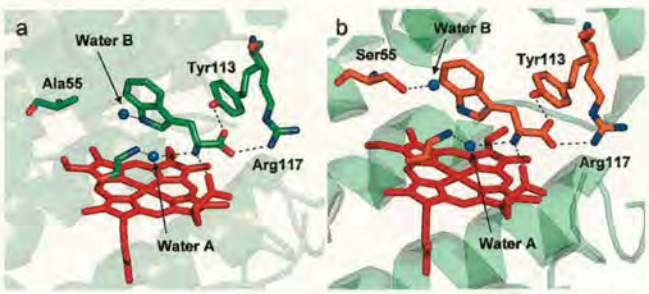

FIGURE 5: The active site of (a) H55A TDO and (b) H55S TDO. Hydrogen-bonding interactions are indicated by dashed lines. The subtly different positions of water B in the mutant enzymes can be seen. This figure was generated using PYMOL (*30*).

second L-Trp molecule is observed at the intersubunit interface close to each of chains A, B, C, D, and E in the H55A TDO structure, and in the H55S model there is one interfacial L-Trp per monomer. In addition, the H55A and H55S models contain 1026 and 1955 water molecules, respectively. The atomic coordinates have been deposited in the Protein Data Bank, accession codes 3BK9 (H55A) and 3E08 (H55S).

Binding Mode of L-Trp to H55A and H55S Mutants. The binding orientation of L-Trp at the active site of the H55A mutant enzyme is slightly different from that observed in the WT TDO structure. An overlay of the active sites of WT TDO and the H55A and H55S enzymes (based on α-C overlay) is shown in Figure 4. The bound L-Trp substrates belonging to the H55A and H55S mutant enzymes (in green and orange, respectively) are shifted toward the side chain of residue 55 relative to the position of L-Trp in the wild-type enzyme (in yellow). Due to the substitution of histidine 55 by alanine or serine the hydrogen-bonding interaction between residue 55 and the substrate indole nitrogen atom is lost. The remaining interactions between the substrate and active site residues that are observed in the wild-type enzyme are maintained in both mutant enzymes (Figure 5).

The active sites of WT TDO and both of the H55A and H55S mutant enzymes contain a water molecule above the distal face of the heme (water A in Figure 5). In all three enzymes this water is H-bonded to the ammonium group of L-Trp and the main-chain amide nitrogen of glycine 125 but is too far (≥2.7 Å) from the heme iron to be a ligand. Further to this, an additional water molecule is found in the active site of the H55A and H55S mutant enzymes (water B in Figure 5) in a position which would be sterically inhibited by the histidine 55 side chain in WT TDO. In the H55A mutant enzyme water B is H-bonded to the substrate indole nitrogen (Figure 5a), but in the H55S model water B is instead H-bonded to the side-chain hydroxyl group of serine 55 (Figure 5b), too far away (~3.4 Å) from L-Trp to maintain a hydrogen-bonding interaction.

In WT TDO the histidine 55 imidazole moiety H-bonds to a water molecule in the substrate-free ferrous state, which is displaced upon binding of substrate. The removal of the histidine side chain in either mutant enzyme would almost certainly result in the absence of a water molecule in such a position.

Steady-State Kinetics and Substrate/Substrate Analogue Binding. It has been previously reported that WT TDO shows catalytic activity toward L-Trp, 6-F-Trp, and 5-F-Trp. We have also observed activity toward 5-methyl-DL-tryptophan and 6-methyl-DL-tryptophan. H55A and H55S mutant enzymes show catalytic activity toward L-Trp, 6-F-Trp, 5-F-Trp, 5-methyl-DL-tryptophan, and 6-methyl-DL-tryptophan but no activity with any other compounds investigated. Kinetic parameters are shown in Table 2, and there is about a 7-fold decrease in k_{cat} values, compared to WT TDO, for both mutant enzymes. As previously reported, there is no inhibition of WT TDO catalytic activity on addition of 1-Me-DL-tryptophan, and the same result is obtained for the mutant enzymes (*1*). This contrasts with findings on IDO, where 1-Me-DL-tryptophan is a known inhibitor of L-Trp dioxygenation activity (*11*). Catalytic activity is observed only by the ferrous enzyme for both WT TDO and its mutant forms, in contrast to recent findings that show catalytic activity by ferric human TDO.

The substitution of histidine 55 may have been expected to render the enzyme inactive if a base is required in the catalytic cycle, but the possibility that a water molecule could be bound, in the vacant space made by the substitution of histidine 55, must be considered. This water molecule could, possibly, act as an active site base dependent on its pK_a in the active site. A water molecule is found near this position in both of the mutant enzymes, but it is not optimally aligned for the deprotonation of L-Trp. It is also located 3.3 Å away from the indole nitrogen atom, outside the range of a normal H-bonding interactions, and we propose that it plays no role in the catalytic cycle (Figure 1). These data, and the relative insensitivity of the WT TDO k_{cat} to pH (Supporting Information Table 1), support the idea that histidine 55 or a solvent molecule is not required to deprotonate the indole nitrogen atom. In IDO where the active site is devoid of solvent, the equivalent residue to histidine 55 is serine 167, which is incapable of acting as a catalytic base. Turnover still occurs, and like TDO k_{cat} is observed to be insensitive to pH (*26*).

The decrease in k_{cat} for L-Trp oxidation in both the H55A and H55S mutants may be explained by the movement of L-Trp in the active site. It can be seen from the crystal structures that for both mutants L-Trp has rotated toward the substituted amino acid (and away from the iron atom) relative to the position of L-Trp in WT TDO. The L-Trp indole ring has also shifted toward the heme (shown in Figure 4). These movements are accompanied by a slight increase in the

Table 2: Kinetic Parameters for *X. campestris* TDO Wild Type and Mutants

	WT TDO			H55A			H55S		
	k_{cat} (s^{-1})	K_m (μM)	k_{cat}/K_m	k_{cat} (s^{-1})	K_m (μM)	k_{cat}/K_m	k_{cat} (s^{-1})	K_m (μM)	k_{cat}/K_m
L-Trp[a]	19.5 ± 1.2	114 ± 1	1.711 (100)	2.86 ± 0.10	133 ± 7	0.215 (100)	2.6 ± 0.01	197 ± 2	0.132 (100)
6-F-D/L-Trp[a]	37.3 ± 0.6	186 ± 12	2.005 (117)	3.78 ± 0.10	195 ± 1	0.194 (90)	3.80 ± 0.04	546 ± 36	0.070 (53)
5-F-D/L-Trp[a]	2.40 ± 0.10	100 ± 6	0.240 (14)	0.68 ± 0.14	194 ± 25	0.035 (16)	0.80 ± 0.01	183 ± 12	0.044 (33)
6-Me-D/L-Trp[a]	41.0 ± 1.2	975 ± 48	0.421 (25)	1.65 ± 0.03	386 ± 4	0.0443 (21)	4.66 ± 0.18	1980 ± 170	0.024 (18)
5-Me-D/L-Trp[a]	3.59 ± 0.05	357 ± 12	0.101 (6)	0.40 ± 0.01	395 ± 20	0.010 (5)	1.45 ± 0.01	1302 ± 21	0.011 (8)

[a] Experiments were performed at 25 °C in 100 mM phosphate buffer, pH 7.5, by varying the concentration of the substrate. It should be noted that these rates are determined under normal atomospheric conditions; therefore, the rates determined are "apparent" for k_{cat} as oxygen is not present at a saturating level. The peak positions of the oxyferrous complex (O_2−TDO) are at 420, 548, and 578 nm, and V_{max}, K_m, and K_i are calculated using L-Trp.

Table 3: Substrate Binding to Oxidized and Reduced *X. campestris* TDO Wild Type and Mutants[a]

	TDO WT (K_d)		H55A (K_d)		H55S (K_d)	
substrate	Fe^{3+} (mM)	Fe^{2+} (μM)	Fe^{3+} (μM)	Fe^{2+} (μM)	Fe^{3+} (μM)	Fe^{2+} (μM)
L-Trp	3.84 ± 0.14	4.1 ± 0.2	11.8 ± 0.2	3.7 ± 1.3	18.4 ± 3.0	5.3 ± 1.0
6-F-D/L-Trp	1.51 ± 0.08	<1.00[b]	165 ± 44	73 ± 3	86 ± 12	6.2 ± 0.9
5-F-D/L-Trp	2.45 ± 0.42	<1.00[b]	67 ± 20	9.0 ± 1.7	73 ± 5	<5.00[b]

[a] Experiments were performed at 25 °C in 100 mM phosphate buffer, pH 7.5. Absorbance changes upon substrate binding are small (~5−10% of initial peak absorbance) but easily quantifiable due to tight substrate binding. [b] Binding was too tight to be measured. Values quoted represent the minimum K_d that can be measured under standard assay conditions.

substrate K_m values, implying a small decrease in the stability of the Michaelis complex. The rotation has resulted in the displacement of the tryptophan indole ring from the dioxygen binding site, thus decreasing overlap of the molecular orbitals involved in catalysis. The transition state for the reaction will be less stable, thus increasing the activation energy for catalysis. This will decrease the turnover rates for both mutants compared to WT TDO.

In WT TDO there is a large increase in the affinity of the enzyme for L-Trp for ferrous vs ferric enzyme ($K_d(Fe^{3+})$ = 3.8 mM, $K_d(Fe^{2+})$ = 4.1 μM) (Table 3). This is in contrast to recent findings for human TDO, where there was found to be little discrimination of binding between the ferric and the ferrous enzymes (*27*). For both mutant proteins this effect is essentially destroyed, with only a small increase shown in the affinity of the ferrous enzyme for L-Trp relative to ferric (Table 3). This trend in K_d is repeated for other substrates. These findings suggest that one role of histidine 55 is to disfavor substrate binding to the oxidized protein, and its removal increases binding affinity by a factor >300. It can therefore be hypothesized that histidine 55 is responsible for controlling the binding affinity of the active site for L-Trp, effectively gating the binding of substrate to WT TDO. In this way histidine 55 greatly disfavors the mechanistically unproductive binding of L-Trp to the oxidized enzyme, promoting the productive binding of L-Trp to the reduced enzyme.

Electrochemical Studies. Electrochemical data for WT TDO and the H55A mutant are shown in Figure 6, and the measured midpoint potentials are displayed in Table 4. There is a much smaller shift in the reduction potential upon binding of substrate ($\Delta E_{mid\ H55A}$ = +23 mV) ($\Delta E_{mid\ H55S}$ = +57 mV) for the mutant enzymes compared to WT TDO ($\Delta E_{mid\ WT}$ = +136 mV). The shift in reduction potential of 23 mV for the H55A mutant enzyme almost perfectly correlates with the increase in affinity for L-Trp for the ferrous vs the ferric form (K_d (Fe(II)) = 3.7 μM vs K_d (Fe(III)) = 11.8 μM), both giving an estimated $\Delta\Delta G$ of 3.5 kJ mol^{-1}. In fact, the difference in these $\Delta\Delta G$ values calculated for WT TDO and the H55A mutant enzyme is

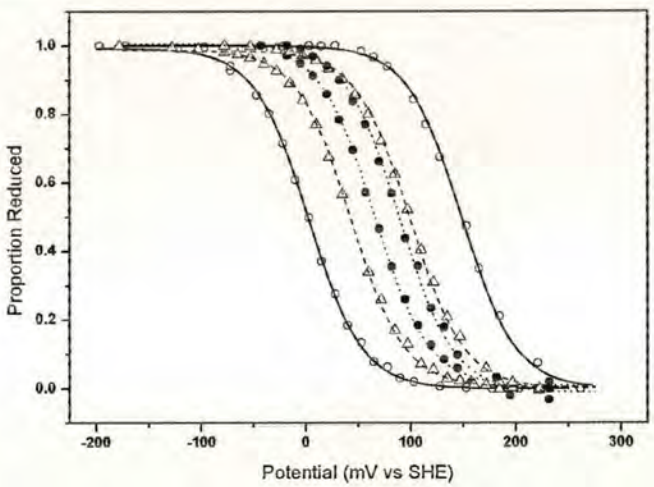

FIGURE 6: OTTLE potentiometric curves for wild-type TDO (open circles), H55A mutant (closed circles), and H55S mutant (open triangles) with (right-hand plots) and without (left-hand plots) L-Trp substrate present (±L-Trp). Each curve is produced from both reduction and oxidation of the layer of interest.

Table 4: Electrochemical Midpoint Potentials

	potential (mV vs SHE)		
	no L-Trp	+L-Trp	change
TDO WT	8 ± 5	144 ± 6	+136
H55A	64 ± 3	87 ± 2	+23
H55S	44 ± 2	101 ± 2	+57
rlTDO[a]	100	160	+60
rhIDO[b]	−30 ± 4	16 ± 3	+46

[a] See ref *29*. [b] See ref *26*.

approximately 11.5 kJ mol^{-1}, within the range of energies for a single hydrogen bond. The data are less clear for H55S, with a 57 mV shift in the reduction potential on L-Trp binding. The increase in affinity for L-Trp to the ferrous H55S vs the ferric give an estimated $\Delta\Delta G$ of 5.5 kJ mol^{-1}. It is possible that the lower affinity of oxidized WT TDO for substrate may be attributed to subtle changes in the structure of the active site (in terms of the hydrogen-bonding pattern) between the oxidized and reduced enzymes. Binding of L-Trp

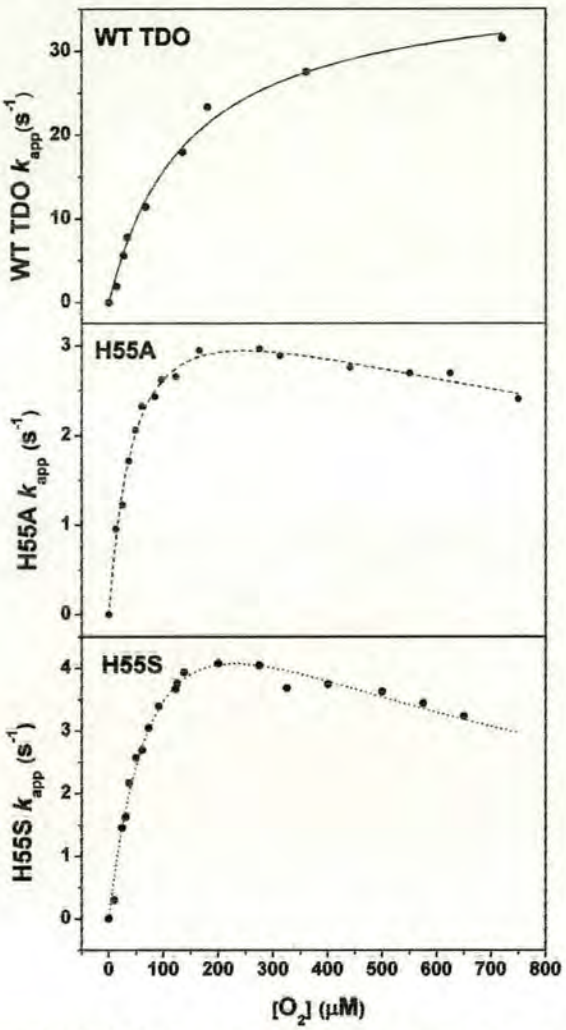

FIGURE 7: Plot of the observed steady-state turnover rate (k_{app}) versus O_2 concentration for wild-type TDO (top) and H55A (middle) and H55S (bottom) mutant forms. The maximum turnover rate (k_{max}), the Michaelis constant (K_m), and the inhibition constant (K_i (for oxygen)) are reported.

accompanies expulsion of solvent from the active site and results in the formation of a hydrogen bond between histidine 55 and the pyrrole nitrogen of the indole L-Trp moiety.

In the H55A mutant enzyme the alanine side chain is unable to form the same hydrogen bonds that histidine 55 can in WT TDO. Consequently, there may be less rearrangement of the active site hydrogen-bonding interactions necessary to allow L-Trp binding, and the K_d for substrate binding to ferric enzyme is correspondingly low. All other amino acid interactions binding L-Trp to the active site are analogous to WT TDO. Consequently, the absence of significant oxidation-state-dependent changes in the active site in H55A TDO results in decreased specificity of binding to the oxidized or reduced enzyme.

The case is similar for the H55S mutant enzyme as the serine side chain is unable to form the same hydrogen bonds that histidine 55 can in WT TDO. It is possible that the serine could form a bonding interaction with a nearby solvent molecule (water 250), but the data suggest that less rearrangement of active site hydrogen-bonding interactions is necessary to allow L-Trp binding than for WT TDO.

Stability of the Michaelis Complex. Figure 7 shows how the observed rate constant for turnover (k_{app}) is dependent

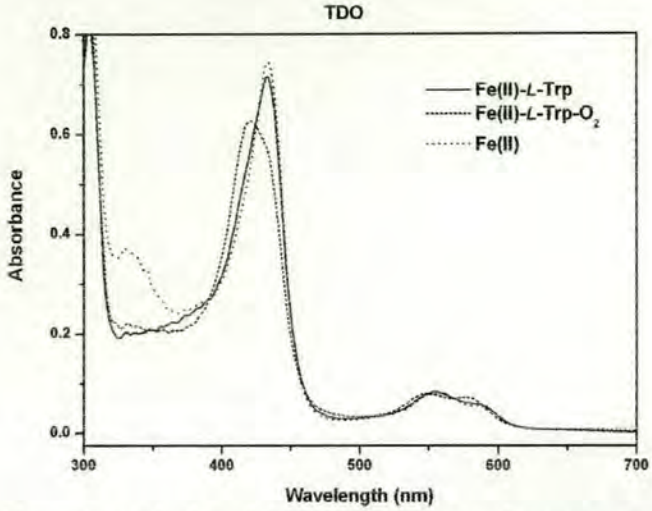

FIGURE 8: Production of the wild-type TDO oxyferrous ternary complex. The peak positions of the oxyferrous ternary complex are at 420, 548, and 578 nm. This decays back to ferrous enzyme and product (*N*-formylkynurenine, peak position 321 nm).

on dioxygen concentration, [O_2], under saturating L-Trp concentrations (25 mM). In phosphate buffer (pH 7.5) at 25 °C, $K_m(O_2)$ is approximately 120 μM and k_{app} for WT TDO is only 60% of maximum; however, in the case of the H55A and H55S mutant enzymes, k_{app} is nearly maximal (Table 2). These data seem contrary to the Michaelis model (based on steady-state kinetics) that predicts a lower O_2 binding affinity for the mutant forms.

WT TDO has an ordered catalytic cycle in which the reduced enzyme−substrate complex must be formed prior to O_2 binding for turnover to occur (*11, 28*). No ferrous−oxy complex is observed, and addition of oxygen to ferrous WT TDO or the mutant forms in the absence of substrate leads to direct decay to the ferric state. This is also the case for human TDO (*27*), suggesting that instability of the ferrous−oxy species may be common in TDO species. The similar L-Trp binding affinity of the reduced mutant enzymes compared to WT TDO (3.7 and 5.2 μM versus 4.1 μM) and similar K_m values for substrates (Table 2) show that all enzymes can bind substrate and then dioxygen in productive ternary complex formation. Structural data indicate that movement of the indole moiety of L-Trp in the active site is responsible for the decrease in k_{cat} for H55A and H55S. The increased L-Trp binding affinity to the oxidized H55A and H55S enzymes, compared to WT TDO, will lead to a higher probability of nonproductive oxidized enzyme−substrate complex formation, possibly decreasing k_{cat}, but this effect would be small compared to the effect of the destabilized transition state.

Formation and decay of the oxyferrous ternary species generated (Figure 8) for WT TDO show that the (Fe^{2+}−L-Trp) complex displaying a Soret peak at 432 nm binds O_2, producing (Fe^{2+}−L-Trp−O_2), with a corresponding shift in the Soret peak to 419 nm. This then decays to *N*-formylkynurenine (shown by an increase in absorbance at 321 nm) and ferrous enzyme (displaying a Soret peak at 432 nm). This is also observed with 6-F-Trp as the substrate, but for 5-F-Trp some uncoupling is seen, leading to production of the inactive ferric enzyme and the superoxide anion (O_2^-) and release of the substrate. These trends are repeated for H55A and H55S, with uncoupling observed only with 5-F-Trp as substrate. However, the initial

Table 5: Oxygen Dependence of Steady-State Turnover of L-Tryptophan by *X. campestris* TDO Wild Type and Mutants

	TDO WT	H55A	H55S
k_{max} (s^{-1})	35.4 ± 0.9	3.86 ± 0.26	7.88 ± 0.60
K_m (μM)	119 ± 2	45.7 ± 5.6	99 ± 16
K_i (μM)		1380 ± 140	480 ± 50

rates of formation of the ternary complexes are slower, with a rate constant of approximately 50 s^{-1} compared to 100 s^{-1} for WT TDO. Oxyferrous decay parallels this with rate constants of 0.4 s^{-1} and 2 s^{-1} for the mutant enzymes and WT TDO, respectively. This indicates that both mutations do not destabilize the ternary complex significantly, but as the rate of decay is decreased compared to WT TDO, this correlates with a higher activation energy for catalysis due to the movement of the tryptophan indole ring destabilizing the catalytic transition state.

Substrate inhibition is observed at high oxygen concentrations for both mutant forms (Table 5), while none is observed for WT TDO. This unexpected result may be plausibly explained by the lower rate of decay and subsequent slower expulsion of product from the active site by the mutant enzymes. As the active site cavity is larger due to the removal of histidine and its replacement by alanine or serine in the mutant forms, the product, *N*-formylkynurenine, may be less readily expelled at high oxygen concentrations and dioxygen may be able to bind before the product has left. This would trap the product in the active site, causing inhibition of catalytic activity.

CONCLUSIONS

In this study we have investigated whether a putative active site base, histidine 55, is necessary for catalytic activity in TDO. The data we have presented show that in the mutant enzymes H55A and H55S turnover still occurs. This indicates clearly that histidine 55 is not an essential base. Instead, a different role for histidine 55 in controlling substrate binding at the active site has been revealed. On the basis of structural, kinetic, and electrochemical data we have proposed that the role of histidine 55 is to prevent the formation of the nonproductive ferric enzyme−substrate complex. This is most likely achieved by histidine 55 controlling the water content of the substrate-free active site.

SUPPORTING INFORMATION AVAILABLE

A table presenting data on the pH dependence of L-Trp dioxygenation by wild-type TDO and the H55A and H55S mutant forms of the enzyme. This material is available free of charge via the Internet at http://pubs.acs.org.

REFERENCES

1. Forouhar, F., Anderson, J. L. R., Mowat, C. G., Vorobiev, S. M., Hussain, A., Abashidze, M., Bruckmann, C., Thackray, S. J., Seetharaman, J., Tucker, T., Xiao, R., Ma, L.-C., Zhao, L., Acton, T. B., Montelione, G. T., Chapman, S. K., and Tong, L. (2007) Molecular insights into substrate recognition and catalysis by tryptophan 2,3-dioxygenase. *Proc. Natl. Acad. Sci. U.S.A. 104*, 473–478.
2. Takikawa, O. (2005) Biochemical and medical aspects of the indoleamine 2,3-dioxygenase-initiated L-tryptophan metabolism. *Biochem. Biophys. Res. Commun. 338*, 12–19.
3. Yamamoto, S., and Hayaishi, O. (1967) Tryptophan pyrrolase of rabbit intestine. D- and L-tryptophan-cleaving enzyme or enzymes. *J. Biol. Chem. 242*, 5260–5266.
4. Botting, N. P. (1995) Chemistry and neurochemistry of the kynurenine pathway of tryptophan metabolism. *Chem. Soc. Rev. 24*, 401–412.
5. Takikawa, O., Truscott, R. J. W., Fukao, M., and Miwa, S. (2003) Age-related nuclear cataract and indoleamine 2,3-dioxygenase-initiated tryptophan metabolism in the human lens. *Adv. Exp. Med. Biol. 527*, 277–285.
6. Sanni, L. A., Thomas, S. R., Tattam, B. N., Moore, D. E., Chaudhri, G., Stocker, R., and Hunt, N. H. (1998) Dramatic changes in oxidative tryptophan metabolism along the kynurenine pathway in experimental cerebral and noncerebral malaria. *Am. J. Pathol. 152*, 611–619.
7. Mellor, A. L., and Munn, D. H. (2001) Extinguishing maternal immune responses during pregnancy: implications for immunosuppression. *Semin. Immunol. 13*, 213–218.
8. Grohmann, U., Fallarino, F., and Puccetti, P. (2003) Tolerance, DCs and tryptophan: much ado about IDO. *Trends Immunol. 24*, 242–248.
9. Munn, D. H., and Mellor, A. L. (2007) Indoleamine 2,3-dioxygenase and tumor-induced tolerance. *J. Clin. Invest. 117*, 1147–1154.
10. Mellor, A. L., and Munn, D. H. (2004) IDO expression by dendritic cells: tolerance and tryptophan catabolism. *Nat. Rev. Immunol. 4*, 762–774.
11. Sono, M., Roach, M. P., Coulter, E. D., and Dawson, J. H. (1996) Heme-containing oxygenases. *Chem. Rev. 96*, 2841–2887.
12. Sugimoto, H., Oda, S., Otsuki, T., Hino, T., Yoshida, T., and Shiro, Y. (2006) Crystal structure of human indoleamine 2,3-dioxygenase: catalytic mechanism of O_2 incorporation by a heme-containing dioxygenase. *Proc. Natl. Acad. Sci. U.S.A. 103*, 2611–2616.
13. Kotake, Y., and Masayama, I. (1936) The intermediary metabolism of tryptophan. XVIII. The mechanism of formation of kynurenine from tryptophan. *Z. Physiol. Chem. 243*, 237–244.
14. Miller, C. L., Llenos, I. C., Dulay, J. R., Barillo, M. M., Yolken, R. H., and Weis, S. (2004) Expression of the kynurenine pathway enzyme tryptophan 2,3-dioxygenase is increased in the frontal cortex of individuals with schizophrenia. *Neurobiol. Dis. 15*, 618–629.
15. Ishiguro, I., Naito, J., Saito, K., and Nagamura, Y. (1993) Skin L-tryptophan-2,3-dioxygenase and rat hair growth. *FEBS Lett. 329*, 178–182.
16. Littlejohn, T. K., Takikawa, O., Truscott, R. J. W., and Walker, M. J. (2003) Asp274 and His346 are essential for heme binding and catalytic function of human indoleamine 2,3-dioxygenase. *J. Biol. Chem. 278*, 29525–29531.
17. Zhang, Y., Kang, S. A., Mukherjee, T., Bale, S., Crane, B. R., Begley, T. P., and Ealick, S. E. (2007) Crystal structure and mechanism of tryptophan 2,3-dioxygenase, a heme enzyme involved in tryptophan catabolism and in quinolinate biosynthesis. *Biochemistry 46*, 145–155.
18. Bradford, M. M. (1976) A rapid and sensitive method for the quantitation of microgram quantities of protein utilizing the principle of protein-dye binding. *Anal. Biochem. 72*, 248–254.
19. Berry, E. A., and Trumpower, B. L. (1987) Simultaneous determination of hemes *a*, *b*, and *c* from pyridine hemochrome spectra. *Anal. Biochem. 161*, 1–15.
20. Collaborative Computational Project, Number 4. (1994) The CCP4 suite: programs for protein crystallography. *Acta Crystallogr. D50*, 760–763.
21. Adams, P. D., Grosse-Kunstleve, R. W., Hung, L.-W., Ioerger, T. R., McCoy, A. J., Moriarty, N. W., Read, R. J., Sacchettini, J. C., Sauter, N. K., and Terwilliger, T. C. (2002) PHENIX: building new software for automated crystallographic structure determination. *Acta Crystallogr. D58*, 1948–1954.
22. Roussel, A., and Cambillau, C. (1991) TURBO-FRODO, in *Silicon Graphics Geometry Partners Directory 86*, Silicon Graphics, Mountain View, CA.
23. Murshudov, G. N., Vagin, A. A., and Dodson, E. J. (1997) Refinement of macromolecular structures by the maximum-likelihood method. *Acta Crystallogr. D53*, 240–255.
24. Ishimura, Y. (1970) L-Tryptophan 2,3-dioxygenase (tryptophan pyrrolase) (*Pseudomonas fluorescens*). *Methods Enzymol. 17*, 429–434.
25. Ost, T. W. B., Clark, J. P., Anderson, J. L. R., Yellowlees, L. J., Daff, S., and Chapman, S. K. (2004) 4-Cyanopyridine, a versatile spectroscopic probe for cytochrome P450 BM3. *J. Biol. Chem. 279*, 48876–48882.
26. Papadopoulou, N. D., Mewies, M., McLean, K. J., Seward, H. E., Svistunenko, D. A., Munro, A. W., and Raven, E. L. (2005) Redox

and spectroscopic properties of human indoleamine 2,3-dioxygenase and a His303Ala variant: Implications for catalysis. *Biochemistry 44*, 14318–14328.

27. Basran, J., Rafice, S. A., Chauhan, N., Efimov, I., Cheesman, M. R., Ghamsari, L., and Raven, E. L. (2008) A kinetic, spectroscopic, and redox study of human tryptophan 2,3-dioxygenase. *Biochemistry 47*, 4752–4760.

28. Ishimura, Y., Nozaki, M., Hayaishi, O., Nakamura, T., Tamura, M., and Yamazaki, I. (1970) The oxygenated form of L-tryptophan 2,3-dioxygenase as reaction intermediate. *J. Biol. Chem. 245*, 3593–3602.

29. Makino, R., Sakaguchi, K., Iizuka, T., and Ishimura, Y. (1980) L-Tryptophan 2,3-dioxygenase; structure, function and interaction with substrate. *Dev. Biochem. 16*, 179–187.

30. DeLano, W. L. (2002) The PyMOL molecular graphics system, DeLano Scientific, Palo Alto, CA.

BI801202A

Indoleamine 2,3-dioxygenase and tryptophan 2,3-dioxygenase

Sarah J Thackray[†], *Chiara Bruckmann*[†], *Christopher G Mowat*[†], *Farhad Forouhar*[‡], *Stephen K Chapman*[†] *and Liang Tong*[‡]

[†] EaStCHEM, School of Chemistry, University of Edinburgh, West Mains Road, Edinburgh, UK
[‡] Department of Biological Sciences, Northeast Structural Genomics Consortium, Columbia University, New York, NY, USA

FUNCTIONAL CLASS

Indoleamine 2,3-dioxygenase, E.C. 1.13.11.52; tryptophan 2,3-dioxygenase, E.C. 1.13.11.11.

Indoleamine 2,3-dioxygenase (IDO, also known as *tryptophan pyrrolase*) and tryptophan 2,3-dioxygenase (TDO, also known as *tryptophan oxygenase* and L-*tryptophan pyrrolase*) are oxidoreductase enzymes that contain one noncovalently bound iron–protoporphyrin IX per monomer. These enzymes catalyze the dioxygenation of L-tryptophan (L-Trp) to *N*-formyl-L-kynurenine in the first and rate-limiting step of the kynurenine pathway[1,2] (Figure 1).

OCCURRENCE

IDO and TDO are members of a family of enzymes that also includes sIDO from *Shewanella oneidensis*[3] and PrnB, the second enzyme in the pyrrolnitrin biosynthesis pathway from *Pseudomonas fluorescens*,[4] although dioxygenase activity has not been demonstrated for either as yet. Recently, a new enzyme with the ability to catalyze L-tryptophan dioxygenation, INDOL1, was identified. It is encoded by a gene adjacent to that for IDO in many eukaryotes and is predicted to be closely related to IDO in terms of its structure and function.[5]

IDO was first isolated from rabbit intestine in 1967[6] and is found in many eukaryotes where it is expressed throughout the body, except in the liver.[7–9] Its production can be induced in many tissues in response to various stimuli, and this specific expression in different cellular locations suggests a distinct role for IDO.[10] Bacteria are also believed to use members of this family for the aerobic metabolism of L-tryptophan *via* the kynurenine pathway, although prokaryotic IDO-like proteins bear little sequence similarity to eukaryotic IDO proteins and very little is yet known about them.

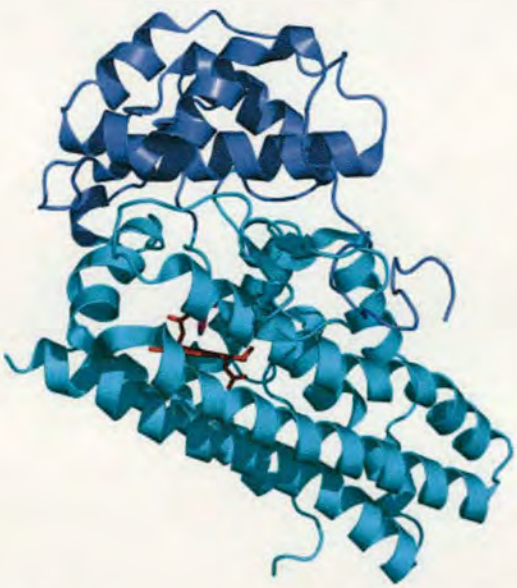

3D Structure The structure of human IDO, comprising two domains. The smaller N-terminal domain is shown in blue and the larger domain in cyan. An iron-containing porphyrin shown in red forms the active site. This figure was prepared using PyMOL[37] based on coordinates from PDB code 2D0T.

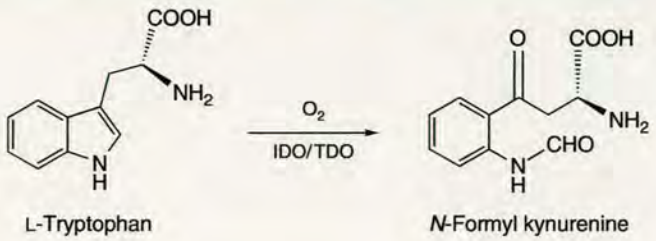

Figure 1 Reaction catalyzed by IDO and TDO.

TDO was initially discovered in the 1930s[11] and is found in both eukaryotes (human,[12] rat,[13] and rabbit[14]) and prokaryotes (*Xanthomonas campestris*,[3] *Ralstonia metallidurans*, and *P. fluorescens*.[15,16]) Expression of TDO in mammals is normally restricted to the liver, but it has been identified in the brain and epididymis of some species, and, in some tissues, its production can be induced in response to stimuli.

BIOLOGICAL FUNCTION

IDO and TDO both play a central role in the physiological regulation of tryptophan flux in the human body, controlling the kynurenine pathway and influencing serotogenic regulation.[17] However, many studies have implicated these proteins in wide-ranging and seemingly unconnected physiological and pathophysiological conditions. Although both enzymes catalyze the same reaction, the compartmentalization of IDO and TDO expression is thought to reflect their differing biological roles. Production of IDO and TDO can be induced in many tissues in response to various stimuli, and this specificity of cellular induction suggests little crossover of function.

The kynurenine pathway

The kynurenine pathway accounts for the processing of over 90% of L-tryptophan utilized by humans.[13] It is important not only as a source of metabolites but also because of the effect of IDO/TDO on the local tryptophan concentration. The buildup of pathway metabolites due to IDO/ TDO induction or poor metabolism further along the pathway can lead to numerous conditions.[1] High levels of quinolinic acid and L-kynurenine in cerebrospinal fluid[18] (CSF) may be involved in various neurological disorders (e.g. cerebral malaria, ischemic brain injury, multiple sclerosis, and acquired immune deficiency syndrome (AIDS)-related dementia[18–20]). Concentrations of these metabolites increase with the severity of neurological dysfunction or brain injury under a wide range of inflammatory conditions. For example, the kynurenine pathway metabolites 3-hydroxyanthranilic acid and 3-hydroxykynurenine are UV filters that can bind to the lens protein in the eye and they have been implicated in cataract formation when present at high concentrations.[21] In addition, some kynurenine pathway metabolites are immunomodulatory and can consequently contribute to immunosuppressive pathways and suppress proliferation (or even cause apoptosis) of T cells.[10,22,23] However, the mechanisms of action of such metabolites are unknown.

The local depletion of tryptophan by enzymatic action is mainly associated with an antimicrobial response by IDO or TDO, or immune regulation by IDO.[24] Some pathogens are sensitive to tryptophan degradation, including viruses (herpes viruses), intracellular bacteria (*Chlamydia* and *Rickettsia*), and extracellular bacteria (*Staphylococci*), and this may be an effective mechanism for controlling their ability to proliferate.

Immune regulation

IDO plays an active role in the human body's immune response, but there is little evidence to suggest that TDO plays a part in this process. Immune regulation by IDO is extremely complex and is influenced by many factors including tryptophan depletion, the accumulation of immunosuppressive metabolites, and interactions with signaling or immunoregulatory pathways.[25]

Initially, IDO was associated with peripheral tolerance and immunosupression by the immune system. IDO is a normal effector of peripheral tolerance in the immunoregulatory pathway of tryptophan metabolism and helps create a balanced immune response between inflammation and tolerance, suppressing excessive immune activation.[26] The delicate balance between suppression and activation of the immune response by the body is not well understood. However, the effects observed when IDO activity is disturbed are widespread and suggest that its role is an important one.

IDO is now also thought to play an essential role in acquired immune tolerance. Inhibition of IDO activity in mice has been shown to lead to allogenic fetal rejection,[27,28] and increased IDO activity is thought to be responsible for renal allograft rejection.[29] In both cases, the body must acquire immune tolerance. It has also been discovered that IDO helps tumors induce tolerance from the host's immune system by interacting with T cells and

Table 1 TDO and IDO proteins characterized by crystallography

Protein	Organism	Molecules bound	Resolution (Å) & PDB ID code	
IDO[30]	*Homo sapiens*	4-Phenyl imidazole	2.3	2D0T
		Cyanide	3.4	2D0U
TDO[3]	*Xanthomonas campestris*	None	2.7	2NW7
		L-Tryptophan	1.6	2NW8
		6-Fluoro-tryptophan	1.8	2NW9
TDO[15]	*Ralstonia metallidurans*	None	2.4	2NOX

depleting L-tryptophan levels.[22] Consequently, IDO has emerged as an attractive drug target in cancer and transplant treatments.[2]

AMINO ACID SEQUENCE INFORMATION

IDOs and TDOs from a number of eukaryotic species have been sequenced and can be found in protein databases. Those species whose crystal structures are mentioned in the text are described in Table 1. Homology between members of this family is apparent from their 3D structures and from the conservation of certain amino acids in their active sites, but sequence similarity between family members is low and sequence alignment based on their structures often gives an identity of approximately 10%.

IDO is monomeric and contains approximately 400 amino acids, displaying high sequence similarity between eukaryotic species. TDO is homotetrameric; eukaryotic TDOs contain approximately 400 amino acids, while prokaryotic TDOs contain approximately 300 amino acids. Sequence identities between prokaryotic and eukaryotic TDOs are around 20–30%.

PROTEIN PRODUCTION, PURIFICATION, AND MOLECULAR CHARACTERIZATION

Both IDO and TDO can be purified directly from mammalian sources. Initial studies used these methods of preparation. Recent studies into both enzymes have used genetic engineering to overproduce the proteins in bacterial hosts, thus making it possible to construct site-directed mutant forms of the enzymes. The recent examples of expression and purification protocols for these enzymes are given below.

Expression of recombinant human IDO

For the efficient expression of His-tagged recombinant human IDO, Raven and coworkers cloned the cDNA into a pQE-30 vector previously modified *via* polymerase chain reaction (PCR) to incorporate KpnI and SalI restriction sites and an N-terminal hexa-histidine tag. *Escherichia coli* BL21-Gold (DE3) cells were used for protein production. The protein was purified using nickel-affinity chromatography.[31]

Expression of *Xanthomonas campestris* TDO

Production of full-length *X. campestris* TDO was achieved by cloning the genomic DNA into a pET-21d derivative, with a C-terminal hexa-histidine tag, and overexpression in *E. coli* BL21(DE3) pMGK cells. The protein was purified using nickel-affinity and gel-filtration chromatography; the details are given in the supplementary material of Forouhar *et al.*[3]

METAL CONTENT AND COFACTORS

Both IDO and TDO bind one *b*-type heme (protoporphyrin IX) per monomer. This has been confirmed by both UV–vis spectrophotometry and pyridine hemochromogen assays on active protein samples. Neither protein associates with any other metals or cofactors, although IDO may be purified with up to 5% of its relative atomic mass as attached carbohydrate; this appears to have little or no function. It is thought that TDO may possibly bind ligands that act as allosteric effectors *in vivo*,[32] but to date none have been identified.

SPECTROSCOPY

The UV–vis absorbance spectra for this family of proteins are characteristic of *b*-type heme-containing proteins with histidine as an axial heme ligand. Spectrochemical data are shown in Table 2. EPR (electron paramagnetic resonance) data of the substrate-free and L-tryptophan-bound forms of IDO and TDO, in the ferric state, are shown in Table 3. Resonance Raman, MCD (magnetic circular dichroism), and NMR (nuclear magnetic resonance) spectroscopies have also been used to characterize this family of proteins, and the results of these studies, along with those determined by EPR, are discussed in the section 'Heme Iron Coordination'.

CRYSTAL STRUCTURES

Crystallization and structure determination

The crystal structure of recombinant human IDO was published in 2006.[30] IDO crystals were obtained using the hanging-drop vapor diffusion method at 20 °C. Hanging drops of 6 μl volume were prepared using

Table 2 Absorption spectra maxima

Enzyme	Derivative	Ferric	Ferrous
H. sapiens IDO[31a]	Substrate-free	404	425
		500, 535/633	527[b], 558
	L-Tryptophan	411	425
		540, 576	556
	O_2		412
			539, 576[b]
	CO		419
			539, 565
H. sapiens TDO[12c]	Substrate-free	406	432
		633	556
	L-Tryptophan	433	421
		455	537, 567
X. campestris TDO[3d]	Substrate-free[e]	405	431
		503, 633	555, 588
	L-Tryptophan[e]	405	433
		585	555, 588
	L-Tryptophan-O_2		420
			548, 578

[a] Data recorded in pH 7.0 100 mM sodium phosphate buffer, 25 °C.
[b] Shoulder.
[c] Data recorded in pH 7.0 100 mM KP_i buffer, 25 °C.
[d] Data recorded in pH 7.5 100 mM KP_i buffer, 25 °C.
[e] SJ Thackray, CG Mowat, SK Chapman, unpublished results.

Table 3 EPR identification of all species observed in the absence or presence of L-tryptophan for IDO and TDO

Enzyme	Species	*g* values
H. sapiens IDO[31]	High spin (H_2O)	5.96 and 1.99
	Low spin (N)	2.94, 2.25, and 1.50
	Low spin (OH^-)[a]	2.52 2.19, and 1.86
H. sapiens TDO[b]	High spin	5.71 and 2.01
	Low spin	2.89, 2.30, and 1.62
	Low spin[c]	2.63, 2.20, and 1.84
Pseudomonas acidovorans TDO (1)[33,c]	High spin	5.8
	Low spin[a]	3.67, 2.20, and 1.80

[a] Only observed in the presence of L-tryptophan.
[b] J Basran, S Rafice, N Chauhan, I Efimov, MR Cheesman, L Ghamsari and EL Raven.[46]
[c] Similar data are observed in the study by Brady *et al.*[34]

a 1:1 ratio of protein (40 mg ml^{-1} in 10 mM 2-(*N*-morpholino)ethanesulfonic acid buffer (pH 6.5), 25 mM NaCl, 1 mM 4-PI (4-phenylimidazole)) and the well solution.[35] The well solution comprised 100 mM *N*-cyclohexyl-2-aminoethanesulfonic acid buffer (pH 9.0), 200 mM ammonium acetate, and 10% polyethylene glycol (PEG) 8000. Using this method, crystals of IDO in complex with the inhibitor 4-phenyl imidazole were obtained, and the model has been deposited in the protein data bank (PDB) (Table 1). In addition to this, the structure of the IDO cyanide adduct (PDB ID 2D0U; 3.4 Å resolution) was obtained by soaking these crystals in a cryoprotectant buffer containing 5 mM KCN for 5 min.

For TDO, the structures of the *R. metallidurans*[15] (PDB ID 2NOX; 2.4 Å resolution) and *X. campestris*[3] (PDB IDs 2NW7 (2.7 Å resolution), 2NW8 (1.6 Å resolution), 2NW9 (1.8 Å resolution)) enzymes have been published (Table 1). The *R. metallidurans* enzyme was crystallized using a construct lacking 18 N-terminal residues (Δ18TDO). Crystals were obtained by vapor diffusion at 22 °C using 25 mg ml^{-1} Δ18TDO (in 50 mM sodium phosphate buffer pH 8.0, 200 mM imidazole, 300 mM sodium chloride) with a well solution comprising 0.8–1.2 M tri-sodium citrate dihydrate (pH 6.5) supplemented with 1 mM L-tryptophan. For *X. campestris* TDO, crystals of the reduced enzyme were obtained by carrying out crystallization in a glovebox under a nitrogen atmosphere. Crystals were obtained by the sitting-drop vapor diffusion method with a well solution comprising 100 mM sodium 2-(*N*-morpholino) ethanesulfonic acid (MES) buffer (pH 6.3), 10–12% PEG 4000, 60 mM $MnCl_2$, 10 mM sodium dithionite, and 2 mM L-tryptophan. In order to ensure the presence of L-tryptophan at the active site, crystals were soaked in a cryoprotectant solution supplemented with 50 mM L-tryptophan.

Overall structure

IDO

The structure of human IDO revealed that the enzyme is folded into two distinct domains (see 3D Structure). The larger (and C terminal) of these is completely helical, with 13 α helices and two 3_{10} helices, and belongs to the family of IDO-like protein folds,[36] while the smaller N-terminal domain consists of six α helices, two short β strands, and three 3_{10} helices and is similar to the C-terminal domain of GST (glutathione *S*-transferase).[36] The heme is bound within the larger domain, but is close to the domain interface. The loop region connecting the two domains (residues 250–267) lies above the distal face of the heme, close to the active site. The interdomain contact is extensive, with a buried surface area of 3100 Å^2.

TDO

The enzymes from *R. metallidurans* and *X. campestris* share 47% sequence identity, and their overall structures are essentially identical. Indeed, the regions of highest sequence conservation are those that are close to the active site. For this reason, we limit the discussion of the TDO structure to that of the highest resolution

Figure 2 The structure of *X. campestris* TDO. The 'dimer of dimers' arrangement can be seen, with one 'dimer' colored green and magenta and the other blue and gray. Heme groups are shown in red and L-tryptophan molecules are in cyan. This figure was prepared using PyMOL based on coordinates from PDB code 2NW8.

structure. This is the 1.6-Å-resolution model of the *X. campestris* enzyme in the ferrous form and in complex with L-tryptophan.[3]

The structure of TDO is an intimately associated homotetramer (Figure 2) with approximately 4500 Å^2 of the surface area of each monomer being buried within the tetramer interface. The structure of the monomer contains 12 α helices and no β strands and belongs to the family of bacterial TDO-like protein folds.[36] The tetramer may be considered as a dimer of dimers, and the N-terminal regions (residues 21–40 of *X. campestris* TDO) of each monomer interact with the adjacent subunit to form part of its L-tryptophan binding site.

Comparison of IDO and TDO

With the exception of the smaller N-terminal domain of IDO, the structures of IDO and TDO are very similar. Indeed, in comparing 201 structurally equivalent Cα atoms between TDO and the large domain of IDO, the rmsd (root mean square difference) is only 3.1 Å. An overlay of the structures is shown in Figure 3. The above-mentioned 'dimeric' arrangement in TDO, which involves the N-terminal region of one monomer comprising part of the substrate binding site in the adjacent monomer, is clearly not possible in monomeric IDO. However, the two tyrosine residues in TDO that are proposed to be important

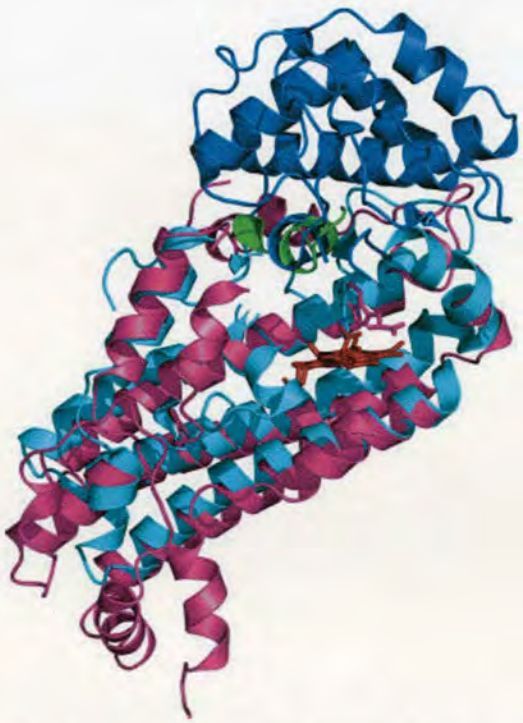

Figure 3 An overlay of human IDO (same coloring as Figure 2) with one monomer of *X. campestris* TDO (in magenta). Also shown is the N-terminal region (in green, residues 21–40) of the adjacent monomer, which forms part of the active site. The heme groups are shown in red. This figure was prepared using PyMOL based on coordinates from PDB codes 2D0T and 2NW8.

in this arrangement, Tyr24 and Tyr27, are in equivalent positions to Tyr126 and Cys129 in IDO. In TDO, the side chain of Tyr27 occupies a space that is taken by the side chain of Phe164 in IDO.

The active site

The active sites of IDO and TDO have several similarities. The substrate binding site of TDO is well characterized owing to the presence of L-tryptophan in the crystal structure (Figure 4). The interactions of the substrate with the active site include an electrostatic interaction between the side chain of Arg117 and the substrate carboxylate group, which is also hydrogen bonded to the phenolic oxygen of Tyr113 and the main chain amide group of Thr254. The substrate ammonium group is hydrogen bonded to the side chain hydroxyl group of Thr254, the 7-propionate group of the heme, and a water molecule. The substrate indole ring is located approximately 3.5 Å above and is perpendicular to the heme plane. It maintains van der Waals interactions with the side chain of Phe51 as well as those of Tyr24 and Tyr27 from the adjacent monomer. In addition to these interactions, there is a hydrogen-bonding interaction between the substrate indole nitrogen and one of the side chain nitrogen atoms of His55. This extensive network of enzyme–substrate interactions serves to stabilize the active site and control substrate binding and catalysis.

In contrast to TDO, the structure of IDO is not available with any substrate bound, but has been solved with the inhibitor 4-PI at the active site (Figure 5). This model shows that 4-PI binds to the heme iron as expected, but does not yield any information regarding the mode of substrate binding in IDO. Given the similarity between the active sites of both dioxygenases, it is perhaps reasonable to assume a similar substrate binding mode in IDO. This is supported by comparison of the active sites of IDO and TDO (Figure 6). Active site bond distances are shown in Table 4.

For example, it can be seen that Arg117 in TDO is equivalent to Arg231 in IDO, while Phe51 in TDO is in the same position as Phe163 in IDO and Tyr24 in TDO is equivalent to Tyr126 in IDO. Similarly, the position

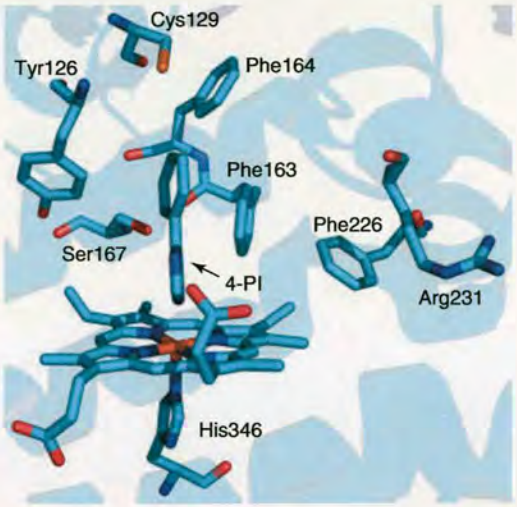

Figure 5 The active site of human IDO. Potentially important active site residues are shown, along with the bound inhibitor 4-phenylimidazole (4-PI). This figure was prepared using PyMOL based on coordinates from PDB code 2D0T.

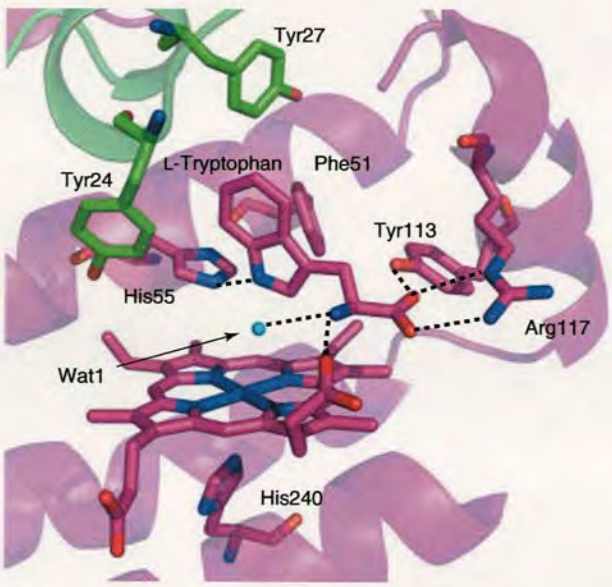

Figure 4 The active site of *X. campestris* TDO. Some of the interactions between the bound L-tryptophan and the active site residues are shown. This figure was prepared using PyMOL based on coordinates from PDB code 2NW8.

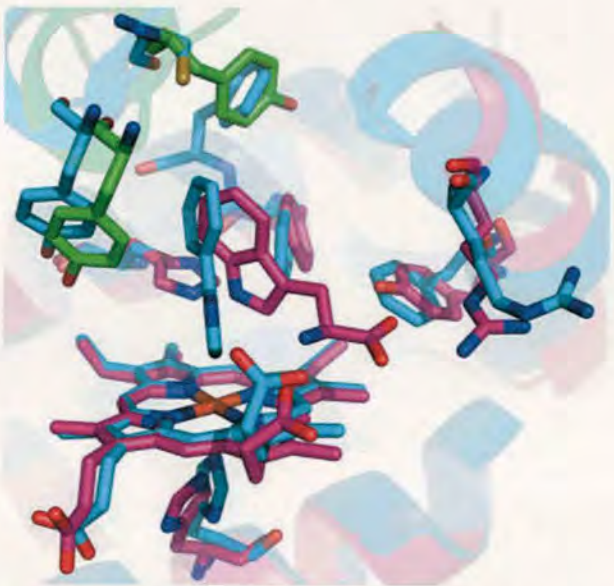

Figure 6 An overlay of the active sites of IDO (cyan) and TDO (magenta). This is a composite image of Figures 4 and 5 with the labeling removed for clarity. This figure was prepared using PyMOL based on coordinates from PDB codes 2D0T and 2NW8.

Table 4 Active site distances and interactions

Enzyme	Atoms	Distance (Å)
H. sapiens IDO[a]	NE2 H346 – Fe	2.1
	Fe – N3 4-PI	2.1
X. campestris TDO[b]	NE2 H240 – Fe	2.3
	Fe – O Wat1	3.5
	O Wat1 – G125 amide N	2.8
	O Wat1 – L-tryptophan α-amino N	3.0
	O Wat1 – L-tryptophan indole N	3.3
	NE2 H55 – L-tryptophan indole N	2.6
R. metallidurans TDO[c]	NE2 H257 – Fe	2.2

[a] PDB ID 2D0T. All distances are ±0.3 Å.
[b] PDB ID 2NW8. All distances are ±0.2 Å.
[c] PDB ID 2NOX. All distances are ±0.3 Å. In the majority of monomers there was found to be no distal water bound to the heme iron.

occupied by Tyr113 in TDO is taken by Phe226 in IDO. However, in addition to these similarities, it should be noted that the equivalent region in IDO of the loop comprising residues 250–260 of TDO is disordered in the IDO structure. This region is particularly important in TDO because it includes Thr254 that, as mentioned above, is involved in binding the ammonium and carboxylate moieties of L-tryptophan. It is interesting to note that in the absence of L-tryptophan this loop region is also disordered in the TDO structure, and that substrate binding is required to induce its ordering. This may also be the case for IDO, but the possibility exists that there is no equivalent interaction between IDO and L-tryptophan.

Perhaps the most obvious difference between the active sites of the two enzymes is the presence of His55 in TDO and its equivalent Ser167 in IDO. In TDO, the histidine side chain is hydrogen bonded with the indole nitrogen atom of L-tryptophan, and the role of His55 would appear to be for regulating substrate binding. The role of Ser167 in IDO is less clear in the absence of a substrate-bound crystal structure, but it is unlikely that this residue plays any crucial role in IDO.

Secondary binding site – allosteric effectors

In the crystal structure of L-tryptophan-bound *X. campestris* TDO in the ferrous state, there is a second L-tryptophan binding site in the tetramer interface with a well-defined electron density (Figure 7). It would appear that this is a specific interaction with L-tryptophan, and in light of reports of allosteric activation of TDO by L-tryptophan,[38,39] it could be possible that this site represents an allosteric effector site.

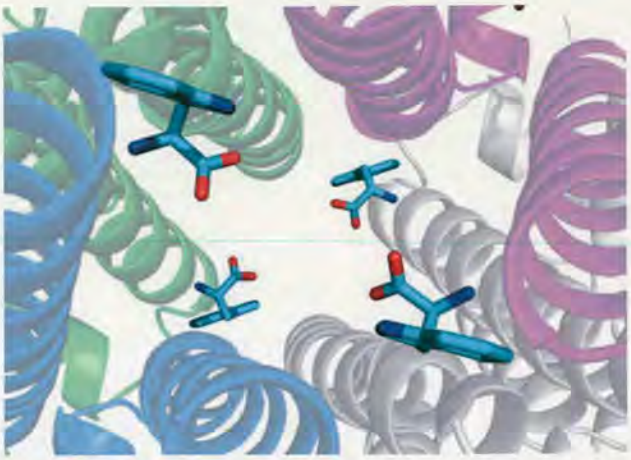

Figure 7 The L-tryptophan binding site in the tetramer interface. Each L-tryptophan molecule occupies an identical site with respect to the four monomers. This figure was prepared using PyMOL based on coordinates from PDB code 2NW8.

HEME IRON COORDINATION

IDO

UV–vis, EPR, and MCD spectra of ferric human IDO show the presence of two distinct species in solution, high-, and low-spin heme, in approximately equal population at pH 6.0[31,40] (Table 3). The two species are shown to be in equilibrium, and, on increasing the pH, there is an increase in the low-spin component, with a concomitant decrease in the high spin component. Histidine is the proximal ligand to the heme iron in both species, with a nitrogen–iron bond distance of 2.1 Å (Table 4). The high-spin species is confirmed by MCD and resonance Raman spectroscopy as arising from water ligation in the distal position. The sixth ligand in the low-spin species is thought to be an as yet unidentified nitrogenous ligand, as there is no available nitrogen ligand in the active site. The spectra are shown to be pH independent – indicating that no ionizable residue affects binding, and there is no formation of hydroxide-bound heme while substrate is absent.

In the presence of L-tryptophan at pH 8, MCD and EPR confirm that there are three distinct species in solution, one of which is high spin and the other two are low spin. The sixth heme ligand for the additional low-spin species is hydroxide, and this is the predominant species in solution. The bound L-tryptophan provides a hydrogen bond acceptor to stabilize deprotonation of the bound water molecule. Ferric substrate-free human IDO does not form a hydroxide-bound species as IDO lacks a hydrogen-bond acceptor to facilitate deprotonation of the bound water molecule. In contrast, for the ferric-substrate-bound enzyme, the spectra are pH dependent due to an ionizable interaction affecting the formation of the hydroxide species in the active site. L-Tryptophan is thought to act as a proton acceptor, deprotonating the bound water molecule

and forming the hydroxide-bound species; this is supported by resonance Raman studies.[12] The relation of these studies and those above to the active site structure is currently limited by the lack of a substrate-bound crystal structure.

TDO

The substrate binding site of TDO is well characterized due to the presence of L-tryptophan in the crystal structure. The active site bond distances are shown in Table 4. EPR experiments on human, rat liver, and *Pseudomonas* TDOs in the ferric state have shown the presence of two distinct species in solution, a high-spin form and a low-spin form[33] (Table 3). At acidic pH, only the high-spin state has been reported, and, on increasing the pH, a transition to a mixed-spin state occurs, containing a mixture of the two forms. The spin state of the alkaline form of ferric TDO is temperature dependent, and the proportion of high-spin species increases with elevating temperature. Histidine occupies the axial coordination position to the heme iron. The bond lengths are shown in Table 4. The nature of the sixth ligand for the high-spin species is postulated to be a water molecule, while that of the low-spin species is postulated to be hydroxide. This is possible for substrate-free TDO as a histidine residue is present in the active site to deprotonate a bound water molecule, which is present in the *X. campestris* substrate-free active site (PDB ID 2NW7). This is in contrast to IDO where no equivalent residue is available, but data so far are inconclusive.

EPR data on rat liver and *Pseudomonas* enzymes show that addition of L-tryptophan to the ferric enzyme causes an increase in the low-spin component at neutral pH, with a decrease in the high-spin component.[34] MCD studies have suggested that this high-spin component may be distinct from that observed in the substrate-free enzyme, but little data are available for analysis at present.[41] The spectral changes indicate that L-tryptophan binding to the ferric protein causes increased deprotonation of the heme bound water. L-Tryptophan binding to the ferric enzyme also significantly modifies the pH of the spin-state transition, decreasing the pH at which this transition occurs by about 1.6 units. This substrate-induced shift could be caused by the bound L-tryptophan, deprotonating the bound water molecule, as in IDO, rather than the active site histidine. Figure 4 shows that deprotonation of the water by the indole nitrogen is possible, as the bond distance is 3.3 Å (Table 4).

Contrary to the data on the prokaryotic TDO, recent EPR analysis has shown that addition of L-tryptophan to human TDO causes the creation of an additional low-spin species (Table 3). The high-spin and two low-spin species observed have g values similar to those of human IDO under analogous conditions, and they are proposed to have similar ligands in their distal position. This result is clearly different from that of the prokaryotic TDO species studied, and poses many questions regarding the differences in the heme environment and substrate binding interactions between TDO enzymes and between IDO and TDO.

Small molecule binding

Recent resonance Raman spectra of CO and NO binding to ferric, L-tryptophan-bound human TDO and human IDO enzymes suggest that in TDO the C2–C3 double bond of the tryptophan ring faces the distal diatomic ligand of the heme. This is in contrast to IDO, where the indole nitrogen appears to hydrogen bond with the diatomic heme ligand.[12] These differences suggest that the two enzymes may catalyze the dioxygenation of L-tryptophan *via* differing mechanisms, as deprotonation of the indole nitrogen may occur by two distinct processes. These mechanisms are discussed further below under 'catalytic mechanism'.

FUNCTIONAL ASPECTS

Steady-state kinetics

Weak catalytic activity by ferric IDO and TDO has been reported, but the turnover is generally catalyzed by the ferrous protein.[12,42] Reduction of heme iron is therefore required to facilitate the observation of catalytic activity. Upon reduction, some turnover can be observed in the absence of any electron transfer mediators, but full catalytic activity is not observed without their presence. Ascorbate, catalase, and methylene blue are employed in the assay buffer to achieve this. Ascorbate and methylene blue are reducing agents, but also react with dioxygen to form superoxide and peroxide by-products, which can bleach the heme and destroy catalytic activity. Catalase is therefore present to remove any superoxide or peroxide in solution and hence allows an efficient turnover of substrate.[16] The reaction velocity is calculated by monitoring the increase in concentration of *N*-formylkynurenine (or related derivative) at 321 nm, and fitting the data to the Michaelis–Menten or Hill equation.

TDO has been shown to catalyze the dioxygenation of L-tryptophan, 6-F-tryptophan, and 5-F-tryptophan. D-Tryptophan is a competitive inhibitor of the enzyme at high concentrations.[43] IDO displays broader substrate selectivity than TDO, catalyzing the dioxygenation of D-tryptophan, 5-OH-tryptophan, serotonin (5-OH-tryptamine), and tryptamine in addition to those substrates utilized by TDO.[8] Catalytic data is shown in Table 5.

Despite sharing low sequence identity, key active site residues are similar in IDO and TDO (Figure 6) and they may display the same L-tryptophan binding mode. However, IDO may have weaker interactions with the ammonium ion and carboxylate group of L-tryptophan than TDO. In addition, a histidine residue hydrogen bonds

Table 5 Kinetic parameters for substrate dioxygenation

Enzyme	Substrate	pH	k_{cat} (s^{-1})	K_m (μM)	k_{cat}/K_m ($M^{-1}s^{-1}$)	Fe^{III} (μM)	Fe^{II} (μM)
H. sapiens IDO[31]	L-Tryptophan	8.0	1.4[a]	7.1	7.3×10^5	285[a]	nr
Rabbit IDO[43,44]	L-Tryptophan	7.0	2.0	13	1.6×10^5	5800	13
	D-Tryptophan	6.0	1.6	7400	220	nc	nc
H. sapiens TDO[12]	L-Tryptophan	7.0	2.1	190	1.3×10^4	nr	nr
H. sapiens TDO[b]	L-Tryptophan	8.0	1.4	220	6300	~350	~200
X. campestris TDO[3]	L-Tryptophan	7.5	19	110	1.7×10^5	3800	4.1
	D-Tryptophan	7.5	0.0	16500[c]	nc	>50 000	nc

nr, not recorded; nc, no change on binding or no turnover.
[a] N Chauhan, J Basran, I Efimov, DA Svistunenko, HE Seward, PCE Moody and EL Raven.[45]
[b] J Basran, S Rafice, N Chauhan, I Efimov, MR Cheesman, L Ghamsari and EL Raven.[46]
[c] Inhibitory constant, K_i.

with the indole nitrogen atom of L-tryptophan in TDO, providing a precise alignment between the indole ring of the substrate and the heme porphyrin (Figure 4). In IDO, the analogous residue is serine, which is unable to form a hydrogen bond to L-tryptophan. These differences may be the reason why IDO cannot completely distinguish among the indoleamine substrates, and can therefore catalyze a wider range of reactions.

Binding studies

The addition of L-tryptophan and related substrates to IDO and TDO causes significant changes in their UV–vis spectra. Binding affinities are shown in Table 5 and it can be seen that L-tryptophan binds to the ferrous enzyme with a higher affinity than the ferric enzyme for both IDO and TDO. This phenomenon is common in heme enzymes, with increased affinity for substrate being attributed to a large conformational movement upon reduction of the enzyme.

When substrate is bound to either enzyme, there is an apparent activation toward binding of diatomic ligands as evidenced by a decrease in their K_d values. Previous studies have demonstrated that the binding of ligands such as oxygen, carbon monoxide, and nitric oxide to the ferrous enzyme are greatly augmented by the binding of L-tryptophan.[47]

Inhibition studies

The most-studied inhibitor of IDO is 1-methyltryptophan, a competitive inhibitor that exists as two stereoisomers. It is unclear as to which isomer affects the greatest inhibitory response *in vitro*; many derivatives have been studied for their inhibitory properties.[48,49] 1-Methyltryptophan is ineffective against TDO activity. This can be explained by comparison of the active sites of the enzymes (Figure 6). In TDO, the N1 atom of tryptophan is directly hydrogen bonded to the His55 side chain and its methylation clearly causes a steric clash with this residue. In comparison, His55 is replaced by Ser167 in IDO, which creates a small pocket that can accommodate the 1-methyl group, allowing binding. IDO is a therapeutic target for the development of new anticancer drugs and importance has been given to the design of new inhibitors of its action.

A few potent inhibitors of TDO have been discovered, including norharman, a β-carboline derivative,[50,51] and a number of 2-(2-pyridylethenyl)indole derivatives.[52]

Binding requirements and superoxide

IDO and TDO must first form a ternary complex (substrate–Fe^{II}–O_2) to allow productive substrate turnover, and the trapping of this complex for both enzymes confirms its formation.[53,54] What is less clear is the order in which the substrates bind to the enzyme.

Studies have shown that TDO must first form the ferrous binary enzyme–substrate complex (Fe^{II}–Substrate) before dioxygen binding can occur and allow a productive turnover. This binding order appears logical as initial substrate binding to the ferrous enzyme would prevent unproductive coupling of dioxygen to the ferrous enzyme, which could lead to the production of superoxide and the dead-end ferric complex. However, limited turnover of substrate by ferric TDO, possibly utilizing superoxide as an electron source, has recently been observed for human TDO.[12]

IDO operates in the same manner, but can also utilize superoxide as an oxygen source.[43] Ferric and ferrous IDO can react with superoxide (O_2^-) to produce the ferrous oxygenated enzyme (Fe^{II}–O_2), which can then bind L-tryptophan and effect substrate turnover. It is not known if this is important to the biological function of IDO or TDO, but research suggests that *in vivo* utilization of superoxide is probably minimal.[55]

For IDO, studies have shown that binding of L-tryptophan to the ferrous enzyme is more favorable or similar to the binding of dioxygen. This suggests that initial substrate binding may be favored over dioxygen binding by IDO, similar to that for TDO.

Catalytic mechanism

The catalytic mechanisms employed by this family of enzymes are poorly understood, and little characterization of reactive intermediates has been reported. The mechanism employed by TDO and IDO for binding and transferring dioxygen appears to be very different to that of other heme proteins such as hemoglobin and to nonheme dioxygenases such as catechol 3,4-dioxygenase.

The proposed catalytic cycle of tryptophan oxidation by TDO and IDO is schematically illustrated in Figure 8. Under physiological conditions, the enzymes are likely to be in the active ferrous form due to the high reduction potential of the heme. Binding of L-tryptophan and oxygen to the active site to form the ternary complex (**2**) is thought, in the case of TDO, to occur by substrate binding to form the enzyme adduct (**1**), followed by the binding of dioxygen. As described above, formation of the ternary species for IDO is more complex.

In the enzyme active site, O_2 coordinates to the ferrous heme iron to form the heme–O_2 complex. This activates triplet O_2 and allows the otherwise spin-forbidden reaction to proceed. Catalysis can then proceed *via* an ionic or radical mechanism, both of which can be shown to undergo the same choice of intermediates in product formation. The ionic mechanism may be more likely because the radical mechanism is thermodynamically unfavorable,[56] requiring the one-electron oxidation of L-tryptophan; only the ionic mechanism is shown in Figure 8.

In the proposed mechanism, catalysis proceeds *via* the formation of a hydroperoxide intermediate (**3**) and (**6**) in which addition of O_2 to the C3 position of the substrate occurs prior to O–O bond cleavage. Some studies have proposed that this addition could be base catalyzed by the loss of the indole proton. This may be possible for TDO, which has a histidine residue in the active site (Figure 4), although mutation of this histidine residue to alanine leads to only a 10-fold loss in k_{cat}.[3] IDO has no side chain available to act as a catalytic base. Figure 8 displays a nonbase catalyzed mechanism. Proton abstraction by the iron-bound dioxygen is therefore proposed for IDO, where the interaction of the indole NH group with the proximal oxygen atom weakens the oxygen–oxygen bond. It is unclear which route is employed in TDO, but the structure of TDO suggests that a precise alignment between the indole ring of the substrate and the bound dioxygen is necessary for catalysis. This is facilitated by the hydrogen-bonding interaction with His55, and this residue appears to play an important role in the active site. Resonance Raman data have suggested a clear distinction between the mechanisms employed for proton abstraction by IDO and TDO.[12]

The hydroperoxide intermediate may undergo one of two pathways to form the product. The Criegee rearrangement requires an antiperiplanar arrangement of the O–O bond and the indole C2–C3 bond to form an intermediate (**4**), which further rearranges to form the product *N*-formylkynurenine (**8**). The dioxetane mechanism requires a sin-coplanar configuration of intermediate (**7**), which then undergoes a retro [2 + 2] cycloaddition to form the product. The dioxetane mechanism is thought to be less favorable owing to the excess endothermicity involved in forming the strained dioxetane intermediate and the exothermicity of its decomposition to form the product.[57]

It is thought that the proximal histidine ligand may play a role in determining the bond order of the iron–dioxygen (Fe–OO) and oxygen–oxygen (FeO–O) bonds.[12] This may be important for electron rearrangement in the transition state of both IDO and TDO, but the precise nature of the mechanisms employed by IDO and TDO needs to be further investigated.

Oxidation/reduction potentials

Electrochemical midpoint reduction potentials are shown in Table 6. Few reduction potentials for either IDO or TDO have so far been reported, but those available show clear trends. Upon binding of the substrate, there is an increase in reduction potential for both IDO and TDO, reflecting additional stabilization of the ferrous derivative. The increase is larger for TDO proteins (with the exception of human TDO), compared to IDO proteins, and the shift in reduction potential for *X. campestris* TDO is supported by the almost perfect correlation with the increase in affinity for L-tryptophan upon its reduction. For both IDO and TDO, it is not clear whether heme reduction precedes substrate binding or *vice versa*, but a thermodynamic stabilization of the reduced form would clearly favor reduction prior to substrate binding. The large positive change in the reduction potential for both enzymes suggests that there is a significant stabilization of the ferrous form when substrate is bound. This stabilization could also play a physiological role in keeping the proteins reduced, and therefore active, when L-tryptophan is present.

Allostery

The recent crystal structure of *X. campestris* TDO showed the specific binding of four L-tryptophan residues in the interface of the tetramer, as shown in Figure 7. These additional binding sites raise the possibility that these may be possible allosteric effector sites, where binding of substrate changes the conformation of the protein, affecting the binding of further molecules.

When L-tryptophan is bound to TDO, there is an apparent activation toward binding of diatomic ligands, such as oxygen, carbon monoxide, and nitric oxide, as evidenced by dramatically decreased K_d values.[47] In addition, there is an increased affinity for oxygen in the

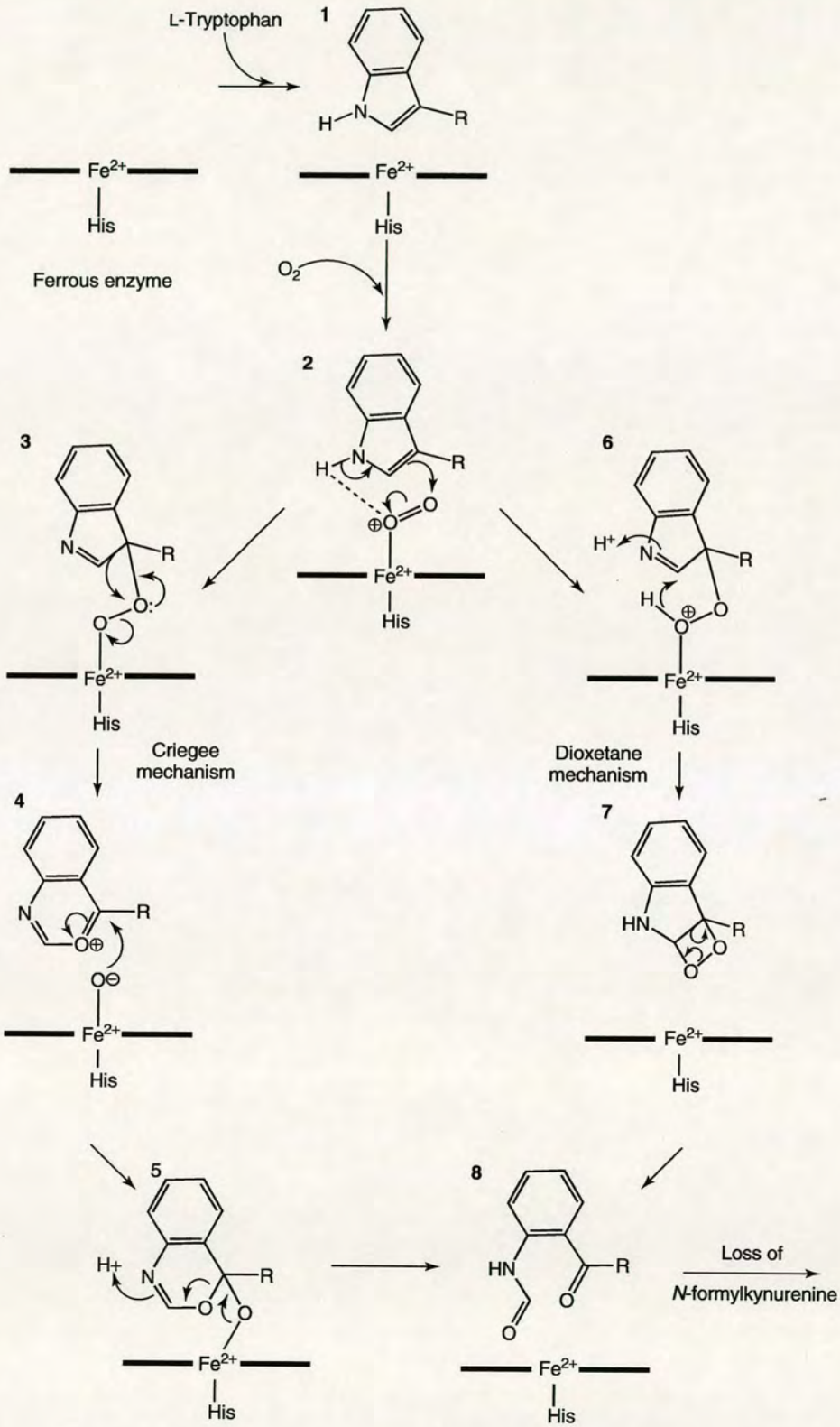

Figure 8 Proposed catalytic mechanisms of IDO and TDO. The figure displays ionic, nonbase catalyzed mechanisms of L-tryptophan dioxygenation. First, substrate binds to the protein (1), followed by dioxygen binding to form the ternary complex (2). The mechanism proceeds by the formation of a hydroperoxide intermediate (3) and (6), which can undergo two different rearrangements to form the product, *N*-formylkynurenine (8), a Criegee rearrangement (4), and (5) or a dioxetane rearrangement (7). The product is then released, leaving the protein in the active ferrous state.

Table 6 Electrochemical midpoint reduction potentials (mV vs standard hydrogen electrode)

Protein	Substrate-free	Substrate-bound[a]	ΔE_{mid}
H. sapiens IDO[31]	-30 ± 4	$+16 \pm 3$	+46
H. sapiens TDO[b]	-92 ± 3	-76 ± 6	+16
X. campestris TDO[3]	$+8 \pm 5$	$+144 \pm 6$	+136
Rat liver TDO[58]	+100	+160	+60

[a] Substrate is L-tryptophan for all enzymes. Potentials for *H. sapiens* IDO, *H. sapiens* TDO and rat liver TDO obtained at pH 7.0, and those for *X. campestris* TDO obtained at pH 7.5.

[b] J Basran, S Rafice, N Chauhan, I Efimov, MR Cheesman, L Ghamsari and EL Raven.[46]

presence of α-methyl-tryptophan, a substrate analog that is neither a substrate nor an inhibitor of enzyme activity.[44,59]

In the presence of substrate, cyanide binds to ferric TDO in a positively cooperative manner, while no cooperativity is observed in the absence of substrate.[60] This is strong evidence that substrate binding alters the conformation of the protein. In addition, this implies that there is indeed communication between catalytic sites in TDO. This proposed conformational rearrangement appears to be induced by L-tryptophan, tryptamine, and 5-hydroxy-L-tryptophan.

The reaction velocity of allosteric enzymes can be regulated by small changes in substrate concentration and often regulate metabolic pathways where the substrate concentration fluctuates over a narrow range. It is possible that TDO may play such a role, regulating tryptophan concentrations in the liver of mammals, and prokaryotes.

REFERENCES

1 O Takikawa, *Biochem Biophys Res Commun*, **338**, 12–19 (2005).

2 J Khan, F Forouhar, X Tao and L Tong, *Expert Opin Ther Targets*, **11**, 695–705 (2007).

3 F Forouhar, JLR Anderson, CG Mowat, SM Vorobiev, A Hussain, M Abashidze, C Bruckmann, SJ Thackray, J Seetharaman, T Tucker, R Xiao, L-C Ma, L Zhao, TB Acton, GT Montelione, SK Chapman and L Tong, *Proc Natl Acad Sci USA*, **104**, 473–78 (2007).

4 W De Laurentis, L Khim, JLR Anderson, A Adam, RS Phillips, SK Chapman, K-H Van Pee and JH Naismith, *Biochemistry*, **46**, 12393–404 (2007).

5 HJ Ball, A Sanchez-Perez, S Weiser, CJD Austin, F Astelbauer, J Miu, JA McQuillan, R Stocker, LS Jermiin and NH Hunt, *Gene*, **396**, 203–13 (2007).

6 S Yamamoto and O Hayaishi, *J Biol Chem*, **242**, 5260–66 (1967).

7 R Yoshida and O Hayaishi, *Methods Enzymol*, **142**, 188–95 (1987).

8 G Allegri, A Bertazzo, M Biasiolo, CVL Costa and E Ragazzi, *Adv Exp Med Biol*, **527**, 455–63 (2003).

9 TK Littlejohn, O Takikawa, RJW Truscott and MJ Walker, *J Biol Chem*, **278**, 29525–31 (2003).

10 U Grohmann, F Fallarino and P Puccetti, *Trends Immunol*, **24**, 242–48 (2003).

11 Y Kotake and I Masayama, *Z Physiol Chem*, **243**, 237–44 (1936).

12 D Batabyal and S-R Yeh, *J Am Chem Soc*, **129**, 15690–701 (2007).

13 G Allegri, E Ragazzi, A Bertazzo, CVL Costa and R Rocchi, *Adv Exp Med Biol*, **527**, 481–96 (2003).

14 G Allegri, E Ragazzi, A Bertazzo, M Biasiolo and CVL Costa, *Adv Exp Med Biol*, **527**, 473–79 (2003).

15 Y Zhang, SA Kang, T Mukherjee, S Bale, BR Crane, TP Begley and SE Ealick, *Biochemistry*, **46**, 145–55 (2007).

16 Y Ishimura, *Methods Enzymol*, **17**, 429–34 (1970).

17 B Wirleitner, G Neurauter, K Schroecksnadel, B Frick and D Fuchs, *Curr Med Chem*, **10**, 1581–91 (2003).

18 H Ohashi, K Saito, H Fujii, H Wada, N Furuta, M Takemura, S Maeda and M Seishima, *Arch Biochem Biophys*, **428**, 154–59 (2004).

19 K Saito, S Fujigaki, MP Heyes, K Shibata, M Takemura, H Fujii, H Wada, A Noma and M Seishima, *Am J Physiol*, **279**, F565–72 (2000).

20 A Tankiewicz, D Pawlak and W Buczko, *Postepy Hig Med Dosw*, **55**, 715–31 (2001).

21 JA Aquilina, JA Carver and RJW Truscott, *Exp Eye Res*, **64**, 727–35 (1997).

22 DH Munn and AL Mellor, *J Clin Invest*, **117**, 1147–54 (2007).

23 AL Mellor, D Munn, P Chandler, D Keskin, T Johnson, B Marshall, K Jhaver and B Baban, *Adv Exp Med Biol*, **527**, 27–35 (2003).

24 CR MacKenzie, K Heseler, A Mueller and W Daeubener, *Curr Drug Metab*, **8**, 237–44 (2007).

25 G Neurauter, B Wirleitner, K Schroecksnadel, B Frick and D Fuchs, *Aktuel Ernahrungsmed*, **29**, 171–77 (2004).

26 M Platten, PP Ho, S Youssef, P Fontoura, H Garren, EM Hur, R Gupta, LY Lee, BA Kidd, WH Robinson, RA Sobel, ML Selley and L Steinman, *Science*, **310**, 850–55 (2005).

27 AL Mellor, P Chandler, K Lee Geon, T Johnson, DB Keskin, J Lee and DH Munn, *J Reprod Immunol*, **57**, 143–50 (2002).

28 S Suzuki, S Tone, O Takikawa, T Kubo, I Kohno and Y Minatogawa, *Biochem J*, **355**, 425–29 (2001).

29 A Tankiewicz, D Pawlak, J Topczewska-Bruns and W Buczko, *Adv Exp Med Biol*, **527**, 409–14 (2003).

30 H Sugimoto, S-i Oda, T Otsuki, T Hino, T Yoshida and Y Shiro, *Proc Natl Acad Sci USA*, **103**, 2611–16 (2006).

31 ND Papadopoulou, M Mewies, KJ McLean, HE Seward, DA Svistunenko, AW Munro and EL Raven, *Biochemistry*, **44**, 14318–28 (2005).

32 P Feigelson, FO Brady and JA McCray, *J Biol Chem*, **248**, 5267–71 (1973).

33 R Makino, K Sakaguchi, T Iizuka and Y Ishimura, *J Biol Chem*, **255**, 11883–91 (1980).

34 FO Brady, P Feigelson and KV Rajagopalan, *Arch Biochem Biophys*, **157**, 63–72 (1973).

35 SI Oda, H Sugimoto, T Yoshida and Y Shiro, *Acta Crystallogr Sect F: Struct Biol Cryst Commun*, **F62**, 221–23 (2006).

36 AG Murzin, SE Brenner, T Hubbard and C Chothia, *J Mol Biol*, **247**, 536–40 (1995).

37 WL DeLano, *The PyMOL Molecular Graphics System*, DeLano Scientific, Palo Alto, CA (2002).

38 Y Ishimura, R Makino and T Iizuka, *Adv Enzyme Regul*, **18**, 291–302 (1980).

39 M Sono, *Biochemistry*, **28**, 5400–7 (1989).

40 M Sono and JH Dawson, *Biochim Biophys Acta: Protein Struct Mol Enzymol*, **789**, 170–87 (1984).

41 K Uchida, T Shimizu, R Makino, K Sakaguchi, T Iizuka, Y Ishimura, T Nozawa and M Hatano, *J Biol Chem*, **258**, 2526–33 (1983).

42 JS Li, Q Han, J Fang, M Rizzi, AA James and J Li, *Arch Insect Biochem Physiol*, **64**, 74–87 (2007).

43 M Sono, MP Roach, ED Coulter and JH Dawson, *Chem Rev*, **96**, 2841–87 (1996).

44 M Sono, T Taniguchi, Y Watanabe and O Hayaishi, *J Biol Chem*, **255**, 1339–45 (1980).

45 N Chauhan, J Basran, I Efimov, DA Svistunenko, HE Seward, PCE Moody and EL Raven, *Biochemistry*, **47**, 4761–69 (2008).

46 J Basran, SA Rafice, N Chauhan, I Efimov, MR Cheesman, L Ghamsari and EL Raven, *Biochemistry*, **47**, 4752–60 (2008).

47 M Sono, *Biochemistry*, **25**, 6089–97 (1986).

48 MD Southan, RJW Truscott, JF Jamie, L Pelosi, MJ Walker, H Maeda, Y Iwamoto and S Tone, *Med Chem Res*, **6**, 343–52 (1996).

49 D-Y Hou, AJ Muller, MD Sharma, J DuHadaway, T Banerjee, M Johnson, AL Mellor, GC Prendergast and DH Munn, *Cancer Res*, **67**, 792–801 (2007).

50 N Eguchi, Y Watanabe, K Kawanishi, Y Hashimoto and O Hayaishi, *Arch Biochem Biophys*, **232**, 602–9 (1984).

51 M Sono and SG Cady, *Biochemistry*, **28**, 5392–99 (1989).

52 DJ Madge, R Hazelwood, R Iyer, HT Jones and M Salter, *Bioorg Med Chem Lett*, **6**, 857–60 (1996).

53 M Sono and O Hayaishi, *Biochem Rev*, **50**, 173–81 (1980).

54 Y Ishimura, M Nozaki, O Hayaishi, T Nakamura, M Tamura and I Yamazaki, *J Biol Chem*, **245**, 3593–602 (1970).

55 M Sono, *J Biol Chem*, **264**, 1616–22 (1989).

56 PKS Tsang and DT Sawyer, *Inorg Chem*, **29**, 2848–55 (1990).

57 GA Hamilton, *Adv Enzymol Relat Areas Mol Biol*, **32**, 55–96 (1969).

58 R Makino, K Sakaguchi, T Iizuka and Y Ishimura, *Dev Biochem*, **16**, 179–87 (1980).

59 K Kobayashi, K Hayashi and M Sono, *J Biol Chem*, **264**, 15280–83 (1989).

60 M Sono, *Biochemistry*, **29**, 1451–60 (1990).

Exploring the mechanism of tryptophan 2,3-dioxygenase

Sarah J. Thackray, Christopher G. Mowat and Stephen K. Chapman[1]
EastCHEM, School of Chemistry, University of Edinburgh, West Mains Road, Edinburgh EH9 3JJ, U.K.

Abstract

The haem proteins TDO (tryptophan 2,3-dioxygenase) and IDO (indoleamine 2,3-dioxygenase) are specific and powerful oxidation catalysts that insert one molecule of dioxygen into L-tryptophan in the first and rate-limiting step in the kynurenine pathway. Recent crystallographic and biochemical analyses of TDO and IDO have greatly aided our understanding of the mechanisms employed by these enzymes in the binding and activation of dioxygen and tryptophan. In the present paper, we briefly discuss the function, structure and possible catalytic mechanism of these enzymes.

Introduction

Haem-containing proteins have a wide variety of functions ranging from oxygen transport, storage and activation to simple single-electron transfers. TDO (tryptophan 2,3-dioxygenase) and IDO (indoleamine 2,3-dioxygenase) are members of a small family of haem enzymes that catalyse the aerobic metabolism of L-tryptophan to *N*-formylkynurenine. TDO was initially discovered in the 1930s and is found in both eukaryotes and prokaryotes [1]. TDO expression is normally restricted to the liver in mammals, although it has been identified in the brain and epididymis of some species [2,3]. IDO was first isolated from rabbit intestine in 1967 [4], and is found in many eukaryotes where it is expressed ubiquitously throughout the body, except in the liver. Some prokaryotic IDO-like proteins from *Shewanella* species have been identified [5], but to date these have no known function.

Sequence similarity between family members is low, with amino acid sequence alignment indicating an identity of approx. 10% between family members. Homology is only apparent from their three-dimensional structures and the conservation of certain amino acids in their active sites.

Why are TDO and IDO of interest?

A vital biochemical reaction

TDO and IDO activate molecular oxygen and catalyse its insertion into L-tryptophan to form *N*-formylkynurenine, in the first and rate-limiting step in the kynurenine pathway [6]. The kynurenine pathway processes over 90% of L-tryptophan utilized by humans. Although both enzymes catalyse the same reaction, TDO is highly substrate-specific, only dioxygenating L-tryptophan and some tryptophan derivatives substituted in the 5- and 6-positions. IDO displays wider substrate specificity, catalysing the dioxygenation of D-tryptophan, tryptamine and 5-hydroxytryptamine (serotonin) in addition to those substrates dioxygenated by TDO [7].

Tryptophan regulation

Both TDO and IDO play a central role in the regulation of tryptophan in the human body, controlling the kynurenine pathway and influencing serotogenic regulation [8]. IDO and TDO activity alters local tryptophan concentration and the build-up of pathway metabolites can lead to numerous physiological and pathophysiological conditions. These include cataract formation, AIDS-related dementia and ischaemic brain injury [6,8–10]. In addition, the local depletion of tryptophan by IDO or TDO is associated with an antimicrobial response. Some pathogens are sensitive to tryptophan degradation, and this may be an effective mechanism for controlling their ability to proliferate [11].

Immune regulation

Although both enzymes catalyse the same reaction, compartmentalization of IDO and TDO expression is thought to reflect their differing biological roles. IDO plays an active role in the human body's immune response, but there is little evidence to suggest that TDO plays a part in this process. Immune regulation by IDO is extremely complex, but two major roles have become evident [12,13]. First, IDO is a normal effector of peripheral tolerance in the immunoregulatory pathway of tryptophan metabolism. It helps to create an appropriate immune response, influencing the balance between tolerance and attack. Secondly, it is thought to play an essential role in acquired immune tolerance. IDO helps tumours to induce tolerance from the host's immune system by interacting with T-cells and depleting L-tryptophan levels [13], and it has consequently emerged as an attractive drug target in cancer and transplant treatments.

Key words: haem, indoleamine 2,3-dioxygenase, kynurenine, oxygen, tryptophan 2,3-dioxygenase.

Abbreviations used: IDO, indoleamine 2,3-dioxygenase; hIDO, *Homo sapiens* IDO; TDO, tryptophan 2,3-dioxygenase; rmTDO, *Ralstonia metallidurans* TDO; xcTDO, *Xanthomonas campestris* TDO.

[1]To whom correspondence should be addressed (email S.K.Chapman@ed.ac.uk).

Figure 1 | Structures of (a) xcTDO and (b) hIDO

(**a**) Structure of xcTDO. L-Tryptophan is shown in red, haem is grey, and separate monomers are shown in cyan, magenta, grey and blue. (**b**) Structure of hIDO. Haem is shown in grey, the smaller N-terminal domain is shown in grey, and the larger C-terminal domain is shown in marine.

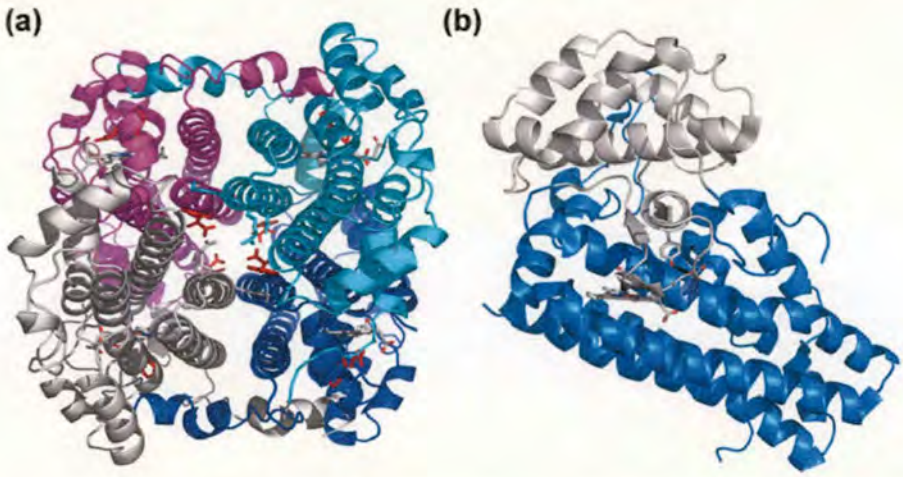

TDO and IDO structures?

Overall structure

Recent crystallographic studies of xcTDO (*Xanthomonas campestris* TDO) [5], rmTDO (*Ralstonia metallidurans* TDO) [14] and hIDO (*Homo sapiens* IDO) [15] have aided our understanding of this family of haem enzymes. The crystal structures of xcTDO and rmTDO are essentially identical, sharing 47% sequence identity, and are intimately associated homotetrameric enzymes (Figure 1a). They are perhaps best described as a dimer of dimers because the N-terminal residues of each monomer form part of the substrate-binding site in an adjacent monomer. The N-terminal region lies above the distal face of the haem, providing part of the binding cavity. The proteins are completely helical, and a flexible loop (comprising residues 250–260 of xcTDO), involved in L-tryptophan binding, is observed just outside the haem pocket. This loop is only ordered in crystals grown in the presence of L-tryptophan, as substrate binding appears to induce its ordering.

IDO is a monomeric protein, folded into two distinct domains: a large (C-terminal) domain and a small (N-terminal) capping domain (Figure 1b). Contact between these domains is extensive, and they are joined by a long loop. The larger domain is essentially topologically identical with a monomer of TDO, and the structures are readily superposable [5,14,15]. The loop region connecting the two domains provides similar interactions in the active site to those provided by the N-terminal arm of TDO, forming part of the active-site cavity. A flexible loop exists just outside the haem pocket, like that of TDO, but is not fully resolved crystallographically, probably due to the lack of bound substrate in the active site.

Active-site environment

TDO and IDO are *b*-type haem proteins with histidine occupying the axial co-ordination position to the haem iron. The only structure available with substrate bound at the active site in the catalytically active ferrous state is xcTDO. The structure clearly shows the important substrate-binding interactions in the active site. The active-site pockets of xcTDO with and without L-tryptophan bound and that of hIDO are shown in Figure 2. Owing to high similarity between the active sites of TDO and IDO, it is reasonable to assume a similar substrate-binding mode in IDO. Interactions of the substrate with the active site can be split into two categories: interactions with the carboxy and ammonium groups of L-tryptophan, and those with the indole ring system.

In the structure of xcTDO, the carboxy group of L-tryptophan interacts with Arg^{117}, Tyr^{113} and Thr^{254}. Amino acid residues equivalent to Arg^{117} and Tyr^{113} are found in nearly all TDO and IDO proteins. This carboxy-binding motif appears to be essential for substrate binding; arginine reorients in the presence of substrate, co-ordinating the carboxy group of L-tryptophan with both 'open' and 'closed' conformations observed (Figures 2a and 2b). The closed conformation is only observed in TDO crystals grown in the presence of L-tryptophan. The substrate ammonium group is hydrogen-bonded to the side-chain hydroxy group of Thr^{254}, the 7-propionate group of the haem, and a water molecule. Thr^{254} is involved in binding both the ammonium and carboxy moieties of L-tryptophan and is part of the flexible loop, just outside the haem pocket.

The substrate indole ring binds into a hydrophobic pocket, where it interacts with the side chain of Phe^{51} and several other hydrophobic residues, including Tyr^{24} and Tyr^{27} from the adjacent monomer. Both of these tyrosine residues

Figure 2 | Active-site residues of xcTDO and hIDO

Active-site residues of (**a**) substrate-free xcTDO, (**b**) L-tryptophan-bound xcTDO, with L-tryptophan shown in red, and (**c**) hIDO, with 4-phenylimidazole (shown in red) bound.

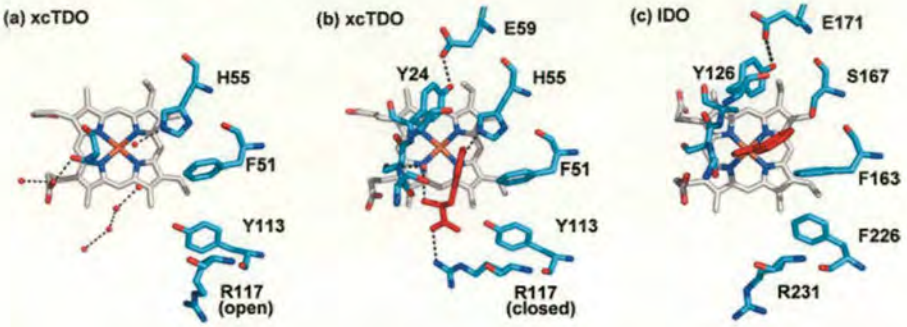

Figure 3 | Proposed catalytic mechanism of IDO and TDO

Initial formation of the ternary complex (**1**) occurs by substrate binding to the ferrous protein, followed by dioxygen binding. The ternary complex activates O_2 and catalysis proceeds via the formation of a hydroperoxide intermediate (**2** and **5**) that undergoes either a Criegee or a dioxetane rearrangement to form the product *N*-formylkynurenine (**7**).

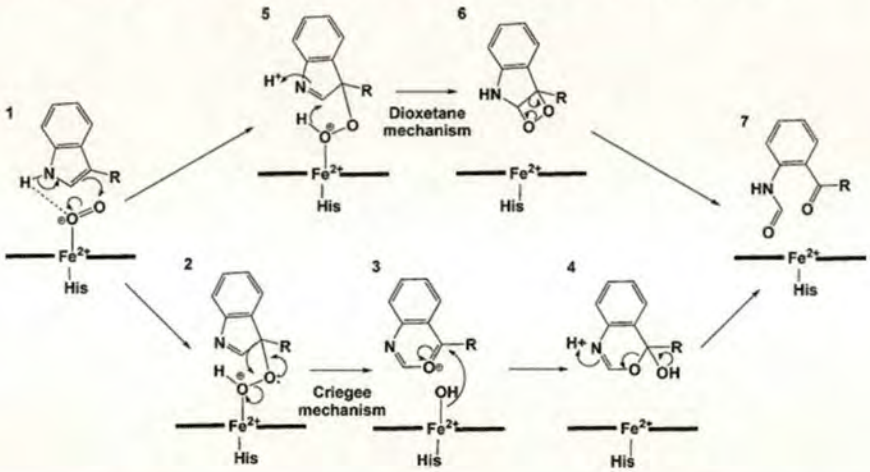

are hydrogen-bonded to a glutamate residue, linking the N-terminal loop of the adjacent monomer to the active site, and this Tyr-Glu motif is conserved throughout TDO and IDO proteins.

Perhaps the most obvious difference between the active sites of TDO and IDO is the presence of His^{55} in xcTDO and its equivalent, Ser^{167} in hIDO (Figure 2). In TDO, the histidine side chain is hydrogen-bonded with the NH group of the indole ring of L-tryptophan, and a role for His^{55} would appear to be in regulating substrate binding. In comparison, Ser^{167} in IDO is incapable of forming this bond, and it appears unlikely that this residue plays any critical role in substrate binding or catalysis by IDO.

What is the catalytic mechanism?

Substrate binding

The proposed catalytic mechanism employed by this family of enzymes is shown in Figure 3. It is thought that the ferrous enzyme is required for catalytic activity and, upon substrate binding, there is an increase in the electrochemical midpoint potential for both TDO and IDO. This shift in the reduction potential reflects additional stabilization of the ferrous form.Such a thermodynamic stabilization of the reduced form would clearly favour reduction before substrate binding [5,16–18]. A recent study has suggested that cytochrome b_5 is the electron transfer partner for IDO, providing ferrous active protein *in vivo*, consistent with these results.

For TDO, the initial formation of the ternary complex (Figure 3, **1**) occurs by substrate binding followed by dioxygen binding to the ferrous protein. For IDO, the order of binding events is more complex, but the ternary complex must still be formed before the reaction can proceed. The ternary complex activates O_2 and allows the otherwise spin-forbidden reaction to proceed.

Formation of the hydroperoxide intermediate

It has been proposed that formation of the hydroperoxide intermediate (Figure 3, **2** and **5**) is catalysed by the loss

of the indole proton. Two mechanisms are thought to be probable: base-catalysed deprotonation or proton abstraction by bound dioxygen [7]. If the substrate-binding mode in IDO is similar to that seen in xcTDO, proton abstraction by a proteinaceous base is only possible in TDO, with the active-site histidine (His^{55} in xcTDO) being the only basic residue in the active site of either enzyme (Figure 2). However, catalytic activity is maintained upon substitution of alanine for His^{55} in xcTDO, suggesting that base-catalysed deprotonation may not be essential for enzymatic activity [5]. Catalysis by the iron-bound dioxygen is generally proposed for IDO in the absence of a base, and seems reasonable from modelling simulations.

Rearrangement of the hydroperoxide intermediate

The rearrangement of the hydroperoxide intermediate to form the product could occur via either a Criegee or a dioxetane intermediate [7]. Little biochemical information currently exists to discriminate between these two differing pathways, and all discussion has been based on thermodynamic considerations and computer modelling simulations [7,14]. Thermodynamic considerations indicate that formation of the highly strained dioxetane intermediate and its high exothermicity of decomposition make this an unlikely route to be employed by an enzyme. In addition, no chemiluminescence has been detected on decomposition of the dioxetane. These data alone support the Criegee rearrangement for both IDO and TDO. However, further investigation is necessary to determine the nature of this rearrangement.

Conclusion

Recent crystallographic and biochemical analyses of TDO and IDO have aided our understanding of the mechanisms employed for binding and activating dioxygen by allowing identification of key active-site residues. Analysis of the active-site pockets of TDO and IDO shows that there are differences in the choice of residues employed in catalysis. However, how these changes have an impact on the catalytic mechanism and reaction intermediates employed by these enzymes is still unclear. Recent studies have led to possible future routes of investigation. These include: substitution of newly identified key active-site residues to identify their roles in catalysis; EPR and ENDOR (electron nuclear double resonance) studies of reaction intermediates, and computer modelling simulations.

Note added in proof (received 23 September 2008)

In a recent article by Chung et al. [19], density functional theory calculations on the catalytic mechanism of TDO and IDO have cast doubt on the relevance of the Criegee mechanism and raised the possibility of a radical addition pathway.

We thank the Wellcome Trust for financial support.

References

1 Kotake, Y. and Masayama, I. (1936) The intermediary metabolism of tryptophan. XVIII. The mechanism of formation of kynurenine from tryptophan. Z. Physiol. Chem. **243**, 237–244
2 Ishiguro, I., Naito, J., Saito, K. and Nagamura, Y. (1993) Skin L-tryptophan-2,3-dioxygenase and rat hair growth. FEBS Lett. **329**, 178–182
3 Haber, R., Bessette, D., Hulihan-Giblin, B. and Durcan, M.J. (1993) Identification of tryptophan 2,3-dioxygenase RNA in rodent brain. J. Neurochem. **60**, 1159–1162
4 Yamamoto, S. and Hayaishi, O. (1967) Tryptophan pyrrolase of rabbit intestine: D- and L-tryptophan-cleaving enzyme or enzymes. J. Biol. Chem. **242**, 5260–5266
5 Forouhar, F., Anderson, J.L.R., Mowat, C.G., Vorobiev, S.M., Hussain, A., Abashidze, M., Bruckmann, C., Thackray, S.J., Seetharaman, J., Tucker, T. et al. (2007) Molecular insights into substrate recognition and catalysis by tryptophan 2,3-dioxygenase. Proc. Natl. Acad. Sci. U.S.A. **104**, 473–478
6 Tankiewicz, A., Pawlak, D. and Buczko, W. (2001) Enzymes of the kynurenine pathway. Postepy Hig. Med. Dosw. **55**, 715–731
7 Sono, M., Roach, M.P., Coulter, E.D. and Dawson, J.H. (1996) Heme-containing oxygenases. Chem. Rev. **96**, 2841–2887
8 Wirleitner, B., Neurauter, G., Schrocksnadel, K., Frick, B. and Fuchs, D. (2003) Interferon-γ-induced conversion of tryptophan: immunologic and neuropsychiatric aspects. Curr. Med. Chem. **10**, 1581–1591
9 Wang, R. and Tang, A.-G. (2005) Detection and clinical significance of kynurenine. Guowai Yixue Linchuang Shengwu Huaxue Yu Jianyanxue Fence **26**, 835–837
10 Ohashi, H., Saito, K., Fujii, H., Wada, H., Furuta, N., Takemura, M., Maeda, S. and Seishima, M. (2004) Changes in quinolinic acid production and its related enzymes following D-galactosamine and lipopolysaccharide-induced hepatic injury. Arch. Biochem. Biophys. **428**, 154–159
11 MacKenzie, C.R., Heseler, K., Muller, A. and Daubener, W. (2007) Role of indoleamine 2,3-dioxygenase in antimicrobial defense and immunoregulation: tryptophan depletion versus production of toxic kynurenines. Curr. Drug Metab. **8**, 237–244
12 Munn, D.H. (2006) Indoleamine 2,3-dioxygenase, tumor-induced tolerance and counter-regulation. Curr. Opin. Immunol. **18**, 220–225
13 Mellor, A.L., Munn, D., Chandler, P., Keskin, D., Johnson, T., Marshall, B., Jhaver, K. and Baban, B. (2003) Tryptophan catabolism and T cell responses. Adv. Exp. Med. Biol. **527**, 27–35
14 Zhang, Y., Kang, S.A., Mukherjee, T., Bale, S., Crane, B.R., Begley, T.P. and Ealick, S.E. (2007) Crystal structure and mechanism of tryptophan 2,3-dioxygenase, a heme enzyme involved in tryptophan catabolism and in quinolinate biosynthesis. Biochemistry **46**, 145–155
15 Sugimoto, H., Oda, S., Otsuki, T., Hino, T., Yoshida, T. and Shiro., Y. (2006) Crystal structure of human indoleamine 2,3-dioxygenase: catalytic mechanism of O_2 incorporation by a heme-containing dioxygenase. Proc. Natl. Acad. Sci. U.S.A. **103**, 2611–2616
16 Basran, J., Rafice, S.A., Chauhan, N., Efimov, I., Cheesman, M.R., Ghamsari, L. and Raven, E.L. (2008) A kinetic, spectroscopic, and redox study of human tryptophan 2,3-dioxygenase. Biochemistry **47**, 4752–4760
17 Papadopoulou, N.D., Mewies, M., McLean, K.J., Seward, H.E., Svistunenko, D.A., Munro, A.W. and Raven, E.L. (2005) Redox and spectroscopic properties of human indoleamine 2,3-dioxygenase and a His303Ala variant: implications for catalysis. Biochemistry **44**, 14318–14328
18 Makino, R., Sakaguchi, K., Iizuka, T. and Ishimura, Y. (1980) L-Tryptophan 2,3-dioxygenase; structure, function and interaction with substrate. Dev. Biochem. **16**, 179–187
19 Chung, L. W., Li, X., Sugimoto, H., Spiro, Y. and Morokuma, K. (2008) Density functional theory study on a missing piece in understanding of heme chemistry: the reaction mechanism for indoleamine 2,3-dioxygenase and tryptophan 2,3-dioxygenase. J. Am. Chem. Soc. **130**, 12299–12309

Received 13 June 2008
doi:10.1042/BST0361120

Reassessment of the Reaction Mechanism in the Heme Dioxygenases

Nishma Chauhan,[†] Sarah J. Thackray,[‡] Sara A. Rafice,[†] Graham Eaton,[†] Michael Lee,[†] Igor Efimov,[†] Jaswir Basran,[§] Paul R. Jenkins,[†] Christopher G Mowat,[‡] Stephen K. Chapman,*[,‡] and Emma Lloyd Raven*[,†]

[†] *Department of Chemistry, University of Leicester, University Road, Leicester, LE1 7RH, U.K.,* [‡] *EaStCHEM, School of Chemistry, University of Edinburgh, West Mains Road, Edinburgh EH9 3JJ, U.K, and* [§] *Department of Biochemistry, University of Leicester, Lancaster Road, Leicester, LE1 9HN, UK.*

RECEIVED DATE (automatically inserted by publisher); **Email: s.k.chapman@ed.ac.uk; emma.raven@le.ac.uk.**

Indoleamine 2,3-dioxygenase (IDO) and tryptophan 2,3-dioxygenase (TDO) are heme enzymes that catalyse oxidation of L-tryptophan to *N*-formyl-kynurenine (Scheme 1),[1-3] in a mechanism that involves binding of dioxygen to reduced iron. The mechanistic details of this oxidation are not yet known, but early studies[3] suggested base-catalysed deprotonation of the indole NH group (Scheme 2A). This was based largely on the observation that 1-methyl-L-tryptophan (1-Me-L-Trp) is an inhibitor of dioxygenase activity, and was plausible since base-catalysed abstraction is not possible with the methylated compound. There are problems with this mechanism, however. To begin with, it is inconsistent with the chemistry of indoles,[4] which typically react by electrophilic addition across the C_3 position and subsequent formation of a cation at N_1. In addition, the structure of human IDO (hIDO)[5] reveals that there is no active-site base close enough for proton abstraction at N_1. The only polar active site residue is Ser167, but this is not essential for activity.[5,6] Although *X. campestris* TDO (*Xc*TDO) does contain an active site histidine (His55, equivalent to Ser167 in hIDO)[7] which hydrogen bonds to the indole N_1, it is not essential for activity.[7,8] Together, this led to the hypothesis[5,7] that the bound dioxygen might act as the active-site base (Scheme 2B), with no involvement from active site residues.

Here, we examine the activity of three heme dioxygenases (hIDO, human TDO (hTDO) and *Xc*TDO[9]) with 1-Me-L-Trp, including a number of site-directed variants focused on the His55/Ser167 location. In contrast to previous work,[10] we find that 1-Me-L-Trp is a slow substrate. These observations are inconsistent with current proposals for the mechanism of substrate oxidation, and we propose an alternative.

Scheme 1. Reaction catalysed by IDO and TDO.

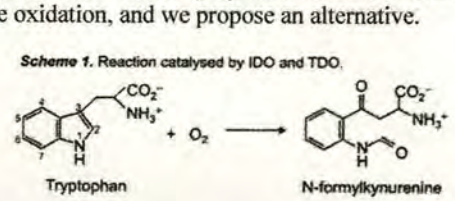

To determine if the purified enzymes could utilize 1-Me-L-Trp as a substrate, identification of the methylated product was essential.[11,12] Formation of *N*-formyl-kynurenine and *N*-formyl-methylkynurenine was confirmed at 321 nm (Figure S2, solid and dashed line, respectively). The reaction with 1-Me-L-Trp was repeated in the absence of enzyme (Figure S2, dotted line) and no absorbance change at 321 nm was observed, confirming that product formation is from enzymatic oxidation. LC-MS analysis using selected ion monitoring (shown for hIDO, Figure 1A) was then carried out. For the reaction with L-Trp, this gave an ion with m/z = 237 (Figure 1B, *top*) which corresponds to the mass of *N*-formyl-kynurenine (m/z = 236); for the reaction with 1-Me-L-Trp, an equivalent ion is detected at m/z = 251 (Figure 1B, *bottom*) as expected for *N*-formyl-methylkynurenine (m/z = 250).

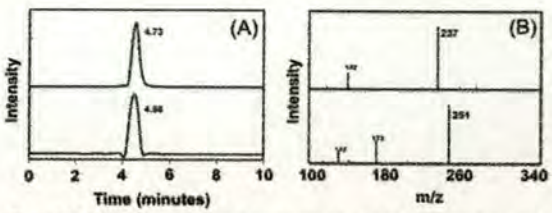

Figure 1. LC-MS analyses of products obtained on reaction of hIDO with *N*-formylkynurenine (top) and *N*-formylmethylkynurenine (bottom). Panel A: elution profiles for selected ion chromatograms with *m/z* of (top) 237 and (bottom) 251, corresponding to *N*-formylkynurenine and *N*-formylmethylkynurenine, respectively. Panel B: corresponding positive ESI mass spectra for the products eluted at 4.73 min and 4.50 min (top and bottom, respectively).

Steady-state kinetic parameters for the oxidation of 1-Me-L-Trp were also determined.[6,7] (Figure S3 and Table 1).[13] Clear increases in absorbance, corresponding to product formation, are observed for hIDO (Figure S3), as well as for the S167A variant of hIDO and variants of both hTDO and *Xc*TDO (Table 1).[13]

These data clearly indicate that formation of *N*-formyl-methylkynurenine occurs upon reaction of 1-Me-L-Trp with hIDO and variants of hIDO, hTDO and *Xc*TDO. However, no activity was detected for hTDO and *Xc*TDO with 1-Me-L-Trp in either steady-state or LC-MS analyses. The structure of *Xc*TDO[7] reveals a hydrogen bond (2.6 Å) between the indole NH of L-Trp and His55, which would be expected to lead to a steric clash between His55 and the methyl group of 1-Me-L-Trp. Indeed, a model of 1-Me-L-Trp binding to *Xc*TDO (Figure S4) shows a non-bonding distance of ~1.5 Å between the N^{ε} of His55 and the carbon atom of the Me group on 1-Me-L-Trp. We propose that binding of 1-Me-L-Trp to *Xc*TDO is weak as a consequence. Sequence alignments[7] indicate that hTDO also contains a histidine (His76) in the same position (in fact this histidine residue is conserved in all TDOs), so that the same steric restrictions apply and thus explain the observed inactivity. Substitution of histidine in *Xc*TDO (H55A, H55S) and hTDO (H76S) allows accommodation of

Table 1. Steady-state parameters (k_{cat}, K_M) for oxidation of 1-Me-L-Trp.

	Variant	k_{cat} (s^{-1})	K_M (μM)
hIDO	native	0.027 ± 0.001	150 ± 11
	S167A	0.032 ± 0.002	31 ± 5.0
hTDO	native	-	-
	H76S	0.023 ± 0.001	2300 ± 230
*Xc*TDO	native	-	-
	H55A	0.048 ± 0.011	59 ± 16
	H55S	0.052 ± 0.009	70 ± 11

the additional methyl group and turnover of 1-Me-L-Trp occurs (Table 1). This hypothesis is further supported by the fact that hIDO and S167A, which are both able to accommodate the bulky Me group in their active sites, are also able to oxidise 1-Me-L-Trp (Table 1).

Overall, turnover numbers for 1-Me-L-Trp are lower than for L-Trp.[6,8,14] When X=Me (Scheme 2D), the inductive effect of the Me group would presumably stabilise the cation intermediate. This would not be expected to slow down the electrophilic attack but might affect other steps in the mechanism that our experiments do not address. A completely different binding location/orientation for 1-Me-L-Trp (and therefore a different mechanism) is also possible, but this is not supported by inhibition data (Table S1 and [10]) which show 1-Me-L-Trp as a competitive inhibitor for L-Trp.

***Scheme* 2.** Possible mechanisms for oxidation of Trp (C_2, C_3 and N_1 of the substrate are labelled). (A) Abstraction of the indole proton by an active site base.[3,15] (B) Abstraction of the indole proton by the heme-bound dioxygen.[5,16] (C) Direct electrophilic addition. (D) A revised mechanism for product formation in heme dioxygenases, where X=H or Me. The conversion to product is proposed to occur either by a Criegee or a dioxetane mechanism.[3]

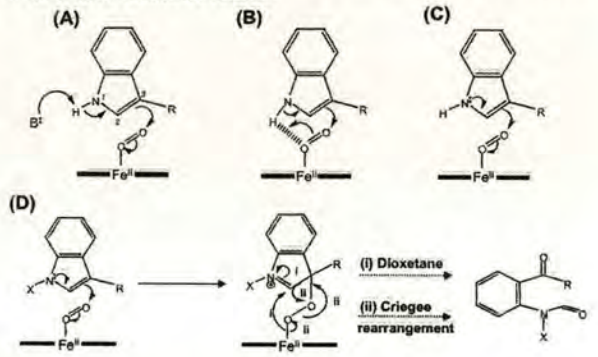

Since hIDO and variants of both hTDO and *Xc*TDO can oxidise 1-Me-L-Trp, deprotonation of the indole NH cannot be essential for catalysis. Mechanisms involving abstraction of the indole proton, either using an active site base[3,15] or dioxygen[5,16] (Schemes 2A, B), are therefore unlikely as they cannot proceed with a Me group on N_1.

The chemistry of indoles is very well documented[4] and does not occur by loss of the indole proton. Instead, when an indole reacts with an electrophile (*e.g.* O_2) the lone pair on N_1 initiates the process (Scheme 2C) and the electrophile becomes attached preferentially at C_3 (Scheme 2D).[17] We propose this as a more likely mechanism for tryptophan oxidation in the heme dioxygenases, allowing both L-Trp and 1-Me-L-Trp to react (Scheme 2D), with the role of the iron merely as a donor of the required oxygen molecule. This mechanism is compatible with the absence of an active site base in IDO, and avoids the need to deprotonate an N_1 atom with a pK_a (≈17[18]) that is out of range.[18] In addition, a recent density functional theory study[19] found that direct electrophilic addition has a lower activation energy than a base-catalysed deprotonation mechanism, consistent with our observations.

In conclusion, we report that 1-Me-L-Trp is a substrate for hIDO and variants of hTDO and *Xc*TDO in which the active site histidine has been replaced. This shows that deprotonation of the indole N_1 is not essential for catalysis and we propose that direct electrophilic addition to dioxygen, facilitated by the lone pair on the indole N_1, occurs instead.

Acknowledgement. We thank Dr Sharad Mistry for helpful discussions. This work was supported by The Wellcome Trust (grants 083636 to SKC and ER).

Supporting Information Available: HPLC/NMR of 1-Me-L-Trp, spectra of *N*-formyl-kynurenine and *N*-formyl-methylkynurenine, steady-state data, and a model of the *Xc*TDO/Me-Trp complex.

References

1. Yamamoto, S.; Hayaishi, O. *J. Biol. Chem.* **1967**, *242*, 5260.

2. Knox, W. E.; Mehler, A. H. *J. Biol. Chem.* **1950**, *187*, 419.

3. Sono, M., Roach, M. P., Coulter, E. D., and Dawson, J. H. *Chem. Rev.* **1996**, *96*, 2841.

4. Joule, J. A.; Mills, K. *Heterocyclic Chemistry* **2000**, *Fourth Edition*, Blackwell, Oxford, p319.

5. Sugimoto, H.; Oda, S.; Otsuki, T.; Hino, T.; Yoshida, T.; Shiro, Y. *Proc. Natl. Acad. Sci. USA* **2006**, *103*, 2611.

6. Chauhan, N.; Basran, J.; Efimov, I.; Svistunenko, D. A.; Seward, H. E.; Moody, P. C.; Raven, E. L. *Biochemistry* **2008**, *47*, 4761.

7. Forouhar, F.; Anderson, J. L.; Mowat, C. G.; Vorobiev, S. M.; Hussain, A.; Abashidze, M.; Bruckmann, C.; Thackray, S. J.; Seetharaman, J.; Tucker, T.; Xiao, R.; Ma, L. C.; Zhao, L.; Acton, T. B.; Montelione, G. T.; Chapman, S. K.; Tong, L. *Proc. Natl. Acad. Sci. USA* **2007**, *104*, 473.

8. Thackray, S. J.; Bruckmann, C.; Anderson, J. L.; Campbell, L. P.; Xiao, R.; Zhao, L.; Mowat, C. G.; Forouhar, F.; Tong, L.; Chapman, S. K. *Biochemistry* **2008**.

9. All proteins were isolated as described previously.[6,7,14].

10. Cady, S. G.; Sono, M. *Arch. Biochem. Biophys.* **1991**, *291*, 326

11. Commercially available 1-Me-L-Trp (95% purity) was purified by HPLC to remove contaminating species which could act as substrate (Figure S1A) and the purity confirmed by further HPLC and ^{1}H NMR (Figure S1B,C).

12. Steady-state assays contained sodium ascorbate (20 mM), methylene blue (10 μM) catalase (10 μg), 1-Me-L-Trp (variable) and enzyme (1-5 μM)[6,7], in either 50 mM Tris/HCl buffer, pH 8.0 (hIDO and hTDO and respective variants) or 100 mM phosphate buffer, pH 7.5 (*Xc*TDO and variants). Reactions were allowed to proceed for at least 1 hour, and then quenched by addition of 30% (v/v) trichloroacetic acid, followed by centrifugation to remove the enzyme. Values for K_i were measured in the same way by varying varying [L-Trp] as above differing concentrations of 1-Me-L-Trp. Data were analysed by plotting 1/v (the observed rate) against 1/[L-Trp].

13. The corresponding LC-MS data for these proteins also showed ions at 251, as for hIDO (data not shown).

14. Basran, J.; Rafice, S. A.; Chauhan, N.; Efimov, I.; Cheesman, M. R.; Ghamsari, L.; Raven, E. L. *Biochemistry* **2008**, *47*, 4752.

15. Leeds, J. M.; Brown, P. J.; McGeehan, G. M.; Brown, F. K.; Wiseman, J. S. *J. Biol. Chem.* **1993**, *268*, 17781.

16. Terentis, A. C.; Thomas, S. R.; Takikawa, O.; Littlejohn, T. K.; Truscott, R. J.; Armstrong, R. S.; Yeh, S. R.; Stocker, R. *J. Biol. Chem.* **2002**, *277*, 15788.

17. Attack at C_3 generates a positive charge on C_2 which is resonance stabilized by the lone pair on N_1 (Scheme D). Attack at C_2, as proposed recently,[19] is less favourable and not observed in indole chemistry because this generates a positive charge on C_3, which is less well stabilized (through the benzene ring). This preference for attack at C_3 would also apply for radical addition.[19]

18. Yagil, G. *Tetrahedron* **1967**, *23*, 2855.

19. Chung, L. W.; Li, X.; Sugimoto, H.; Shiro, Y.; Morokuma, K. *J. Am. Chem. Soc.* **2008**, 12299.